Dynamic of intra-continental extension in magmatic rift context: Turkana Rift (Northern Kenya) from Eocene to Present

William Vetel

Unit Mixte de Recherche CNRS
" Domaines Ocaniques"

ECOLE DOCTORALE DES SCIENCES DE LA MER
GROUPE DE FORMATION DOCTORALE GEOSCIENCES MARINES

THESE DE DOCTORAT DE
L'UNIVERSITE DE BRETAGNE OCCIDENTALE

William VETEL

Dynamique de l'extension intra-continentale en contexte de rift magmatique : le Rift Turkana (Nord Kenya) de l'Eocène à l'Actuel

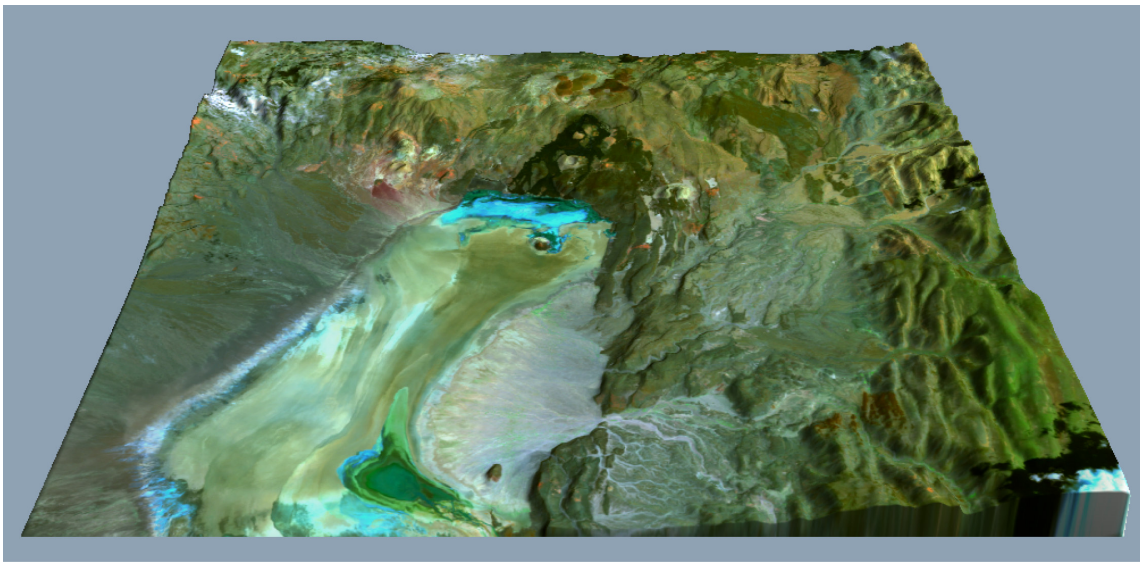

Soutenance prévue le 21 janvier 2005 devant le jury composé de :

O. Dauteuil	**DR/CNRS, Univ. Rennes**	**Rapporteur**
D. Delvaux	**Professeur, Univ. Tervuren**	**Invité**
J. Deverchère	**Professeur, IUEM, Brest**	**Examinateur**
Y. Klinger	**CR/CNRS, Inst. Physique du Globe, Paris**	**Examinateur**
B. Le Gall	**CR/CNRS, IUEM, Brest**	**Directeur de thèse**
J. Rolet	**MC, IUEM, Brest**	**Examinateur**
M. Sébrier	**DR/CNRS, Univ. Paris VI**	**Rapporteur**
J. Walsh	**Professeur, Univ. Dublin**	**Invité**

BREST, 2005

I.U.E.M.
U.M.R. 6538
Unit Mixte de Recherche CNRS
" Domaines Ocaniques"

ECOLE DOCTORALE DES SCIENCES DE LA MER
GROUPE DE FORMATION DOCTORALE GEOSCIENCES MARINES

THESE DE DOCTORAT DE
L'UNIVERSITE DE BRETAGNE OCCIDENTALE

William VETEL

Dynamique de l'extension intra-continentale en contexte magmatique : le cas du Rift Turkana (Nord Kenya) de l'Eocène à l'Actuel

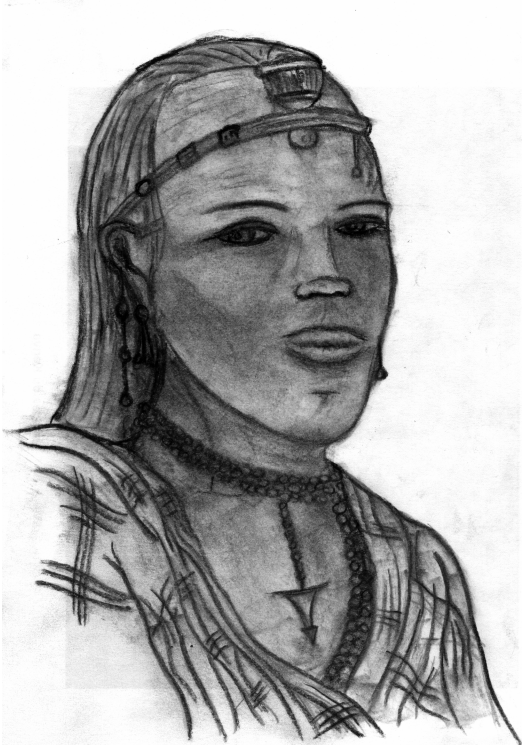

BREST, 2005

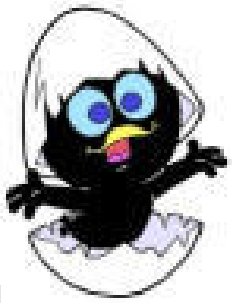

REMERCIEMENTS

A l'issue de ces trois années de doctorat, je tiens à exprimer ma plus vive reconnaissance à toutes les personnes qui m'ont apporté leur aide, de près ou de loin, pour la réalisation et la concrétisation de ce travail.

Tout d'abord, je tiens à remercier les membres du jury qui ont accepté et pris le temps de juger ce travail : Olivier Dauteuil, Damien Delvaux, Jacques Deverchère, Yann Klinger, Joël Rolet, Michel Sébrier et John Walsh.

Je remercie particulièrement Bernard Le Gall qui, en tant que directeur de thèse, a toujours su être disponible, malgré un emploi du temps bien rempli (Maroc, Djibouti, Tanzanie, …). Son apport a largement dépassé le cadre de la géologie (from Poullic to Kerziou …). Il a su guider, orienter et corriger mon travail avec un enthousiasme et un dynamisme à toute épreuve. Il m'a permis de découvrir le plaisir de l'investigation géologique, aussi bien sur le terrain à la recherche des failles 'perdues' du Turkana, qu'à l'IUEM.

Je remercie le programme ECLIPSE INSU (Paléoenvironnements des Hominidés Mio-Plio-Pléistocènes en Afrique centrale et orientale ; responsable H. Roche) qui nous a permis d'acheter les données d'imagerie Landsat et de financer une mission de terrain (été 2002). Je remercie Hélène Roche et son équipe de paléontologues pour leur accueil dans leur camp trois étoiles au bord du laga Nariokotome (Turkana).
J'exprime également ma gratitude aux chercheurs qui m'ont accueilli au sein de leur laboratoire et m'ont permis de me former à de nouvelles techniques, je citerai John Walsh (Dublin, Irlande), Tom Johnson (Duluth, USA), Richard Gloaguen (Freiberg, Allemagne), l'équipe de Rennes (Stéphane Bonnet, François Guillocheau, Olivier Dauteuil,…) avec qui les discussions ont toujours été très enrichissantes.
Dans ce cadre, je ne saurais oublier les membres du département Géosciences de l'IUEM : mes collègues thésards (Mickey *et al.,* B-133), ainsi que Jean-Luc Travers, Dominique Gac, Danièle Hureau, Eric Hardy , …

Plus proche de moi, je remercie plus particulièrement Muriel et Morticia (le chat de l'amour), de leur compréhension, leur soutien et leur patience au quotidien.

Illustration de couverture : *Extrait de l'image Landsat ETM+ (169-058) drapé sur le MNT SRTM. Vue 3D vers le nord de la terminaison de la vallée de la Suguta et du complexe volcanique du Barrier.*
Illustration seconde couverture : *Dessin personnel d'un jeune guerrier Masaï.*

TABLE DES MATIERES

RESUME

La dynamique de l'extension continentale et la géométrie des rifts qui en découlent sont régies par la combinaison de nombreux paramètres (thermiques, mécaniques, cinématiques) qui interagissent à différentes échelles, dans le temps et dans l'espace. L'exemple choisi dans cette étude, afin d'apporter des éléments de réponse à la compréhension de la mise en place des structures extensives, est celui du rift Turkana (Nord Kenya) qui appartient à la branche est du Rift Est Africain (REA). Cette portion de rift cénozoïque atypique s'est développée selon un axe NS depuis ~45 Ma. entre les terminaisons de deux bassins d'un rift antérieur oblique (bassins Anza-Soudan N140°E Crétacé). Sa structure profonde est dominée par un ensemble d'hemi-grabens syn-rifts oligo-pliocènes et sa géométrie de surface est actuellement marquée par une topographie peu contrastée et une sismicité faible qui rendent difficile l'étude des mouvements récents/actifs dans ce secteur.

Ce mémoire, basé sur l'interprétation d'imagerie satellitale Landsat ETM+, corrélée aux données topographiques (SRTM) et aux données de sismique réflexion, permet :

- A l'échelle régionale, une reconstitution tectono-magmatique de l'histoire polyphasée du rift Turkana établie sur la base de cinq cartes 'restaurées' successives (45-23 Ma., 23-15 Ma., 15-6 Ma., 6-2.6 Ma. et 2.6 Ma.-Actuel), auxquelles ont également été intégrées les structures pré-existantes (socle précambrien, structures crétacées). Ce modèle démontre clairement l'influence de : 1) deux couloirs transverses de socle faillés d'échelle régionale (NKFZ : N'Doto-Karisia N140°E, 100x600 km ; KBFZ : Kataboi-Buluk N50°E, 30x250 km) et 2) de domaines magmatiques, sur la nucléation et la propagation des structures extensives à différents stades du rifting. Les bassins syn-rifts se développent et migrent en premier lieu à l'intérieur du couloir N140°E NKFZ à la faveur de relations angulaires entre les structures N140°E et les failles néoformées NS, ces dernières sont par la suite bloquées lors de leur interaction avec les structures N50°E KBFZ qui peuvent également agir comme des zones de transfert et aboutissent à l'élargissement de la zone riftée (200x200 km). La description des relations entre les domaines magmatiques et la déformation met en avant le rôle déterminant des structures internes des dômes volcaniques (fentes d'extrados, failles syn-magmatiques) sur la propagation des bassins à travers ces paleo-dômes après cessation de l'activité magmatique.

- A l'échelle lithosphérique, les interactions panache/lithosphère durant la migration de la plaque Afrique (~1000 km vers le NE) depuis 50 Ma. à la verticale de deux plumes cénozoïques permettent de proposer deux hypothèses sur l'absence de soulèvement thermique le long de la dépression du Turkana. Il peut s'agir, soit de la migration latérale de la tête du panache sous la lithosphère pré-étirée crétacée selon un mécanisme de 'thin-spot', soit du 'durcissement' de cette même lithosphère en réponse au refroidissement du matériel mantellique sous-plaqué (crétacé) qui entrave le soulèvement de l'ensemble de la zone.

- Concernant les déformations récentes/actives (<5 Ma.) du rift Turkana, l'étude du développement des inversions tectoniques positives (<3.7 Ma.), distribuées uniquement dans les bassins situés à la verticale du couloir transverse N140°E NKFZ, confirme l'importance du rôle joué par cette discontinuité de premier ordre sur l'évolution du rift Turkana depuis l'Eocène jusqu'à l'Actuel. La reconstitution de la mise en place de ces structures compressives aboutit à un modèle cinématique polyphasé comprenant les trois stades suivants : 1) un régime purement extensif avant 5 Ma. ($\sigma3$ horizontal orienté EW, $\sigma1$ vertical), 2) une rotation horaire (~20°) de l'axe $\sigma3$ entre 5 et 3.7 Ma. qui entraîne la réactivation en dextre de la NKFZ et la formation d'un réseau de fractures N20°E et 3) un stade compressif (permutation des axes $\sigma1/\sigma2$) accompagné de la rotation horaire de $\sigma3$ (~20°) qui induit la réactivation en inverse des failles N20°E après 3.7 Ma.

- A l'échelle plus locale, dans la partie orientale du rift Turkana, le réseau récent (<3 Ma.) de failles N170°-N10°E du Kino Sogo (150x40 km) s'organise selon une succession régulière de horsts et grabens, exceptionnellement bien exposés, qui recoupent des laves mio-pliocènes peu épaisses (~200 m) mises en place sur un horst asymétrique de socle, limité par des structures N140°E, N50°E et NS. L'étude géométrique et statistique de la population de failles du Kino Sogo révèle plusieurs particularités : 1) ce réseau accommode peu d'extension (<1%) et implique des taux d'extension et de déformation faibles (~0.1 mm/an et 10^{-16} s^{-1}, respectivement), 2) l'analyse des longueurs de failles se corrèle avec une loi mathématique de type exponentielle en opposition avec celles classiquement admises de type lois de puissances, et 3) malgré des longueurs

importantes (9-40 km), les failles présentent des rejets ≤ 100 m, ce qui leur confère un rapport rejet/longueur inférieur à ceux décrits sur des réseaux de failles similaires. Ce caractère mature, mais sous-déplacé des failles, est attribué à un modèle de croissance de failles dominé par la réactivation de structures pré-existantes présentes dans le socle sous-jacent (foliation/failles) ou au toit d'un paléo-dôme volcanique antérieur.

- Enfin, d'un point de vue méthodologique, l'intérêt de l'étude des réseaux de drainage en contexte morphologique peu contrasté est confirmé par une analyse détaillée de l'intense réseau de drainage développé dans le secteur occidental du Turkana. En effet, l'interprétation structurale de trois anomalies de drainage met en évidence : 1) la déviation de la rivière Turkwell (NS puis EW) le long d'un couloir transverse faillé EW intra-socle de second-ordre (Turkwell-Mont Porr ; ~20x100 km), 2) le blocage d'un réseau dense de rivières par la réactivation récente (<5 Ma.) du plan de faille bordière Ouest Napedet d'âge oligo-miocène 3) la formation d'une anomalie de type circulaire autour d'une structure antiforme initiée lors de l'inversion d'un dépocentre au pied de la faille de Kerio et associée aux inversions tectoniques positives décrites pour la période récente (<3.7 Ma) dans une partie du rift Turkana.

D'une façon générale, ce travail apporte des résultats et des modèles nouveaux ayant des implications directes sur l'étude de la nucléation et de la propagation des bassins syn-rifts et des réseaux de failles associés aux segments de rift magmatiques marqués par un héritage structural important (socle, système rifté antérieur).

ABSTRACT

Continental extension and rift geometry are widely controlled by the interaction of various parameters (thermal, mechanical, kinematical) that interplay at different space and time scales. So as to provide some new insights about the dynamic of magmatic rift segments emplacement, this study focuses on the Turkana rift (Northern Kenya) which belongs to the eastern branch of the reference East African Rift System (EARS). This NS atypical Cenozoic rift portion developed since 45 Ma. between the termination of two previous oblique cretaceous basins (N140°E Anza and Soudan). Its deep geometry is dominated by a set of syn-rift Oligo-Miocene half-grabens whereas its present-day surface arrangement is marked by a subdued topography and a weak seismicity that makes difficult to study recent/active movements in the Turkana rift area.

This work, based on interpretation of Landsat ETM+ satellite imagery correlated with digital topography (SRTM) and seismic reflection dataset, leads us to propose and discuss a tectono-magmatic reconstruction of the poly-phased evolution of the Turkana rift by five successive 'restored' maps (45-23 Ma., 23-15 Ma., 15-6 Ma., 6-2.6 Ma., 2.6 Ma.-Actual), completed by two additional maps dealing with pre-existing structures (Precambrian basement, previous Cretaceous rift). Our model fully demonstrates the influence of: 1) two regional-scale transverse corridors (NKFZ: N'Doto-Karisia N140°E, 100x600 km; KBFZ: Kataboi-Buluk N50°E, 30x250 km) and 2) the existence of magmatic domains, on the nucleation and propagation of extensional structures during different stages of rifting. Both location of newly-formed basins and their final geometry are directly imposed by transverse fault zone dimensions. Syn-rift basins firstly develop and migrate north and eastwards within the N140°E NKFZ transverse corridor, according to favourable angular relations between N140°E and rift-parallel NS structures, whereas faults are next locked by N50°E KBFZ structures due to acute unfavourable fault interaction types. N50°E discontinuities could also act as transfer zones and tend to distribute the deformation over a wide-rifted area (200x200 km). Description of relation between magmatic domain and extension widely highlights the key-role plays by inner volcanic domes structures (extrados faults/fractures, syn-magmatic faults) on the propagation of basin throughout those paleo-domes after the cessation of volcanic activity. At a greater scale, considering plume/lithosphere interactions, during the migration of Africa plate (~1000 km to the NE) since 50 Ma. above two Cenozoic mantle plumes, permits to propose two hypothesis so as to explain the lack of thermal uplift along the persistent Turkana depression: 1) the lateral migration of plume head material beneath the pre-stretched cretaceous lithosphere or 2) the strengthening of the lithosphere in response to the cooling of the cretaceous underplating that prevent any bending of the lithosphere at a large wavelength.

Concerning the recent/active deformations (<5 Ma.) of the Turkana rift, the kinematical study of recent inversions tectonics (<3.7 Ma.), only distributed within some of the Oligo-Pliocene basins located above the NKFZ N140°E transverse fault zone, confirms the key-role plays by this first-scale discontinuity on the evolution of the Turkana rift from Eocene to Actual rifting stages. The comprehension of the formation of those compressive structures leads us to propose a three-stages kinematic model: 1) a pure extensional regime before 5 Ma. ($\sigma3$ horizontal oriented EW, $\sigma1$ vertical), 2) a slight clockwise rotation (~20°) of $\sigma3$ axis between 5 and 3.7 Ma. that induced the dextral reactivation of the NKFZ and the formation of a N20°E T-type fault network and 3) a clockwise rotation of $\sigma3$ (~20°) after 3.7 Ma. coeval to a permutation of $\sigma1/\sigma2$ axes that induced the reversed reactivation of N20°E fault network.

In the oriental area of the Turkana rift, the exceptionally well-exposed recent Kino Sogo fault network (<3 Ma.; 150x40 km) comprised a series of horsts and grabens within an arcuate 40 km-wide zone that dissects Mio-Pliocene lavas overlying an earlier asymmetric fault block bounded by N140°E, N50°E and NS structures. The geometrical and quantitative analysis on the scaling properties reveals several particularities of the Kino Sogo dense fault network : 1) this pattern accommodates very low strains (<1%) and implies a weak rate of extension and deformation (~0.1 mm/yr and 10^{-16} s^{-1}, respectively), 2) fault length distribution subscribe to a negative exponential scaling law, as opposed to the power-law scaling typical of other fault systems, 3) the long faults (length up to 40 km) are characterised by maximum throws of no more than 100 m, hence providing displacement/length ratios which are significantly below of other fault systems. The under-displaced nature of the Kino Sogo fault system is attributed to early stage rapid fault propagation possibly arising from reactivation of earlier magmatic-related fractures and/or underlying basement structures/fabrics.

Finally, a detailed analysis of the Turkana drainage network, exceptionally developed on the occidental part of the Turkana area, confirms the general structural and kinematic framework of the Turkana rift segment. Three drainage anomalies are studied and highlight: 1) the virgation of the Turkwell River (from NS to EW) along an EW second-order faulted corridor (Turkwell-Mount Porr; 20x100 km), 2) the locking of a dense river pattern by the recent rejuvenation (<5 Ma.) of the West Napedet Oligo-Miocene border fault plane and 3) the formation of the Kalabata circular drainage anomaly surrounding an antiformal structure associated to the recent phase of structural inversions (<3.7 Ma.).

More generally, the new insights fully discussed in this work have direct implications on the study of the processes of nucleation and propagation of a magmatic rift segment recording a low deformation rate and being influenced by a strong structural inheritance (basement, previous rifted system).

INTRODUCTION et PROBLEMATIQUES

La dynamique de l'extension continentale et la complexité structurale des rifts qui en découlent sont directement fonction de la combinaison d'une multitude de facteurs qui interagissent, en surface et en profondeur, à des échelles de temps et d'espace très variables (Morley, 1994 ; Ziegler & Cloetingh, 2004). La compréhension d'un rift donné implique donc d'identifier les facteurs en présence, puis de préciser leur rôle respectif dans les processus de la déformation.

- A l'échelle mantellique, les interactions entre des mouvements convectifs (panache) et la lithosphère continentale, soumise ou non à des sollicitations tectoniques externes, ont mené à la distinction classique entre rifts 'actifs' ou 'passifs' qui se démarquent principalement par la chronologie des évènements tectoniques et magmatiques (e.g. Bott & Kusznir, 1979 ; Spohn & Schubert, 1982 ; McKenzie & Bickle, 1988).

- A une échelle intermédiaire, la nature initiale de la lithosphère joue également un rôle déterminant dans la géométrie finale du rift. Le profil thermique, et donc rhéologique, de cette dernière est primordial, d'autant plus qu'il s'agit de dispositifs extensifs polyphasés pour lesquels il convient alors de considérer, après chaque processus de rifting, le temps nécessaire au rééquilibrage thermique de la lithosphère (Negredo et al., 1995).

- A l'échelle de la croûte supérieure, deux autres facteurs sont prépondérants sur les mécanismes et la cinématique de l'extension. Il s'agit :

- Du contrôle exercé par les discontinuités pré-existantes (fragiles et/ou ductiles) sur l'initiation et le développement des structures syn-rifts. Aborder cette notion d'héritage structural, déjà largement débattue à différentes échelles (e.g. McConnell, 1972 ; Cordell, 1978 ; Chorowicz & Mukonki, 1980 ; Illies, 1981 ; Dunbar & Sawyer, 1988 ; Daly et al., 1989 ; Versfelt & Rosendahl, 1989 ; Smith & Mosley, 1993 ; Hetzel & Strecker, 1994 ; Theunissen et al., 1996 ; Morley, 1999a), implique de restituer la géométrie et la cinématique des déformations à des stades successifs du rifting jusqu'au dispositif initial.
- De l'influence du magmatisme sur le comportement mécanique de la croûte continentale déformée (Corti et al., 2003). La nature de ces interactions a été récemment discutée à propos de la formation des marges passives volcaniques (Callot et al., 2001, 2002), ce qui aboutit aboutit à la notion de 'points-mous' plus facilement déformables et donc points de nucléation potentiels de la déformation. Concernant les systèmes de rift intra-continentaux, la notion de 'points-mous' n'a été discutée, à notre connaissance, qu'à l'échelle d'édifices volcaniques individuels (De Chabelier & Avouac, 1994 ; Van Wyk de Vries & Merle, 1996; Lahitte et al., 2003) ou de portions de rift très restreintes (Lezzar et al., 2002), mais pas à celle de véritables segments de

rifts de dimensions ~100x200 km, comparables à celles de la zone d'étude du Turkana.

Aux principaux facteurs évoqués ci-dessus s'ajoutent encore, par exemple, le caractère polyphasé des rifts, la durée de l'extension, le taux d'extension ou les variations du champ de contrainte appliqué au domaine étudié.

La quasi-totalité de ces problématiques peut être discutée de façon déterminante à propos du segment de rift du Turkana au nord du Kenya (1-5° de latitude nord et 35-39° de longitude est) (Fig. 1). Cette portion de rift magmatique, d'environ 16 000 km² de superficie et active depuis 45 Ma. (Morley et al ., 1992 ; Wolfenden et al., 2004), appartient à la branche orientale du Rift Est Africain (REA). Ce secteur polyphasé a enregistré l'extension en continu sur 45 Ma. et présente de nombreuses caractéristiques atypiques, à toutes les échelles évoquées ci-dessus, qui en font un des secteurs-clés pour une meilleure compréhension des processus de l'extension continentale.

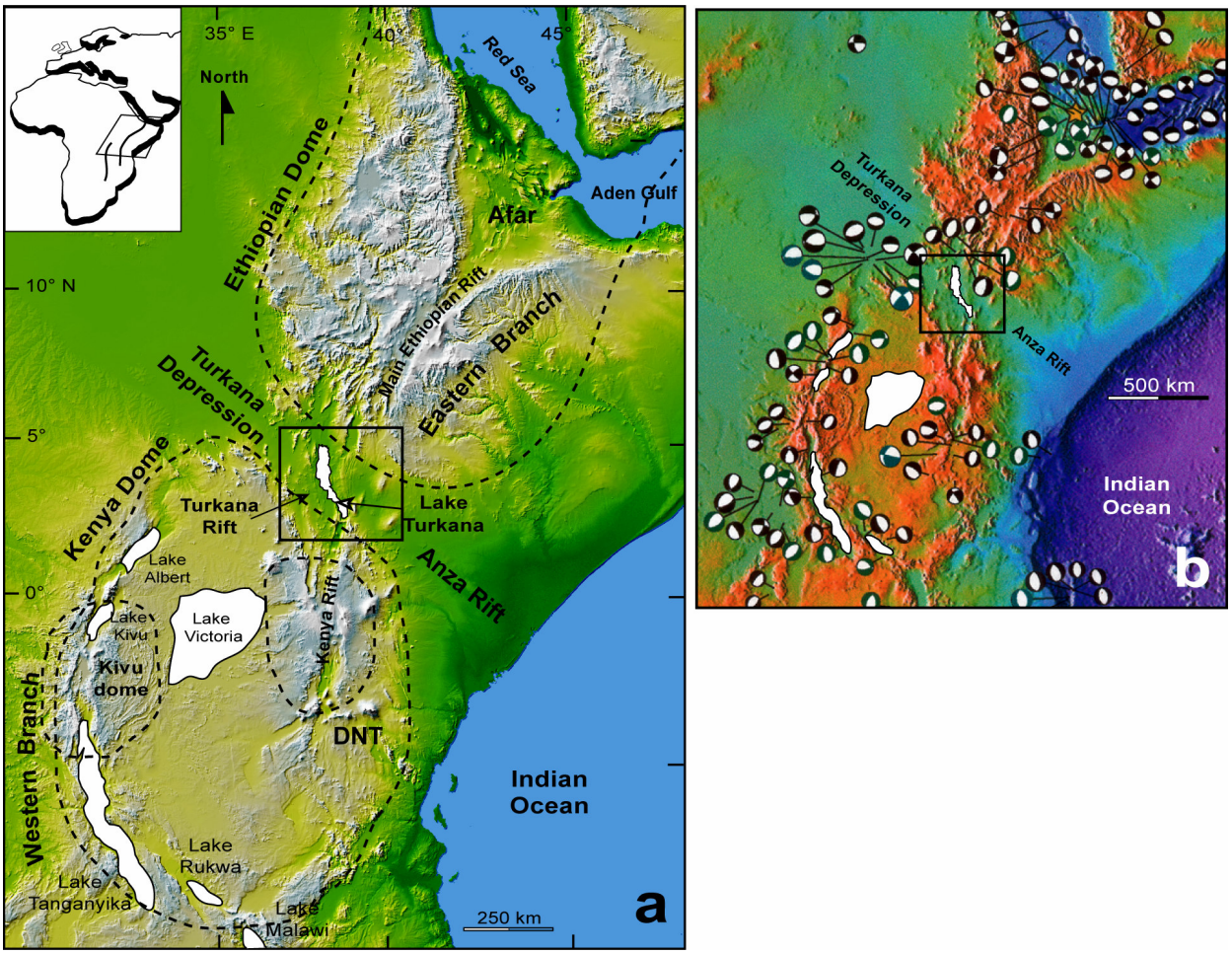

Figure 1. *Topographie générale et sismicité du Rift Est Africain. (a) Modèle numérique de terrain du REA (modifié d'après les données SRTM, http://photojournal.jpl.nasa.gov/catalog/PIA03395). La dépression transverse du Turkana sépare les dômes Ethiopien et Kenyan (pointillés). La trace du rift tertiaire Turkana est faiblement marquée en comparaison de la vallée axiale entaillant les deux dômes. Le carré noir localise notre secteur d'étude, DNT : Divergence Nord Tanzanienne. (b) Carte des mécanismes au foyer des séismes, reportée sur un fond topographique Gtopo 30 (modifié d'après Gloaguen, 2000). On note le caractère peu sismique des rifts du Turkana et du Kenya par rapport aux zones sismiques de l'Afar et de la branche ouest du REA.*

- A l'échelle du REA, le rift Turkana se marque en surface par la disparition longitudinale du fossé axial du rift dont la morphologie de graben étroit (~50 km de large) au niveau du Kenya central passe vers le nord à une zone à morphologie très atténuée où la déformation semble se distribuer sur une largeur d'environ 200 km (Fig. 1). Une telle topographie peu marquée ainsi qu'une sismicité réduite voire inexistante (Tongue et al., 1992) rendent particulièrement difficile l'étude de la tectonique active dans le secteur du rift Turkana (Fig. 1b). Cette rupture de style structural intervient entre les dômes topographiques éthiopien et kenyan qui sont l'expression en surface de deux panaches mantelliques cénozoïques (George et al., 1998 ; George & Rogers, 2002). Compte tenu de la migration de la plaque Afrique d'environ 1000 km vers le NE au cours des derniers 50 Ma. (Bonavia et al., 1995 ; George et al., 1998), le rift Turkana a donc interagi vers 35 Ma. avec l'un des deux panaches mantelliques. Ce dispositif permet donc d'aborder la nature des interactions panache/lithosphère.

- A l'échelle lithosphérique, le rift cénozoïque du Turkana est également un secteur unique où le rift NS tertiaire recoupe, avec un angle fort (~40°), l'axe d'un dispositif rifté antérieur, d'âge crétacé, exprimé en subsurface par les bassins N140°E du Soudan (NW) et d'Anza (SE) le long desquels se localise la dépression du Turkana (Fig. 1). Toutefois, le rift cénozoïque présente la particularité de s'être initié et propagé au niveau d'une étroite portion de lithosphère (~300-400 km de large) épargnée par l'extension mésozoïque. Ces paramètres permettent d'aborder les questions relatives à 1) l'initiation d'un rift à la périphérie d'une lithosphère pré-étirée et 2) le comportement de ce système hétérogène à la verticale d'un panache mantellique. En outre, les données de sismique réfraction (KRISP, 1991) révèlent un amincissement crustal important, de l'ordre de 20 km, au niveau du Turkana (Prodehl et al., 1994) ainsi qu'une forte remontée de la limite asthénosphère/lithosphère proche de la base de la croûte (Morley, 1994 ; Hendrie et al., 1994). De tels profils crustaux/lithosphériques ne peuvent pas uniquement résulter d'une extension 'passive' mais doivent aussi porter l'empreinte de phénomènes actifs liés aux panaches cénozoïques (Morley, 1994).

- A l'échelle de la croûte supérieure, des campagnes de sismique réflexion pétrolière (Amoco, 1986) ont mis en évidence au niveau du Turkana un ensemble de bassins syn-rifts, d'âge oligo-pliocène (~35 Ma.) (Morley et al. 1992), contemporains des bassins de la Mer Rouge au nord et de Kerio-Baringo dans le rift Central Kenya (Hautot et al., 2000 ; Wolfenden et al, 2004). Le rift Turkana comprend également les laves les plus anciennes (~45

Ma.) du REA dont la mise en place pourrait marquer l'impact d'un des panaches mantelliques sous la lithosphère du nord Kenya (Stewart & Rogers, 1996 ; George et al., 1998). L'évolution structurale et stratigraphique des bassins oligo-miocènes ainsi que l'émission de laves à diverses périodes de développement du rift Turkana offrent donc un enregistrement continu de l'évolution tectono-magmatique d'un segment de rift sur une période d'environ 45 Ma.

Les études antérieures consacrées au rift Turkana se sont focalisées sur la structure et le potentiel pétrolier des bassins sédimentaires oligo-pliocènes, en se basant principalement sur les données de sismique réflexion et quelques données de surface (datations K/Ar) (Dunkelman et al., 1989; Morley et al., 1999a). Par conséquent, seule la partie occidentale du rift Turkana était correctement connue pour la tranche de temps 35-3 Ma., tandis que l'organisation du secteur oriental restait largement incomprise. De plus, peu ou pas d'études se sont intéressées aux déformations récentes/actives (5 Ma.-Actuel) malgré de nombreux indices de complications tectoniques atypiques (inversions positives, réseau de failles en lanière,…). Ces travaux ont toutefois brossé les grands traits du développement du rift Turkana en évoquant, notamment, à une large échelle spatio-temporelle, une migration latérale vers l'est à la fois du magmatisme et de la déformation au cours de 35 derniers Ma. Néanmoins, les mécanismes de nucléation/propagation de la déformation n'ont jamais été intégrés dans un modèle global prenant en compte l'histoire complexe enregistrée par ce secteur pendant 45 Ma.

L'objectif de ce mémoire, présenté sous la forme de quatre publications, est de préciser, depuis l'Eocène, les mécanismes du rifting responsables de la structure actuelle du segment du Turkana, avec toutefois un intérêt majeur pour les déformations récentes (<5 Ma.). A notre connaissance, c'est la première fois qu'une telle approche, intégrant 45 Ma. d'évolution syn-rift ainsi que l'héritage structural antérieur, est tentée à l'échelle d'un segment de rift du REA. Ce travail repose principalement sur l'interprétation de nouvelles données de surface (imagerie satellitale Landsat ETM+, topographie SRTM et terrain), complétée par l'ensemble des données disponibles sur ce secteur (sismique réflexion pour l'essentiel).

Plan du mémoire

Après un premier chapitre consacré à une description brève des données et des méthodes utilisées dans ce travail, certaines des problématiques citées en introduction sont abordées par le biais de quatre publications. Cette présentation entraîne inévitablement des répétitions (contexte géologique, méthodologie) que nous avons tentées de minorer en ne rédigeant notamment qu'une seule liste de référence à la fin du mémoire. De plus, dans la mesure où les quatre publications n'ont pas été rédigées dans un ordre chronologique, et que le chapitre 2,

rédigé en dernier nécessite une vue d'ensemble du système, certaines structures ou processus peuvent sembler manquer dans les papiers les plus anciens (chapitre 5 en particulier).
Afin de faciliter la lecture du manuscrit, qui comporte une toponymie relativement abondante et complexe, une carte générale du rift Turkana est disponible sous la forme d'un dépliant à la fin du mémoire.

Chapitre 2 : Dynamic of continental extension in magmatic rifts. The study case of the Turkana Rift since the last 45 Ma. (Northern Kenya).
(Vétel, W. & Le Gall, B.; submitted to Journal of the Geological Society, London).

Il s'agit dans ce papier de discuter les mécanismes tectono-magmatiques de mise en place du rift Turkana depuis l'Eocène (~45 Ma.) par le biais de cinq cartes 'restaurées' spécifiques aux intervalles 45-23 Ma., 23-15 Ma., 15-6 Ma., 6-2.6 Ma. et 2.6 Ma.-Actuel. Nous cherchons dans ce chapitre à préciser plus particulièrement le mode de développement du segment de rift du Turkana en relation avec 1) l'héritage structural (zones transverses faillées intra-socle, système rifté oblique antérieur) et 2) la présence de domaines magmatiques.
Ce chapitre apporte au lecteur une vision complète du système du Turkana et lui permet ensuite d'aborder plus aisément les articles suivants qui traitent principalement des déformations récentes (<5 Ma.) en relation avec des structures pré-existantes décrites dans cette première partie.

Chapitre 3 : Inversion tectonics during continental rifting : the Turkana Cenozoic rifted zone, Northern Kenya.
(Le Gall, B., Vétel, W. & Morley, C. K.; in press to Tectonics).

Dans ce chapitre, nous cherchons à comprendre l'origine et le développement d'inversions tectoniques positives récentes (<3.7 Ma.), mises en évidence dans certains bassins du rift Turkana, et mises en relation avec la cinématique d'une zone de fracture transverse pré-existante et les variations du champ de contraintes au cours des cinq derniers Ma.

Chapitre 4 : Geometrical properties and growth of an inner rift fault pattern : the Kino Sogo Fault Belt, Turkana Rift (North Kenya)
(Vétel, W., Le Gall, B. & Walsh, J. J.; submitted to Journal of Structural Geology).

Le réseau de failles en lanière du Kino Sogo correspond à une alternance de horsts et grabens affectant des laves oligo-pliocènes (~200 m d'épaisseur) déposées au toit du socle protérozoïque. Cette fracturation récente (<3 Ma.) est exceptionnellement bien exposée sur le flanc est du lac Turkana, dans un secteur qui, resté en position haute tout au long du rifting, est exempt de couverture sédimentaire. Cette configuration est favorable à l'extraction du

réseau de fracture à partir d'images satellites et topographiques, puis à son analyse géométrique et statistique. Les résultats quantitatifs obtenus procurent de nouvelles contraintes sur 1) le mode de croissance des failles et 2) le taux de déformation cumulé à travers les 40 km du réseau de failles. Ces résultats, spécifiques à une seule partie du rift Turkana, sont comparés à ceux décrits dans la littérature à propos des populations de failles également initiées en contexte extensif.

Chapitre 5 : Recent tectonics in the Turkana rift (North Kenya) : an approach from drainage network, satellite imagery and reflection seismic analyses.
(Vétel, W., Le Gall, B. & Johnson, T. C.; published in Basin Research).

Ce travail s'inscrit directement dans la thématique dédiée aux déformations récentes (<5 Ma.). Sur la base de l'étude du réseau hydrographique, extrêmement bien développé dans le secteur SW du Turkana, nous cherchons à interpréter d'un point de vue structural, l'origine de certaines anomalies de drainage en relation avec de faibles mouvements récents/actifs qui sont difficilement identifiables à partir des données de topographie.

Chapitre 6 : Synthèse générale et conclusions

Ce chapitre synthétise les principaux résultats de ce travail.

Enfin, un ultime chapitre (7) propose des perspectives de recherche sur deux thématiques consacrées : 1) à des modélisations analogiques des processus de contrôle de la déformation par des structures transverses pré-existantes et 2) au couplage soulèvement/érosion le long d'escarpements de failles majeures.

1. DONNEES ET METHODES

Les résultats discutés dans ce travail de thèse se basent principalement sur l'analyse et l'interprétation de quatre images satellites Landsat Enhanced Thematic Mapper Plus (ETM+) et de modèles numériques de terrain (essentiellement SRTM : Shuttle Radar Topography Mission). L'imagerie satellitale a déjà été utilisée par des travaux antérieurs consacrés à la l'étude de certains secteurs du REA (Thoué, 1993 ; Coussement, 1995 ; Le Turdu, 1998 ; Cardon, 1999 ; Gloaguen, 2000), toutefois ces derniers se focalisaient sur les déformations récentes affectant la vallée axiale et l'âge des séries déformées n'était donc pas différencié. Notre approche s'intéresse à l'évolution polyphasée du rift du Turkana, initiée il y a 45 Ma., marquée par une succession de phases de magmatisme et de fracturation, il a donc été essentiel de discriminer les différents ensembles en présence (socle métamorphique, laves oligocènes-quaternaires, sédiments récents) afin de contraindre l'âge des déformations observées. De ce fait, l'imagerie satellitale a été utilisée d'une part pour extraire les populations de failles et d'autre part pour établir une cartographie régionale des affleurements. Les résultats obtenus ont également été compilés avec l'ensemble des documents disponibles sur la zone d'étude, principalement représenté par le jeu de profils de sismique réflexion pétrolière (Amoco et Probe) qui permet de corréler les structures de surface avec les structures profondes des bassins (profondeur maximale de ~7-8 km).

Ce chapitre développe des compléments aux différents paragraphes de méthodologie disponibles dans les quatre publications qui constituent ce travail. Seule la méthodologie concernant l'étude du réseau de drainage n'est pas rappelée car largement argumentée dans le chapitre 5. Nous décrivons dans un premier temps les principales caractéristiques des images utilisées (Landsat ETM+, MNT), puis nous présentons les traitements effectués afin d'améliorer la dynamique des images et obtenir une meilleure résolution des structures.

Les conditions d'affleurement exceptionnelles de la fracturation affectant des laves récentes (<3 Ma.) dans le secteur du Kino Sogo, sur le flanc est du lac Turkana, ont permis d'extraire la population de faille et de procéder à une étude géométrique et statistique. Cette étude permet une approche quantitative de la déformation selon les principes qui sont brièvement évoqués ci-dessous. L'ensemble des données complémentaires également intégré dans cette étude (terrain, sismique réflexion, …) est présenté en fin de chapitre.

1.1. L'IMAGERIE SATELLITALE

Notre étude structurale utilise l'imagerie satellitale dans un but précis, à savoir, identifier les différents ensembles lithologiques en présence et cartographier en détail la fracturation syn-rift. Pour ce faire, nous disposions de quatre images optiques à haute résolution de type

Landsat Enhanced Thematic Mapper Plus (ETM+) en format numérique, imageant l'ensemble de la zone d'étude (169/057, 27/10/2000 ; 169-058, 21/10/1999 ; 170-057, 12/07/2000 ; 170-058 ; 18/01/2000) (Fig. 1). Chaque image couvre une surface d'environ 170x185 km correspondant à une échelle courante de l'ordre du 1/50 000. Une image contient 9 bandes spectrales de longueurs d'ondes distinctes, avec une résolution au sol (taille du pixel) variable selon les canaux (Tableau 1). Les pré-traitements classiques (étalement de la dynamique de 0 à 255 niveaux de gris, compositions colorées en Rouge Vert Bleu des bandes 3, 2 et 1, …) ne suffisant pas à rehausser correctement la dynamique des images, nous avons appliqué des traitements annexes sur des extraits d'images couvrant des secteurs d'intérêt majeur comme décrit ci-dessous.

Bandes spectrales	Domaine spectral	Résolution spatiale (mètres)
1. [0.45 - 0.51 µm]	Bleu	30x30
2. [0.52 - 0.60 µm]	Vert	30x30
3. [0.63 - 0.69 µm]	Rouge	30x30
4. [0.75 - 0.90 µm]	Proche infrarouge	30x30
5. [1.55 - 1.75 µm]	Infrarouge moyen	30x30
6. [10.40 - 12.50 µm]	Infrarouge thermique	60x60
7. [2.09 - 2.35 µm]	Infrarouge lointain	30x30
P. [0.52 - 0.90 µm]	Panchromatique	15x15

Tableau 1. *Caractéristiques des bandes spectrales composant les images Landsat ETM+.*

1.1.1. Traitement des images satellites

Dans un premier temps, l'orthorectification des images a été réalisée grâce au logiciel Geomatica 9.2 en calant les 4 coins de l'image fournis dans l'encodage GeoTiff, afin de corriger leur géoréférencement initial (inexact) et leur étirement en latitude. Chaque scène a été projetée selon le géoréférencement World Geodetic System 1984 (WGS 84).
Par la suite, nous leur avons appliqué divers traitements, sous les logiciels Geomatica 9.2 et Envi 4.1, qui ont considérablement améliorés la vision des structures et donc permis l'extraction exhaustive du réseau de fractures. La topographie actuelle du rift Turkana est constituée pour l'essentiel par des affleurements de socle métamorphique, de laves (réflectance faible) et de sédiments récents (réflectance forte).

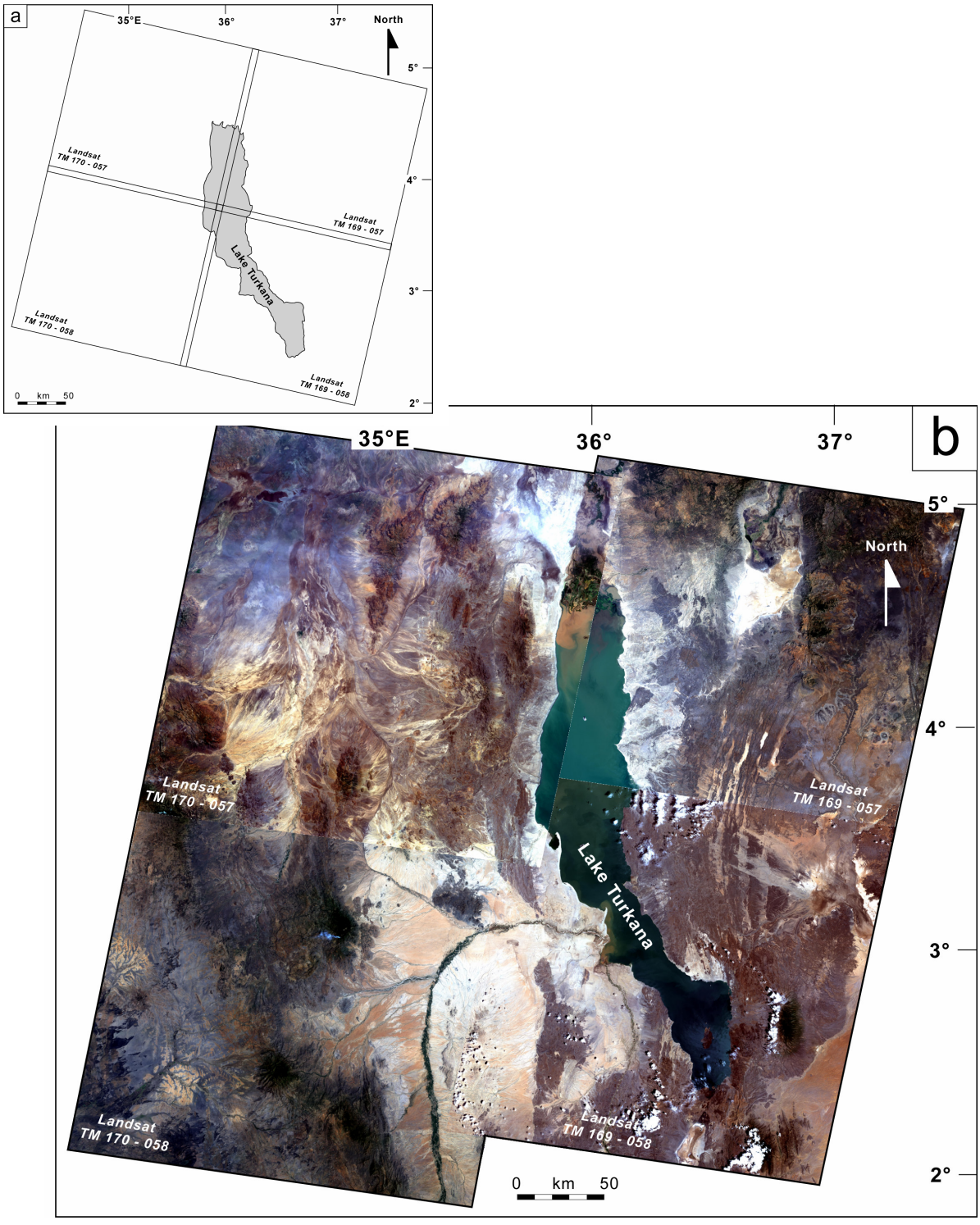

Figure 1. *Couverture de l'imagerie satellitale Landsat ETM+. (a) Plan de position et référence des images. (b) Mosaïque des quatre images utilisées pour cette étude. Composition colorée en couleurs 'naturelles', bandes 321 (Rouge Vert Bleu).*

Ces derniers présentent de faibles contrastes qui n'autorisent pas une cartographie fine, limitée par la résolution de l'image (30x30 m). Les divers traitements appliqués aux images sont illustrés sur les figures 2 et suivantes à partir d'un exemple unique, extrait de l'image 170-058, qui représente un pli d'échelle plurikilométrique impliquant des orthogneiss bordés par des sédiments récents, au SW de la zone d'étude.

1.1.1.1. Fusion

Les différentes bandes qui constituent l'image Landsat présentent chacune des paramètres qui leur sont propres (résolution spatiale, longueur d'onde, …) (Tableau 1) et qu'il est intéressant de combiner afin de faire apparaître le maximum d'informations sur l'image traitée. Un traitement par fusion de la bande panchromatique n° 8, celle qui offre la meilleure résolution spatiale (15x15 m), avec les bandes 7 (infrarouge lointain), 4 (proche infrarouge) et 2 (vert), permet d'obtenir un maximum de résolution au sol avec une réponse colorée très contrastée faisant apparaître plus clairement les structures (Fig. 2). Ce mode de traitement s'est révélé être le plus efficace dans la recherche d'une meilleure vision des linéaments et des réseaux de fractures. Néanmoins, des traitements complémentaires ont également été appliqués (filtres, analyse en composantes principales et classification) afin de mieux contraindre l'analyse structurale des images.

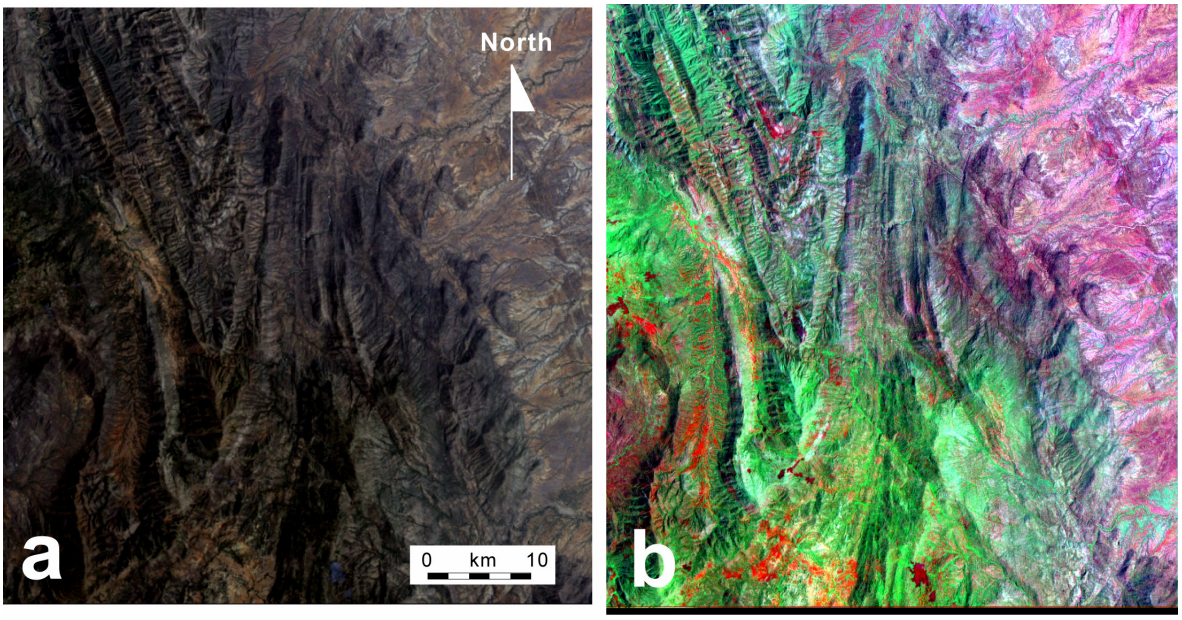

Figure 2. *Extrait de l'image Landsat 170-058 sur le socle de Turkwell. On note la présence d'un pli d'échelle plurikilométrique avec un plan axial NS, parallèle à la foliation, et recoupé par des réseaux de fractures N140°E et N50°E. (a) Composition colorée classique RVB (bandes 321) non traitée. (b) Traitement d'image par fusion des bandes panchromatiques 8 et des bandes 7, 4 et 2.*

1.1.1.2. Filtres

Afin d'optimiser l'extraction des réseaux de fractures, l'application de filtres directionnels (Marr & Hildreth, 1980) permet d'accentuer l'expression de réseaux de fractures selon une direction imposée (de 0 à 180°) (Fig. 3). La méthode la plus classiquement utilisée est le filtrage directionnel par convolution. Un filtre est représenté sous la forme d'une matrice de n x n pixels (n impair ; 5x5 dans le cas présent) qui se déplace pixel par pixel sur l'image entière (Fig. 3). Une opération de convolution entre les éléments de la matrice et chaque point-unité est alors réalisée, ce qui rehausse le tracé des structures existantes selon la direction choisie. Ceci permet par exemple de confirmer l'existence d'un réseau de fractures associé à un couloir déformé discontinu.

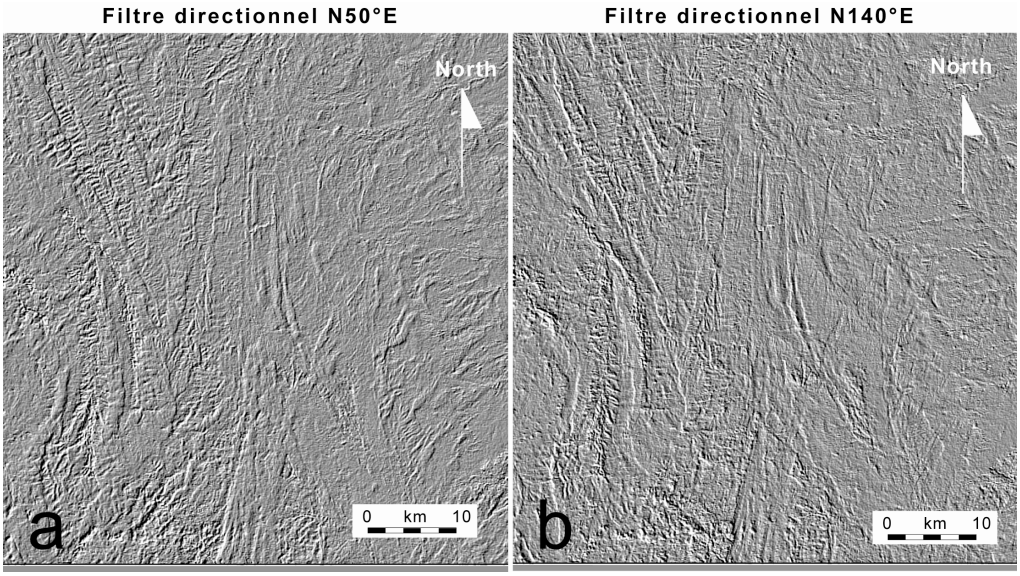

-1.4088	-1.4088	-0.7660	-0.1233	-0.1233
-1.4088	-1.4088	-0.7660	-0.1233	-0.1233
-0.6428	-0.6428	0.0000	0.6428	0.6428
0.1233	0.1233	0.7660	1.4088	1.4088
0.1233	0.1233	0.7660	1.4088	1.4088

c

0.1233	0.1233	-0.6428	-1.4088	-1.4088
0.1233	0.1233	-0.6428	-1.4088	-1.4088
0.7660	0.7660	0.0000	-0.7660	-0.7660
1.4088	1.4088	0.6428	-0.1233	-0.1233
1.4088	1.4088	0.6428	-0.1233	-0.1233

d

Figure 3. *Traitement d'un extrait de l'image Landsat ETM+ 170-058 (cf. figure 2) par application de filtres directionnels. (a) Résultat d'un filtre directionnel orienté N50°E (5x5). (b) Résultat d'un filtre directionnel N140°E (5x5). (c) Matrice 5x5 de filtre directionnel N50°E. (d) Matrice 5x5 de filtre directionnel N140°E.*

1.1.1.3. Analyse en Composantes Principales

L'analyse en composantes principales (ACP) est une méthode statistique qui permet de représenter des données fortement corrélées selon un système d'axes minimisant cette corrélation. Le taux de données initiales (bruit) est ainsi réduit relativement aux

représentations significatives qui sont conservées (Girard et Girard, 1999 ; Mouchot, 2000). L'application d'une ACP sur les six canaux d'une image Landsat TM (visible et proche, moyen et infrarouge thermique) conduit à projeter l'ensemble des pixels sur les axes décorrélés suivants : premier axe (somme des canaux sauf le 4) ; second axe (canal 4) ; troisième axe (bandes 1, 2 et 3 opposées aux bandes 5 et 7) ; quatrième axe (oppose l'axe 1 au 2 et 3) ; cinquième axe (bandes 5 et 7) et sixième axe (oppose les axes 2 et 3) (Girard et Girard, 1999). La visualisation de ces résultats aboutit à une vision différente et complémentaire des résultats de fusion afin de confirmer ou compléter les interprétations (Fig. 4).

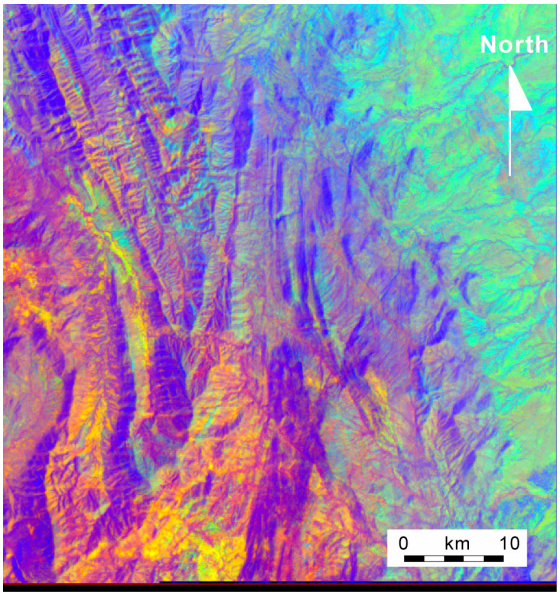

Figure 4. *Traitement de l'extrait de l'image ETM+ 170-058 selon une analyse en composantes principales. Représentation selon les axes 531.*

1.1.1.4. Classifications

Une opération de classification tend à regrouper des pixels ayant des caractéristiques radiométriques proches (Fig. 5). Lorsque l'on effectue une composition colorée de trois bandes, les pixels correspondants se distribuent dans un diagramme orthonormé à 3 axes (chaque axe allant de 0 à 255 niveaux de gris) et ils se concentrent par zones de réflectance comparable sur l'image. Ces regroupements peuvent être isolés les uns des autres par une opération de classification qui définit chaque classe de pixel par (1) un centre de classe, (2) une moyenne d'écart des points par rapport au centre, (3) une variance, … Les classifications peuvent être (1) non supervisées, on indique alors au logiciel le nombre de classes désirées et on ne fait aucune supposition quant aux valeurs des pixels à regrouper, ou (2) supervisées, et dans ce cas où le nombre de classes est connu, on possède un échantillon de chaque classe (Mouchot, 2000). Une classe correspond à une signature spectrale particulière liée à la nature

des objets exposés en surface (eau, basalte ou végétation). On peut ainsi isoler plus aisément les différents ensembles lithologiques et, dans le cas présent, un type de lave d'un autre à la condition qu'ils ne présentent pas les mêmes réflectances. Par exemple, des intrusions de type rhyolitique mises en place dans un ensemble basaltique peuvent être plus facilement discriminées et cartographiées.

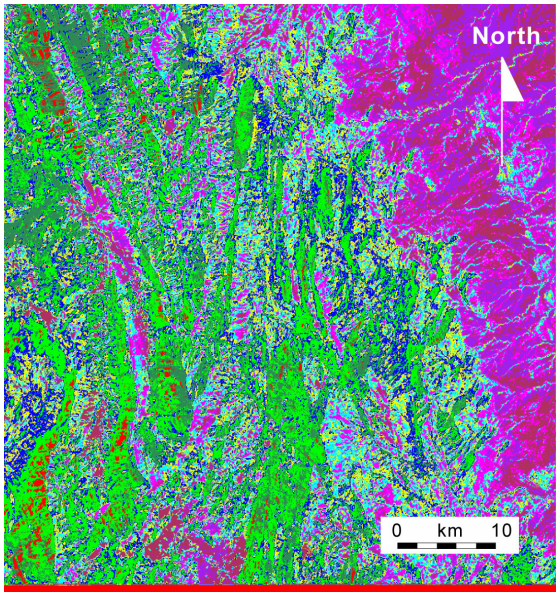

Figure 5. *Résultat d'une classification non supervisée (10 classes maximum) sur un extrait de l'image Landsat ETM+ 170-058. Chaque couleur correspond à une classe de pixels aux caractéristiques radiométriques proches sur l'image d'origine.*

1.2. LES DONNEES TOPOGRAPHIQUES

Afin de préciser l'organisation néotectonique du rift Turkana, il était indispensable d'en définir le cadre morphostructural, en complément des interprétations d'images satellites.
Au démarrage de ce travail de thèse (année 2001), seules les données de type GTopo 30 étaient disponibles sur la zone d'étude (ftp://edcftp.cr.usgs.gov/pub/data/gtopo30/global/). La faible résolution latérale (30'' d'arc soit environ 1 km) et verticale (~100 m) de ce modèle numérique de terrain (MNT) n'offrait qu'une vision 3D émoussée des reliefs et n'autorisait donc pas une étude morphologique précise du rift Turkana.
Au cours de l'année 2002, afin de palier au manque de données topographiques, nous avons fait compiler par l'USGS (http://edcimswww.cr.usgs.gov/pub/imswelcome/) 8 MNT à partir de couples stéréo d'images Aster (Aster L1A Reconstructed Unprocessed Instrument Data V002 et 003) couvrant des structures-clés du secteur d'étude (Fig. 6b). Chaque MNT couvre une surface de 60 x 60 km avec une excellente résolution verticale de 7 m, mais leur

exploitation est difficile compte tenu du manque de continuité de la couverture ainsi que des nombreux 'blancs' liés à la présence de nuages sur les images d'origine.

Au mois de mai 2004, la NASA a mis à la disposition du public sur le site internet (www2.jpl.nasa.gov/srtm) l'ensemble des données de type SRTM 90 (Shuttle Radar Topography Mission, 90 m). Ces données numériques sont disponibles à l'échelle de l'Afrique sous la forme de zones de 1°x1° que nous avons mosaïquées avec les logiciels ENVI 4.1 et 3DEM (http://www.visualizationsoftware.com/3dem/downloads.html) (Fig. 6a).

Avec une résolution de 90 m au sol et 16 m en vertical, chaque scène procure, pour la première fois, une vision 3D fine et complète de la surface du REA, y compris dans le secteur du Turkana caractérisé par une morphologie peu contrastée. Les données SRTM ont donc permis de révéler la géométrie des escarpements et blocs soulevés associés aux failles précédemment identifiées sur les images satellites, jetant ainsi les bases d'une approche qualitative et quantitative de la déformation. Dans certains cas favorables (structures récentes, présence de marqueurs planaires, …), la dimension des escarpements extraits de profils topographiques fournit une estimation minimale du rejet intervenu le long de plan de failles, autorisant ainsi le calcul des taux d'extension cumulés à travers certaines zones faillées (ex. Kino Sogo, chapitre 4). Toutefois, la disponibilité tardive de ces données (6 mois avant le terme de ce travail) ne nous a pas permis de réaliser une étude géomorphologique complète du rift Turkana. Cette thématique est ébauchée à la fin du mémoire en termes de perspectives de recherche.

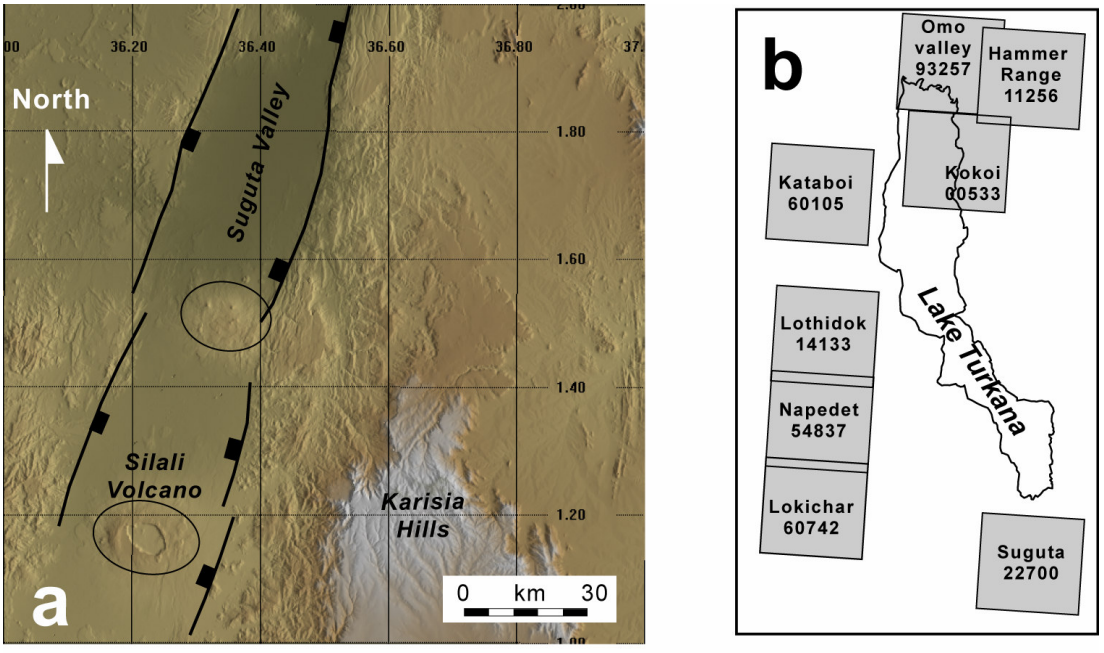

Figure 6. *(a) Exemple de MNT SRTM couvrant une partie de la vallée axiale de la Suguta au sud du lac Turkana. (b) Plan de position des MNT Aster.*

1.2.1. Drapage des données Landsat sur la topographie

Une vision plus 'réaliste' de certains secteurs est apportée par le drapage des données satellites sur le fond topographique (MNT SRTM) (Fig. 7). Ce procédé implique que les deux types de données aient été géoréférencées selon la même projection (WGS 84), puis superposés par le biais du logiciel Geomatica 9.2 ou 3DEM. Les blocs diagrammes 3D ainsi obtenus peuvent permettre de mieux comprendre la géométrie exacte des structures selon différents angles de vue (0 à 360°).

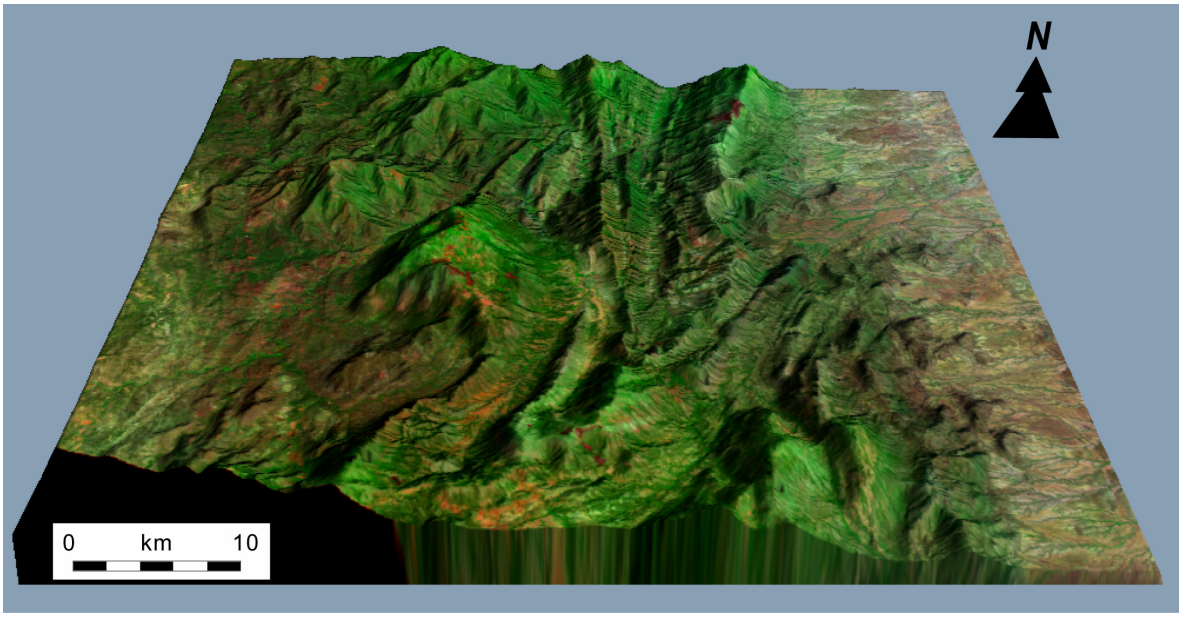

Figure 7. *Résultat de la superposition d' un extrait de l'image Landsat ETM+ 170-058 sur le MNT SRTM (Vue vers le nord,éclairage vers l'ouest, exag. vert. x2).*

1.3. METHODE D'ANALYSE GEOMETRIQUE ET STATISTIQUE DE LA FRACTURATION

Une analyse géométrique et statistique de la fracturation a été menée sur un réseau de failles en lanières exposé de façon exceptionnelle dans le secteur volcanique du Kino Sogo, sur le flanc est du lac Turkana. La population de failles extraite de l'imagerie satellitale et des données de topographie (Fig. 8) a été traitée selon une méthodologie, déjà validée par de nombreuses études antérieures, et donc brièvement expliquée ci-dessous (Villemin & Sunwoo, 1987 ; Velde et al., 1990, Velde et Dubois, 1991 ; Davy, 1993 ; Thoué, 1993 ; Castaing et al., 1995 ; Cowie et al., 1995 ; Fossen & Rornes, 1996 ; Marret, 1996 ; Needham et al., 1996 ; Nicol et al., 1996 ; Yielding et al., 1996 ; Cardon, 1999 ; Gloaguen, 2000).

1.3.1. Numérisation des données

La carte de fracturation obtenue à partir de l'interprétation des images satellites constitue le document de base pour la numérisation, puis l'analyse géométrique et statistique des structures (Fig. 8). Cette étude souffre des limites imposées par la résolution spatiale des images et par conséquent, les objets (failles) ayant une dimension inférieure à celle d'un pixel (15x15 m, bande panchromatique n°8) ne sont pas décelables et comptabilisés dans l'étude statistique. De plus, les images sont prises avec un éclairage (soleil) provenant de l'est de telle sorte que les plans de failles à regard ouest, soulignés par des ombres portées, sont plus aisément identifiables que les failles à regard est, directement éclairées.
Le tracé d'une faille peut être continu ou discontinu. Dans ce dernier cas, il consiste alors en un ensemble de segments distincts dont il est essentiel de préciser la définition afin de distinguer la population de failles de celles des segments qui les constituent. Chaque segment de faille est défini dans ce travail, d'un point de vue purement géométrique, par un changement de direction des structures ou la présence de zone de relais entre deux segments contigus. Nous ne prenons pas en compte les changements de pendage ou de rejet pouvant intervenir le long de certaines structures. Nous avons donc numérisé la population de failles dans un premier temps puis celle des segments de failles dans un second temps. Chacune des deux populations a ensuite été traitée selon les mêmes procédés d'étude géométrique et statistique.

Les données ont été numérisées sur une table à digitaliser Océ Graphics à l'aide du logiciel DigitXY qui permet de numériser des segments de droite compris dans un cadre défini par un point d'origine et deux axes représentant la latitude et la longitude selon une échelle que nous avons précisée (1 cm = 0.28 km). Le curseur permet ensuite de pointer manuellement les extrémités de chaque objet. Les données de la numérisation sont obtenues sous la forme d'un fichier contenant quatre colonnes X1, Y1, X2 et Y2 qui définissent, en kilomètres, les coordonnées des extrémités du segment de droite considéré. L'interprétation structurale du réseau de failles est ainsi décomposée en un ensemble d'éléments simples (vectoriels) qui autorise ensuite une analyse géométrique en termes de longueur, direction, etc….

La principale limitation de la digitalisation est directement conditionnée par le logiciel DigitXY qui ne permet ni de numériser en continu les segments conjoints, ni de les regrouper comme appartenant à la même faille ($\Sigma L^{segments} = L^{segment\ 1} + L^{segment\ 2} + \ldots$) (Fig. 9). On perd donc la relation entre la faille et ses segments associés. Ceci implique de définir la longueur d'une faille comme la distance minimale entre ses deux extrémités (Gloaguen, 2000) (Fig. 9b), ce qui peut induire une erreur non négligeable dans le cas de tracé sinueux où l'on a alors ($L^{faille} < \Sigma L^{segments}$). Le rapport entre la longueur totale de la population de failles et celle des segments nous renseigne néanmoins sur la 'tortuosité' du système étudié.

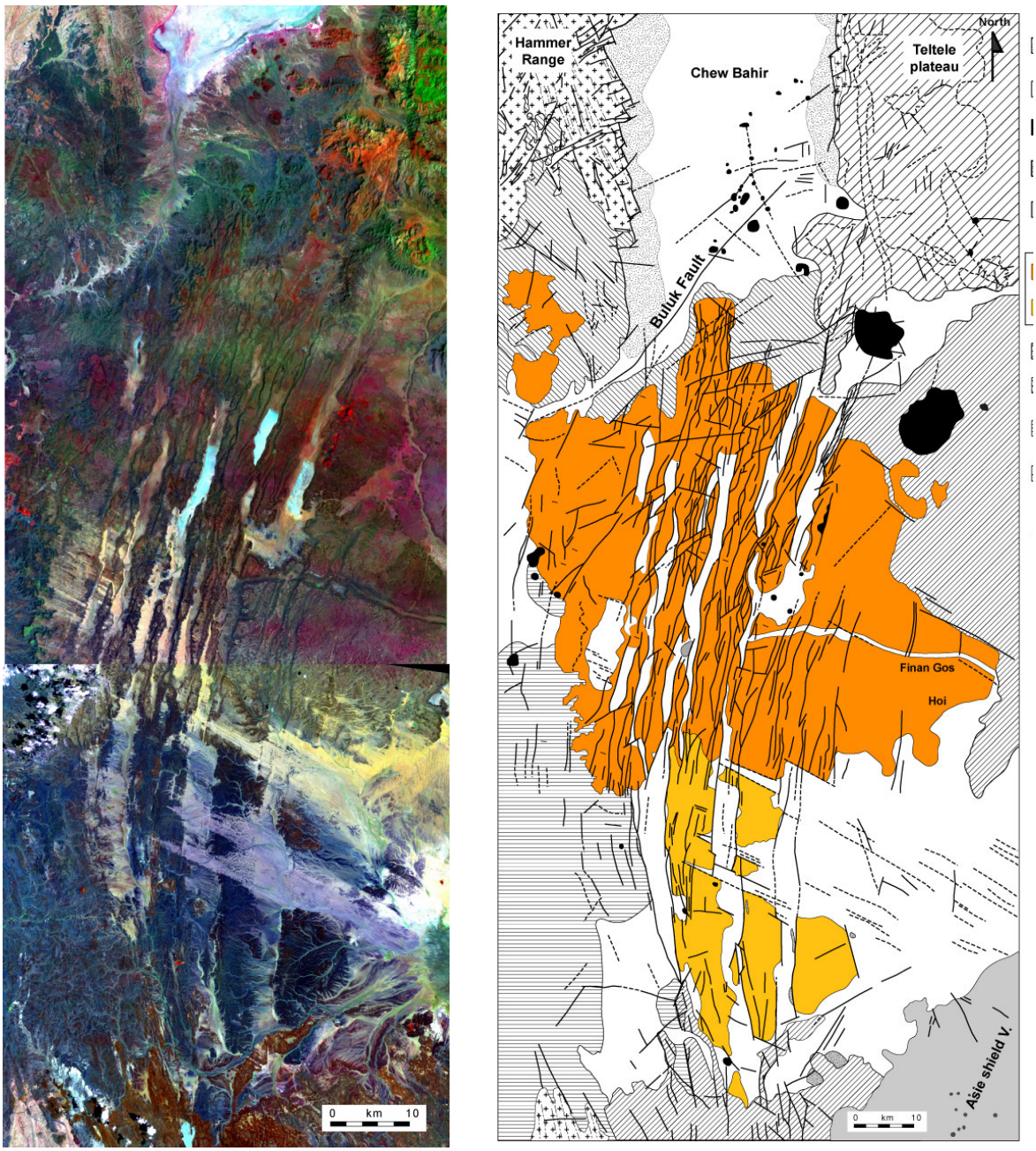

Figure 8. *Réseau de failles en lanières du Kino Sogo, flanc est du lac Turkana (voir dépliant en fin de manuscript). (a) Détails des images Landsat ETM+ 169-058 et 169-057 traités selon le mode de fusion. (b) Carte de fracturation interprétée d'après la figure a.*

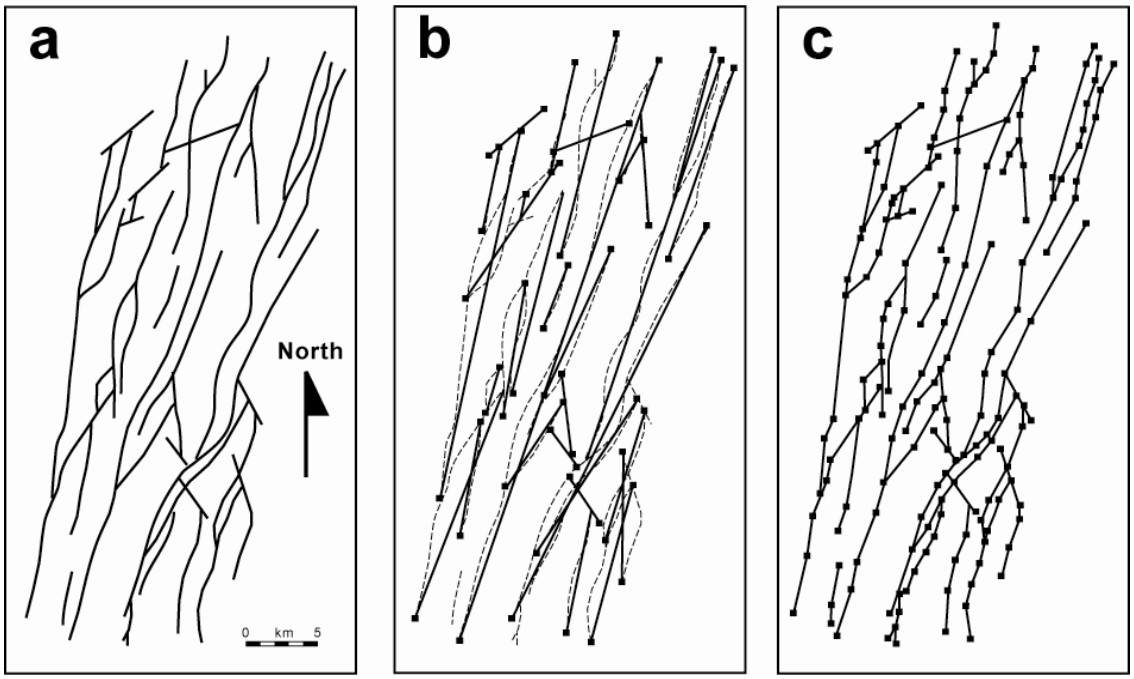

Figure 9. *Exemple de numérisation de failles et segments de failles sur une portion du Kino Sogo. (a) Résultat de l'interprétation de l'image satellite. (b) Numérisation des failles, les carrés noirs figurent les extrémités numérisées. (c) Numérisation des segments de failles.*

A l'inverse, la numérisation des segments de failles (Fig. 9c) reste fidèle à l'interprétation de départ et reproduit l'allure courbe des failles en les réduisant à une succession d'éléments rectilignes de taille variable (Cardon, 1999).

1.3.2. Traitement des données

Différents cas de figures se présentent pour définir les coordonnées d'un segment (X1, Y1, X2 et Y2) en fonction de sa direction et selon que l'on numérise d'abord le point supérieur ou inférieur (Tableau 2). Des calculs géométriques ont donc été effectués à partir des données brutes à l'aide du tableur Excel afin d'obtenir la longueur des segments ainsi que leur direction par rapport au nord (entre 0 et 180°E).

1.3.2.1. Longueur et orientation des failles et segments de failles

Après avoir calculé les deux paramètres 'longueurs et azimut', nous les avons représenté par le biais du logiciel Rockware dans différents diagrammes binaires concernant par exemple, la fréquence des failles ou des segments de failles selon l'azimut, rose de densité, longueur des failles en fonction de leur azimut, fréquence des failles selon leur longueur, etc… L'ensemble de ces diagrammes aboutit dans un premier temps à discuter la géométrie du système.

North	Géométrie du segment de droite	Rapport des coordonnées du segment	Longueur du segment et du côté a	Azimut du segment
CAS N°1 θ >90°	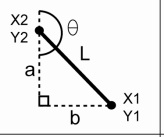	X1 > X2 Y1 < Y2	$L = \sqrt{(X1-X2)^2 + (Y1-Y2)^2}$ $a = \sqrt{L^2 - (X1-X2)^2}$	θ = 180 - (Acos a/L)
CAS N°2 θ >90°	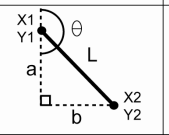	X1 < X2 Y1 > Y2	$L = \sqrt{(X1-X2)^2 + (Y1-Y2)^2}$ $a = \sqrt{L^2 - (X1-X2)^2}$	θ = 180 - (Acos a/L)
CAS N°3 θ <90°	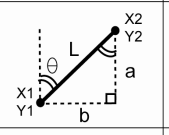	X1 < X2 Y1 < Y2	$L = \sqrt{(X1-X2)^2 + (Y1-Y2)^2}$ $a = \sqrt{L^2 - (X1-X2)^2}$	θ = (Acos a/L)
CAS N°4 θ <90°	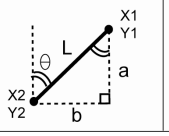	X1 > X2 Y1 > Y2	$L = \sqrt{(X1-X2)^2 + (Y1-Y2)^2}$ $a = \sqrt{L^2 - (X1-X2)^2}$	θ = (Acos a/L)

Tableau 2. *Différents cas de figures de numérisation d'un segment de droite et calculs appliqués sous Excel aux données brutes pour obtenir la longueur et la direction des objets numérisés.*

1.3.2.2. Ajustement du paramètre longueur à des lois mathématiques

Afin de définir le mode de croissance des réseaux de fractures d'après leur longueur, les données sont corrélées à des lois mathématiques de type loi exponentielle *(1)* ou de puissance *(2)*. Ces lois caractérisent, de façon plus au moins fidèle et à un instant donné du processus de croissance, le comportement et l'évolution d'un réseau de faille à un stade précoce, intermédiaire ou final de la déformation. Compte tenu des dimensions de la zone de failles étudiée, (150 x 40 km) et de la résolution des méthodes utilisées, nous avons choisi de représenter les fréquences cumulées des longueurs de failles et segments de failles par pas de 1 km et de 500 m, respectivement, dans les diagrammes Excel.

Loi exponentielle $\boldsymbol{N(L) = \alpha . e^{-\lambda L}}$ *(1)*

N est le nombre de failles ou segments de failles mesurés dont la longueur est supérieure ou égale à une longueur L donnée ; α est le nombre total de mesures ; λ est un paramètre d'échelle. Les données sont représentées dans des diagrammes log/linéaire afin d'établir leur éventuelle corrélation avec cette loi.

Loi de puissance $\boldsymbol{N(L) = \beta . L^{-\nu}}$ *(2)*

N est le nombre de failles ou segments de failles mesurés dont la longueur est supérieure ou égale à une longueur donnée**,** β est lié au nombre de mesures ; ν est l'exposant de la loi et indique la dimension fractale du système (Yielding et al., 1996). Les données sont représentées dans des diagrammes log/log afin d'établir leur éventuelles corrélation avec cette loi.

1.3.2.3. Espacement des failles

Les espacements entre les failles ont été mesurés le long de coupes sériées perpendiculaires à la direction générale des structures. Les résultats sont représentés en fréquences cumulées sur des diagrammes log-log ou log-linéaire afin de les corréler aux lois mathématiques évoquées ci-dessus. Ce paramètre nous renseigne plus particulièrement sur la densité, et donc la saturation, du réseau de fractures considéré.

1.3.2.4. Rejet des failles

Les données topographiques SRTM ont une résolution verticale de l'ordre de 16 m si bien que seuls les rejets apparents de failles supérieurs à cette limite sont directement mesurables sur les coupes (Fig. 10). Des relations trigonométriques simples *(3)* associant le rejet vertical à la quantité d'extension de chaque faille autorisent le calcul de l'extension cumulée le long de transects régulièrement espacés et perpendiculaires au réseau de failles étudié. Le pendage des failles ne pouvant être directement mesuré, il est estimé entre 60° et 70° d'après l'allure des escarpements. Dans notre cas d'étude (Fig. 10), l'organisation cartographique des laves du Kino Sogo démontre que le déplacement le long du système de failles n'excède pas l'épaisseur des laves supérieures (~100 m). L'érosion du bloc soulevé, qui tendrait à minimiser l'importance des mouvements verticaux, est considérée comme négligeable, faute de contraintes spécifiques.

Extension $\boldsymbol{E = Ra / \tan \Phi}$ *(3)*

E est l'extension ; Ra est le rejet apparent mesuré verticalement entre le haut et le pied de l'escarpement de faille ; Φ est le pendage du plan de faille.

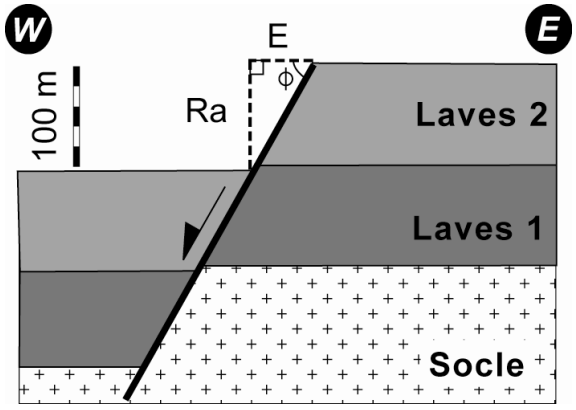

Figure 10. *Coupe schématique des paramètres pris en compte dans le calcul de l'extension le long d'un plan de faille normale (Ra : rejet apparent, E : extension ; Φ : pendage du plan de faille).*

1.3.2.5. Relation rejet/longueur des failles

En dernier lieu, le rejet maximum le long d'une faille individuelle est estimé à partir d'une série de coupes, perpendiculaires à l'escarpement, et régulièrement espacées (~10 km). Une trentaine de failles majeures ont ainsi été mesurées, et leur rejet maximum a ensuite été corrélé avec leur longueur. Cette représentation graphique des résultats débouche sur un modèle de croissance de failles qui contredit les conceptions classiquement admises selon lesquelles la longueur et le rejet d'une faille suivent une relation linéaire (Schlische et al., 1996) (cf. chapitre 3).

1.4. DONNEES COMPLEMENTAIRES

Un jeu de données intégrant à la fois des données de surface et de profondeur a également pris en compte afin de compléter les interprétations obtenues à partir d'imagerie de surface.

1.4.1. Les données de terrain

Au cours de l'été 2002, une mission d'une durée de deux mois nous a permis de travailler à une échelle plus réduite et de compléter l'interprétation des images satellites par des relevés de terrain. Nous avons principalement couvert la partie ouest du lac Turkana allant du secteur de Lapurr au nord, au secteur de Loperot au Sud (Fig. 11). Cette mission, effectuée dans le cadre du projet ECLIPSE 1 INSU (Paléoenvironnements des Hominidés Mio-Plio-Pléistocènes en Afrique centrale et orientale ; directeur : H. Roche), avait pour objectif initial de rechercher des indices de déformations récentes le long du rift Turkana. En complément des observations dans les séries les plus récentes, nous avons également observé et pris des mesures dans les affleurements de socle, les grès Crétacé et les zones volcaniques oligo-pliocènes (Planche photo 1 et annexe 1). Un échantillonnage systématique des différentes formations a donné lieu à une vingtaine de datations K/Ar sur les laves oligo-pliocènes (cf . annexe 2), ainsi qu'a une dizaine de datations C^{14} sur des sédiments récents lacustres, basculés et faillés (cf. annexe 3), dans le but de mieux contraindre l'âge de la déformation dans certains secteurs-clés. Les données acquises dans le cadre d'une mission antérieure (1998) dans le secteur de Mount Porr, sur la partie SE du lac Turkana, ont également été intégrées afin de discuter la déformation et l'âge des 'Turkana Grits' (Crétacé).

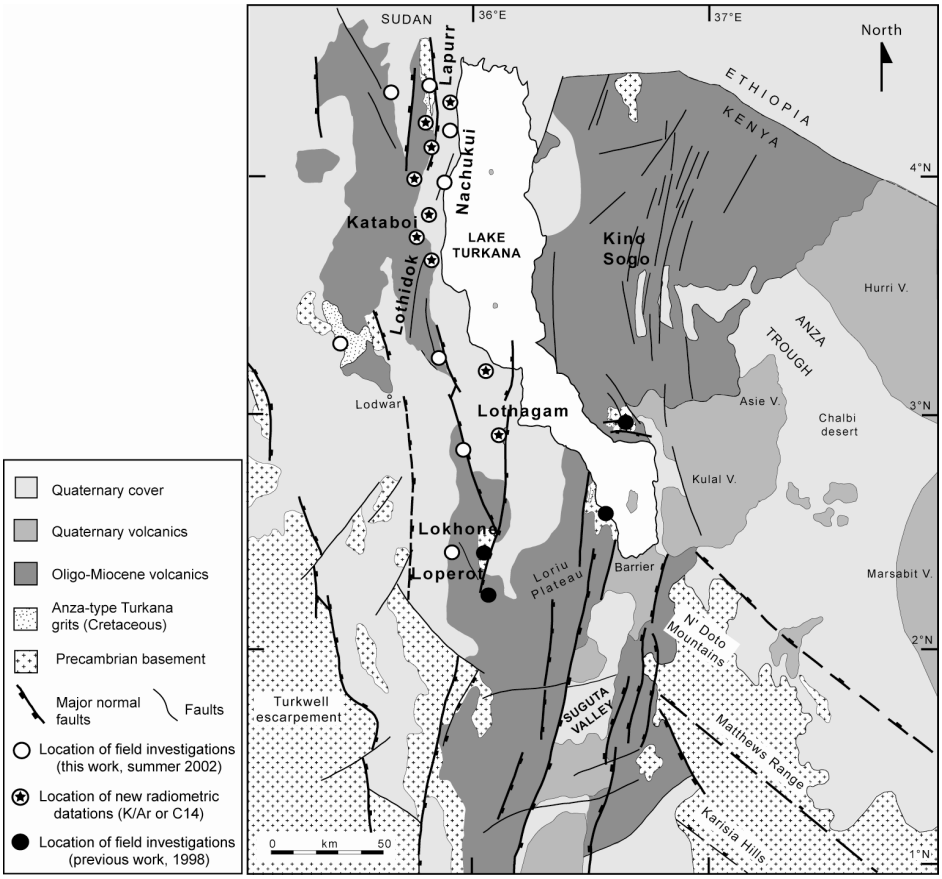

Figure 11. *Localisation des secteurs étudiés lors de la mission de terrain de l'été 2002.*

1.4.2. Sismique réflexion

Nous disposions de la quasi-totalité des lignes sismiques TVK (version papier) acquises dans la partie WSW du lac Turkana par la compagnie pétrolière Amoco en 1986 (Morley et al., 1992) et mises à notre disposition par la NOCK (National Oil Corporation of Kenya) (Fig. 12a). Ces lignes imagent la géométrie profonde (4-5 s. TWTT) des bassins oligo-pliocènes dont le remplissage sédimentaire est calibré par 2 forages (Eliye Springs, 2767 m et Loperot, 2950 m ; Shell, 1992 ; Morley et al, 1999a). Ce jeu de données est complété dans les bassins du lac Turkana par des lignes sismiques TVB (version papier) acquises en 1984 dans le cadre du Projet Probe (Dunkelman et al., 1989). L'espacement régulier entre les profils à terre (~2-5 km) ou dans le lac (5-10 km) autorise la corrélation latérale des failles. Dans le cadre de cette étude, certains des profils sismiques ont parfois été réinterprétés par rapport aux conceptions antérieures de Morley et Dunkelman afin de corréler les failles imagées sismiquement avec celles déduites de notre étude en surface.

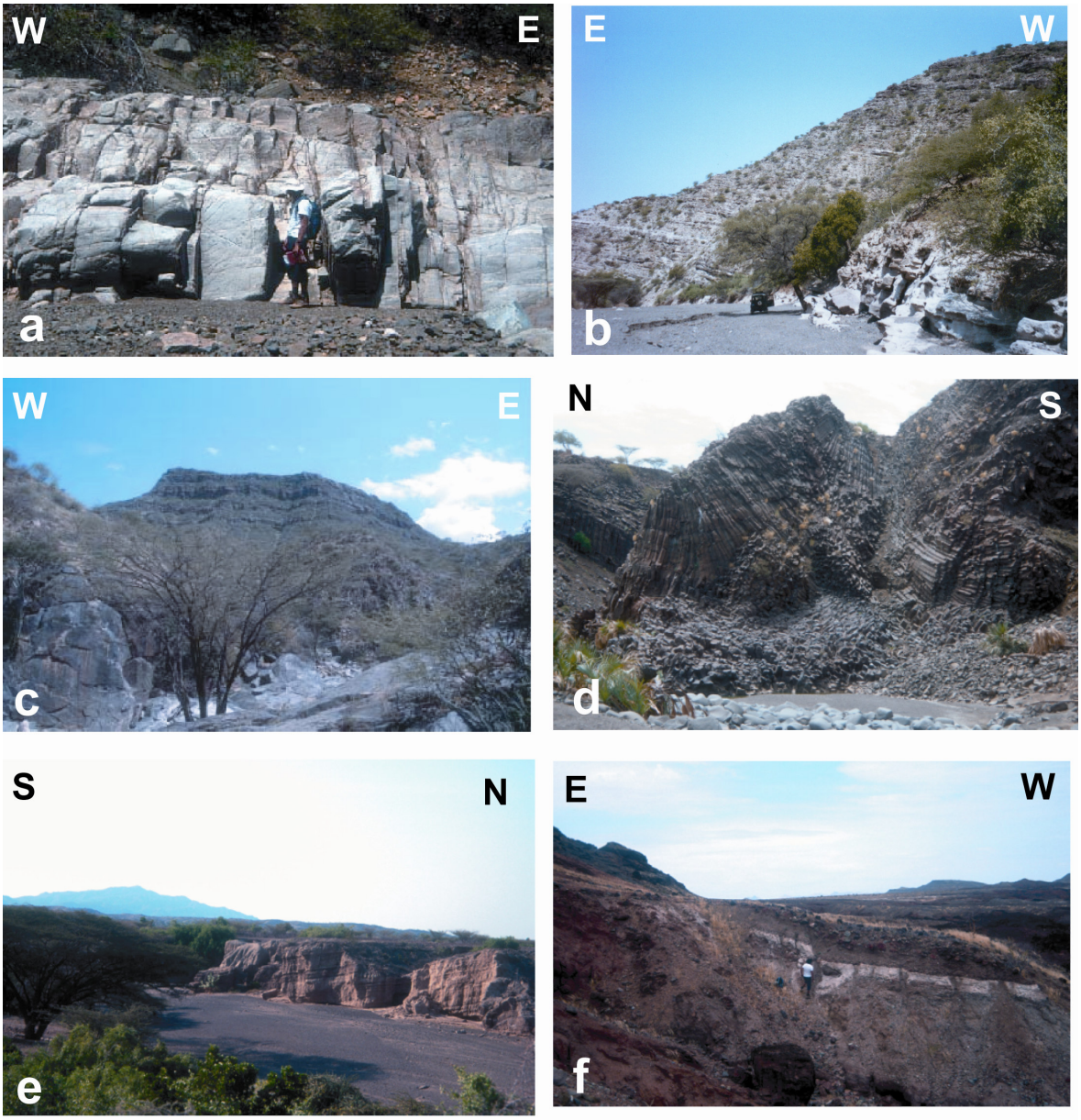

Planche I de photographies de terrain. *(a) Système de fractures EW affectant le socle protéroïque de Lapurr, (b) Grès crétacés de Lapurr, (c) Empilement de laves oligo-miocènes de Lapurr, (d) Basaltes pliocènes de Kataboi, (e) Sédiments récents à Hominidés basculés de Nachukui (2.34 Ma., Roche et al., 1999) (f) Sédiments holocènes lacustres, basculés et faillés, Lothagam (9795+-15 ans , âge C^{14} cf. annexe 3). Voir figure 11 pour localisation.*

1.4.3. Sismique réflexion haute résolution

En complément des lignes TVB 'offshore' (Probe, 1984), 770 km de profils de sismique haute- résolution (1kHz) imagent la structure des 200 derniers mètres de sédiments holocènes déposés dans les bassins du lac Turkana (Johnson et al., 1987) (Fig. 12b). De nombreux indices de déformations récentes/actives (<10 000 ans d'après une surface d'érosion), dont

certaines affectent le plancher du lac, sont clairement identifiables. Toutefois, la mauvaise qualité des données 'papier' ainsi que l'espacement important des profils (~10-20 km) ne permettent pas une cartographie précise des structures. Nous avons toutefois pu mettre en évidence une déformation extensive relativement importante le long de 5 portions du lac Turkana (Fig. 12b).

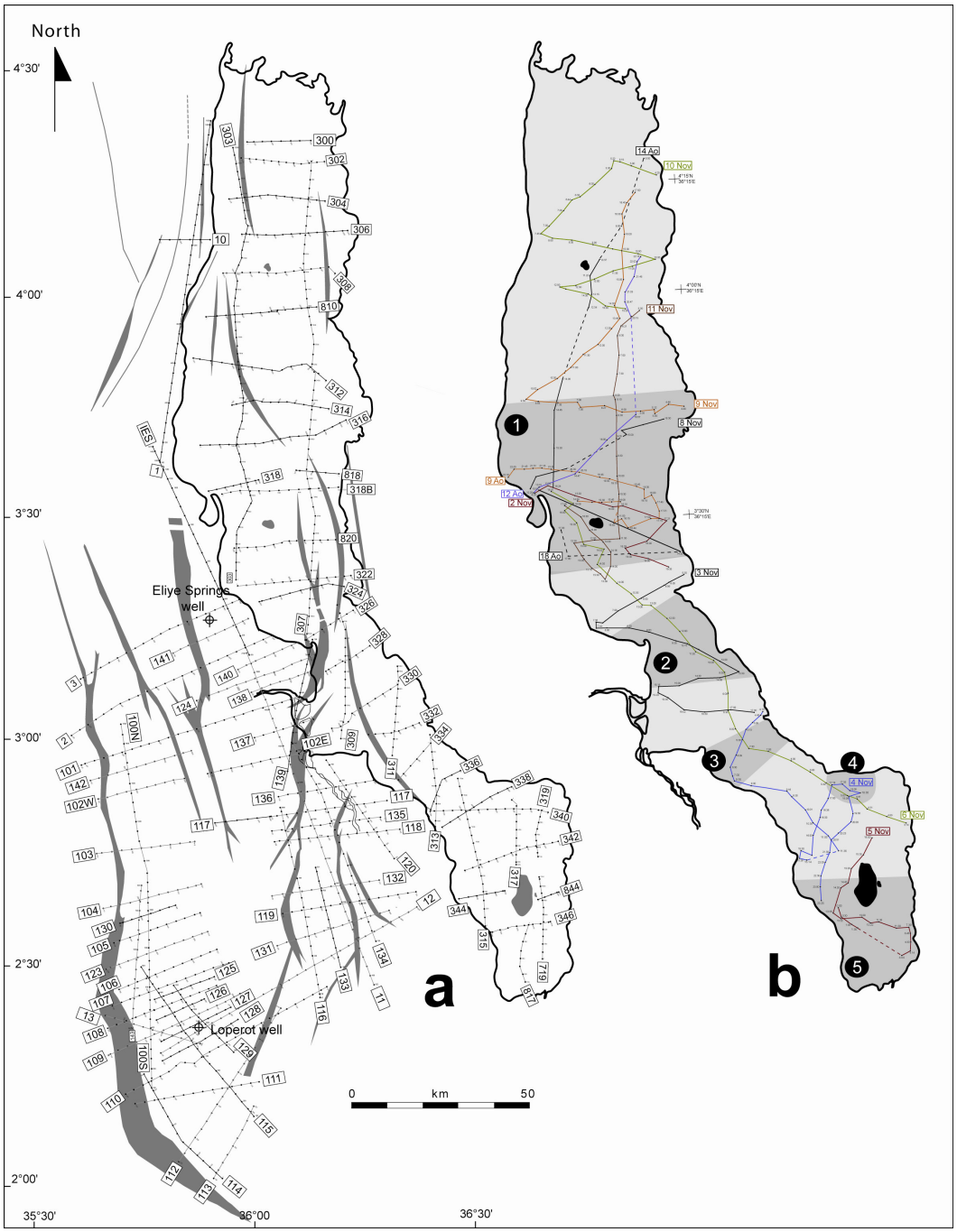

Figure 12. *(a) Plan de position des lignes sismiques TVK Amoco (à terre) et TVB Probe (lac). La trace des failles majeures (en grisé) est dessinée d'après Morley et al. (1999a). (b) Plan de position des lignes sismiques haute résolution. Les zones affectées par des indices de déformations récentes (<10 000 ans.) sont indiquées en gris sombre dans le lac.*

2. Dynamic of continental extension in magmatic rifts. The study case of the Turkana Rift since the last 45 Ma. (Northern Kenya)

William Vétel[1] & Bernard Le Gall[1]

[1] UMR 6538 'Domaines Océaniques', Institut Universitaire Européen de la Mer, UBO, CNRS, 4 Place Nicolas Copernic, 29280, Plouzané - FRANCE

(Submitted to Journal of the Geological Society, London)

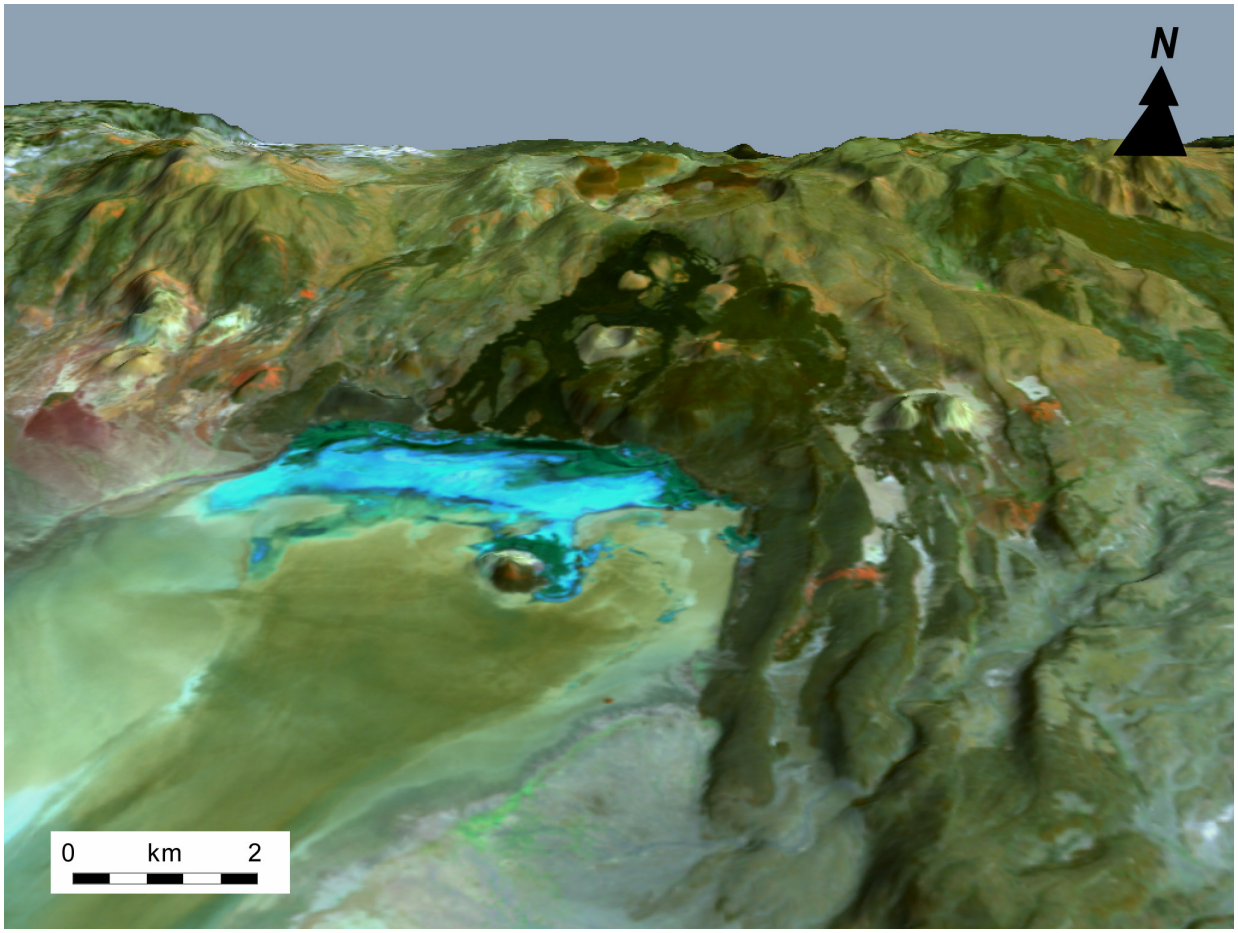

Perspective view of a portion of the Landsat image 169-058 overlain on the digital topography SRTM in the termination of the Suguta Valley and the faulted Barrier volcanic complex (view to the north, light from East, vert. exag. x4).

Abstract: The Turkana magmatic rift (Northern Kenya) initiated at 45 Ma. as one of the nucleation zone of rifting in the EARS. It actually forms an anomalously broad rifted zone (~200 km) extending with a NS trend within a NW-SE topographic depression, floored on both sides of the Turkana area by Cretaceous rifts in the Sudan and Anza plains. From a compilation of available data, combined to newly-acquired remote sensing and DEM dataset, we propose a five-stage tectono-magmatic model for the Turkana rift (45-23 Ma.; 23-15 Ma.; 15-6 Ma.; 6-2.6 Ma. and 2.6 Ma.-Present). The corresponding 'restored' maps clearly show the changing spatial distribution of magmatism and fault/basin network with time, hence supplying some clues to fully discuss key-aspects of continental extension. First-order basement-rooted transverse faults zones are identified and their influence on nucleation and propagation of strain is demonstrated whereas, inversely, the role of magmatic 'soft-spot' as concentrating strain is minimised. Recent (<5 Ma.) stress-field variations result in local basin inversion and emplacement of off-axis volcanism. Lastly, the origin of the Turkana depression is assigned to interaction of lithospheric processes involving the impingement of two mantle plumes on the heterogeneous East African lithosphere migrating to the NE.

Keywords: East African Rift, Turkana, tectonics, magmatism, mantle plume, structural inheritance.

2.1. Introduction

The structural style of continental rifts depends on a combination of thermal, mechanical and kinematical parameters (strain rate, initial conditions, mechanical instabilities) that control the deformation of the stretched lithosphere. In terms of causative processes, a distinction between active (plume-related) and passive rifting is generally proposed (McKenzie & Bickle 1988; Sengör & Burke 1978; Ziegler & Cloetingh 2004; and references therein), whilst from a structural point of view, narrow, wide rifting and core complexes are distinguished as a function of the width of the deformed zone (England 1983; Buck 1991). The deformation processes governing continental extension are strongly influenced by the rheological properties of the extending crust/lithosphere which, in turn, play a key-role in the finite arrangement of surface rift

fault patterns. When a number of parameters interact concomitantly, such as long duration of rifting, strong structural inheritance, volcanic activity and changing stress field conditions, increasing structural complexities of rift domains may occur as it is the case for the ~45 Ma.-old Turkana magmatic rift (northern Kenya) in the central part of the eastern branch of the East African Rift System (EARS) (Fig. 1a). Indeed, with regards to the adjoining Ethiopian and Kenyan plume-related rift domes, the Turkana Cenozoic rift occupies the median part of NW-SE intervening depression whereas its dimensions (~200 km-wide zone of deformation in EW direction), its poor rift topography, and its reduced crustal thickness (20 km) have long been recognized (Prodehl *et al*. 1994). However, many of these structural characteristics remain largely understood and a complete rift model integrating both shallow and deep structures in the time-span of ~45 Ma. has not been so far established. The only accurate kinematic model applied to the Turkana rift is principally focussed upon Oligo-Miocene fault/basins developed during the onset of rifting in the western part of the rifted zone, e.g. west of modern Lake Turkana (Morley *et al.* 1992, 1999a; Hendrie *et al*. 1994).

The aim of this paper is thus to get a structural picture of the long-lived Turkana rift, encompassing the seismically-imaged sedimentary basins, but also the poorly-investigated basement and magmatic domains. Our renewed structural interpretation of surface geology, mainly from remote sensing data, provides some clues about the dynamical processes that govern the Turkana rift evolution since Eocene-Oligocene times onwards. That leads us to elaborate a five-stage kinematic evolutionary model for the 45 Ma.-long rift history emphasing the interplay between strain and magmatism. The time interval of ~10 Ma., as well as the dimension (~100 km) of individual structures investigated here, supply an adequate resolution for discussing the influence of a number of parameters (structural inheritance, distribution of magma, stress field) on the style of rifting. From our tectono-magmatic model, it is clear that the 45 Ma. evolution of the Turkana rift is more complex than a simple and linear propagation of strain and magmatism as generally stated (Hendrie *et al.* 1994; Morley 1994). Structural disturbances are clearly associated with large-scale transverse faulted zones trending at N50°E and N140°E. At a greater scale, some assumptions are also attempted in order to reconcile upper crustal structures and deep thermal lithosphere parameters linked to Cenozoic mantle plume frameworks and their possible interference with two main rift systems present in the Turkana area as a whole.

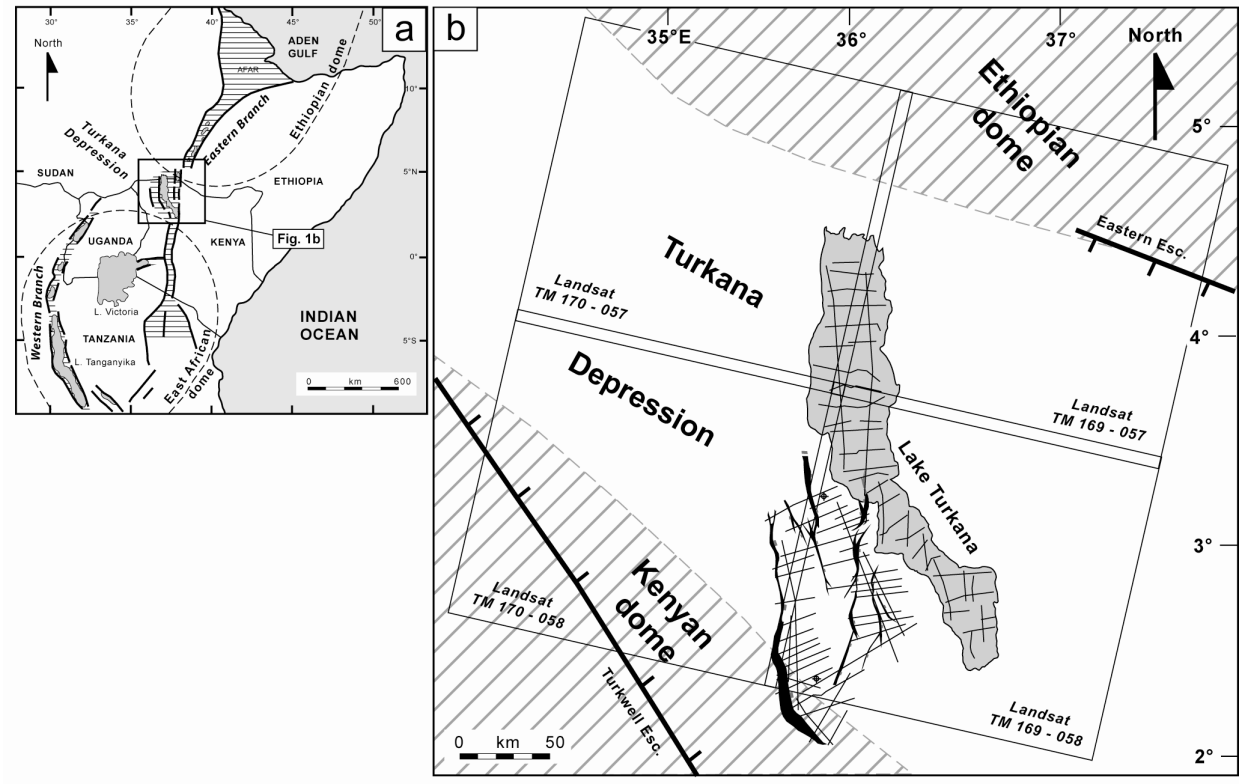

Fig. 1. *(a). General map of the East African Rift System (EARS). Dashed areas show the trace of the inner trough. The broad Turkana rifted zone under study (dark square) is a portion of the eastern rift branch and occurred between the Ethiopian and Kenyan rift along the transverse Turkana depression. (b). Location map of the Turkana area showing the different types of dataset used in this study: four Landsat Enhanced Thematic Mapper Plus satellite images (169-057, 27/01/2000; 169-058, 21/10/1999; 170-057, 12/07/2000; 170-058, 18/01/2000), onshore AMOCO and offshore PROBE seismic lines. Topographic data are shown on figure 2.*

2.2. Dataset and methods

The study area extends over more than 16. 000 km² (~35° to 39°E long. and ~2° to 6°N lat.) along the NW-SE-trending Turkana depression and the distal parts of the Ethiopian and Kenyan adjoining domes (Figs 1 and 2). Our specific objective is to precise the Cenozoic tectono-magmatic evolution of this broad rifted zone from ~45 Ma. (Late Eocene) to Present. For that purpose, the exhaustive analysis of available dataset (seismic imagery and geological maps) has been performed and completed by the structural interpretation of remote sensing data (Landsat images and digital elevation models) (Figs 1 and 2). PROBE (offshore) and AMOCO (onshore) seismic reflection profiles across the synrift basins of the Lake Turkana area *sensu lato* have been

partially reinterpreted from previous published works (Dunkelman *et al*. 1989; Morley *et al*. 1992, 1999a) (Fig. 1a). Four 1/250 000 geological maps (1°x1°) (Charsley 1987; Ochieng *et al.* 1988; Wilkinson 1988; Dunkley *et al*. 1993) help us to correlate surface geology with structures depicted from satellite imagery interpretation. Four Landsat Enhanced Thematic Mapper Plus images (169-057, 27/01/2000; 169-058, 21/10/1999; 170-057, 12/07/2000; 170-058, 18/01/2000), with a ground resolution of 30 m (15 m for panchromatic band) (Girard & Girard 1990), have been processed by using Geomatica 9.2 software in order to enhance the trace of surface rift fault patterns. The recently available SRTM (Shuttle Radar Topography Mission; http://www2.jpl.nasa.gov/strm) topographic data supply supportive evidence for recent fault scarps, hence leading us to elaborate a new and more constrained neotectonic model for the Turkana rift (Fig. 2). More generally, five successive rift stages are distinguished at 45-23 Ma., 23-15 Ma., 15-6 Ma., 6-2.6 Ma. and 2.6 Ma.-Present. The corresponding 'restored' tectono-magmatic maps are completed by two additional pre-rift structural maps of the Anza Cretaceous rift and the underlying Proterozoic basement, in order to further discuss the problem of structural inheritance.

The accuracy of our evolutionary rift model is directly dependant on the validity of the published radiometric dating (a few ten's of K/Ar ages) acquired during the 1980's, principally on the main synrift volcanic complexes (Zanettin *et al*. 1983; McDougall & Watkins 1988; Ochieng *et al.* 1988; Wilkinson 1988; Morley *et al*. 1992; Dunkley *et al*. 1993; McDougall & Feibel 1999). Other limitations of our work are related to the poorly-imaged shallow structures on seismic profiles, and the uncertainties about the strain rate, the cumulative extension and the applied stress-field conditions for each time period. Consequently, the five retrograde tectonic maps proposed in the study are not true 'restored' maps and the orientation of the corresponding principal stress axes is indirectly deduced, in most of cases, from 2D-map fault arrangement and volcanic lineament azimuths. Despite those limitations, some new insights about fault propagation and strain migration are discussed with respect to magmatic distribution and structural inheritance throughout the Turkana broad rifted zone.

2.3. Geological framework

2.3.1. Cenozoic rift setting

The ~16. 000 km² studied rift area encompasses, in addition to the Turkana depressed zone which is the main topics of the paper and benefits from a more complete surface and subsurface (reflection seismics) dataset, the external parts of the Ethiopian and Kenyan plume-related domes (Fig. 2). The ~250 km-wide Turkana transverse depression is bounded by two NW-SE escarpments cutting through the 2000 m-high relief of the Ethiopian and Kenyan domes (Figs 2b and 2c). Its subdued morphology, with an average elevation of 400-900 m, contrasts with the typical graben-like structure of the Suguta axial valley to the south. Its general N140°E trend, parallel to the axis of the Anza-Sudan Cretaceous rift system, is cut at high angle in the Turkana area by dominantly NS-trending fault structures of the Cenozoic rift. Most of these structures are associated with large rift basins, already fully investigated by Morley *et al.* (1999a), and thus briefly described here. On the other hand, emphasis is put on large-scale transverse fault zones assumed to have played a dominant role in the geometry and kinematics of the Turkana Cenozoic rift system (Fig. 2b).

Fig. 2. *Topographical framework of the Turkana rifted zone. (a) General topography of northeastern Africa (Gtopo 30 elevation data). The NS-trending Turkana rift (white square) is located within the transverse Turkana depression flanked by the Ethiopian and Kenyan plume-related domes (dashed-lines). The trace of the Turkana rift, centred on Lake Turkana, is poorly expressed compared to the linear and narrow Kenyan and Ethiopian rift valleys. (b) Shuttle Radar Topography Mission digital elevation model (no vertical exaggeration, ground resolution 90 m, 16 m in vertical) showing the relatively low relief of the Turkana rift. The trace of the rift is diffuse in the vicinity of the lake but is well-expressed along the Suguta Valley to the south of Lake Turkana, and in the Chew Bahir trough to the NE. Three first-order transverse fault zones are indicated (dashed lines): the N140°E-striking N'Doto-Karisia fault zone (NKFZ), the N50°E Buluk and Kataboi fault zones (BFZ and KFZ, respectively). The second-order Turkwell-Mount Porr fault zone (TMFZ) trends at N90°E through Lake Turkana around 3° north. Principal location names used in this paper are also indicated. (c) Topographic profile across the Turkana depression (see figure 2b for location). Note the subdued topographic expression of the ~300 km-wide Turkana depression zone, in contrast with the external Ethiopian and Kenyan relief limited by steep escarpments.*

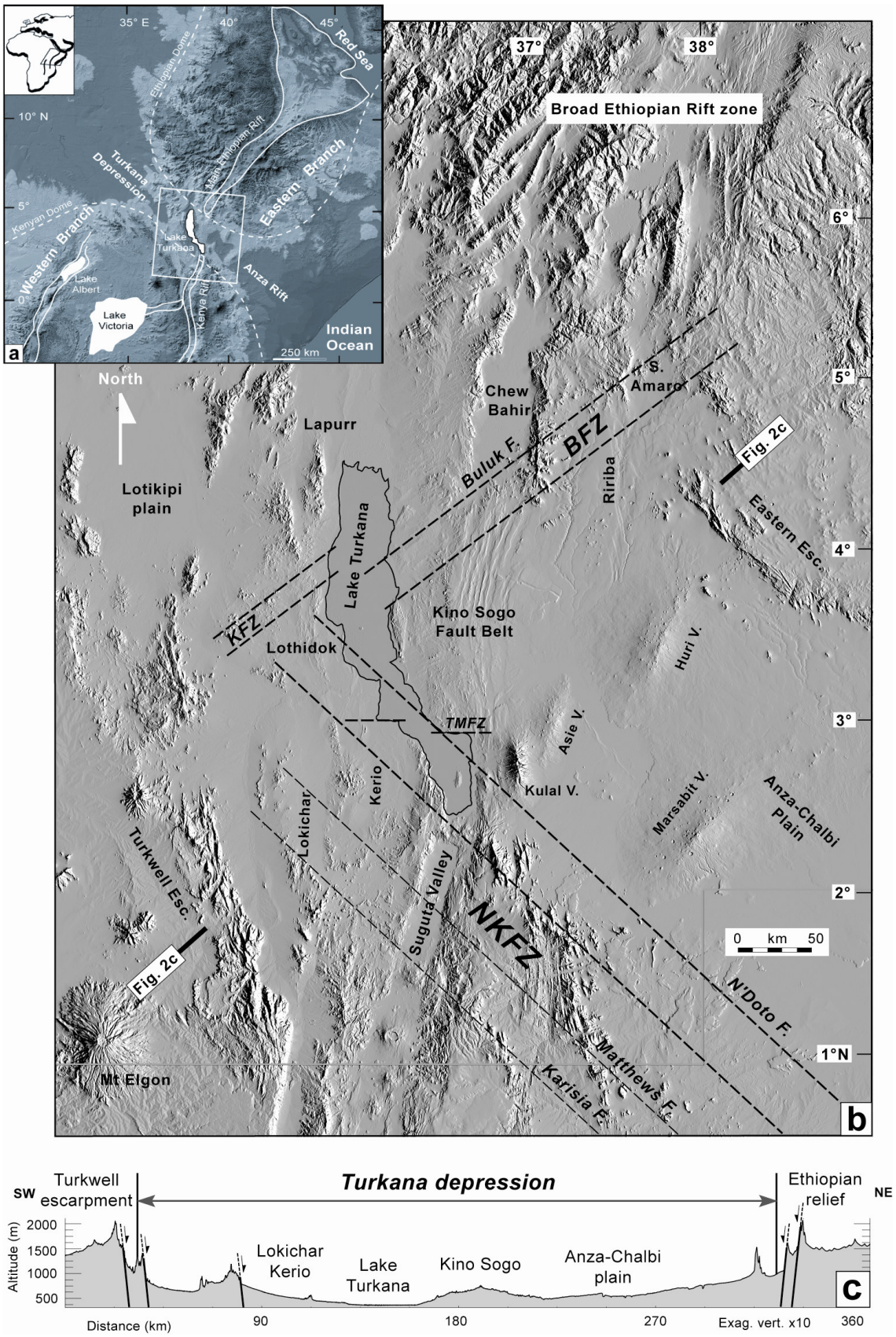
a
35° E
40°
45°
Red Sea
Ethiopian Dome
10° N
Main Ethiopian Rift
Turkana Depression
Eastern Branch
5°
Kenyan Dome
Western Branch
Lake Turkana
Lake Albert
Anza Rift
0°
Lake Victoria
Kenya Rift
Indian Ocean
250 km
North
37°
38°
Broad Ethiopian Rift zone
6°
5°
4°
3°
2°
1°N
Chew Bahir
S. Amaro
Lapurr
Buluk F.
BFZ
Ririba
Fig. 2c
Eastern Esc.
Lotikipi plain
Lake Turkana
KFZ
Kino Sogo Fault Belt
Lothidok
Huri V.
TMFZ
Asie V.
Kerio
Kulal V.
Marsabit V.
Anza-Chalbi Plain
Lokichar
Turkwell Esc.
Suguta Valley
NKFZ
0 km 50
N'Dofo F.
Fig. 2c
Matthews F.
Mt Elgon
Karisia F.
b
SW
Turkwell escarpment
Turkana depression
Ethiopian relief
NE
Altitude (m)
2000
1500
1000
500
Lokichar Kerio
Lake Turkana
Kino Sogo
Anza-Chalbi plain
c
Distance (km)
90
180
270
Exag. vert. x10
360

2.3.2. Major basin and magmatic frameworks

Since the acquisition of seismic reflection profiles in the late 1980's and early 1990's, the rifted domain centered over Lake Turkana is known to be a 200x100 km extensional province comprising three parallel belts of NS half-grabens illustrated on the map and structural dip-sections of figure 3 (Dunkelman *et al.* 1989; Morley *et al.* 1999a). Stratigraphic calibration by two boreholes (Loperot, 2950 m and Eliye Springs, 2964 m) indicates a progressive northwards and eastwards younging of the depocentres from the 6-7 km-deep Lokichar half-graben which is one of the oldest basins (~35 Ma.) of the EARS as a whole (Morley 1999c; Morley *et al.* 1999a) (Fig. 3c). An array of half-grabens with alternating polarity involves to the east the North Kerio, Turkwell, Turkana and Lake basins.

The rifting activity is accompanied since ~45 Ma. by a dominantly mafic volcanism preferentially emplaced along inter-basin structural highs forming the Lapurr, Lothidok, Kino Sogo and Napedet lava plateaus (Zanettin *et al*. 1983; McDougall & Watkins 1988; Ochieng *et al*. 1988; Wilkinson 1988; Morley *et al.* 1992; Dunkley *et al*. 1993; McDougall & Feibel 1999) (Fig. 3a). The available radiometric dataset suggests the easterly shift of the magmatic activity from Oligo-Miocene (Turkana domain) to Present (shield volcanoes in the Anza-Chalbi plain). A quite similar lateral migration of strain during recent time is also indicated by (1) the <3 Ma. dense fault grid across the recent Kino Sogo volcanics (Vétel *et al*. submitted) between the Chew Bahir and Suguta grabens, and (2) the ~1 Ma. Ririba extensional branch further east (Fig. 2).

Fig. 3. *Geological framework and deep geometry of the Turkana rift. (a) Structural map of the Turkana rift on the western termination of N140°E-trending Anza trough. Its occidental part is marked by a serie of NS Oligo-Pliocene half-grabens. Eocene-Miocene volcanism is confined to the west whereas Plio-Quaternary lavas are restricted to the east. (b and c) Representative geological sections (modified from Morley et al. 1999a) across the Turkana synrift basins network from seismic reflection data (Amoco TVK and Probe TVB profiles). See location of the section on figure 3a. Note the dominantly half-graben style of the basins and their progressive younging eastwards and northwards.*

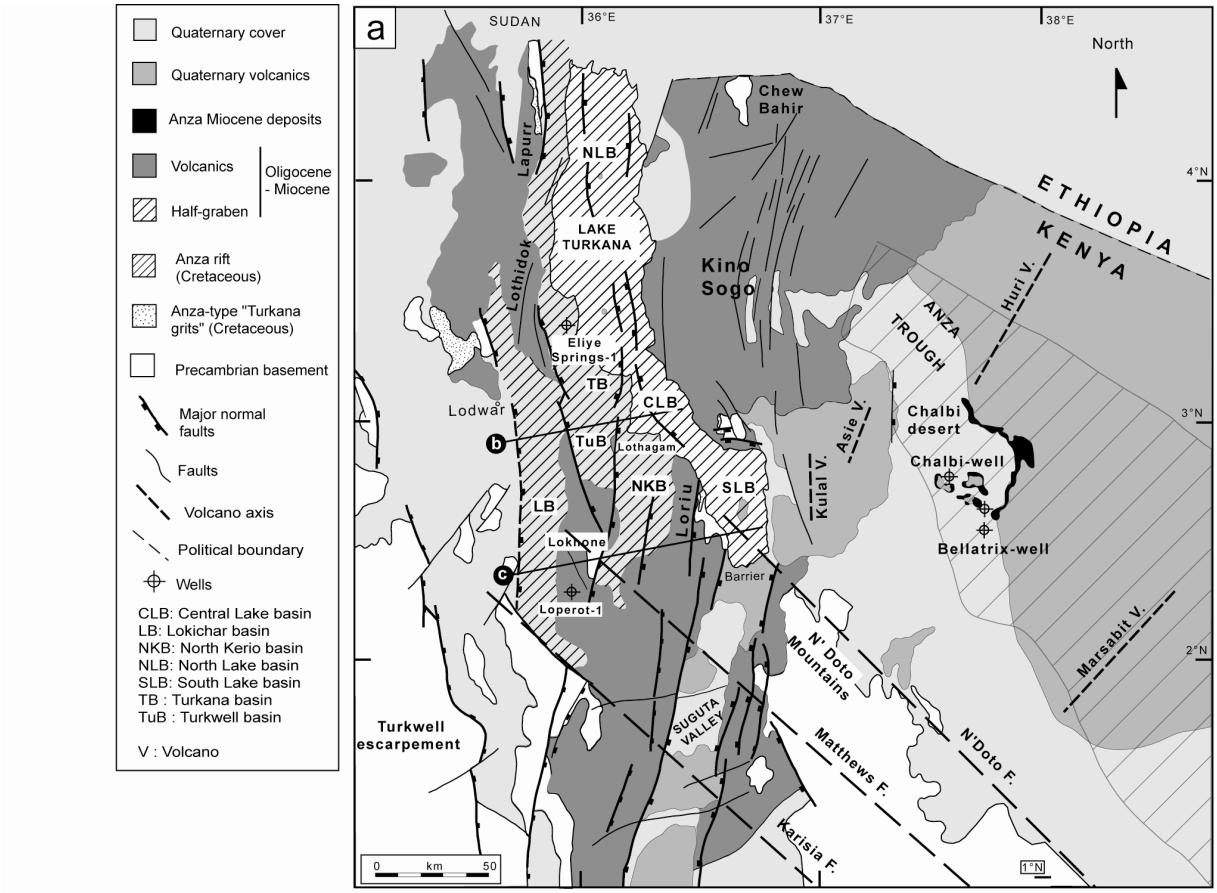
Quaternary cover
Quaternary volcanics
Anza Miocene deposits
Volcanics
Oligocene - Miocene
Half-graben
Anza rift (Cretaceous)
Anza-type "Turkana grits" (Cretaceous)
Precambrian basement
Major normal faults
Faults
Volcano axis
Political boundary
Wells
CLB: Central Lake basin
LB: Lokichar basin
NKB: North Kerio basin
NLB: North Lake basin
SLB: South Lake basin
TB : Turkana basin
TuB : Turkwell basin
V : Volcano
a
SUDAN
36°E
37°E
38°E
North
4°N
3°N
2°N
1°N
ETHIOPIA
KENYA
Chew Bahir
NLB
Lapurr
LAKE TURKANA
Lothidok
Kino Sogo
Eliye Springs-1
TB
CLB
Lodwar
TuB
Lothagam
NKB
LB
Loriu
SLB
Kulal V.
Asie V.
ANZA TROUGH
Huri V.
Chalbi desert
Chalbi-well
Bellatrix-well
Lokhone
Barrier
Loperot-1
N' Doto Mountains
Marsabit V.
Turkwell escarpement
SUGUTA VALLEY
Matthews F.
N'Doto F.
Karisia F.
0 km 50

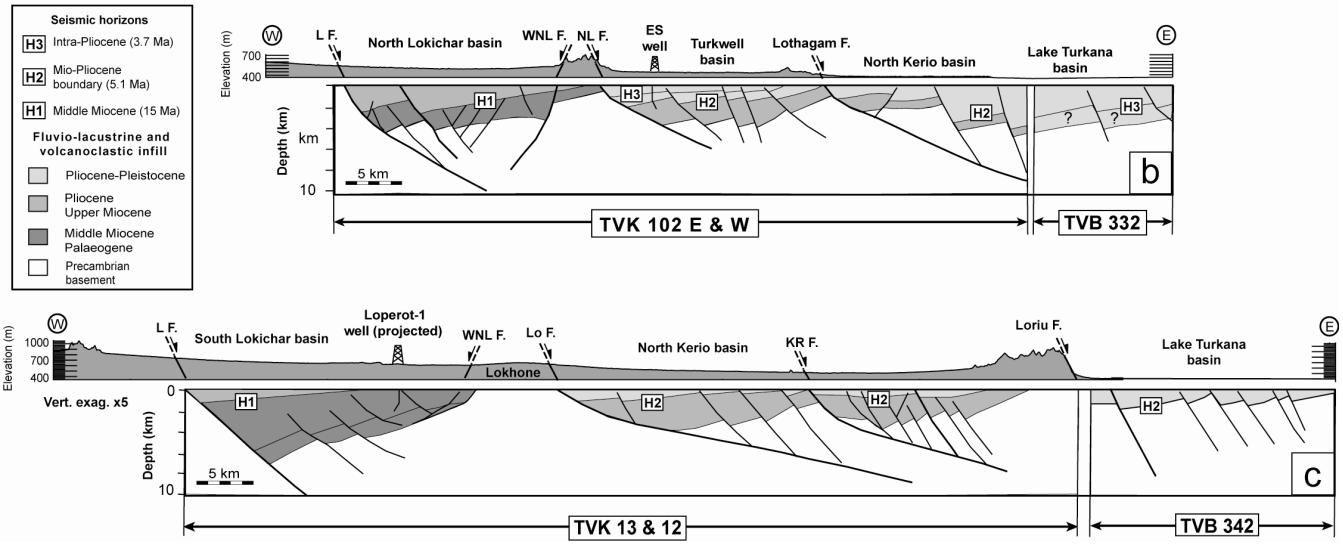
Seismic horizons
H3 Intra-Pliocene (3.7 Ma)
H2 Mio-Pliocene boundary (5.1 Ma)
H1 Middle Miocene (15 Ma)
Fluvio-lacustrine and volcanoclastic infill
Pliocene-Pleistocene
Pliocene Upper Miocene
Middle Miocene Palaeogene
Precambrian basement
Elevation (m)
W
E
L F.
North Lokichar basin
WNL F.
NL F.
ES well
Turkwell basin
Lothagam F.
North Kerio basin
Lake Turkana basin
700
400
Depth (km)
km
10
5 km
H1
H2
H3
?
b
TVK 102 E & W
TVB 332
1000
South Lokichar basin
Loperot-1 well (projected)
Lo F.
Lokhone
KR F.
Loriu F.
Vert. exag. x5
0
5 km
c
TVK 13 & 12
TVB 342

Bulk extension recorded by the Turkana rifted zone since Oligocene times (~35 Ma) is estimated to 30-40 km by Hendrie *et al.* (1994). The fairly detailed image of the crust beneath the Turkana rift (KRISP Working Group 1991) shows the step-like morphology of the Moho along the rift axis, passing northwards from a thinned crust (~20 km-thick) beneath Lake Turkana into a normal thickness (~35 km) at the latitude of Baringo (Mechie *et al.* 1994; Prodehl *et al.* 1994).

2.3.3. Transverse fault zones

On the basis of interpreted satellite and DEM's imagery, a number of first-order oblique fault zones, unknown or underestimated before this work, is identified in the study area as prominent topographic scarps, intra-basin disturbance zones and magmatic lineaments (Fig. 2). Two main trends are recognized at N50°E, along the so-called Buluk and Kataboi fault zones (BFZ and KFZ in the text), and at N140-160°E, along the so-called N'Doto-Karisia fault zone (NKFZ). A more discrete N90°E-trending segmented fault zone reported along the Turkwell-Mount Porr area (TMFZ) is not fully integrated in this paper (see Vétel *et al.* 2004).

2.3.3.1. The Buluk fault zone

The BFZ expresses as a ~30 km-wide faulted corridor between the Chew Bahir graben and the highly-faulted Kino Sogo volcanic plateau (Fig. 4). Its N50°E fault structures cut through fractured lavas as young as 3.3 Ma. (Hackman *et al.* 1990; Vétel *et al.* submitted). It is bounded to the north by the so-called Buluk fault that dies out to the NE in the Quaternary cover of the Chew Bahir trough (Fig. 4c). The BFZ is also outlined by numerous circular intrusions emplaced from Miocene (21-14 Ma.-old Jibisa complex) to Quaternary in the Chew Bahir graben (Hackman *et al.* 1990). The dominant dip-slip extensional component of the faults within the BFZ is suggested by the morphology of the fault scarp limiting the Kino Sogo uplifted fault block to the north (Figs 4b and d). This fault geometry is consistent with the attitude of the normal fault imaged by seismics in 5-3.7 Ma.-old strata of the North Lake Turkana basin, close to the inferred tip zone of the Buluk fault (Fig. 4e).

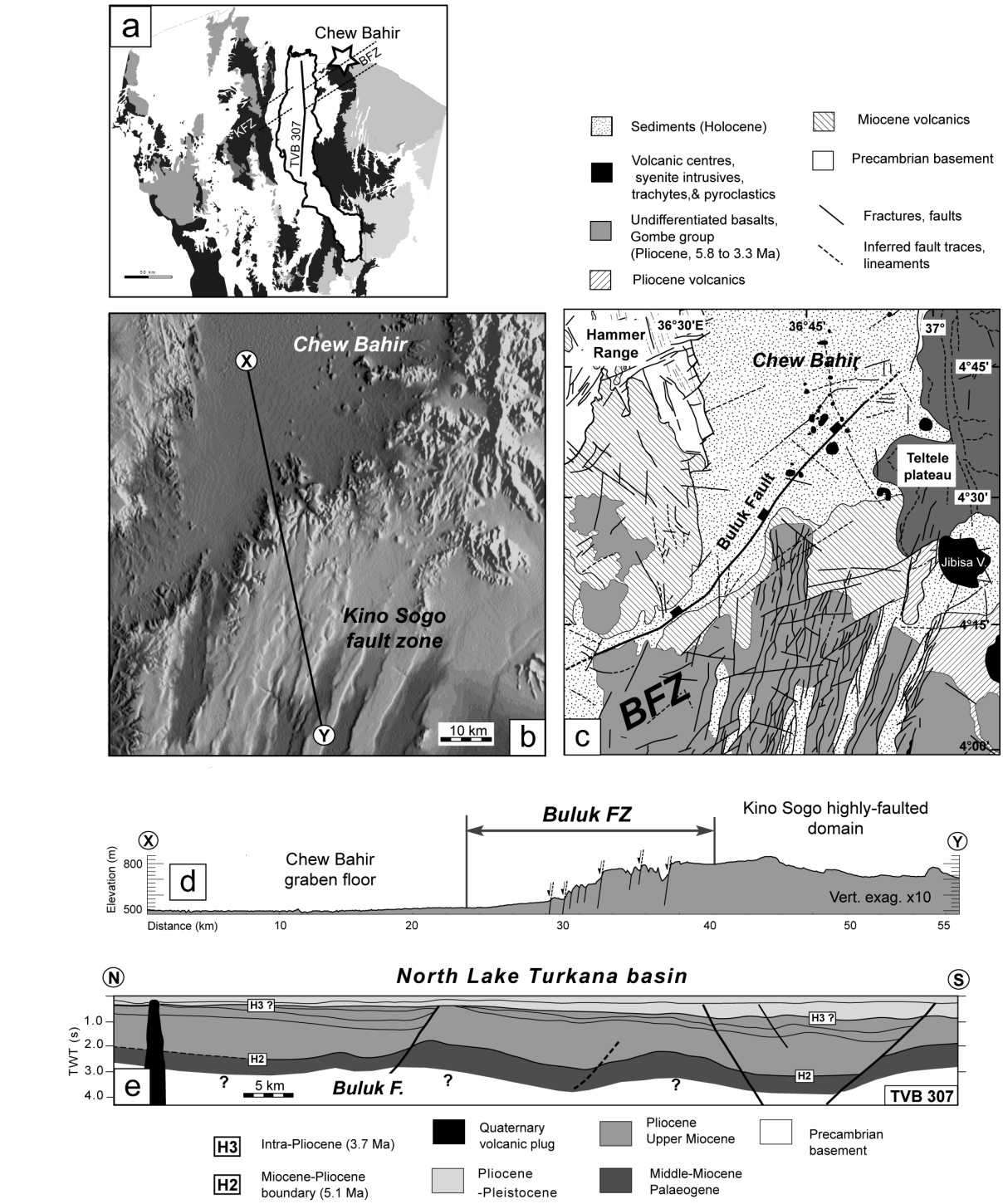

Fig. 4. *Structural evidence for the Buluk Fault Zone (BFZ). (a) Location map of the N50°E BFZ. (b) SRTM digital elevation model on the area showing the trace of the BFZ between the Chew Bahir trough and the Kino Sogo plateau. (c) Structural interpretation of figure 4b. (d) Topographic section across the BFZ illustrating the NW downthrow along the BFZ (see figure 4b for location). (e) Probe seismic line TVB 307 shown the western extremity of the Buluk Fault across the Pliocene basin of North Lake Turkana (modified from Dunkelman et al. 1989) (see figure 4a for location).*

In this offshore fault attenuation zone, the BFZ displays an underlapping convergent geometry (Morley 1999b) with the KFZ discussed below. The BFZ may also extend 70 km further to the NE across the Ririba extensional area where it correlates with a sharp NE-SW fault-like boundary separating the so-called South Amaro graben from the narrow (5 to 10 km-wide) Ririba linear trough to the south (Fig. 2).

2.3.3.2. The Kataboi fault zone

The KFZ lies nearly in the SW prolongation of the BFZ on the western side of Lake Turkana (Figs 2 and 5). It separates two distinct magmatic terrains in the uplifted footwall block of the Lapurr-Lothidok fault system, i.e. the Lapurr-Murua Rith complex (Eocene-Miocene) to the north and the Lothidok-N'Gapoi complex (Miocene) to the south (Fig. 5b). The KFZ is a narrow ~20 km-wide deformed zone comprising a network of ~N50°E faults, facing to the SE (Figs 5b and d). Some of these structures extend with a constant NE-SW strike across the Turkana lacustrine plain where they post-date Plio-Pleistocene Hominid sediments of the Nachukui Formation (Harris *et al.* 1988; Roche *et al.* 1999). Other fault structures in the KFZ swing towards a NS direction and branch to the NE into the Lapurr extensional master fault system. To the south, the KFZ fault network dissects and post-dates the dense rift-parallel fault array developed in the Lothidok southern complex (Figs 5b and d). The present-day downthrown position of this southern volcanic block (Fig. 5e) is indicative of dominantly southeasterly-directed extensional displacement along the KFZ. Such fault kinematics is confirmed by the observation of smaller-scale dip-slip fault planes in the Topernawi area (Fig. 5d). The probably <15 Ma.-old rhyolitic intrusions enclosed within the KFZ (Zanettin *et al.* 1983) are truncated and post-dated by the NE-SW fault network (Figs 5b and c).

Fig. 5. *Structural evidence for the Kataboi Fault Zone (KFZ). (a) Location map of the N50°E KFZ. The KFZ occurs in the SW continuation of the BFZ. (b) Structural map of the Lapurr-Lothidok volcanic area from Landsat imagery interpretation. The KFZ fault/fractures network, outlined by rhyolites intrusions, separates the Eocene-Oligocene Lapurr domain from the highly-faulted Miocene Lothidok domain. KFZ structures also affect the Pliocene/Recent lacustrine sediments to the east. (c and d) Detail view from Landsat ETM+ (170-057) scene and structural interpretation illustrating the emplacement of Miocene rhyolite intrusions along N50°E faults of the KFZ. (e) Topographic section from Murua Rith to Lothidok showing the SE fault downthrown along the KFZ (see figure 5b for location).*

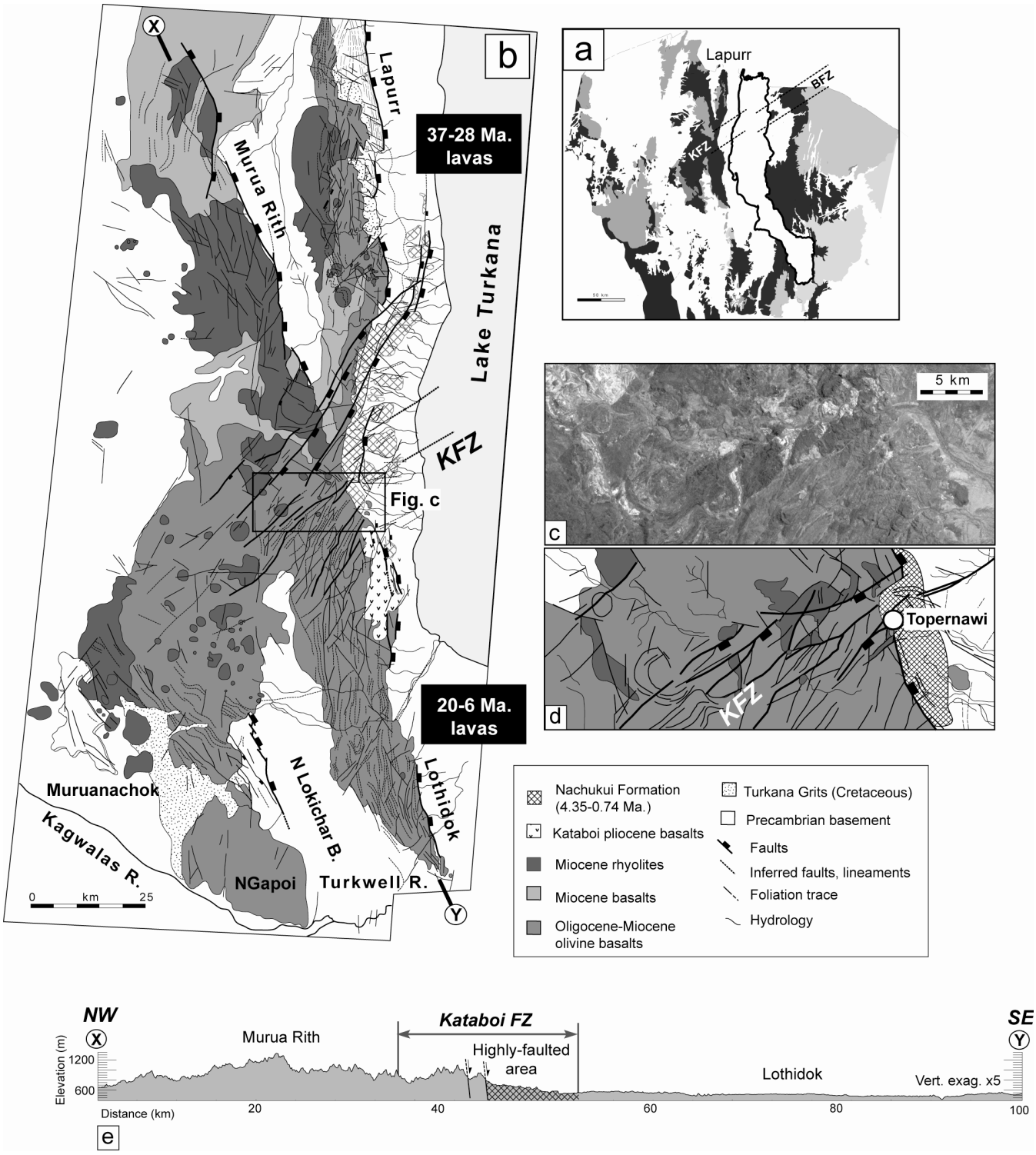
b
Lapurr
Murua Rith
37-28 Ma. lavas
Lake Turkana
KFZ
Fig. c
20-6 Ma. lavas
N Lokichar B.
Lothidok
Muruanachok
Kagwalas R.
NGapoi
Turkwell R.
0 km 25
X
Y
a
Lapurr
BFZ
KFZ
50 km
c
5 km
d
Topernawi
KFZ
Nachukui Formation (4.35-0.74 Ma.)
Kataboi pliocene basalts
Miocene rhyolites
Miocene basalts
Oligocene-Miocene olivine basalts
Turkana Grits (Cretaceous)
Precambrian basement
Faults
Inferred faults, lineaments
Foliation trace
Hydrology
NW
SE
Kataboi FZ
Murua Rith
Highly-faulted area
Lothidok
Vert. exag. x5
Elevation (m)
1200
600
Distance (km)
20
40
60
80
100
e

2.3.3.3. The N'Doto-Karisia fault zone

The NKFZ is the most important oblique fault zone recognized in the Turkana study area (Le Gall *et al.* in press) (Fig. 6). It forms a ~100 km-wide faulted corridor extending over more than 600 km at N140°E to the SE. It first follows the trace of the Finan Gos border fault on the western side of the Anza graben rift, before subdividing the Cretaceous rift into two sub-basins up to Lamu (see below) (Fig. 7a). This long-lived and polyphased transverse fault zone probably roots at depth into a basement brittle weakness zone. In the study area, the NKFZ is bounded by the Karisia (SW) and N'Doto *sensu stricto* (NE) faults. Its NW-SE surface expression corresponds to a typical lineament outlined by a number of discontinuous structures that differ in terms of age and tectonic style, and that consist from NW to SE of: (1) the faulted extremity of the wedge-shaped Lothidok Miocene lava plateau (Fig. 6a), (2) the prominent morphologic scarp between the N'Doto basement relief and the Anza-Chalbi Plain (Fig. 6b), and (3) the Matthews and Karisia linear faults extending on both sides of the Suguta Valley (Figs 2 and 6c). The importance of the NKFZ is also highlighted by subsurface data in the Turkana Cenozoic basins. The anomalous trend and high-density of extensional fault networks seismically-imaged in <3.7 Ma. strata of the North Kerio basin might represent T-type fractures related to the dextral reactivation of a deep basement-rooted discontinuity following the trace of the NKFZ (Le Gall *et al.* in press) (Fig. 6d). However, since there is no significant offset of basins in map-view, right lateral motion was probably minor. The earlier activity of the NKFZ during Cretaceous rifting is also documented in the Anza rift where its SE prolongation subdivides the basin into a non-volcanic (NE) and a highly-intruded (SW) sub-basins (Fig. 7a) (Reeves *et al.* 1987).

Fig. 6. *Structural evidence for the N'Doto-Karisia fault zone (NKFZ). (a) Structural interpretation of the Landsat ETM+ (scene 170-058) in the southern extremity of the Lothidok Miocene plateau (see figure 6c for location). The faulted origin of this boundary is evidenced by both the sharp southern termination of the volcanics and the cartographic virgation of faults and lava flows. (b) Detail view of SRTM digital elevation model showing the transverse faulted boundary of the N'Doto basement relief, SE of Lake Turkana (see figure 6c for location). The NKFZ is expressed by highly-fractured relief with a maximum topographic elevation of 2000 m in the cross-section XY drawn on map 6b. (c) Synthetic structural map of the Turkana rift showing the trace of the NKFZ. (d) Structural sketch illustrating 1) the variation of fault direction from NS to N20°E and 2) the increasing density of faults within the N140°E NKFZ.*

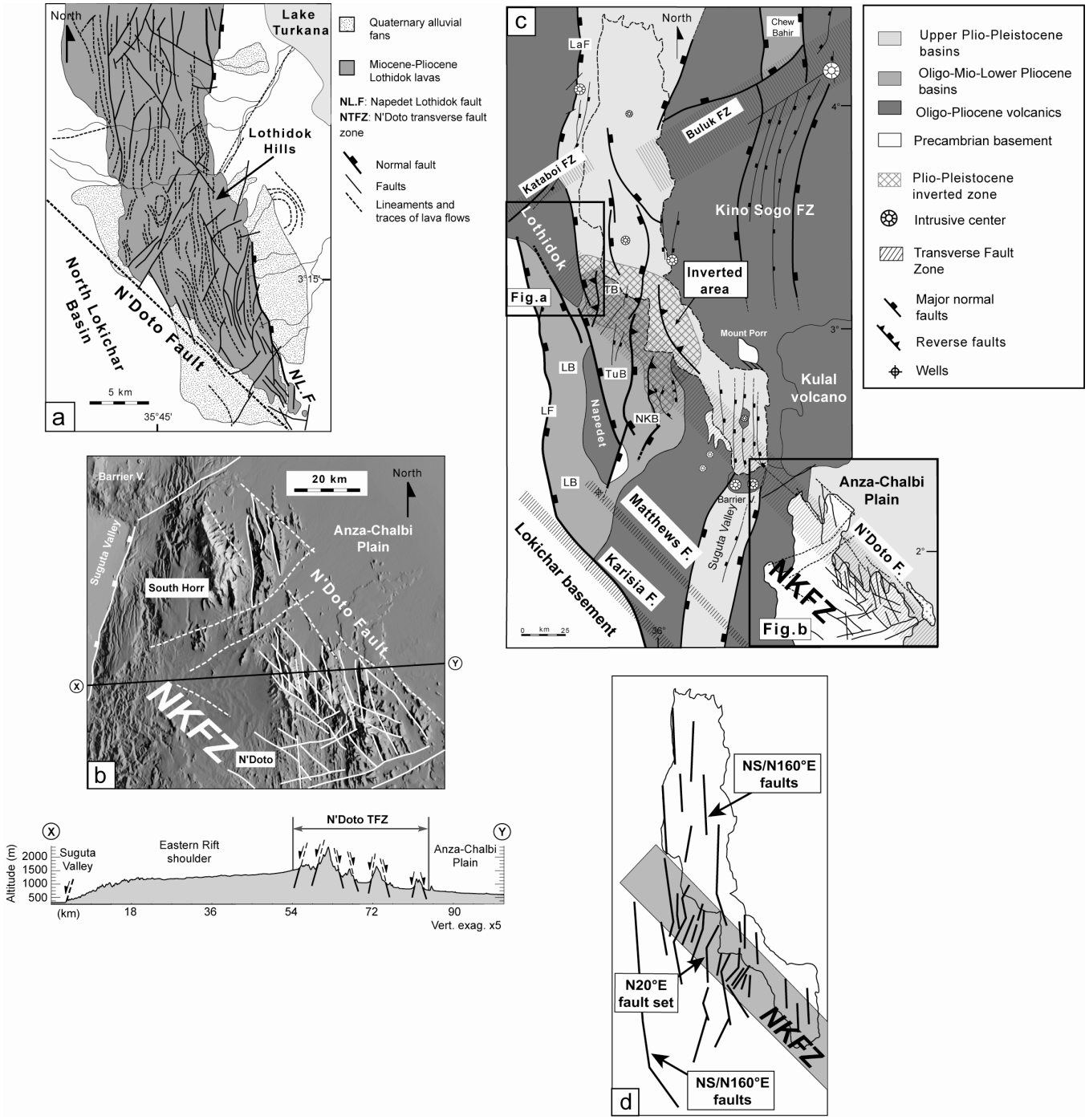
a
North
Lake Turkana
Lothidok Hills
North Lokichar Basin
N'Doto Fault
NLF
5 km
35°45'
3°15'
Quaternary alluvial fans
Miocene-Pliocene Lothidok lavas
NL.F: Napedet Lothidok fault
NTFZ: N'Doto transverse fault zone
Normal fault
Faults
Lineaments and traces of lava flows
b
Barrier V.
20 km
North
Suguta Valley
South Horr
Anza-Chalbi Plain
N'Doto Fault
NKFZ
N'Doto
X
Y
N'Doto TFZ
Altitude (m)
2000
1500
1000
500
Suguta Valley
Eastern Rift shoulder
Anza-Chalbi Plain
(km)
18
36
54
72
90
Vert. exag. x5
c
LaF
North
Chew Bahir
Bulluk FZ
Kataboi FZ
Lothidok
Fig.a
Kino Sogo FZ
Inverted area
TB
TuB
LB
LF
Napedet
NKB
Mount Porr
Kulal volcano
Barrier V.
Suguta Valley
Matthews F.
Karisia F.
Lokichar basement
Anza-Chalbi Plain
N'Doto F.
NKFZ
Fig.b
4°
3°
2°
36°
0 km 25
Upper Plio-Pleistocene basins
Oligo-Mio-Lower Pliocene basins
Oligo-Pliocene volcanics
Precambrian basement
Plio-Pleistocene inverted zone
Intrusive center
Transverse Fault Zone
Major normal faults
Reverse faults
Wells
d
NS/N160°E faults
N20°E fault set
NKFZ
NS/N160°E faults

2.3.4. Pre-rift geology

2.3.4.1. Cretaceous Anza Rift

In the study area, the non-volcanic sub-basin of the N140°E Anza rift forms an asymmetrical graben structure on reflection seismics (Morley *et al.* 1999b) (Fig. 7). Between the Lagh Bogal and Finan Gos bounding master faults, highly-faulted depocentres, as thick as 7 km, involve dominantly terrigeneous series Neocomian-Palaeogene in age (Bosworth & Morley 1994; Morley *et al.* 1999b) (Fig. 7b). The onset of extensional faulting is followed by a thermal sag phase of basin subsidence during Palaeogene time (Morley *et al*. 1999b). The 60 km bulk extension estimated by Dindi (1994) from cumulative fault heave measurements on seismic profiling might have caused significant crust/lithosphere attenuation beneath the Anza rift; however, available gravimetric and refraction data do not further constrain the deep structure of the Anza rift (Dindi 1994; Prodehl *et al*. 1994). The prolongation of the Anza rift to the NW beneath the Lake Turkana area is a long-standing debate. It is here suggested that the high-gradient isobath pattern of the pre-Cretaceous basement top at the northern extremity of the graben (Charsley 1987) (Fig. 7c) should rather indicate a synrift faulted boundary along the Hoi fault than a flexural margin extending to the NW beneath the Lake Turkana Cenozoic basins.

Fig. 7. *Structural framework of the Anza Cretaceous rift. (a) General map of the Anza graben that extends from Lamu (SE) to the eastern part of Lake Turkana (NW). It is subdivided into two subbasins along the 600 km-long NKFZ. (b) Structural cross-section through the Cretaceous-Palaeogene Anza rift (see figure 7a for location) (modified from Morley et al. 1999b). Two main inward-facing border faults control the 8 km-deep basins, e.g. the Lagh Bogal fault to the north and the Finan Gos fault to the south. (c) Structural map of the NW termination of the Anza graben in the vicinity of Lake Turkana (modern Lake Turkana is drawn on following maps as a geographical reference until 5 Ma. where it was formed). Isobath lines of the basement top, drawn from geological cross-sections (Charsley 1987), suggest a NW fault termination of the Anza trough along the N10°E-striking Hoi fault. Origin of discrete Cretaceous outcrops on the western Turkana area is discussed in the text. First-order transverse fault zones (NKFZ and BFZ) are also indicated on maps to illustrate their control of newly-formed structures. (d) Faults and striae diagram (n=12) from deformed 'Turkana Grits' in the Muruanachok area indicates a direction of extension in agreement with inferred Cretaceous extension (Morley et al. 1999b).*

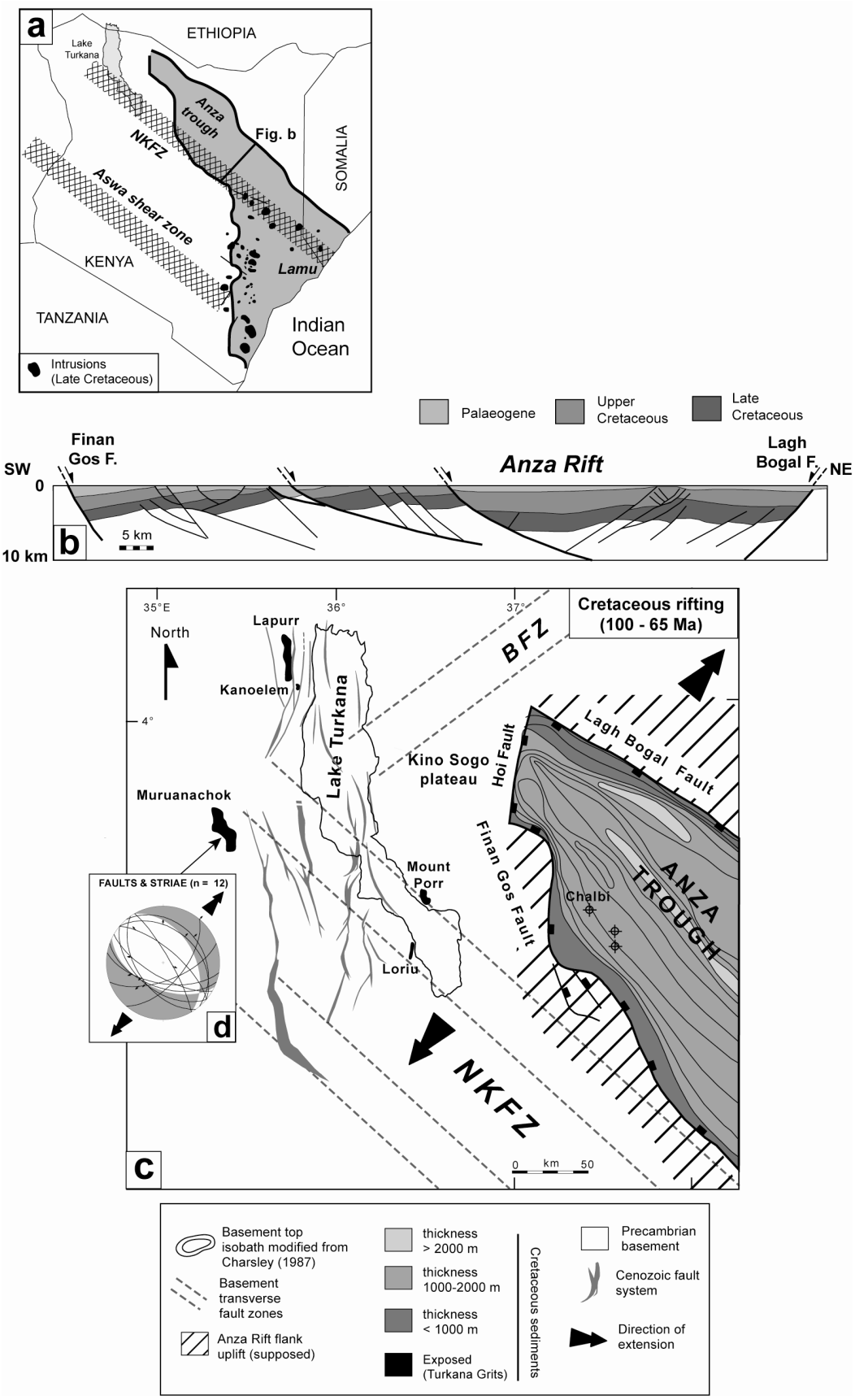
a
ETHIOPIA
Lake Turkana
Anza trough
Fig. b
NKFZ
SOMALIA
Aswa shear zone
KENYA
Lamu
TANZANIA
Indian Ocean
Intrusions (Late Cretaceous)
Palaeogene
Upper Cretaceous
Late Cretaceous
Finan Gos F.
Anza Rift
Lagh Bogal F.
SW
NE
0
10 km
b
5 km
35°E
36°
37°
North
4°
Lapurr
Kanoelem
Lake Turkana
Muruanachok
FAULTS & STRIAE (n = 12)
d
BFZ
Cretaceous rifting (100 - 65 Ma)
Kino Sogo plateau
Hoi Fault
Lagh Bogal Fault
Finan Gos Fault
ANZA TROUGH
Chalbi
Mount Porr
Loriu
NKFZ
c
0 km 50
Basement top isobath modified from Charsley (1987)
Basement transverse fault zones
Anza Rift flank uplift (supposed)
thickness > 2000 m
thickness 1000-2000 m
thickness < 1000 m
Exposed (Turkana Grits)
Cretaceous sediments
Precambrian basement
Cenozoic fault system
Direction of extension

This assumption is confirmed by the absence of Cretaceous and Lower Tertiary sequences between the basement and thin (~200 m) Oligo-Pliocene volcanics in the Kino Sogo plateau to the NW (Fig. 7c) (Wilkinson 1988; Haileab *et al.* 2004; Vétel *et al.* submitted). It is thus suggested that the Anza trough was initially disconnected from the basinal area(s) actually preserved on the western side of the Turkana area as scattered outcrops of quartz-bearing grits, presumably Cretaceous in age (Arambourg 1943; Williamson & Savage 1986; Morley *et al.* 1992) (Fig. 7c). Fault plane analysis in the (undated) Turkana Grits of the Muruanachok Hills (Fig. 7d) indicates a NE-SW direction of extension, i.e. compatible with the Cretaceous palaeo-stress field inferred to have controlled the N140°E-trending Anza rift (Morley *et al.* 1999b). On the other hand, the connection between these badly-constrained 'Turkana' Cretaceous basins and the Sudan rift to the NW is still questionable.

2.3.4.2. Proterozoic basement

Pre-Cretaceous crystalline basement rocks in the Turkana rift are principally exposed SW of the NKFZ and NE of the BFZ (Fig. 8). Their present-day elevated structural position mainly results from footwall block uplift along master Cenozoic extensional faults in the Hammer Range, Lapurr, Lokichar, Lokhone, Loriu and N'Doto areas. The Turkana basement rocks typically consist of highly-deformed granito-gneisses of the ~600 Ma. Proterozoic Mozambique belt (Shakelton 1993). The basement structural grain is dominated by ductile foliation planes, locally involved into coaxial folding (Figs 8b and c), but extending generally with a steep attitude at an almost NS constant azimuth. The ductile fabrics are cut by an intricate network of fault/fractures showing three main structural trends at NS, N50-70°E and N140°E (Fig. 8c).

Fig. 8. *Proterozoic basement framework in the Turkana rift. (a) Structural map of exposed basement rocks. Basement concealed by volcanics and thick sedimentary cover is also indicated. Foliation trace (with a consistent NS trend) and fractures (mainly N50°E and N140°E structures) are drawn on exposed rocks from Landsat images interpretation. (b) Detail view of Landsat ETM+ image (scene 170-058) showing a disrupted fold in Turkwell basement rocks. (c) Structural interpretation of figure 8b. Note the presence of two dominant fault/fracture networks trending at N50°E and N140°E dissecting the NS fold to the north and drawing a fish-bone pattern to the SW.*

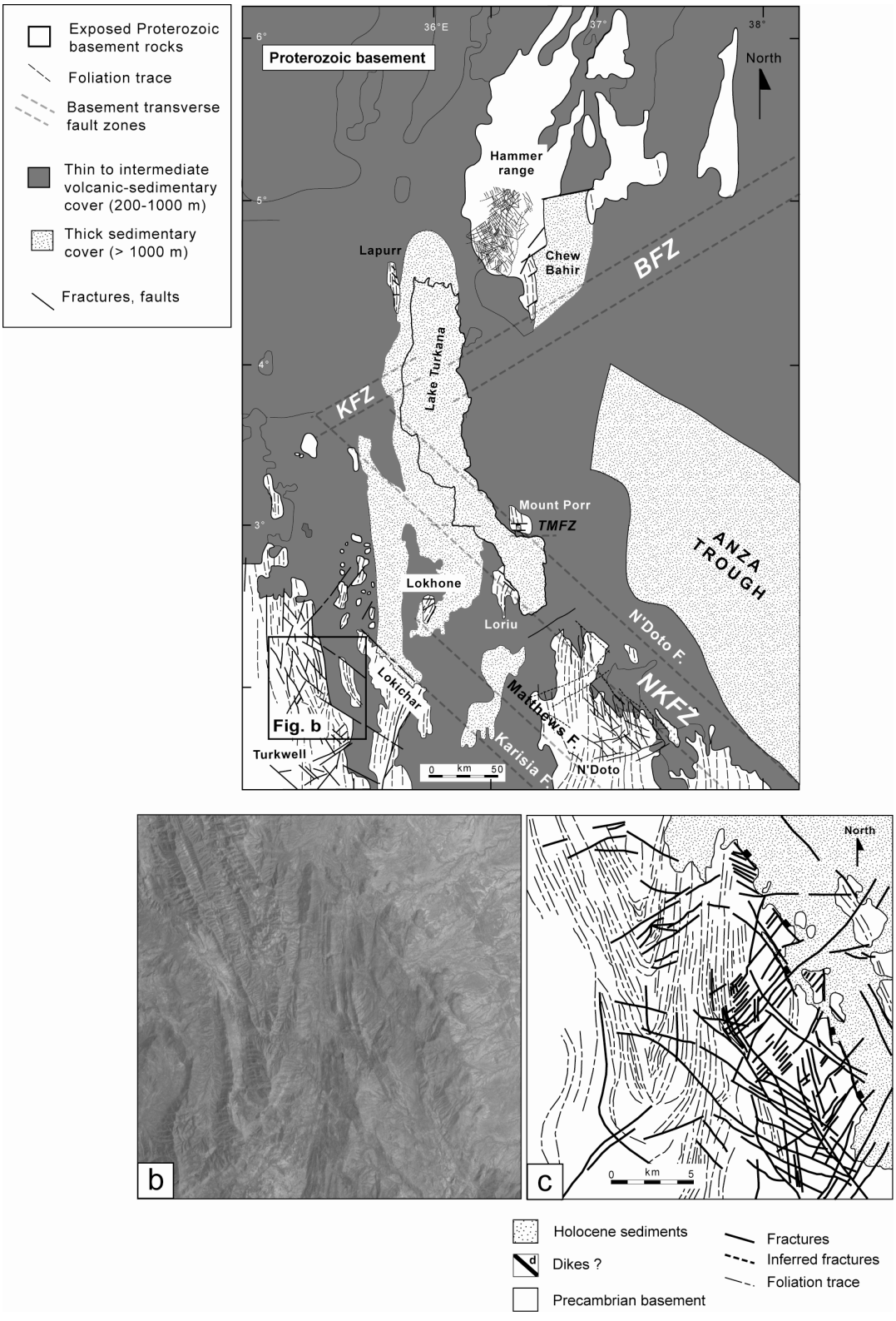
Exposed Proterozoic basement rocks
Foliation trace
Basement transverse fault zones
Thin to intermediate volcanic-sedimentary cover (200-1000 m)
Thick sedimentary cover (> 1000 m)
Fractures, faults
Proterozoic basement
North
Hammer range
Lapurr
Chew Bahir
BFZ
Lake Turkana
KFZ
Mount Porr
TMFZ
ANZA TROUGH
Lokhone
Loriu
N'Doto F.
NKFZ
Lokichar
Matthews F.
Fig. b
Turkwell
Karisia F.
N'Doto
0 km 50
b
c
0 km 5
Holocene sediments
Dikes ?
Precambrian basement
Fractures
Inferred fractures
Foliation trace

These structures are inhomogeneously distributed with an increase number of N50°E structures in the Hammer Range, i.e. in the vicinity of the similarly-trending BFZ, and a high density of N140°E faults on the western side of the NKFZ. Though very few age constraints exist for these brittle structures, most of them are presumed to have initiated as Proterozoic features by comparison with similar basement trends in other parts of the EARS (McConnell 1972; Smith & Mosley 1993; Coussement 1995; Morley 1999a).

2.4. Rift stages (45 Ma. to Present)

The first Cenozoic rifting stage occurs in the Turkana area at ~45 Ma., i.e. after a 15 Ma.-long quiescent period with no stratigraphic and tectonic records following the final synrift deposition (Late Cretaceous) in the Anza graben. The 45 Ma. Cenozoic rift history is marked by a succession of major magmatic pulses and fault/basin activity which both evolve in time and space as illustrated by the five structural maps of figures 9, 10, 11, 12 and 13.

2.4.1. Palaeogene-Lower Miocene (45-23 Ma.)

The earliest manifestation of magmatism in the Turkana area occurred, as early as 45-35 Ma., by the emplacement of dominantly basaltic lava flows in the Lotikipi-Lapurr area to the north (Walsh & Dodson 1969; Bellieni *et al.* 1981; Zanettin *et al.* 1983; Morley *et al.* 1999a) (Fig. 9).

Fig. 9. *Palaeogene-Lower Miocene (45-23 Ma.) event in the Turkana area. (a) 'Restored' structural map showing magmatic and basinal domains. Bounding faults are drawn from the isopach map of Morley et al. 1999a. Contours of volcanic domains are smooth, compared to fault/basin configuration, because of the limitations (dating, ...) mentioned in the text. The losange-shaped South Lokichar basin occurred around 35 Ma. in the southern part of the Turkana area, within the NKFZ area and outside the northern volcanic domain. (b) Diagram of dykes direction from the Kanoelem complex compatible with an EW extension and in agreement with the newly-formed NS Lokichar fault. (c). Interpreted Amoco TVK 110 seismic lines through the westerly-facing Oligo-Miocene South Lokichar half-graben (SLB on figure 9a). (d) The west-facing Allia Bay normal fault within the central magmatic domain controlled the syn-rift shape of the Oligocene Balesa Koromto lavas.*

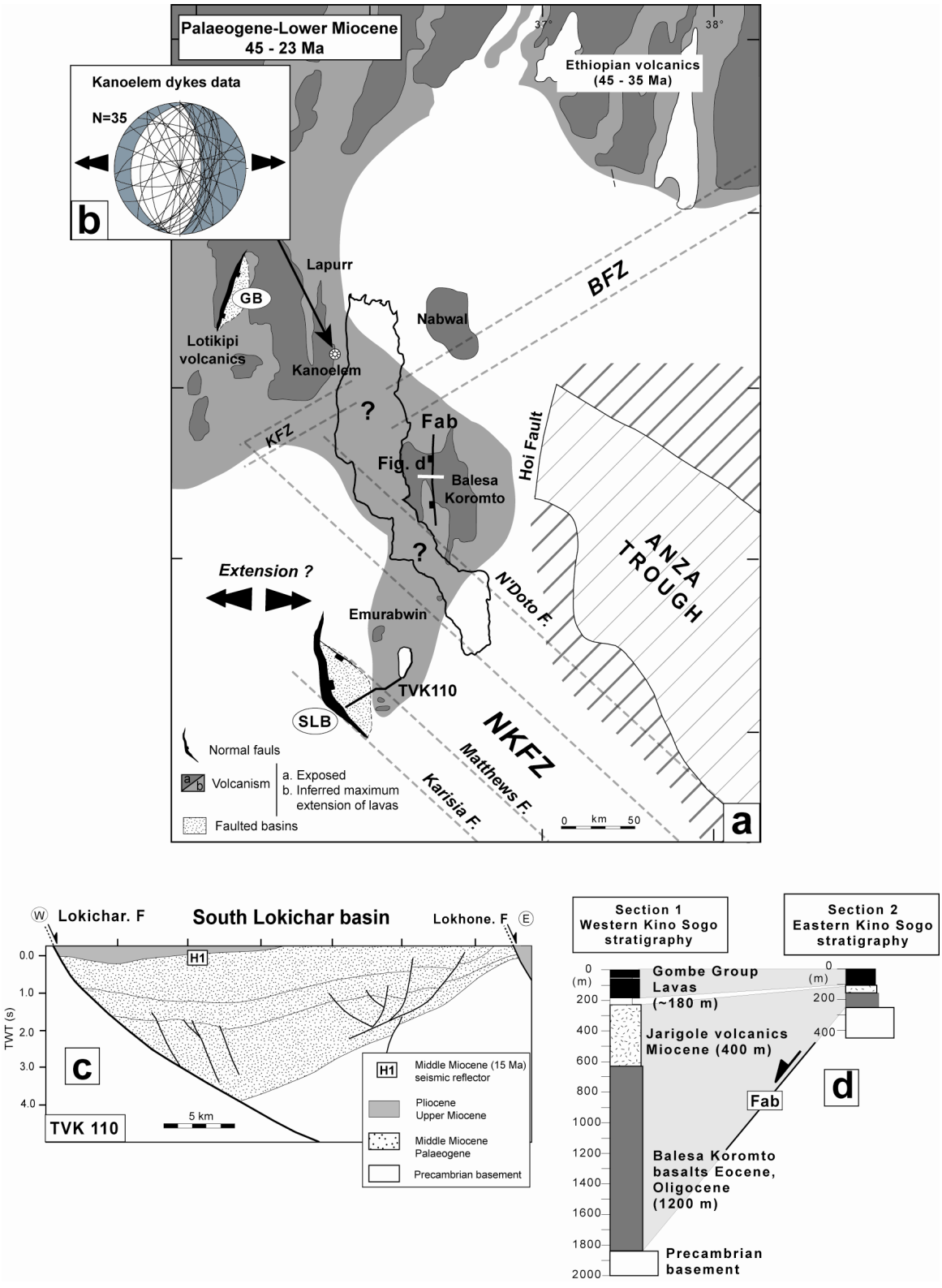
Palaeogene-Lower Miocene
45 - 23 Ma
Ethiopian volcanics
(45 - 35 Ma)
37°
38°
Kanoelem dykes data
N=35
b
Lapurr
GB
Lotikipi
volcanics
Kanoelem
Nabwal
BFZ
KFZ
?
Fab
Fig. d
Balesa
Koromto
Hoi Fault
ANZA
TROUGH
?
Extension ?
N'Doto F.
Emurabwin
TVK110
SLB
NKFZ
Matthews F.
Karisia F.
Normal fauls
Volcanism
a. Exposed
b. Inferred maximum
extension of lavas
Faulted basins
0 km 50
a
W
Lokichar. F
South Lokichar basin
Lokhone. F
E
H1
TWT (s)
0.0
1.0
2.0
3.0
4.0
c
TVK 110
5 km
H1
Middle Miocene (15 Ma)
seismic reflector
Pliocene
Upper Miocene
Middle Miocene
Palaeogene
Precambrian basement
Section 1
Western Kino Sogo
stratigraphy
Section 2
Eastern Kino Sogo
stratigraphy
0
(m)
200
400
600
800
1000
1200
1400
1600
1800
2000
Gombe Group
Lavas
(~180 m)
Jarigole volcanics
Miocene (400 m)
Fab
d
Balesa Koromto
basalts Eocene,
Oligocene
(1200 m)
Precambrian
basement

These volcanic complexes, up to 3 km-thick in the Lotikipi synformal depression (Wescott *et al.* 1999), connect directly northwards into the South Ethiopian volcanic domain, and they probably represent the distal part of the extensive lava flood system linked to the first plume impact to the north, in present Ethiopia (Ebinger *et al.* 2000). Early volcanics extend as far south as modern Lake Turkana, in the Nabwal, Balesa Koromto (proto-Kino Sogo), and Emuruabwin areas, as NS-elongated complexes (Dunkley *et al.* 1993; Morley *et al.* 1999a) limited to the east by the faulted termination of the Anza Cretaceous graben (Hoi fault). Due to the poor resolution of the offshore TVB reflection seismic lines below 2-3 sec. TWT., it is difficult to assert whether the Oligo-Miocene volcanics of the proto-Kino Sogo and Lapurr uplifted fault blocks linked laterally beneath Pliocene series in Lake Turkana basins. NE of the Anza rift, the absence of initial volcanic series might result from Late Cretaceous rift flank uplift relief still preserved in Palaeogene times.

The first occurrence of strain are observed at ~35 Ma., e.g. about 10 Ma. later than initial volcanism, in the Lokichar half-graben south of the magmatic domain (Figs 9a and c). The oldest sediments that accumulated in the hangingwall of the Lokichar NS master fault formed a losange-shaped depocentre (40x20 km), controlled by the N140°E trend of the Karisia and Matthews faults (Figs 2 and 9). The smaller and poorly-constrained Gatome fault-bounded basin in the Lapurr-Lotikipi volcanic area might predate extrusion of Oligo-Miocene lavas (Wescott *et al.* 1999). Evidence for syn-magmatic extensional deformations are documented in the proto-Kino Sogo volcanic domain by rapid lava thickness variations (1200 to 100 m) along the so-called Allia Bay westerly-directed fault (Vétel *et al.* submitted) (Fig. 9d). The EW direction of extension governing the first increment of rifting in the Turkana area is mainly deduced from the dominant NS strike of the main syn-depositional fault network. A similar result is obtained from the swarm of NS-trending dykes in the Kanoelem area which are likely to be the feeder conduits of the Lapurr Oligocene lavas (Figs 9a and b).

2.4.2. Lower Miocene (23-15 Ma.)

The effusive products of a second magmatic pulse (18-11 Ma.) linked to an active plume centred over Ethiopia (the nature of this plume is still debatable) (Stewart & Rogers 1996;

Ebinger & Sleep 1998; George *et al.* 1998; Ebinger *et al.* 2000) overly with no major changes the broad Ethiopian rifted zone to the North (Fig. 10a). Conversely, magmatism distribution changed markedly in the Turkana area resulting in the concentration of the volcanic activity in the Lothidok-Kino Sogo (LKS) province between the BFZ, NKFZ and Hoi faults. The lack of Lower Miocene sedimentary deposits in this elliptic-shaped volcanic area is probably due to its thermal-induced domal topography (see below). At this stage, a number of intrusions are emplaced along rift-parallel faults (Jarigole intrusive centers) and N50°E transverse structures of the KFZ and BFZ (21-14 Ma. Jibisa complex; Hackman *et al.* 1990) (Fig. 10a).

Coeval with the 23-15 Ma. volcanism, extensional strain largely developed over a ~250 km-wide zone encompassing downthrown sedimentary basins around the LKS volcanic dome. Three main types of deformation are reported as a function of (1) the volcanic nature of the terrain, (2) the inherited or (3) the newly-formed origin of the resulting basins. To the west, deformation migrates both northwards and eastwards from the initial, but still active, South Lokichar basin (Figs 10a and b). Thick depocenters (1-2 km) developed in the easterly-facing North Lokichar half-graben, limited to the east by the West Napedet-Lothidok fault, and to the west by the northern prolongation of the Lokichar master fault (Fig. 10a). Concomitantly, two smaller-sized half-grabens (20x30 km) with a dominant western polarity, initiated to the east in the North Kerio area, following N10-20°E basement ductile fabrics. A third discrete basin probably formed further east (South Lake Turkana basin) at the extremity of a wedge-shaped extended zone narrowing to the east and encompassed within the NKFZ. North of the BFZ, extension resulted in the isolated Chew Bahir graben (Gabriel & Aronson 1987; Ebinger *et al.* 2000), on the eastern side of the contemporaneous Nabwal-Nakwele volcanic province (Fig. 10a). Its deep geometry is unknown whereas its surface fault pattern clearly reflects the influence of N50°E (Buluk-type) trends along its southern oblique extremity (Vétel *et al.* submitted) and its dextrally offset border fault to the west. Evidence for extensional fault reactivation are also documented at this stage outside the NKFZ, along Cretaceous faults bounding the northwestern termination of the Anza rift (Figs 10a and c).

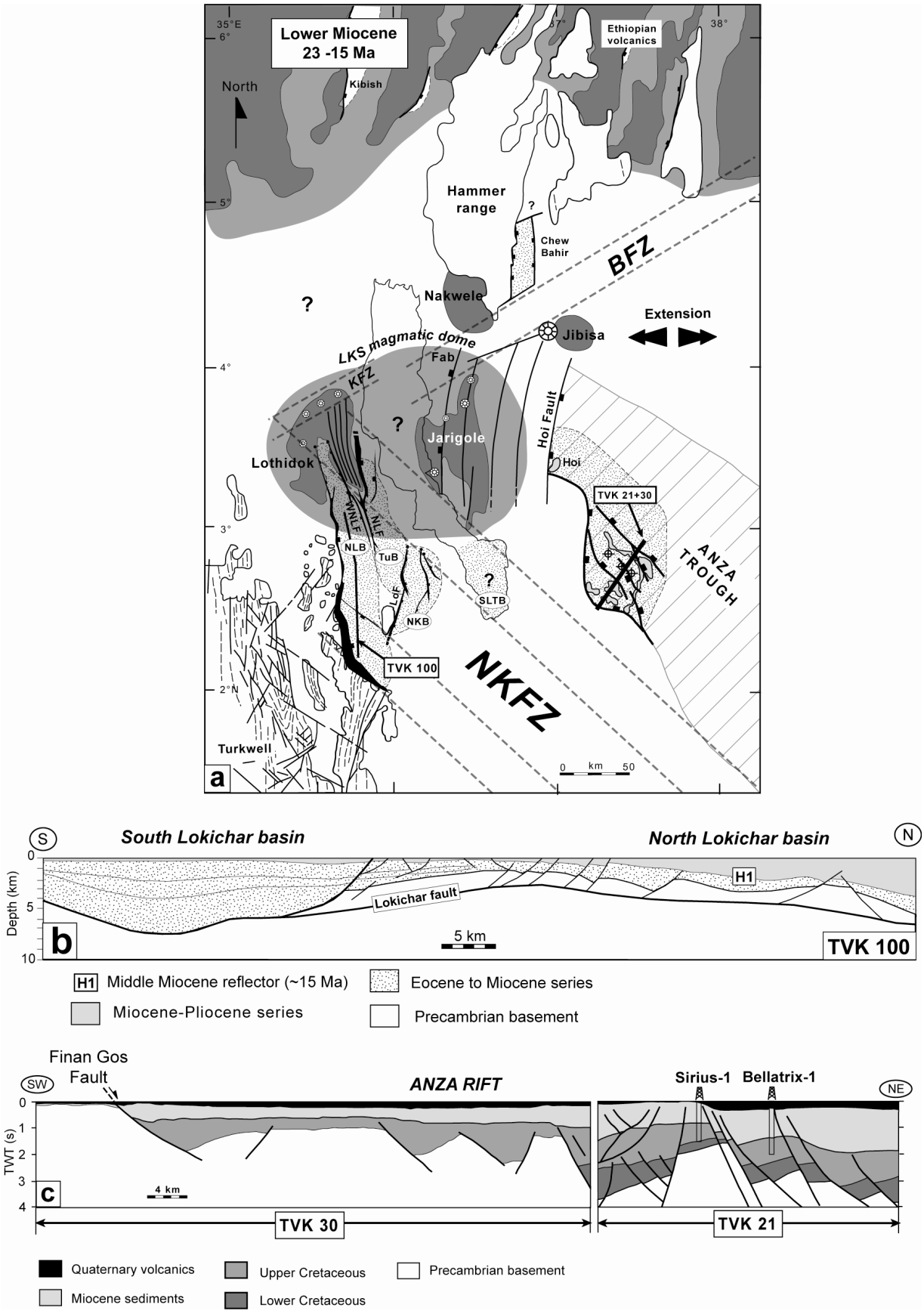
Lower Miocene
23 -15 Ma
North
Kibish
Ethiopian volcanics
Hammer range
Chew Bahir
BFZ
Nakwele
Extension
Jibisa
LKS magmatic dome
Fab
KFZ
Jarigole
Hoi Fault
Hoi
Lothidok
TVK 21+30
WNLF
NLF
NLB
TuB
SLTB
NKB
ANZA TROUGH
TVK 100
NKFZ
Turkwell
0 km 50
a
South Lokichar basin
North Lokichar basin
S
N
Depth (km)
H1
Lokichar fault
5 km
TVK 100
b
H1 Middle Miocene reflector (~15 Ma)
Eocene to Miocene series
Miocene-Pliocene series
Precambrian basement
Finan Gos Fault
SW
ANZA RIFT
Sirius-1
Bellatrix-1
NE
TWT (s)
4 km
c
TVK 30
TVK 21
Quaternary volcanics
Upper Cretaceous
Precambrian basement
Miocene sediments
Lower Cretaceous

Fig. 10. *Lower Miocene (23-15 Ma.) event in the Turkana area. (a) On the structural map, magmatism is confined in a central domain (LKS) which is affected by dense faulting over the Lothidok and Jarigole areas. Three basinal domains are distributed at the periphery of the faulted magmatic domain: the Lokichar-Kerio basins (SW), the NW reactivated part of the Anza rift and the newly-formed Chew Bahir trough to the north. (b) Interpreted Amoco TVK 100 along-strike seismic sections in the Lokichar basin (see location on figure 10a). (c) Composite geological section from interpreted Amoco TVK 30 and 21 seismic lines through the SW Anza reactivated rift basin.*

Stratigraphic correlation between seismic data and surface outcrops leads us to regard the 'Turkana Grits' exposed in the Chalbi Plain as Lower Miocene series deposited in a 150x50 km faulted basin, ~2 km-deep (Bellatrix well; Morley *et al.* 1999b), bounded to the west by the Finan Gos and Hoi rejuvenated faults (Figs 10a and c). North of the main Lokichar-Kerio basinal area, extension is assumed to have also occurred in the LKS volcanic dome as expressed by the dense array of highly-eroded faults actually observed on its flanks in the Lothidok and Jarigole plateaus (Figs 5b and 10a). The deformation in the median (and subsequently depressed) part of the initial magmatic dome is unknown. With respect to the previous rift structures, most of extensional faults developed at this stage with a constant NS-N20°E trend, probably in response to a persistent EW-directed extensional stress.

2.4.3. Upper Miocene (15-6 Ma.)

Major changes occurred in the overall tectono-magmatic organisation of the Turkana rift during Upper Miocene (Fig. 11). Magmatism continued to migrate southwards from the LKS central domain (which became inactive) into the Lokichar-Kerio area where lava flow extrusion and sedimentary deposits interfere for the first time. However, the associated feeding centers, such as the Napedet and Lojamei dyke swarms, dated at 13-17 Ma. (K/Ar) in the present work, were preferentially extruded along NS inter-basinal structural highs (Fig. 11). Further east, the N10°E Longipi-Parkati magmatic axis outlined the trace of the proto-Suguta trough. The only evidence of magmatic activity to the north are the Sabarei basaltic flows, confined within the BFZ, whilst the proto-Kino Sogo to the south was magmatically inactive.

Fault/basin development is dominated by the abandonment of the most external basins (South Lokichar and NW Anza), resulting in the focussing of strain in the median part of the

extended zone. Then, extension propagated northwards across the NKFZ and led to the formation of (poorly-constrained) subsiding depositional areas along the axis of modern Lake Turkana. North of the KBFZ, the synchronous activity of the Chew Bahir (to the east) and the so-called (newly-formed) Lapurr-Murua Rith (to the west) basins determined a three-arm rift system centered on the axial zone. The consistent NS direction of the propagating fault network is still compatible with an EW extension for this time period.

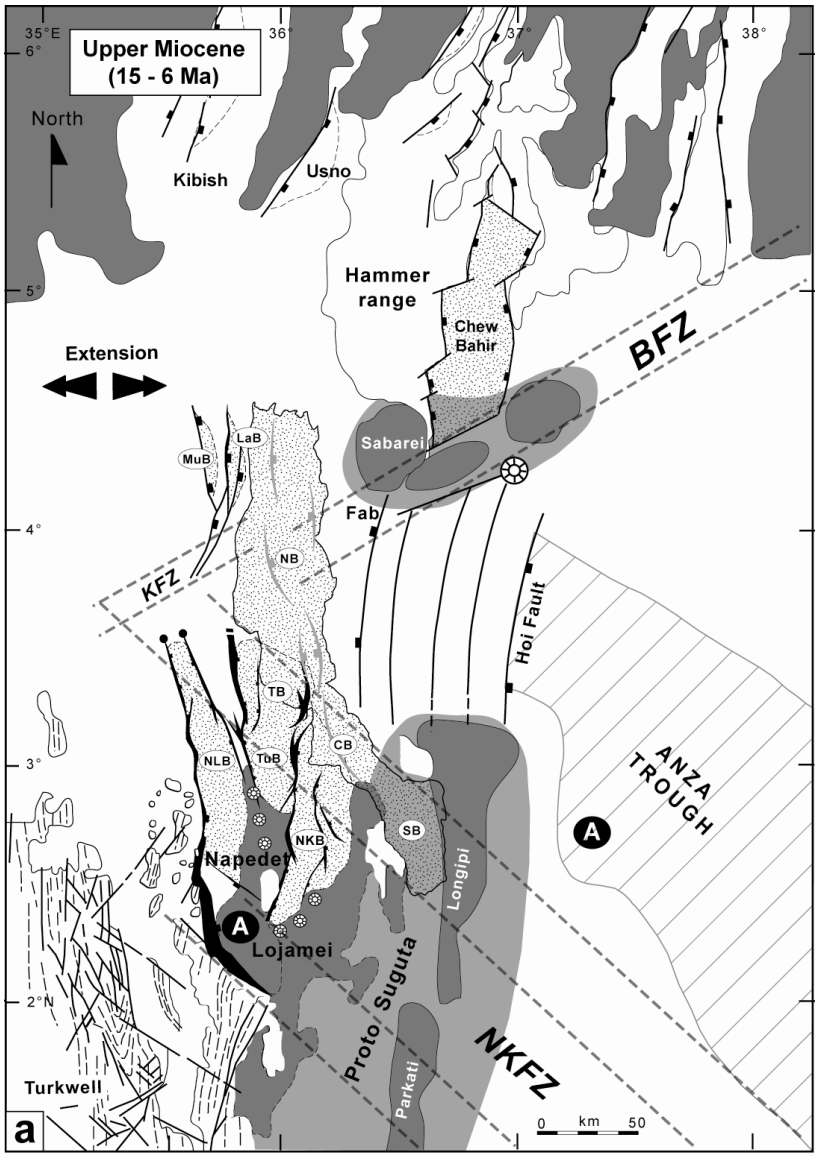

Fig. 11. *Upper Miocene (15-6 Ma.) event in the Turkana area. Magmatism migrates southwards over the Lokichar-Kerio domains. BFZ to the north is also the location of intrusives while the central LKS domain is temporarily abandonated. Deformation migrates northwards and concentrates through the Lake Turkana basins whereas external basins are abandonated (A).*

2.4.4. Pliocene (6-2.6 Ma.)

The 'restored' structural maps applied to the Pliocene (6-2.6 Ma.) and Recent (2.6 Ma.-Actual, see below) periods are better constrained because they benefit from both good resolution seismic images and accurate digital elevation models (Figs 12 and 13).

After a 6 Ma. quiescent phase, Pliocene magmatism shifted markedly to the east and formed a 6000 km² fissure-type volcanic province over the NW-SE Cretaceous Anza rift system (Fig. 12). A huge volume of lava flows, with a cumulative thickness of 10's meters (Hackman *et al.* 1990), was emitted from NE-SW-oriented fissures outlined by the elongated Marsabit and Huri shield volcanoes. This volcanic province encompassed to the west the Gombe Group (5.79-3.28 Ma.; Wilkinson 1988; Haileab *et al.* 2004) in the Kino Sogo plateau (see figure 9d).

A modest, but widely-distributed, intra-basinal volcanic episode also expressed further west in the Turkana basins (excepted the Lokichar half-graben) as a ~30 m-thick interlayered lava sequence (H2 on figure 3), dated at 5.1+-0.2 Ma. (Elyie Springs borehole) (Morley *et al.* 1992; Shell 1992). The 4.41-5.05 Ma. Kataboi basalts (K/Ar ages, present work) formed a NS-trending unit at the western extremity of the Pliocene magmatic province (Fig. 12).

The focusing of strain initiated during Upper Miocene throughout the Lake Turkana area *sensu lato* was amplified by the complete arrest of faulting in the North Lokichar basin to the west, whereas the small half-grabens evolving in the northern half of Lake Turkana with alternating polarities started to link laterally (Dunkelman *et al.* 1989). To the south, the graben-like Suguta trough nucleated along the earlier N10°E volcanic axis (Bosworth & Maurin 1993). At this stage, structural complexities locally recorded by the extensional fault networks in the Kerio and Turkwell basins (increasing fault density and changing strikes) are assigned to the dextral reactivation of the NKFZ at depth under changing stress field conditions (permutation $\sigma1/\sigma2$ and clockwise rotation (~20°) of the principal stress axes) (Le Gall *et al.* in press). The estimated N110°E direction of extension is compatible with the N30°E orientation of the tensile crack/fracture networks that might have guided the ascent of magma beneath the eastern shield volcanoes (see below).

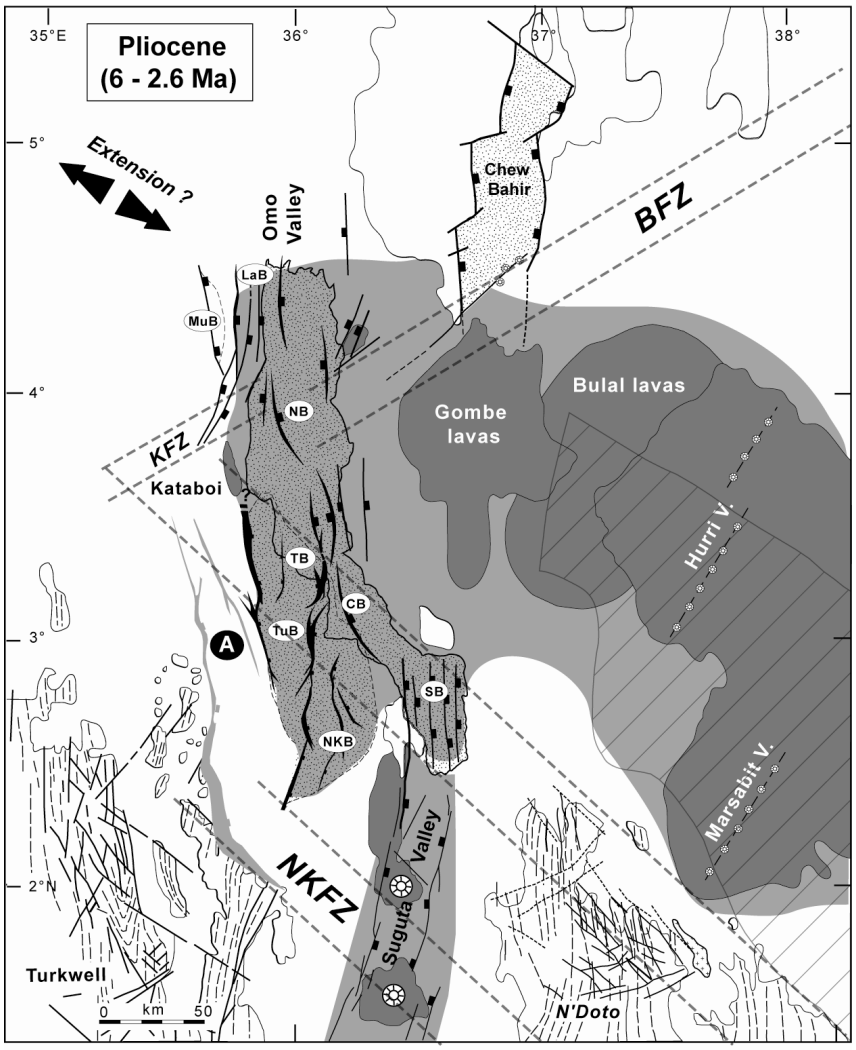

Fig. 12. *Pliocene (6-2.6 Ma.) event in the Turkana area. Modest magmatism is still present in the central Turkana area while the Anza domain is the location of widespread fissural-type lavas for the first time erupted from two major N30°E-elongated shield volcanoes. Deformation continues to concentrate in the central NS axes and propagates southwards via the Suguta trough. The Chew Bahir graben is still isolated to the NE and propagates northwards into the Ethiopian rift.*

2.4.5. Upper Pliocene-Present (< 2.6 Ma.)

During the last rifting stage, a new N10-20°E magmatic axis formed in the northern prolongation of the Suguta axial graben. It is outlined by the Dukana (0.9 Ma.), Asie (2.7 Ma.) and Kulal (1.7 Ma.) volcanoes (Charsley 1987; Dunkley *et al.* 1993) that are partly faulted (Figs

13 and 14e), hence suggesting a lateral shift of strain eastwards into the previous Anza rift. The inferred broadening of the extended zone at this stage is confirmed by the nucleation of a new (poorly-known) rift branch in the Ririba area, to the NE (Figs 2, 13 and 14f). This atypical extensional structure (100x10 km) dies out southwards into the ~1 Ma. Huri lavas and it gives way northwards, *via* the BFZ, into a wider graben-like basin similar to the Chew Bahir, and referred to as the South Amaro basin. In the main central deformed zone, the ongoing extensional development of faulted basins is accompanied by two additional processes.

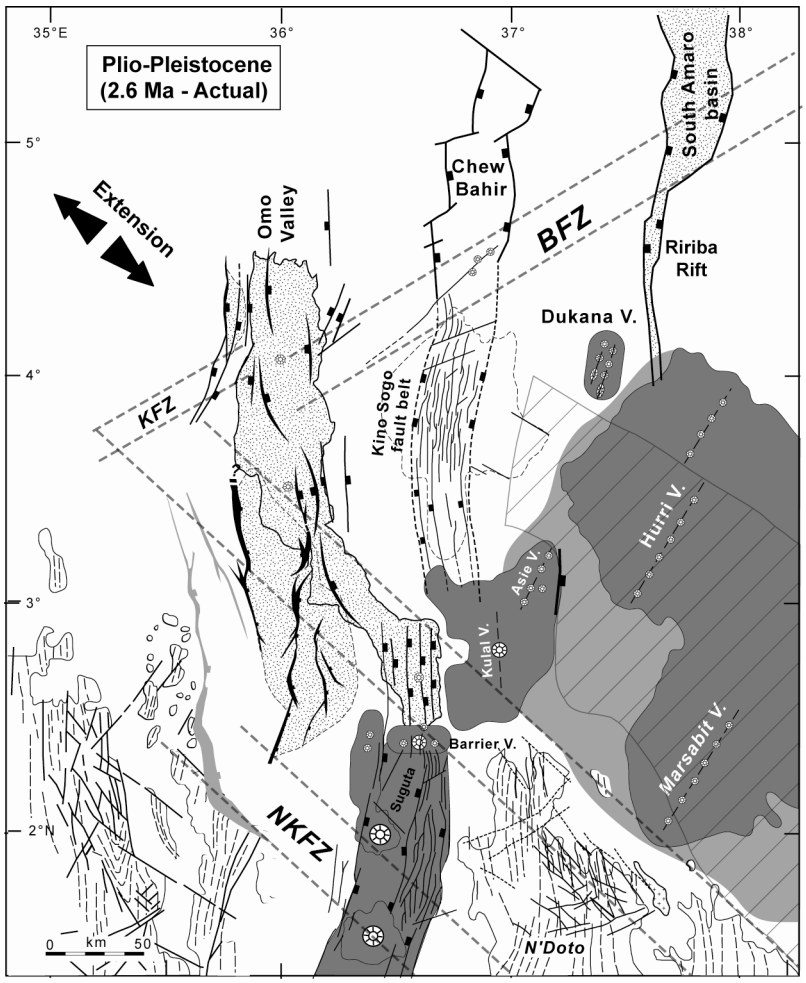

Fig. 13. *Plio-Pleistocene (2.6 Ma.-Present) event in the Turkana area. The Turkana rift acquires its present-day arrangement by a focusing of volcanism along the Suguta axial valley and in the off-axis province to the east (Kulal, Asie, Huri and Marsabit shield volcanoes). Two newly-formed rift branches also developed along the intermediate Kino Sogo area and the eastern Ririba-South Amaro sector which is widely controlled by the BFZ.*

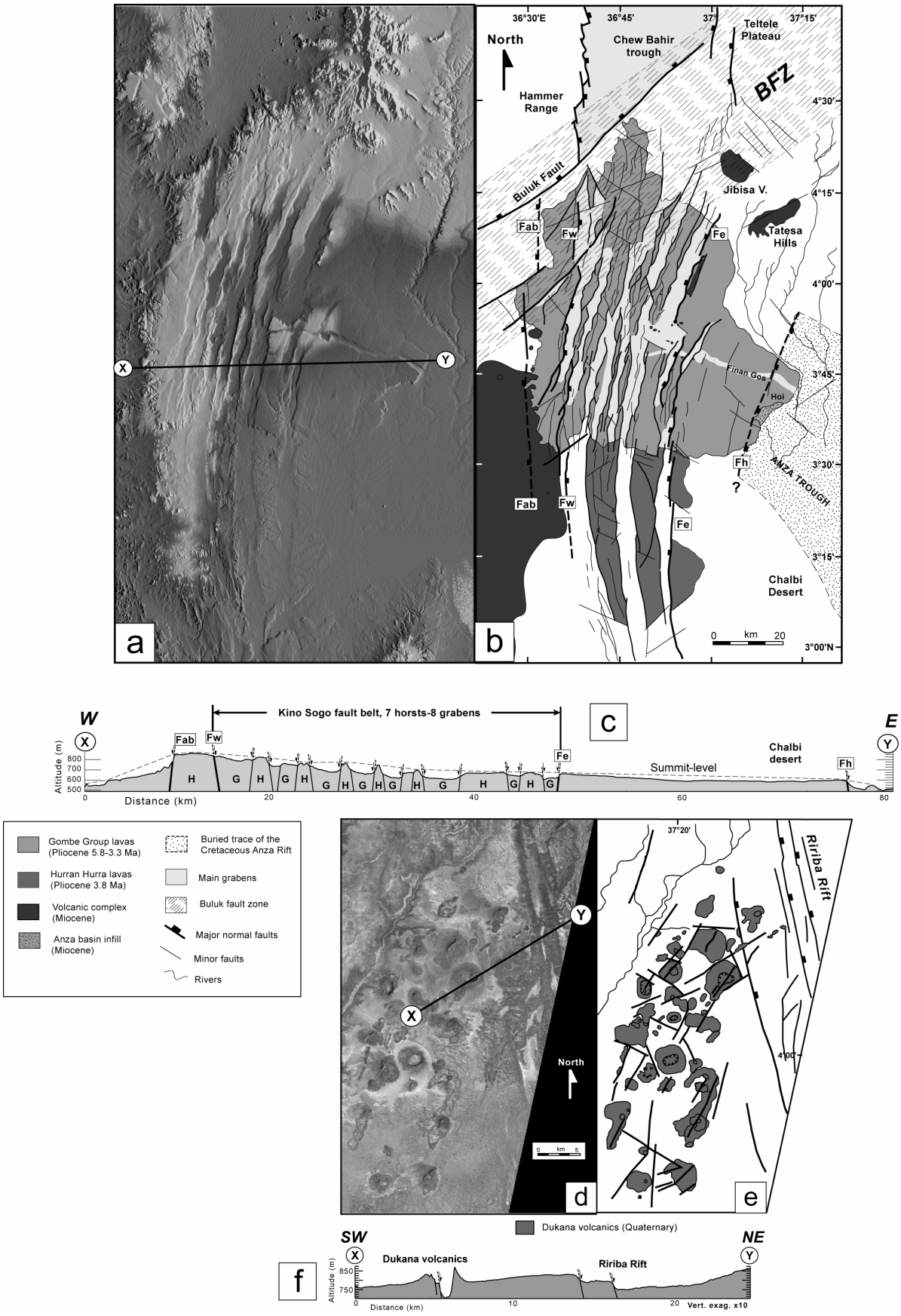
a
b
X
Y
North
36°30'E
36°45'
37°
37°15'
Teltele Plateau
Chew Bahir trough
BFZ
Hammer Range
Buluk Fault
Jibisa V.
Tatesa Hills
Fab
Fw
Fe
Finan Gos
Hoi
Fh
?
ANZA TROUGH
Chalbi Desert
4°30'
4°15'
4°00'
3°45'
3°30'
3°15'
3°00'N
0 km 20
c
W
E
Kino Sogo fault belt, 7 horsts-8 grabens
Summit-level
Chalbi desert
Altitude (m)
800
700
600
500
H
G
Distance (km)
0
20
40
60
80
Gombe Group lavas (Pliocene 5.8-3.3 Ma)
Hurran Hurra lavas (Pliocene 3.8 Ma)
Volcanic complex (Miocene)
Anza basin infill (Miocene)
Buried trace of the Cretaceous Anza Rift
Main grabens
Buluk fault zone
Major normal faults
Minor faults
Rivers
d
e
North
0 km 5
37°20'
Ririba Rift
4°00'
Dukana volcanics (Quaternary)
f
SW
NE
Dukana volcanics
Ririba Rift
Altitude (m)
850
750
0
10
20
Distance (km)
Vert. exag. x10

Fig. 14. *Structural evidence for recent/active deformations in the Kino Sogo and Ririba eastern provinces. (a) Detail view of SRTM digital elevation model on the recent Kino Sogo grid fault (<3 Ma.). (b) Structural interpretation of figure 14a showing the 150x40 km regular horst and graben system of the Kino Sogo fault belt cutting through the Pliocene Gombe lava plateau (see Vétel et al. submitted). (c) Topographic section across the Kino Sogo fault system (vert. exag. x10). The asymmetric easterly-tilted Kino Sogo 'block' is cutted by a regular normal fault system without dominant structures (see figure 14a for location). (d) Detail view of Landsat image (scene 169-057) on the recent (~0.9 Ma.) Dukana volcanic complex (see location on figure 13). (e) The structural interpretation of figure 14d highlights the existence of NS to N50°E faults affecting the recent Dukana volcanic cones and lava flows in the vicinity of the Ririba rift. (f) Topographic section from SRTM data across the Dukana volcanic complex and the Ririba rift (location on figure 14d).*

Firstly, the build-up of a dense NS extensional grid fault across the Kino Sogo volcanic plateau (Figs 14a and c), e.g. between the Chew Bahir and the Suguta-South Lake Turkana basins, tends to form a coalescent and highly-segmented branch, 40 km-wide, on the eastern side of the Lake Turkana fault/basin pattern (Vétel *et al.* submitted). Secondly, partial inversion of the (N10°E) intricate extensional structures linked to the NKFZ in the Kerio and Turkwell basins (see above) is assigned to its more suitable orientation with respect to the still rotating shortening direction (N40°E) (Le Gall *et al.* in press).

2.5. Controlling factors on the Turkana rift evolution

The five rift stages described above for the last ~45 Ma. clearly illustrate the complex tectono-magmatic history of the Turkana area, in relation with a number of parameters, such as structural inheritance, magmatism and stress-field variations, that interacted at various stages of the rift evolution. Although it is difficult to discriminate the respective role of each factor, some new insights about dynamics of crustal extension are discussed below by comparison with concepts recently applied on extensional systems from natural examples and analogue modelling (e.g. Lezzar *et al.* 2002; Corti *et al.* 2003; Ziegler & Cloetingh 2004). Some assumptions about the influence of deeper processes related to the impinging of plume(s) onto a pre-existing heterogeneous lithosphere are also attempted.

2.5.1. Shallow/surface processes

The pre-rift arrangement of the Turkana area is dominated by both Proterozoic basement fabrics and Cretaceous rift structures (Fig. 15a). The consistent NS-striking foliation trace in the basement is cut by two first-order transverse fault zones (NKFZ and BFZ-KFZ) that intersect at high angle (~90°) and are bisected by the inferred EW extension that prevailed during Cenozoic rifting until ~5 Ma. The sequential rift development depicted on cartoons of figure 15 highlights the key-role played by the N50-70°E and N140°E inherited discontinuities on (1) kinematics of the rift fault pattern and (2) the spatial distribution of magmatism. Additional complexities are also due to the mutual interaction between magmatic and faulting processes.

2.5.5.1. Role of N140°E discontinuities

The N140°E fault network in the Turkana rift, referred to as the ~100 km-wide NKFZ, is part of a first-order transverse discontinuity extending 600 km further SE throughout the Cretaceous rift system (see above) (Figs 6 and 7). This long-lived transverse fault zone probably roots at depth into a basement brittle weakness zone. During Cenozoic rifting, kinematics of fault structures within the NKFZ varied as a function of changing stress field conditions, and consequently their influence on fault/basin development evolved with time. Four successive kinematic stages are distinguished within the ~45 Ma. rift history (Fig. 15).

(1) During initial increment of strain (Fig. 15b), the main basinal area in the South Lokichar sector is strictly confined within the NKFZ. Timing and 3D-architecture of the oldest depocentres in this area (Morley *et al.* 1992) provide important clues about the sequential development of fault propagation in relation with the reactivation of pre-existing transverse discontinuities recording EW extension. The locking of the northerly-propagated Lokichar fault along the Matthews transverse fault suggests that the arrest of fault-tip propagation is caused by the acute angle (~50°) and the opposite sense of dip of the two intersecting fault networks (fault interaction type FIT_1 on figure 16). In contrast, the obtuse angle (140°) and the similarly-facing direction of the two cross-cutting fault systems to the south (Karisia) are more favorable for extension (FIT_2 on figure 16).

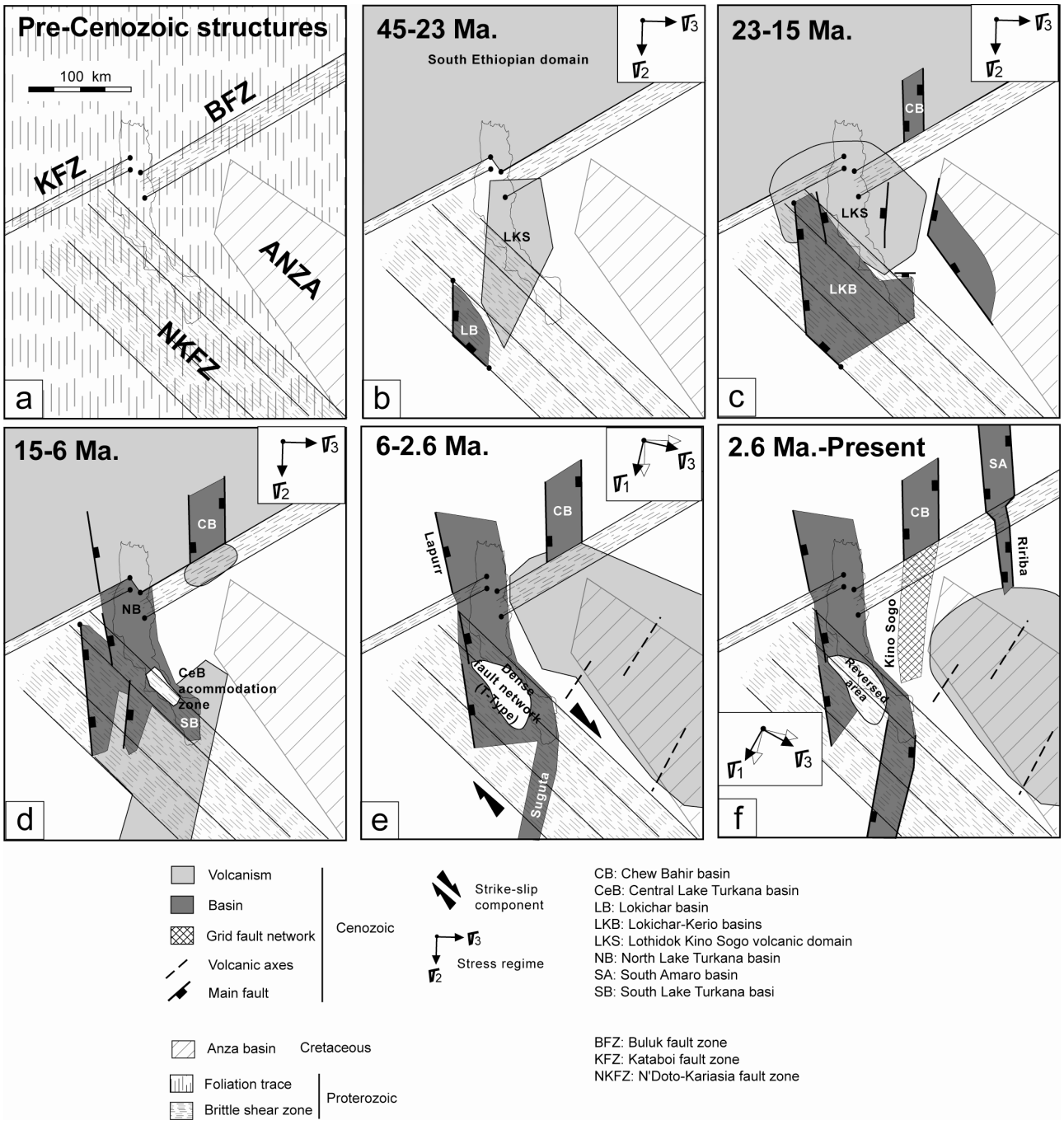

Fig. 15. *Cartoons synthetizing the 45 Ma. rifting history of the Turkana area. (a) Sketch map of pre-rift structural framework. (b,c,d,e,f) Structural sketches elaborated from the restored maps of figures 9, 10, 11, 12 et 13.*

In these conditions, an asymmetrical and losange-shaped sedimentary cell initiated with dimensions (~40x20 km) directly controlled by the transverse fault spacing (~30 km) in the NKFZ.

(2) At a later stage (Fig. 15c), strain propagates northwards into the North Lokichar basin until the definite locking of the Lokichar fault close to a sort of triple junction where the NKFZ and KFZ intersect in the Lothidok magmatic area. In response to this fault propagation inhibition, extension shifted eastwards throughout the eastern part of pre-fractured NKFZ which might have behaved as a weakness zone under EW tensile stress. The arrest of the northerly fault/basin propagation outside the NKFZ results, in map-view, in a triangle-shaped extended zone involving regularly-spaced (~20 km) basins (North Kerio and possibly South Lake Turkana) that decrease in size eastwards (Figs 10a and 15c). This fault/basin system gives way northwards, throughout the Lothidok-Kino Sogo (LKS) updomed volcanic domain, on the NE side of the NKFZ, to a more diffuse fault/fractures array that accomodates extension, probably in association with dyke intrusion (strain/magmatism relations are fully discussed below). At the same period, the ~50 km jump of strain eastwards from the Lokichar-Kerio extended zone into reactivated parts of the previous Anza rift (Cretaceous) results in an anomalously wide rifted zone, ~250 km in EW direction parallel to the inferred extension. The origin of this atypical rift arrangement, with a ratio length/width <1 (0.8), might be related to the difficulty of strain in propagating northwards into the LKS domain probably because of either its magmatic (and less brittle) nature, or its location outside the pre-fractured NKFZ.

(3) The shallow NW-SE basin outlining the oblique central segment of modern Lake Turkana likely formed in the time interval 15-6 Ma. (Fig. 15d), still under an EW extension, along the external structures of the NKFZ. It should have acted as an accommodation zone, subparallel to the NKFZ trend, linking the youngest basin (South Lake Turkana) of the wedge-shaped extended zone to the south with the North Lake Turkana basin that formed later in a more focussed strained area. The coalescence of these diachronous basins led to a more elongated and continuous rift pattern with a length/width ratio of ~2.

(4) Finally, during the last rifting stages (<6 Ma.) (Figs 15e and f), the clockwise rotation of stress axes (~40° from N90°E to N130°E), coupled to the transition from pure extension to compressional regime, is assumed to have caused (1) the dextral reactivation of the (20-30 km-

wide) external corridor of the NKFZ, hence generating a closely-spaced network of N20°E (T-type) extensional fault/fractures in the basins (North Kerio, Turkana and Turkwell) overlying the shear zone; and (2) the local inversion of these basins (Le Gall *et al.* in press) (Fig. 6c).

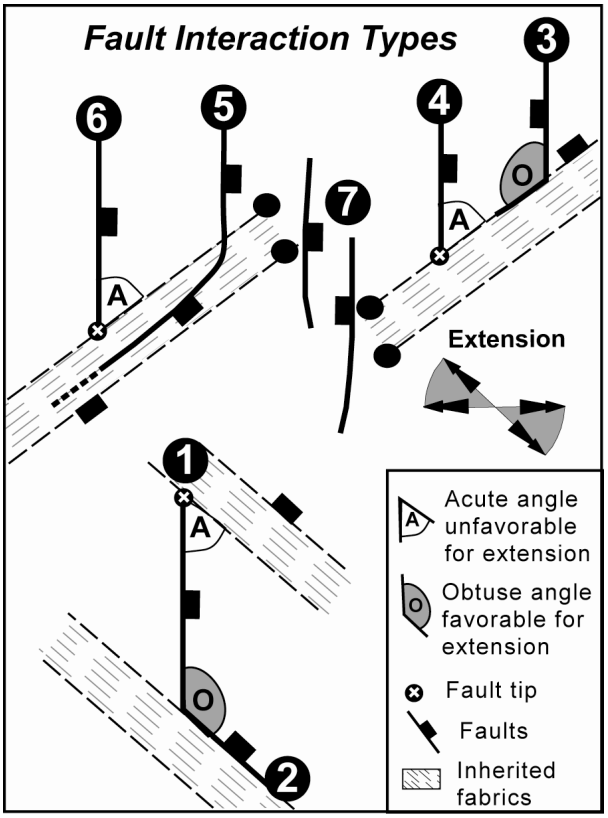

Fig. 16. *Various types of Fault Interaction (FIT) between NS Cenozoic faults and transverse fault zones. The numbers refer to structures that are approximatively in the present-day geographic location.*

2.5.1.2. Role of N50°E discontinuities

The BFZ and KFZ forming the composite N50°E fault network in the North Turkana area contrast with the N140°E system with regards to their nature and influence on rift fault development. They consist of two narrow (~20-30 km-wide) highly-faulted zones extending at N50°E over more than 400 km, with opposite dip direction, and displaying in map-view convergent underlapping geometries in the Lake Turkana area (Fig. 2). Intermitently, they have been the locus of magmatic intrusions (Figs 15c and d) whereas their interaction with the

propagating rift-parallel fault network led to different fault interaction types (Fig. 16). The cartoon of figure 15c first suggests that in the interval 23-15 Ma. the Chew Bahir graben initiated as the consequence of the dextral transfer of extension to the NE along the KBFZ. The lateral offset of strain, in addition to the 'rift' jump evidenced before in the Anza basin to the south, appears as one preferential way for accommodating the ongoing extension outside the Lokichar-Kerio deformed area. With respect to the Lokichar fault system, the Chew Bahir shows a symmetrical fault pattern with greatest fault displacement on the eastern side where NS and N50°E structures intersect at obtuse angle, in agreement with the present-day morphology (Fig. 2 and $FIT_{3\text{-}4}$ on figure 16). In more recent time (<2.6 Ma.), the renewed transfer of extension further east along the KBFZ, from the Chew Bahir into the nascent South Amaro-Ririba rift, leads to the present-day rift network with three parallel and regularly-spaced arms that connect northwards into the broad Ethiopian rift zone (Figs 13 and 15f). The interaction of the N50°E faults with the NS rift-parallel fault network leads to three types of fault arrangement that are well documented in the Lapurr area *sensu lato*, north of the KFZ ($FIT_{5\text{ to }7}$ on figure 16).

(1) The first FIT (n°5) corresponds to the tendency for the NS Lapurr master fault to curve into alignment with the KFZ to the south. The decrease of extensional displacement from the NS (Lapurr) to the N50°E (KFZ) fault segment is consistent with their respective orientation with regards to the EW extension (if assuming their synchronous activity). A quite similar fault arrangement is reported for the <2 Ma. Nachukui fault system further east (Fig. 5b).

(2) The second FIT (n°6) concerns the Murua Rith border fault which limits to the west a half-graben-like depression narrowing to the south towards the KFZ. In addition with the southerly attenuation of the relief in the western uplifted block, this cartographic fault configuration indicates that the lateral propagation of the NS fault system was restricted by the presence of N50°E discontinuities to the south. A quite similar fault attenuation process is likely to have occurred, with an opposite sense, along the North Lokichar symmetrical depressed zone, south of the KFZ (Fig. 5b). To the east, the juxtaposition of the Chew Bahir (N) and Kino Sogo (S) fault systems during recent times (<3 Ma.), on both sides of the BFZ, is also indicative of a sort of strain partitionning between a long-lived and more extended domain to the north and a younger and less strained domain to the south (Vétel *et al.* submitted) (Fig. 13). It is not certain whether the barrier effect exerted by the transverse faulted zones on the southerly propagation of axial rift

structures (Chew Bahir, Murua Rith) is due to their orientation (N50°E) with respect to the applied stress or to the presence of syn-tectonic intrusions.

(3) Additional supportive evidence for the role of the KBFZ volcanic/fault lineament as a mechanical barrier during rift fault development are also supplied by the pathway of the 15-6 Ma. fault network in the North Lake Turkana basin (Figs 11 and 15d). In map-view, the main fault structures strictly propagate in the underlapping approaching zone between the disconnected KFZ and BFZ segments (FIT_7 on figure 16). This fault arrangement is consistent with the fact that step-over regions within segmented fault systems are low-strength areas that facilitate fault propagation (Morley 1999b). It is thus concluded that the location of the North Lake Turkana basin is directly conditioned by a weakness zone along the segmented transverse fault system. Propagation of rift-parallel faults across transverse discontinuities finally contributes to the NS elongation of the Turkana rift zone, and it might have also been enhanced to some extent by the spatial distribution of magmatism as discussed in the following section.

2.5.2. Strain/magmatism relation

The overall Eocene-Present lavas series covering the ~400 km-wide zone in the Turkana rift are generally regarded as resulting from the easterly shift of magmatism with time (Morley 1994). However, a more complex time/space magmatic distribution is evidenced on the 'restored' maps presented above when considering both lower scale structures (~100 km) and shorter time intervals (~10 Ma.). In fact, an EW but also a NS migration of magmatic activity coexist and led to complex relationships between strain and magmatism with times.

In the Lothidok-Kino Sogo domain (LKS), the ~35-3 Ma. volcanic activity is interrupted in the interval 15-6 Ma. At this stage, volcanism starts at ~12 Ma., for the first time, further south in the Napedet-Longipi-Suguta domain (Morley *et al.* 1992), and continues until Recent times. Lastly, a system of fissure-type shield volcanoes is emplaced during Plio-Quaternary in an off-axis position to the east, over part of the Anza rift, as already mentioned in previous models (Hackman *et al.* 1990). The Lotikipi and South Ethiopian long-lived volcanic provinces to the NNW, probably fed by far-travelled melts generated at Eocene time by the initial plume to the north, supply no accurate timing constraints for further discussing the nature of strain/magmatism interaction. The

most fruitful data about strain/magmatism relationships are provided by the evolving fault and magmatic arrangement in central LKS volcanic province during the 23-15 and 15-6 Ma. time periods (Fig. 17).

During stage 23-15 Ma., downthrown faulted basins (Lokichar-Kerio, Chew Bahir and part of Anza) are distributed at the periphery of the LKS volcanic domain that might have formed a thermal-induced topographic dome above an inferred low-density magmatic body at depth (Figs 17a and b). Most of the major extensional faults emplaced at this stage (Hoi, Lothidok and South Chew Bahir faults) show an outward vergence with regards to the LKS domal structure, hence suggesting that they might have formed in response to the combined effect of the EW applied extension and gravity-driven collapse on the flank of the uprising volcanic dome (Fig. 17b). A similar kinematic explanation could account for the still badly-understood (post-Turkana Grits) normal fault array lying in the Mount Porr area with an atypical EW strike parallel to the regional extension (Vétel *et al.* 2004) (Fig. 17a). Extension in the LKS itself should have been accomplished through intense dyking at depth whereas brittle failure at shallow level probably occurred in response to the coupled effects of EW extension and bending stress that gives rise to a network of extrados-type fault/fractures (Fig. 17b). Quantifying extension in the LKS volcanic faulted domain is not an easy task and that makes difficult to assess whether the changing style of deformation from the sedimentary downthrown basins (S) to the uprising volcanic dome (N) is also accompanied by strain rate variations.

Fig. 17. *Fault/magmatism interaction model. (a) Before 15 Ma., deformation migrates eastwards and northwards from the South Lokichar nucleation point and is transferred towards the Chew Bahir via the KBFZ. Strain is distributed over a 250 km-wide zone encompassing basinal areas around the elliptic-shaped LKS faulted magmatic dome. (b) Two schematic structural sections across the Lothidok-Kino Sogo magmatic dome (see figure 17a for location). Before 15 Ma. a system of bending stress fractures develops at the top of the dome, while after 15 Ma., cessation of magmatism induced the deflation of the dome which is disrupted along reactivated domal faults. (c) After 15 Ma., a similar thermal-induced doming/strain relation is stated to the NE about the formation of the Kino Sogo fault belt. With regards to the fissural lava type, magmatic chamber should not be present at the vertical of Anza, but should rather originate from the lateral migration of magmatic underplating beneath the southern shoulder of the Suguta Valley.*

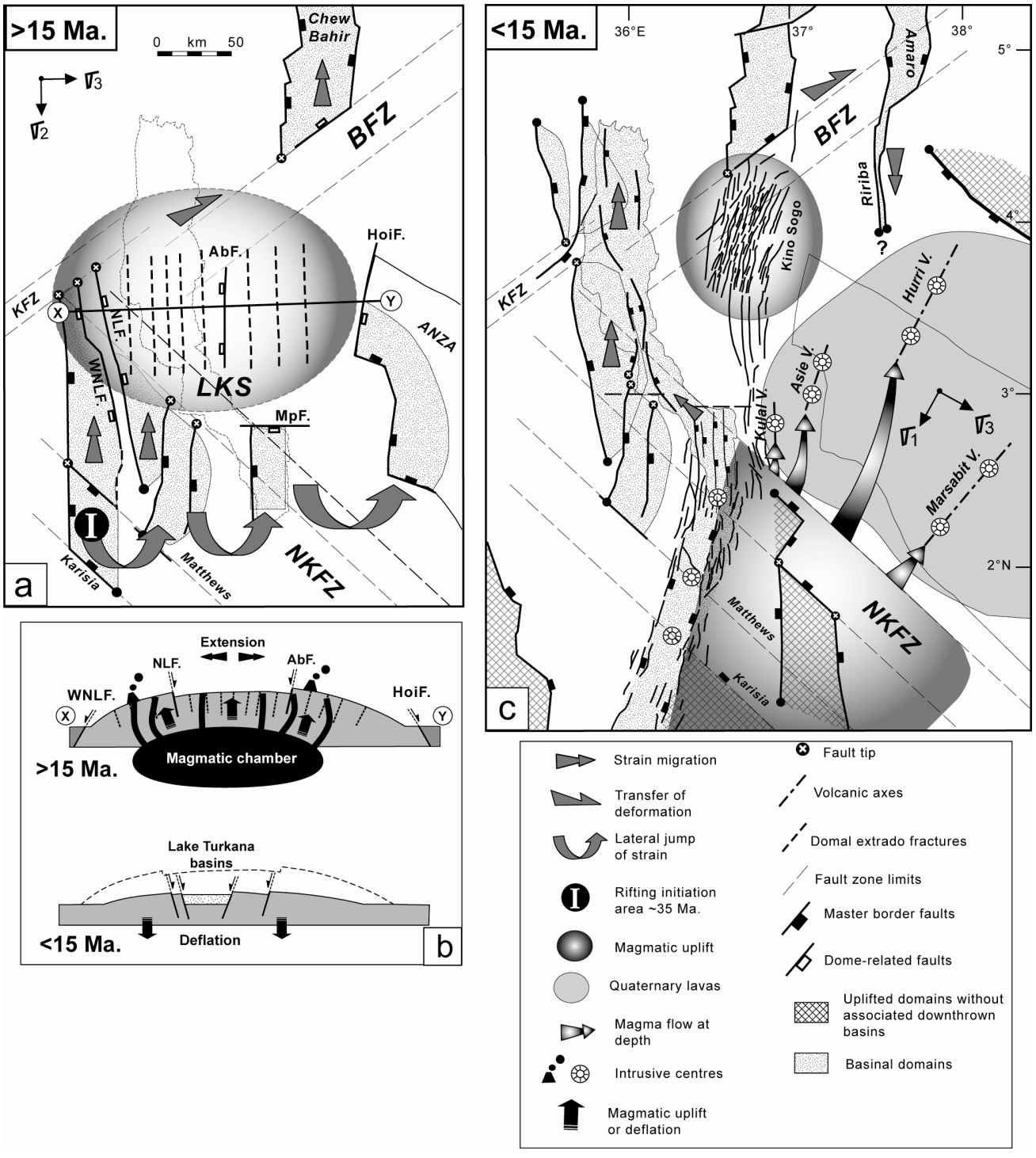
>15 Ma.
0 km 50
Chew Bahir
BFZ
HoiF.
AbF.
KFZ
NLF.
WNLF.
LKS
ANZA
MpF.
Karisia
Matthews
NKFZ
a
Extension
NLF.
AbF.
WNLF.
HoiF.
Magmatic chamber
>15 Ma.
Lake Turkana basins
Deflation
<15 Ma.
b
<15 Ma.
36°E
37°
38°
5°
4°
3°
2°N
Amaro
BFZ
Ririba
Kino Sogo
KFZ
Hurri V.
Asie V.
Huri V.
Marsabit V.
Matthews
NKFZ
Karisia
c
Strain migration
Transfer of deformation
Lateral jump of strain
Rifting initiation area ~35 Ma.
Magmatic uplift
Quaternary lavas
Magma flow at depth
Intrusive centres
Magmatic uplift or deflation
Fault tip
Volcanic axes
Domal extrado fractures
Fault zone limits
Master border faults
Dome-related faults
Uplifted domains without associated downthrown basins
Basinal domains

During stage 15-6 Ma., magmatism migrates southwards from the LKS into the Lokichar-Kerio area, e.g. in the opposite sense of a northerly-propagating fault/basin network throughout the deflated median part of the previous magmatic dome (Fig. 17b). There, earlier development of suitably-oriented (NS) 'extrados' fractures in the tensile part of the LKS volcanic dome might have further helped the northerly migration of faulting beyond the NKFZ. The resulting antagonist spatial distribution of faulting *versus* volcanism leads to envisage that the longitudinal propagation of faults is made easier throughout a crustal domain getting cooler and more brittle during an inter-volcanic stage. This statement, already applied by Lezzar *et al.* (2002) about the ~10 Ma. rift evolution of the Kivu magmatic province in the Lake Tanganyika (western branch of the EARS, see Fig. 1a), is in contradiction with classical concepts that inversely predict the more deformable state of crustal material weakened by thermal event (Callot *et al.* 2001, 2002; Corti *et al.* 2003). From our evolutionary kinematic model, it is therefore suggested that winthin a heterogeneous domain, involving both a weak faulted corridor (NKFZ) and a softened crustal province (LKS sector, similar to the soft spot of Calllot *et al.* (2001)), and undergoing extension, strain preferentially focuses in the brittle pre-faulted areas and then migrates laterally along thermal-induced fractures in the adjoining palaeo-volcanic domes.

About the easterly shift of Plio-Quaternary magmatism over the Anza province, one should note that it nearly coincides in our kinematic model (Le Gall *et al.* in press) with major changes of the regional stress field and the corresponding ~N30°E-directed shortening axis is likely to have facilitated the opening of NNE fissure swarms (inherited or newly-formed?) later exploited by off-axis magma beneath the Asie, Hurri and Marsabit fissure-type shield volcanoes (Fig. 17c).

2.6. Deep processes: Plume/lithosphere interaction and rift surface expression

With regards to the Ethiopia-Kenya plume-related domal context, the Turkana depression is a first-order topographic anomaly which is poorly known (Fig. 18). A number of assumptions are proposed here about its origin from simple considerations dealing with (1) the existence of stationary mantle rising plumes beneath East Africa, (2) the northeastwards migration of the Africa plate since Eocene times, and (3) the interference between plumes and a heterogeneous lithosphere resulting from two distinct rifting events (Cretaceous and Cenozoic).

The East African topographic domes are generally assigned to two diachronous and still active mantle plumes, labelled P1 and P2 on figure 18 (Ebinger *et al.* 1993; McDonald 1994; Bonavia *et al.* 1995; Stewart & Rogers 1996; George *et al.* 1998; Ebinger *et al.* 2000; Rogers *et al.* 2000; George & Rogers 2002), and above which the East Africa plate is assumed to have migrated ~1000 km to the NE from Eocene to Present with an absolute plate motion of 1-3 cm/yr. (Bonavia *et al.* 1995; George *et al.* 1998; Collet *et al.* 2000; George & Rogers 2002). On a pre-rift reconstruction at ~50 Ma. (Figs 18a1 and c1), initial plume (P1) impinged the base of the lithosphere north of present Lake Turkana whereas the second plume head (P2) took place at ~33 Ma. ~900 km further north (Figs 18a2 and c2). They both expressed by the extrusion of huge volumes of flood basalts, ~15 Ma. prior to rifting (George *et al.* 1998). The common origin of P1/P2 from a unique deeper superplume has been evoked by Ebinger & Sleep (1998), in agreement with tomographic records showing a large low-velocity anomaly 500 km-deep in the mantle (Zhang & Tanimoto 1992) (Fig. 18b).

With respect to the plume track proposed by Bonavia *et al.* (1995), the Turkana area should have occurred above P1 at around ~35 Ma. (Figs 18a2 and c2). Though being volcanically active since Oligocene, there is no strong supportive evidence for regional domal uplift in the Turkana depression that would indicate the presence of a Neogene thermal plume (erosion surfaces, …). Instead, the Turkana rift zone evolved as a long-lived downwarping domain where only local-scale domes (~100 km in diameter) existed in relation with individual magmatic centres. This subdued rift topography must reflect two possible mechanical behaviour of the lithosphere beneath northern Kenya during plume (P1) impingement at ~35 Ma (Figs 18e1 and e2).

Firstly, the Cretaceous rift process recorded by the Anza and Sudan domains on both sides of the Turkana area is known to have produced up to 8 km-deep basins (with ~60 km of cumulate extension) which point to strong crustal thinning and lithosphere attenuation, but without (or little) synrift magmatism at shallow level (Reeves *et al.* 1987; Dindi 1994; Morley *et al.* 1999b) (Fig. 18a1). By analogy with a number of works devoted to rift systems (e.g. Ziegler & Cloetingh 2004), the Anza-Sudan stretched lithosphere is likely to have increased its strength by assimilation and cooling of mantle-derived material to the lower crust at the end of Cretaceous rifting. The underplating process beneath the Anza and Sudan rigid ‘blocks’ might have later prevented any bending of the weaker and normal thickness lithosphere occurring in the ~300 km-

wide intervening zone (Turkana) when passing at ~35 Ma over the ~1000 km-diameter plume (P1) (Fig. 18e1).

Secondly, the residual topography possibly preserved at the base of the Cretaceous stretched lithosphere (Anza-Sudan rift) during the onset of P1 plume rising (even in the case of a previous underplating process that did not compensate earlier stretching) should have helped the lateral channelling of melts generated from the plume head (Figs 18a2 and e2). According to this 'thinspot' model, based on the concept of Thompson & Gibson (1991), the dissipation of heat over a broad area (~1500 km), as well as the lateral drainage of plume head material, should have result in a dramatical decrease of thermal-induced uplift throughout the Turkana rift zone. The lateral flowing of plume head melts implies a drastic reduction of magma production at the apex of the plume, e.g. beneath the Turkana area. That is confirmed by the contrast between the eruption rates and total volumes of basaltic material in the Ethiopian and Kenyan domes, on one hand, and in the Turkana depressed rifted zone, on the other hand (Ebinger *et al.* 1993; Stewart & Rogers 1996; George *et al.* 1998). In the proposed model, the lack of Eocene-Pliocene volcanism at shallow level in the Anza-Sudan domain means that far-travelled melt bodies remained trapped beneath the strong Cretaceous lithosphere until Recent times.

Fig. 18. *Deep interactions between thinned Cretaceous lithosphere and impinging of two diachronous Cenozoic mantle plumes. (a1-a4) Cartoons of the Africa plate migration (1000 km towards the NE) during the last 50 Ma. above mantle plumes P1 and P2 which are considered as fixed points. The track of P1 passed through the unstretched Turkana lithosphere. (b) Along-strike tomographic section from S-waves speed anomaly (modified from Zhang & Tanimoto 1992) showing a deep-rooted rising mantle superplume beneath East Africa. (c) Simplified lithospheric sections showing the migration of Africa plate above P1 and P2 during the last 50 Ma, note the persistent downthrow position of the Turkana depression whereas lateral areas are uplifted in response to plume impinging. (d) Two plume-induced domes flank the Turkana depression which outline the trace of the previous Cretaceous stretched lithosphere on the Present-day topography of East Africa (Gtopo 30 data). (e1, e2) Two possible models for the lack of plume-induced uplift along the Turkana area, (e1) Lithosphere strengthening occurred in response to the cooled previous Cretaceous underplating that prevent any bending of the lithosphere during Cenozoic times, (e2) The residual topography preserved at the base of the Cretaceous lithosphere (Anza-Sudan rift) leads the plume head material to migrate laterally hence resulting in the decrease of the thermal-induced uplift (modified from Thompson & Gibson 1991).*

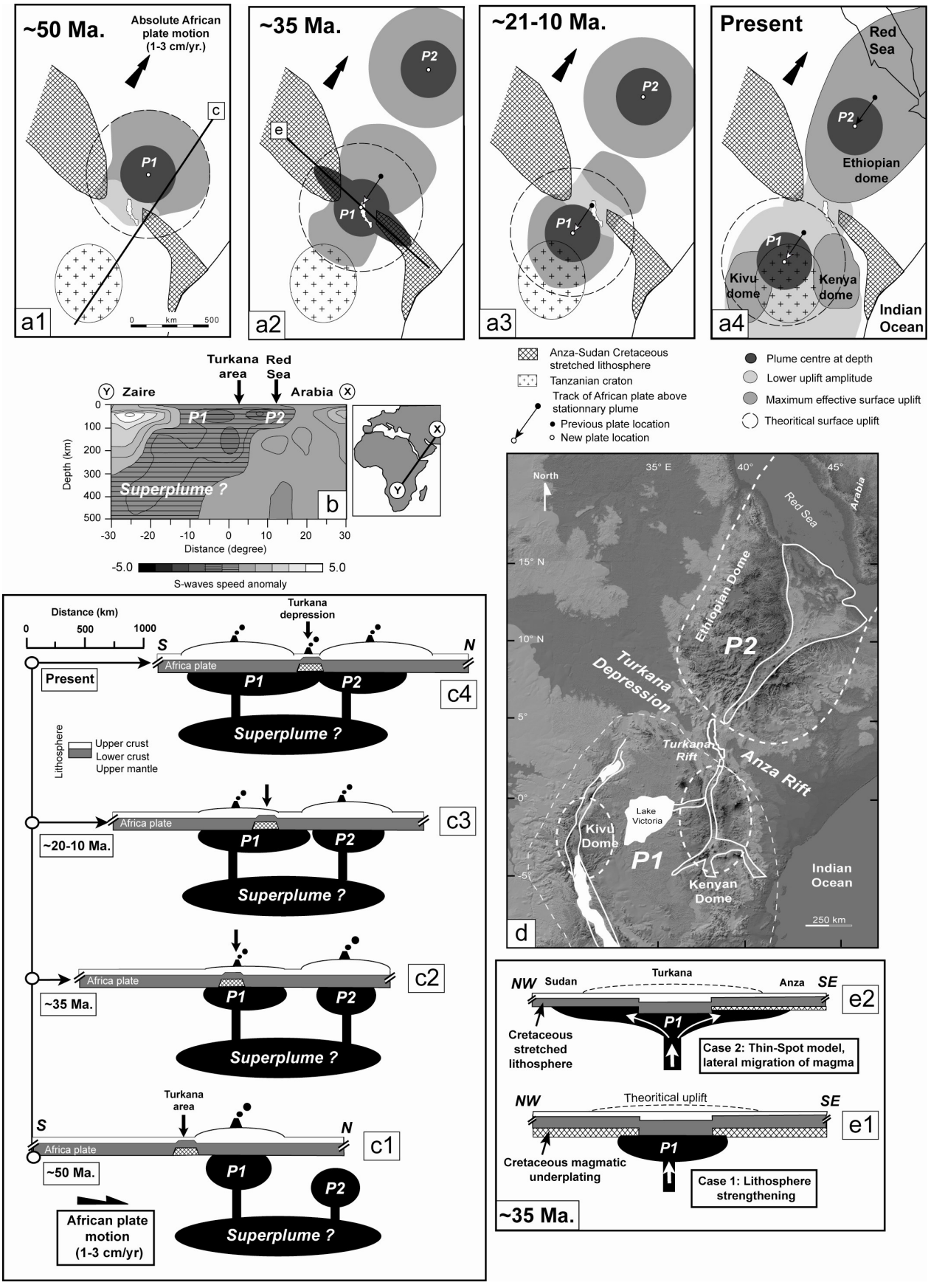
~50 Ma.
Absolute African plate motion (1-3 cm/yr.)
P1
c
a1
0 km 500
~35 Ma.
P2
P1
e
a2
~21-10 Ma.
P2
P1
a3
Present
Red Sea
P2
Ethiopian dome
P1
Kivu dome
Kenya dome
Indian Ocean
a4
Anza-Sudan Cretaceous stretched lithosphere
Tanzanian craton
Track of African plate above stationnary plume
Previous plate location
New plate location
Plume centre at depth
Lower uplift amplitude
Maximum effective surface uplift
Theoritical surface uplift
Turkana area
Red Sea
Zaire
Arabia
Depth (km)
P1
P2
Superplume ?
b
Distance (degree)
-5.0
5.0
S-waves speed anomaly
Distance (km)
Turkana depression
S
N
Present
Africa plate
P1
P2
Superplume ?
c4
Lithosphere
Upper crust
Lower crust
Upper mantle
~20-10 Ma.
c3
~35 Ma.
c2
Turkana area
~50 Ma.
African plate motion (1-3 cm/yr)
c1
North
35° E
40°
45°
Red Sea
Arabia
15° N
Ethiopian Dome
10° N
Turkana Depression
P2
5°
Turkana Rift
Anza Rift
0°
Lake Victoria
Kivu Dome
P1
-5°
Kenyan Dome
Indian Ocean
250 km
d
NW
Sudan
Turkana
Anza
SE
Cretaceous stretched lithosphere
Case 2: Thin-Spot model, lateral migration of magma
e2
Theoritical uplift
Cretaceous magmatic underplating
Case 1: Lithosphere strengthening
e1
~35 Ma.

The extrusion of fissure-type magmatism during Quaternary over part of the Anza rift should have occurred in response to the transition from a tensional to a compressional stress regime (with σ1 oriented NE-SW) that permits the uprising of magmas along N30°E open fault/fracture networks (Le Gall *et al.* in press) (Fig. 17c).
Alternatively, the Quaternary off-axis magmatism in the Anza domain might have been fed, still *via* N30°E fracture networks, by recent magma chambers located on the eastern uplifted side of the Suguta trough, e.g. in the zone of influence of present-day Kenya dome (Fig. 18d).

2.7. Conclusion

A reconstruction of the long-lived and poly-phased tectono-magmatic development of the Turkana Cenozoic rift segment (200x200 km, Northern Kenya) is discussed in this study on the basis of five 'restored' structural maps for the periods 45-23 Ma., 23-15 Ma., 15-6 Ma., 6-2.6 Ma., 2.6 Ma.-Actual. These rift maps are completed by additional documents dealing with pre-existing structures (Proterozoic basement discontinuities, Cretaceous rift). Our evolutionary model highlights the key-role role played by 1) two regional-scale transverse faulted corridors, the so-called N'Doto-Karisia (NKFZ oriented N140°E; 100x600 km) and the Kataboi-Buluk (KBFZ oriented N50°E; 30x200 km) fault zones, and 2) magmatic domains, on the nucleation and propagation of extensional structures at different stages of rifting.
- Both location and final geometry of newly-formed basins are directly imposed by inherited transverse fault zone dimensions. Syn-rift basins firstly develop and migrate north and easterwards within the N140°E NKFZ, according to favourable angular relations between N140°E and rift-parallel NS structures. Faults are next locked by N50°E structures of the KBFZ due to acute and unfavourable fault interaction types in agreement with the fault propagation model published by Lezzar *et al.* (2002) for the Tanganyika rift basins. In the study area, the rift-parallel fault network propagated through the N50°E segmented discontinuity (KBFZ) where this latter displays a convergent underlapping zone that should have acted as a low-strength area.
- Timing and spatial distribution of volcanic and basin/fault areas allows us to discuss magmatic/strain relations at various scales. When a crustal domain recording extension involves both a pre-existing mechanical weakness zone (in the present case, oriented at an angle (~40°) to

extension), and a synrift magmatic province (equivalent to a 'soft spot' of recent modelling), the first increments of strain are not exclusively focussed on the soft spot, as predicted by most of the models, but rather concentrate over the brittle and previously fractured terrains. Later on, propagation of fault/basin network throughout the magmatic province occurs after the cessation of volcanic activity, under probably reduced thermal conditions and over a deflated palaeo-dome. The fault pathway is highly controlled by the previous inner volcanic domes structures (extrados fault/fracture network, syn-magmatic faults). This alternative kinematic model is documented for two rifting stages (Miocene and Pliocene) about two magmatic domes in the central part of the Turkana rift.

- About the interactions between the Cretaceous (N140°E) and Cenozoic (NS) rifts in the Turkana area, it is proposed that the Anza-Sudan rift basins are disconnected on both sides of a ~300 km-wide unstretched crust/lithosphere, centred on the Turkana area, and where Cenozoic rifting will subsequently nucleate.

- At a greater-scale, plume/lithosphere interactions along the eastern branch of the EARS supply some clues for the still debatable origin of the Turkana transverse depression. In the framework of the migration of the African plate (~1000 km to the NE since 50 Ma.) above two Cenozoic mantle plumes, the lack of thermal-induced uplift along the Turkana depression during its entire rift history is here assigned to two (interacting or not) lithospheric processes: (1) the NW and SE migration of plume head material at ~35 Ma. beneath pre-stretched Cretaceous lithosphere in agreement with the thin-spot model of Thompson & Gibson (1991) or (2) the strengthening of the lithosphere in response to the cooling of the Cretaceous underplating (Ziegler & Cloething 2004) that prevent any bending of the lithosphere at large wavelength.

More generally, this study provides some new insights about processes of nucleation and propagation of deformation along a long-lived magmatic rift segment (~45 Ma.), recording a low deformation rate, and widely influenced by structural inheritance due to basement structures and a previous oblique rift.

3. Inversion tectonics during continental rifting: The Turkana Cenozoic rifted zone, Northern Kenya

Bernard Le Gall[1], William Vétel[1] & Christopher Morley[2]

[1] UMR 6538 'Domaines Océaniques', Institut Universitaire Européen de la Mer, UBO, CNRS, 4 Place Nicolas Copernic, 29280, Plouzané - FRANCE

[2]Universiti Brunei Darussalam, Jalan Tungku Link, Gadong BE1410 Negara, Brunei, Darussalam

In press to Tectonics
(Received, February, 23; Revised, September, 3; Accepted, November, 25, 2004)
Manuscript reference, 2004TC001637RR; IUEM publication n°935

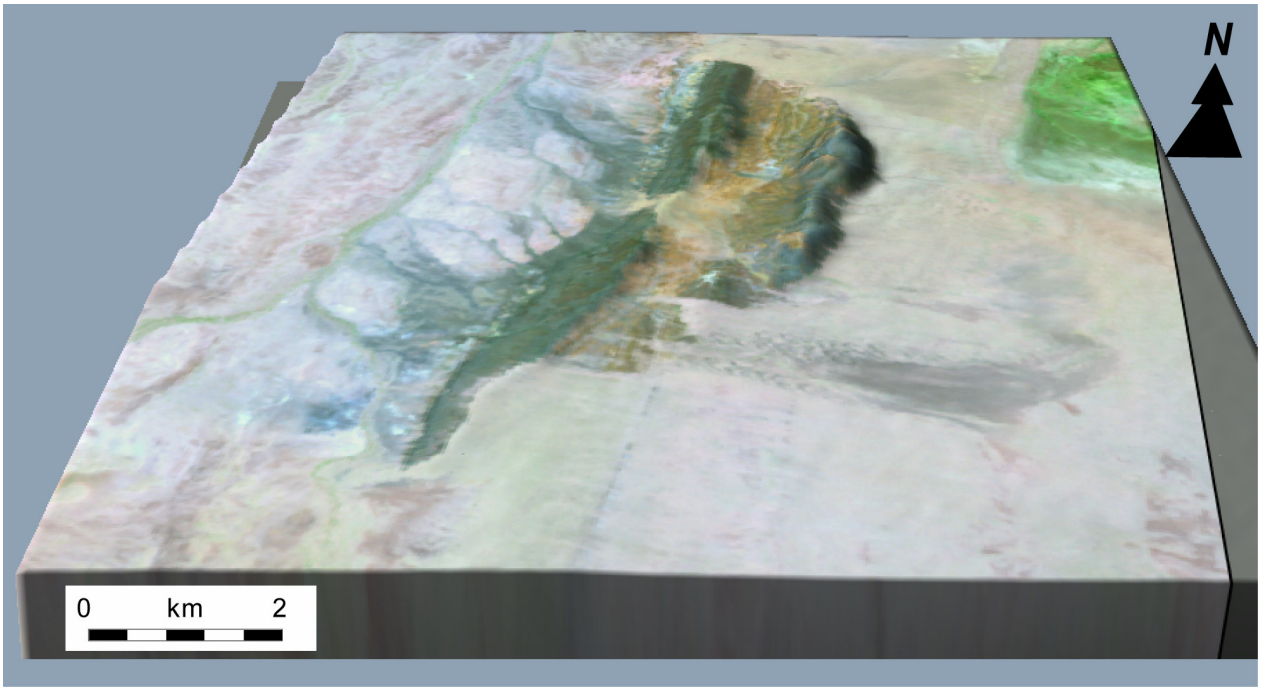

Perspective view of a portion of the Landsat image 169-058 overlain on the digital topography SRTM in the region of Lothagam Hills (view to the north, light from West, vert. exag. x2).

Abstract

Remote sensing data and revised seismic reflection profiles provide new insights about the origin of inverted deformation within Miocene-Recent basins of the Turkana rift (northern Kenya) in the eastern branch of the East African Rift System. Contractional structures are dominated by weakly inverted sets of fault blocks within <3.7 Ma.-old synrift series. Most of reverse extensional faults involve components of oblique-slip whereas associated hangingwall folds are characterised by large wavelength upright folding. The area of basin inversion is restricted to a 40x100 km elongated zone overlying a first-order N140°E-trending fault zone in the basement, referred to as the N'Doto transverse fault zone (NTFZ). In the proposed kinematic model, inversion tectonics is assigned to permutation of principal stress axes ($\sigma1/\sigma2$) in addition to the clockwise rotation of extension (from nearly N90°E to N130°E) during Pliocene. The transition from pure extension (Miocene) to a wrench faulting regime (Pliocene) first results in the development of T-type fault networks within a dextrally reactivated shear zone (NTFZ). Inversion tectonics occurred later (<3.7 Ma.) in response to a still rotated (~20°) shortening axis ($\sigma1$) oriented N40°E that caused the oblique compression of earlier (NS to N20°E) extensional structures within the NTFZ. The origin of basin inversion and strain concentration in the Turkana rift is thus directly linked to a crustal weakness zone, transverse to the rift axis, and involving steep pre-rift anisotropies.

3.1. Introduction

This paper deals with aspects of positive inversion in intracontinental rift setting. The term 'inversion' is used to describe regions which have experienced a reversal from subsidence to uplift [*Harding,* 1983; *Gillcrist et al.,* 1987] during the contractional reactivation of previously extensional faults and basins [*Hill and Cooper,* 1996]. Inversion tectonics is a common feature of many mature sedimentary basins formed on continental crust, prior or after oceanic spreading [*Ziegler,* 1988]. Well developed examples of basin inversion occur along the northeast Atlantic margins of Norway and Britain, and their origin has been variously interpreted as a response to either local stress induced by shearing [*Brekke and Riis,* 1987], or far-field stress in relation to Alpine compression [*Ziegler,* 1989; *Doré et al.,* 1999], oceanic ridge-push [*Price et al.,* 1997], or oceanic transform motion [*Doré and Lundin,* 1996]. Inversion tectonics occurs also quite widely in continental rifts, and areas of inversion in the reference Cenozoic East African Rift System (EARS in the text) are reported to the Afar [*Arthaud et al.,* 1980; *Gaulier and Huchon,* 1991], and Rukwa sectors [*Ring,* 1994; *Morley et al.,* 1992], as well as to the Turkana area [*Morley et al.,* 1999c] which is the subject of the present work (Figure 1a).

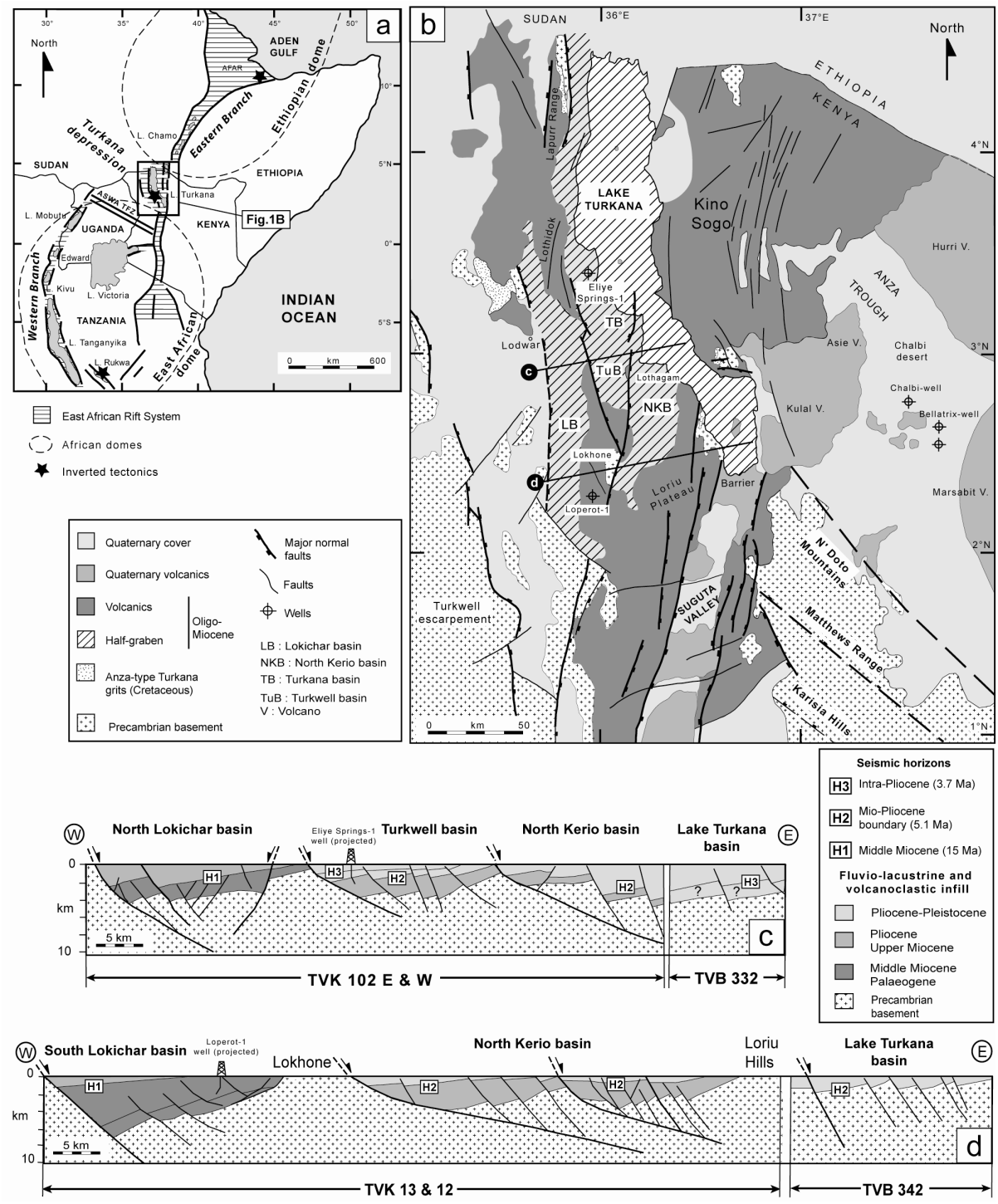

Figure 1. *Tectonic framework of the Turkana Cenozoic Rift, Northern Kenya. (a) Location of the Turkana rift in a large-scale Turkana transverse depression between the Ethiopian and Kenyan (plume-related) domes. (b) Outline geological map of the Turkana Rift in Kenya. (c and d) Representative geological sections across the Turkana synrift basins network from seismic reflection data (Amoco TVK profiles and Probe TVB profiles) discussed in the text, modified from Morley et al. [1999a]. See location of the sections in Figure 1b. Note 1) the dominantly half-graben style (facing to the east) of the basins, and 2) their progressive younging eastwards and northwards.*

The various kinematic models so far proposed for inverted basins in the EARS imply disturbances of the stress field in relation with transform fault in the Afar rift [*Arthaud et al.,* 1980], plate-scale mechanisms in the Turkana rift [*Morley et al.,* 1999c], and permutation and/or rotation of stress axes in the Rukwa rift [*Ring et al.,* 1992]. According to *Morley et al.* [1999c], the Turkana inverted rift basins (northern Kenya) are the consequence of either external or more local lithospheric-scale processes linked with, respectively, the Red Sea-Gulf of Aden spreading centres, and thermo-mechanical processes occurring under the Turkana rift itself (magmatic underplating, reduction of buoyancy forces, ...). However, the short duration and frequency of inversion process (<3.7 Ma.) in the Turkana rift are difficult to reconcile with the long-term stress conditions caused by the inferred plate-scale driving forces [*Morley et al.,* 1999c]. Conversely, newly-acquired structural data showing the restricted spatial distribution of inverted structures favour local-scale contractional mechanism as the main contributing factor for rift basin inversion in the Turkana extensional province.

Some implications of our model deal with the importance of strike-slip versus extensional deformation during the latest rifting stage, whereas the role of pre-existing oblique discontinuities on the overall architecture of the rifted zone is also discussed. Because of the young age (<3.7 Ma.) of inverted structures, our study encompasses the time interval 5 Ma-Present, in contrast with most of previous works that concentrated on Oligo-Miocene structures typically formed during the onset of extension and basin development in northern Kenya. In addition to (partly revised) conventional seismic reflection profiles previously interpreted by *Dunkelman et al.* [1989] for the offshore basins (PROBE TVB profiles of Lake Turkana), and *Morley et al.* [1992, 1999a] for the onshore basins (AMOCO TVK profiles), our work integrates satellite imagery (Landsat Enhanced Thematic Mapper Plus, x 4) in order to correlate surface geology with seismically-imaged basinal structures.

3.2. Regional rift setting

Within the EARS, the Turkana Cenozoic rifted zone lies in a pronounced N140°E-trending oblique depression between the Ethiopian and East African domes (Figure 1a). In this area, the roughly NS-striking Cenozoic rift structures are oblique to earlier NW-SE rift basins that developed during Cretaceous-Palaeogene times in the Anza (SE) and South Sudan (NW) sectors [*Schull,* 1988; *Bosworth and Morley,* 1994]. From gravity data, these early rift systems are assumed to die out laterally towards Lake Turkana [*Reeves et al.,* 1987; *Dindi,* 1994]. Alternatively, the Cretaceous basins may link *via* a putative EW transfer zone lying in southern

Ethiopia, north of the present lake [*Bosworth,* 1992; *Hendrie et al.,* 1994; *Ebinger and Ibrahim*, 1994].

The Turkana rift forms a nearly 120 km-wide broad deformed zone that narrows progressively southwards in Central Kenya where the rifted zone attains a maximum width of ca. 80 km across the Elgayo-Baringo transect. To the north, the Turkana rift gives way into the 300 km-wide complex system of basins and ranges within the broadly rifted zone of southwestern Ethiopia [*Ebinger et al.,* 2000].

Following acquisition of seismic reflection profiles in the late 1980's and early 1990's, the subsurface data of the Turkana area was further calibrated by two boreholes in the Loperot (2950 m) and Eliye Springs (2964 m) areas (Figure 1b). The Turkana Cenozoic rifted zone is known to form a 200 x 100 km extensional province comprising a series of nearly NS-trending half-grabens, arranged into three parallel basin belts as far east as the eastern shore of modern Lake Turkana [*Morley et al.,* 1992] (Figures 1c and 1d). The structural organization of the recent basins occupying Lake Turkana was previously defined by offshore seismic reflection data [*Dunkelman et al.,* 1989].

East of Lake Turkana, a discrete Miocene fault-controlled depocenter is also documented in the Chalbi desert from industrial reflection seismic profiles crossing the easternmost part of the Anza trough (Figure 1b). There, Miocene terrigeneous synrift sequences, as thick as 800 m in the Bellatrix well (Figure 1b), unconformably overlie Cretaceous rifted series [*Winn et al.,* 1993; *Morley et al.,* 1999b].

Cretaceous and younger fault-bounded basins have not yet been observed beneath the Miocene and Quaternary volcanic complexes of the Kino Sogo plateau and the Suguta valley (Figure 1b). These regions are deformed by a dense recent/active grid fault network trending at N10°E [*Mohr and Wood,* 1976; *Bosworth and Maurin,* 1993; *Vétel et al.,* submitted]. The large-scale geometry of the Turkana rift basins is illustrated on the structural dip-sections of figures 1c and 1d from onshore TVK seismic lines [*Morley et al.,* 1999a], and a number of offshore TVB profiles [*Dunkelman et al.,* 1989], further calibrated by the Loperot and Eliye Springs deep boreholes (Figure 1b). Three regional stratigraphic horizons are identified from bottom upwards as H_1 (~15 Ma.), H_2 (5.1 Ma.) and H_3 (3.7 Ma.) [*Shell report,* 1992]. The high-amplitude horizon H_2 marks a regionally-distributed volcanic event [*Haileab et al.,* 2004], almost constantly present on the whole seismic dataset, and previously reported in the Lake Turkana basins as the 'Turkana Reflector' [*Dunkelman et al.,* 1989]. The 3.7 Ma-old horizon is a volcanoclastic episode with a more localized distribution. The age of the youngest overlying series is not well calibrated, hence preventing any precise upper limit for timing of inversion tectonics in the Turkana basins.

The Lokichar (ca. 70 x 20 km), North Kerio, Turkwell and Turkana (ca. 25 x 50 km each) onshore basins define a relatively intricate extensional system to the west. Its overall structure partly results from multiple pulses of deformation, accompanied by reversal in half-graben asymmetry, switch of half-graben polarities along-strike, and lateral shift of strain with time eastwards towards modern Lake Turkana [see *Morley et al.,* 1992; 1999a, for further details]. Very few intrabasinal faults exist within the Lochichar east-facing half-graben if compared to the North Kerio, Turkwell and Turkana basins. Its southwestern part contains the oldest (ante-H_1) and thickest synrift deposits in the Turkana sector. They form a westerly-thickening wedge of Palaeogene to middle Miocene fluvio-lacustrine sediments, capped by a 300-m thick basaltic sequence dated from 12.5 to 10.7 Ma [*Morley et al.,* 1992]. The maximum infill thickness (6-7 km) occurs in the immediate hangingwall of the Lokichar easterly-dipping master fault [*Morley et al.,* 1992; 1999a] (Figures 1c and 1d).

Further east, the North Kerio and Turkwell basins form two easterly-facing half-grabens, Mio-Pliocene in age, where younger synrift deposits (post- H_{2-3}) are still preserved on top of a 4 km-thick (maximum) volcano-clastic package [*Dunkelman et al.,* 1989]. They pass laterally northwards into the Turkana and Lake Turkana basins that conversely display a prominent westerly polarity. *Dunkelman et al.* [1989] interpreted the rift basins in Lake Turkana in terms of the Tanganyika and Malawi styles of alternating half-grabens separated by oblique accommodation zones [*Rosendahl,* 1987; *Spetch and Rosendahl,* 1989]. These basins are not all confirmed in the present work, and, for ease of discussion, the Lake Turkana is basically subdivided into three major basins comprising the South and North basins, oriented at NS and linked by the intermediate Central basin lying with a N140°E oblique direction. The youngest stratigraphy (<5.1 Ma.) of the northern basins is directly tied by the Eliye Springs borehole (Figure 1c), whereas the presence of early Miocene sequences in the deepest part of the basin is not yet proved [*Hendrie et al.,* 1994].

The total extension recorded by the Turkana rifted zone since Miocene times is estimated to 30-40 km by *Hendrie et al.* [1994] from geophysical evidence and modelling of 'unseen' erosion due to footwall uplift. A lower amount of extension at ca. 20-25 km is applied here from the geometry of the rifted basins drawn on the 80 km-long transect of figure 1d, when using the ´antithetic shear model, with $\alpha = 30°$' of *Gibbs* [1984]. The amount of extension within the poorly-imaged Lake Turkana basins is badly constrained.

3.3. Hangingwall fold-fault structures

The synrift sedimentary sections of the Turkana basins show a great number of fold/fault structures that resemble inverted features. From geometrical and kinematical indicators observed on interpreted seismic data, the folds appear to be of three origins. They are exhaustively listed below and referred to as 'Type A, B and C' structures. Since both types A and B features are interpreted to have arisen as the consequence of, respectively, extensional displacement along faults and emplacement of igneous intrusions, they are not reported in the main body of the text which instead deals with inversion structures *sensu stricto* (Type C) caused by large-scale contractional mechanisms.

3.3.1. Extensional-related fold structures (Type A)

On the strike-line TVK 114 that cuts through the main depocentre of the Lokichar half-graben (Figure 2b), part of the Lower Miocene synrift sequences lying in the hangingwall of the Lokichar master fault is involved into a pair of km-wavelength upright folds with a vertical amplitude of nearly 0.5 sec. TWT (approximately 800 m) (Figure 2c). These folds occur within a synrift sedimentary section that thickens northwards from 0.2 to 1.0 sec. (TWT) above a step-like segment of the Lokichar fault [*Boulet,* 2003]. Since antiformal structures are not observed on the dip-sections, they are likely to have formed during the extensional development of the Lokichar bounding fault in response to varying displacement along the fault plane. Similar mechanisms are applied by *Morley et al.* [1992] to local hangingwall deformations along the Lupa master fault in the Rukwa rift (Figure 1a).

Above inflection point 'Y', middle Miocene lacustrine series are involved in the anticline, whilst about 7 km further north, above inflection point 'X', they clearly seal and post-date the folded strata. Folding in the Lokichar hangingwall strata is thus assumed to have developed diachronously as propagating southwards.

The anticline structures imaged on line TVK 114 are the only folded features so far documented in the Lokichar fault-bounded basin. Because of their inferred extensional origin in connection with the development of the Lokichar master fault, they are not indicative of inversion tectonics, and as such are not considered in the following text.

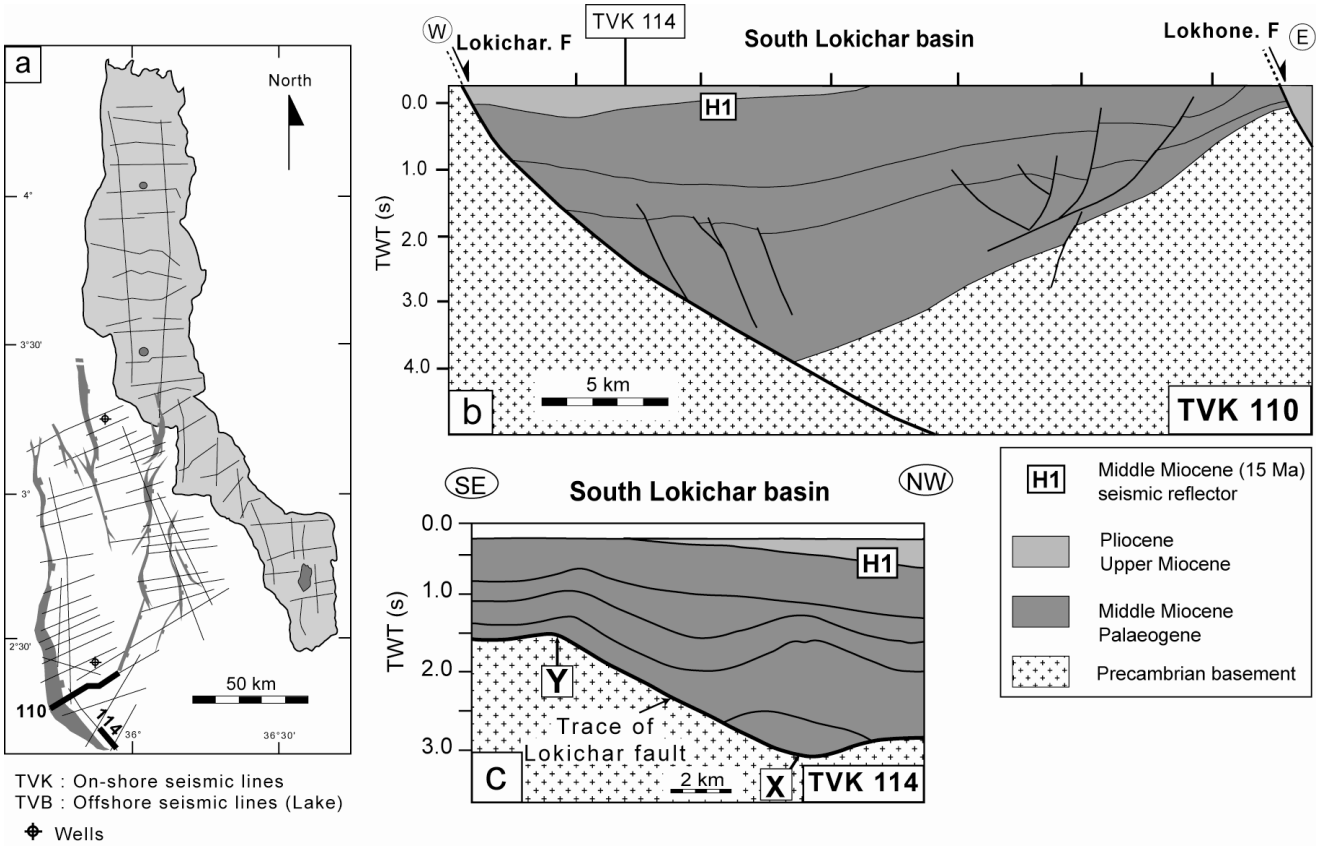

Figure 2. *Example of extension-related fold-like structures (Type A) in the hangingwall of the Lokichar master fault. (a) Location map of onshore (TVK) and offshore (TVB) seismic lines recorded in the Turkana rift basins. The trace of the main rift bounding faults is also drawn, as well as the Eliye Springs and Loperot wells. (b) Sketch structural cross-section of the Lokichar half-graben showing the location of line TVK 114 in Figure 2c. (c) Km-wavelength synform-antiform structures imaged on the strike-section TVK 114 in Palaeogene-Middle Miocene series forming the immediate hangingwall of the Lokichar fault.*

3.3.2. Igneous intrusion-induced fold structures (Type B)

A second type of folded structures is clearly imaged on a number of TVB seismic lines through the North (TVB 308), Central (TVB 318) and South (TVB 340) basins of modern Lake Turkana (Figure 3).

The best examples of folds are observed in the uppermost layered sequences (<1 sec. TWT) overlying H_2 horizon on the TVB 318 migrated section (Figure 3c). They express as upright and symmetrical antiforms, with a wavelength ranging from 1 to 0.5 km. Most of them occur at the apex of steep seismically transparent bodies, typically 2 km-wide. Similar chaotic seismic facies are visible on lines TVB 308 and TVB 340 as elliptic and horizontal bodies totally surrounded by sediments (Figures 3b and 3e).

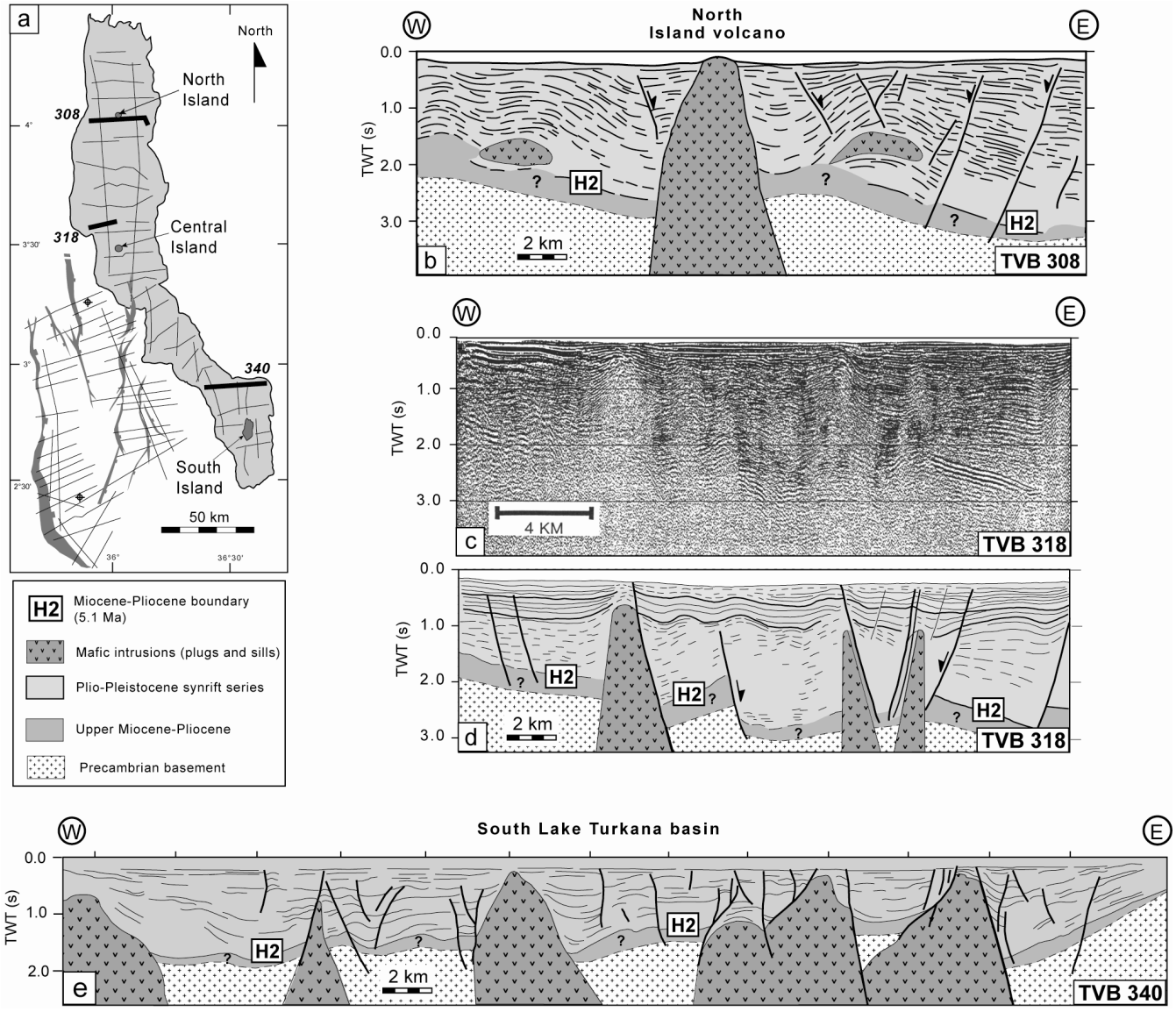

Figure 3. *Evidence of intrusion-related fold structures (Type B) in Plio-Pleistocene sediments of Lake Turkana basins. (a) Similar location map as Figure 2a. (b) Structural interpretation of TVB 308 seismic reflection line (North basin). (c and d) Migrated and interpreted sections of TVB 318 seismic line (Central basin). (e) Interpreted section of TVB 340 line (South basin). In the following, seismic data are illustrated by both raw and interpreted sections when concerning structures of interest and as a function of the quality of the available data. (Much of the data was made available to us only as variably degraded paper records).*

The vertical transparent body of section TVB 308 connects directly upwards into the North island volcano (Figure 3b) and, by extrapolation, all of them are regarded as recent mafic intrusions (plugs and sills), dated at <3.2 Ka in the South island volcanics [*Ferguson and Harbott,* 1982]. Emplacement of magmatic bodies within the middle/upper crust is known to modify stress conditions and to build up temporary horizontal high-compressive stress [*Rubin and Pollard,*

1988], as exemplified along mid-oceanic ridges [*Opheim and Gudmundsson,* 1989; *Villemin et al.,* 1994; *Curewitz and Karson,* 1998]. The deformed and highly fractured strata imaged along the walls of some shallow intrusions (Figures 3d and 3e) are thus likely to have been induced by both doming above underlying intrusions and buckling from temporary high horizontal compressive stress during forceful emplacement of magma. The abundance of intrusions and associated deformation increases markedly southwards in the South basin (Figure 3e). There, the dense network of steep faults, with locally reverse displacement, that dissect the synrift sequences might result from the shortening necessary to accommodate magmatic intrusions which occupy 35% of the area of the complete dip-section TVB 340 (Figure 3e). However, enhanced horizontal compressional stress resulting from magma pressure alone cannot account for the totality of inversion tectonics within the Turkana rift, since a number of fold/fault inverted structures occur within areas totally devoid of recent high-level intrusive centres. This last type of structures (Type C) is particularly abundant in the Turkana and North Kerio onshore basins, but a few of them also occur in parts of the Lake Turkana offshore basins.

3.3.3. Inverted structures (Type C)

As recognized in most of inverted basins [*Ziegler,* 1987; *Coward,* 1996], inversion tectonics in the Turkana rift is dominated by the reactivation of pre-existing extensional fault networks. On the basis of the geometry and the inherited or newly-formed origin of the reverse faults, as well as on the structure of the associated deformed strata, four main sorts of 'Type C' fold/fault structures are distinguished below. They correspond for most part of them to those described by *Morley et al.* [1999c]. The nature of the driving forces responsible for the Turkana inversion structures is then discussed from an integrated analysis of both seismic dataset and onshore surface geology deduced from remote sensing imagery.

3.3.3.1. Geometry of inverted structures

1. A first type of structures involve (Upper?) Pliocene-Recent (<5.1 Ma.) sediments imaged on seismic dip-lines across the Central basin of Lake Turkana (Figure 4).

- The line TVB 330 (Figure 4b) shows km-wavelength and low-amplitude upright folds developed at the upper tip zones of steep faults (Fa, Fb and Fc in Figure 4c). The folded sequences form triangle-shaped wedges bounded or dissected by diverging small-scale faults that branch downwards into the main fault (Figure 4c).

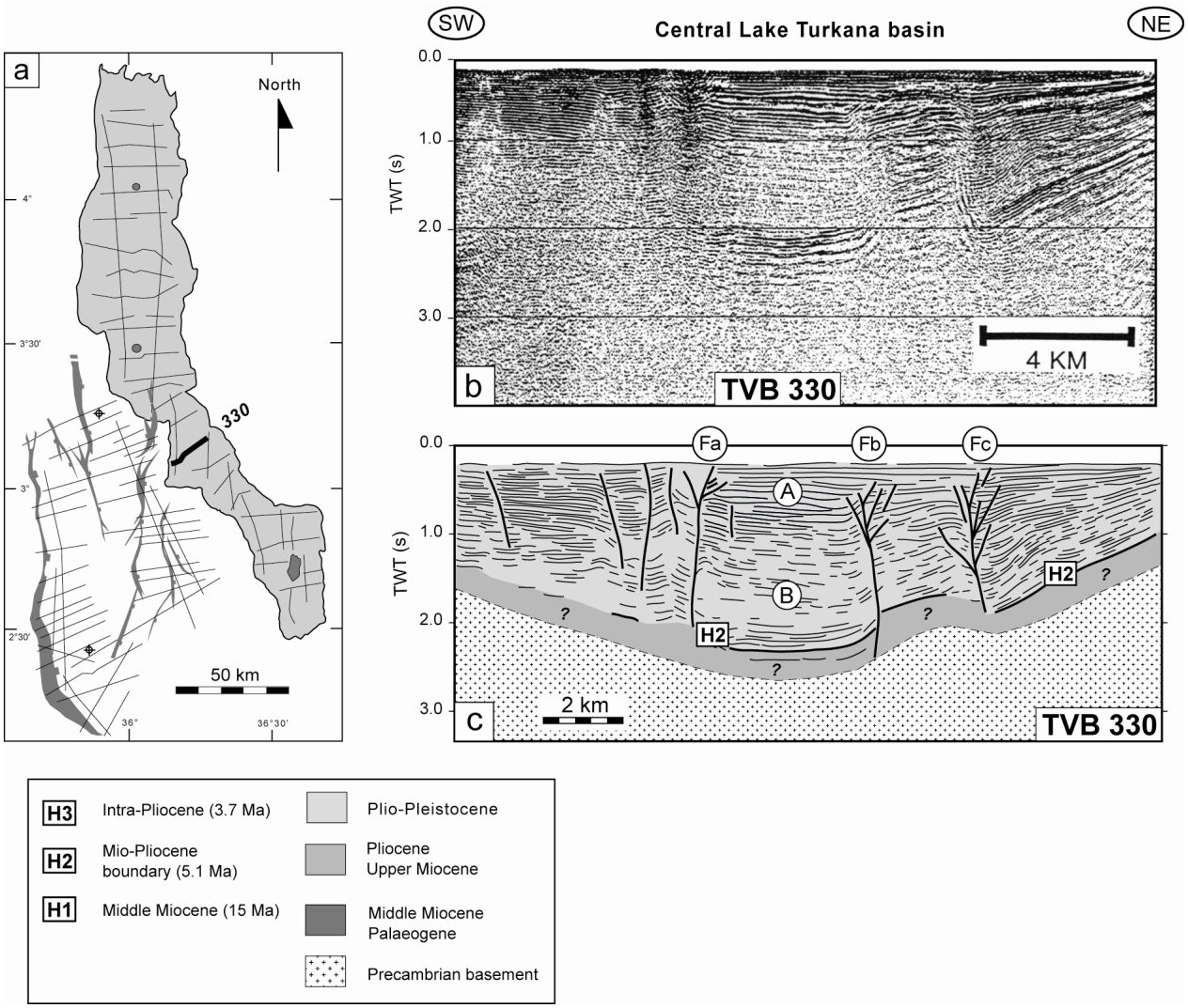

Figure 4. *Strike-slip fault-induced deformation involving recent synrift series in the Central basin of Lake Turkana. (a) Similar location map as Figure 2a. (b and c) Migrated and interpreted sections of line TVB 330 showing flower-like structures developed in sediments (<3.7 Ma) on top of steep faults (named Fa and Fb). These faults, inferred to strike at ca. N140°E, show an extensional displacement at depth close to horizon H_2. Letters refer to structures (faults and sedimentary packages) cited in the text.*

Marked variations of post-H_2 sediment thicknesses on both sides of faults Fb and Fc suggest that differential vertical movement took place along synsedimentary structures showing a NNW-SSE orientation on the post-H_2 sediments isopach maps of *Dunkelman et al.* [1989]. The present-day slightly reverse attitude of faults Fb and Fc indicates some component of horizontal shortening (post-H_2) parallel to the section (NE-SW). On the other hand, the fan-shaped branching fault network resembles flower-like structures typically formed in strike-slip fault regime [*Harding,* 1983; *Sylvester,* 1984]. Indeed, the fault diffraction geometry observed at the branching point of

each diverging fault set, e.g. at a depth of about 1 sec. (TWT), is close to the interface between highly reflective series (A) and a more transparent underlying sedimentary package (B) (Figure 4c). Hence, the observed fault pattern resembles that commonly obtained in experimental modelling of strike-slip fault systems through lithologically contrasted superposed sequences [*Richard et al.,* 1995]. It is therefore suggested that the deformation recorded by the NNW-SSE-trending faults Fa, Fb and Fc during or after synsedimentary activity involves both shortening and strike-slip displacement.

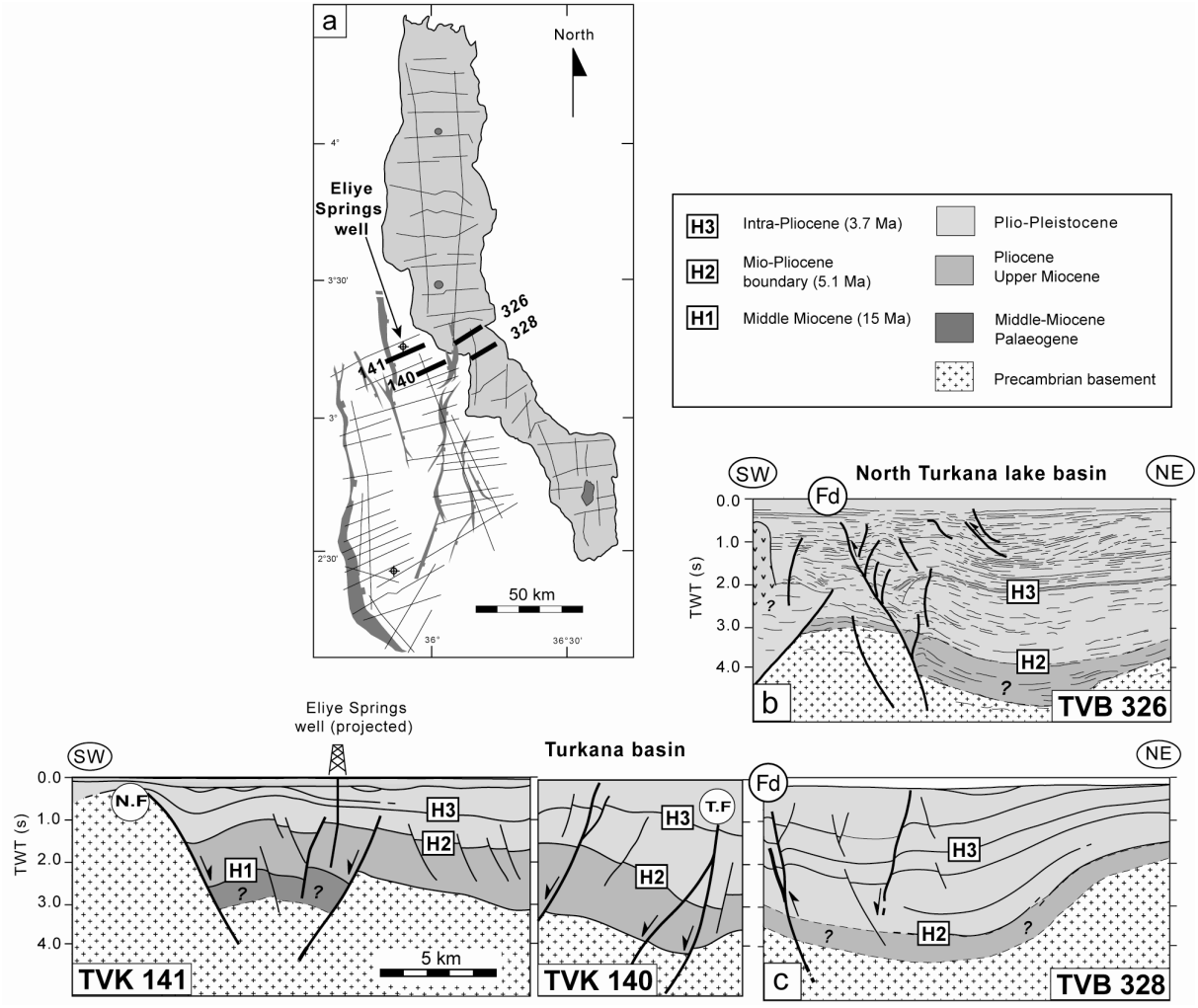

Figure 5. *Slightly inverted basins in the Turkana rift resulting from reverse reactivation of earlier extensional faults. (a) Similar location map as Figure 2a. (b) Westerly-verging drag-folds in Pliocene sediments of the North basin (Lake Turkana) resulting from reversal of movement along an earlier extensional fault (Fd). The minor fault splay branching along the uppermost part of fault Fd may indicate a slight component of oblique slip displacement. (c) Similar fold-fault geometry observed at the southern extremity of fault Fd on the calibrated seismic sections TVK 141, TVK 140, TVB 328. The infill stratigraphy of this composite line is tied with the Eliye Springs well (projected).*

- A nearly similar reactivated fault system is observed further north on seismic line TVB 326 (Figure 5b), close to the steep easterly-dipping fault (Fd) that represents an early extensional structure involving to the east a thick H_2-H_3 hangingwall sequence calibrated by the Eliye Springs well. Modest reversal of movement along Fd fault plane is indicated by the asymmetric and westerly-verging large wavelength drag fold developed in its immediate hangingwall series. The gentle fold can be traced onto the adjacent line TVB 328 (Figure 5c) and its inferred NS/N160°E direction is thus likely to result from a nearly EW-oriented shortening. As stated above for the inverted faults of section TVB 330, reactivation of fault Fd might also integrate some lateral slip, as expressed by minor antithetic faults splay branching on the eastern side of the fault that still shows a preserved extensional geometry.

2. A second type of folded structures still results from reactivated extensional fault, but without any strong evidence for strike-slip motion. The best examples are illustrated on the onshore seismic line TVK 11 that supplies a complete structural section, ~100 km-long, of the North Kerio basin and the southern extremity of the Turkana basin (Figure 6). The oblique section of figure 6d lies at low angle (~20°) to the NS axis of the basins, and it shows two main depocenters (H_2-H_3 sequences) in the hangingwall of the Lothagam (Lo.F) and Kerio (K.F) faults. The wedge-shaped Pliocene sequences in the hangingwall of the Lo.F are folded into a ~5 km-wavelength anticline, and they seem to override to the NNW the thinner footwall sequences, in turn, moderately inclined (apparent dip of ~15°) to the NNW. The dip-line TVK 102 cuts at high angle the fault trace and thus supplies the exact 2D-geometry of the structures (Figure 6e). This reverse faulting pattern is confirmed by field observations along the exceptionally well-exposed Lo.F scarp where tilted footwall volcanics, 4.7 Ma-old [*Haileab et al*., 2004], are cut by the steep east-facing Lo.F plane (Figure 6f). The highly-plunging (55° to the ESE) slickenside striations measured on the fault surface are indicative of reverse displacement to the WNW, with a minor lateral component (Figure 6g). Further SSE on the seismic line TVK 11, the K.F also appears to have been inverted, with footwall series that are furthermore gently folded in an upright anticline. In both cases, the deformed footwall sequences are sharply truncated by the present-day erosion level. Additional supportive evidence for contractional deformation in the central part of the North Kerio basin are supplied by a series of upright folding and associated diverging faults that preferentially involve pre-H_2 sequences (Figures 6b and 6c). The overall hangingwall/footwall structures depicted on line TVK 11 can be thus regarded as the consequence of coeval uplift and shortening processes developed in the vicinity of major rift faults.

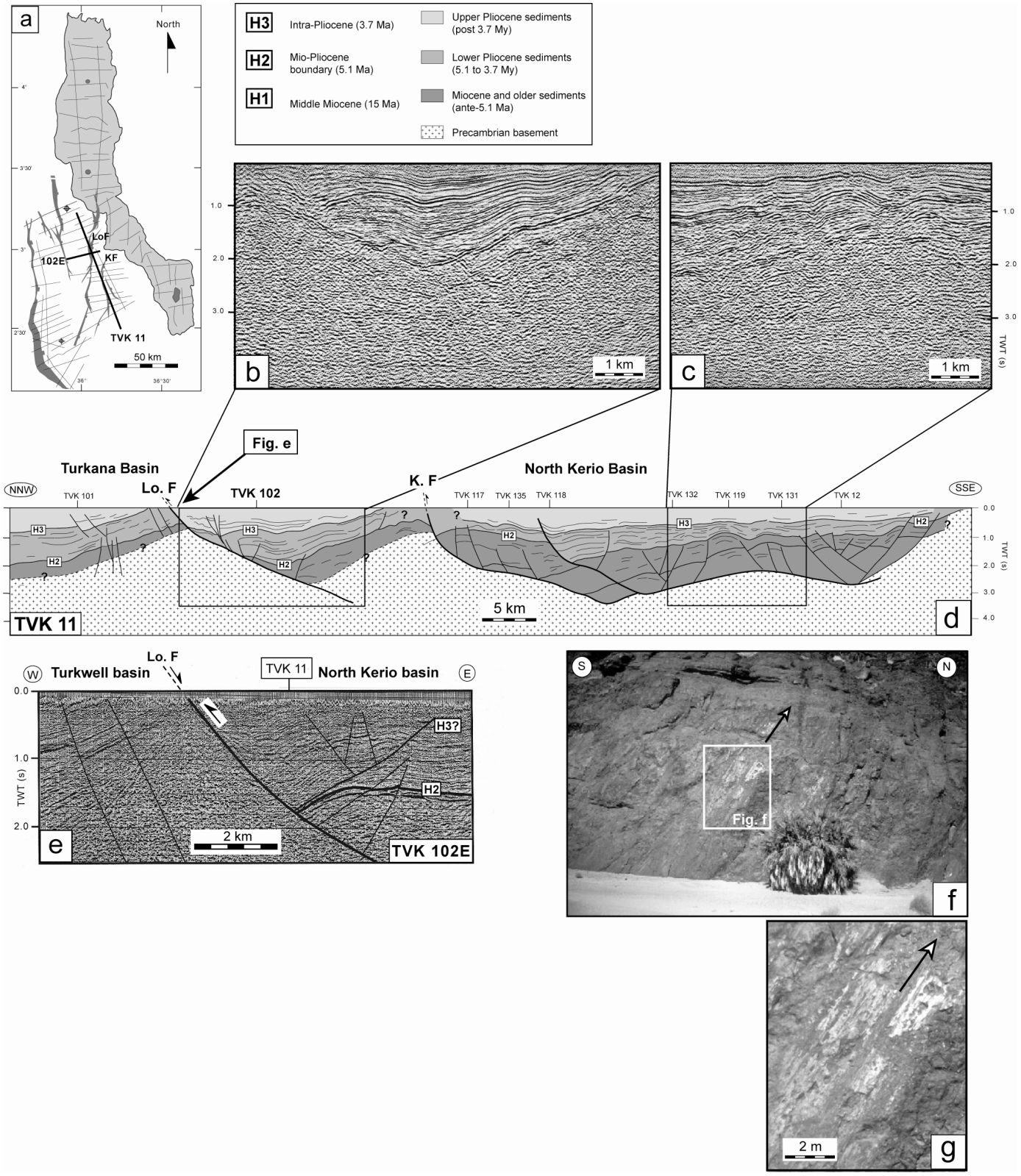
a
North
4°
3°30'
3°
2°30'
LoF
KF
102E
TVK 11
50 km
36°
36°30'
H3
Intra-Pliocene (3.7 Ma)
H2
Mio-Pliocene boundary (5.1 Ma)
H1
Middle Miocene (15 Ma)
Upper Pliocene sediments (post 3.7 My)
Lower Pliocene sediments (5.1 to 3.7 My)
Miocene and older sediments (ante-5.1 Ma)
Precambrian basement
b
1 km
c
1 km
1.0
2.0
3.0
TWT (s)
Fig. e
Turkana Basin
North Kerio Basin
NNW
SSE
Lo. F
K. F
TVK 101
TVK 102
TVK 117
TVK 135
TVK 118
TVK 132
TVK 119
TVK 131
TVK 12
H3
H2
5 km
TVK 11
d
W
Turkwell basin
Lo. F
TVK 11
North Kerio basin
E
H3?
H2
2 km
e
TVK 102E
S
N
Fig. f
f
2 m
g

Figure 6. *Contractional folding and reverse faulting in the Turkana and North Kerio onshore basins. (a) Similar location map as Figure 2a. (b and c) Focussed view of the migrated seismic line TVK 11 showing (b) folded synrift sequences (post-H3) in the hanging wall of the master fault Lo.F and (c) a fault/fold linked system developed in the synrift series above the Kerio master fault. (d) Structural interpretation of TVK 11 reflection seismic line cutting obliquely the Turkana and North Kerio basins. The two main distinct depocentres associated with the Lothagam and Kerio faults are clearly depicted. The inclined and eroded strata forming a monoclinal beneath the Lo.F may result from footwall uplift prior to or coeval with the reverse reactivation of Lo.F. (e) Interpreted seismic reflection line TVK 102E cutting at high angle the Lothagam fault system and illustrating upward arching of post-H2 synrift series [after Morley et al., 1999c]. (f) Field evidence for oblique sense of motion along the Lothagam master fault. Striations are plunging 50° to the SSE. Black arrow indicates the attitude of the striaes of the fault surface. The palm-tree is about 10 m-high. (g) Focussed view of striation on the Lothagam fault plane.*

---

3. A third type of inverted structures corresponds to newly-formed low-angle reverse faults in the Pliocene series of the Turkana and North Kerio onshore basins [*Morley et al.,* 1999c]. Their geometry in the southernmost part of the Turkana basin is depicted on the seismic sections in Figures 7b and 7c.

The Pliocene-(Miocene?) sequences define an asymmetrical graben deepening to the east as the result of greater displacement along the westerly-dipping Turkwell border fault network to the east. On line TVK 3, across the median part of the basin, a shallowly-dipping reverse fault cuts through the basement top and dies rapidly upwards to the west within the sedimentary section (Figure 7b). The amount of throw is estimated at 0.5 km from basement top offset. This low-angle reverse fault forms, together with a steeper inverted normal fault (Fe), a triangle-shaped undeformed zone. This composite compressional fault system is absent on the seismic line TVK 141, about 10 km further south (Figure 5). With regards to the large-scale graben-like profile imaged on the line TVK 3 (Figure 7b), the low-angle reverse fault initiates close to the inflection point Y between a flat-lying and shallow segment of the basin floor to the west, and an easterly-dipping portion, reaching a maximum depth of 2.5-3.0 sec. (TWT) to the east.

Other low-angle reverse faults also exist in the easternmost part of the Turkana graben. On line TVK 138 (Figure 7c), a west-verging imbricate contractional wedge occurs in the hangingwall of the Turkwell fault zone, suggesting that this latter acted as a buttress. The entire reverse fault network roots at shallow depth along an easterly-dipping decollement close to the base Pliocene level. It seems that the overall inverted deformation in the Turkana asymmetric graben preferentially develops within the thickest part of the synrift sedimentary infill, in agreement with experimental modelling of graben inversion tectonics [*Brun and Nalpas,* 1996].

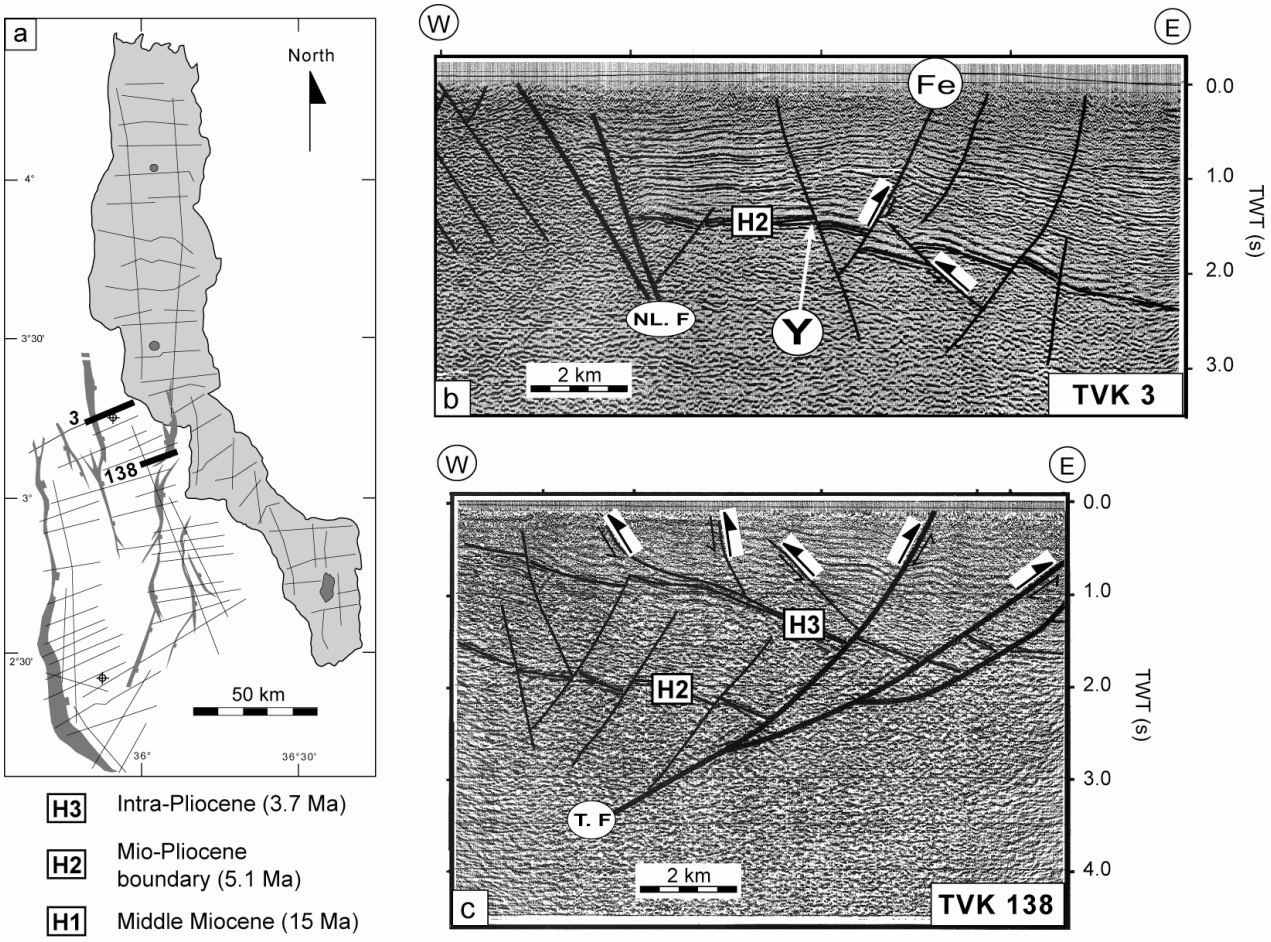

***Figure** 7. Examples of low-angle and newly-formed reverse faults in Pliocene series of the Turkana onshore basin (see location on Figure 1b). (a) Similar location map as Figure 2a. (b) Steep (reactivated) and low-angle (newly-formed) reverse faults in the Turkana asymmetric graben (line TVK 3). Note that inverted structures occur at depth close to basement top. NL.F, Napedet-Lothidok fault. (c) Similar reverse fault geometry in youngest series (post-H_3) at the eastern faulted border of the Turkana basin. T.F, Turkwell fault.*

4. The last type of contractional features is imaged on the onshore seismic lines TVK 136-117-135-118-131 within the northernmost part of the North Kerio basin (Figure 8). Representative inverted deformations are imaged on the dip-profile TVK 117 where shallow (<1.5 sec. TWT) Pliocene sediments [*Morley et al.,* 1999c] are affected by a series of km-wavelength upright anticlines, further disrupted by a closely-spaced (1-2 km) fanning fault network with locally reverse displacements. Contrasts in sediment thicknesses within adjacent fault-bounded blocks indicate that most of faults originated as extensional structures, prior to H_3. A system of dominantly east-facing tilted blocks (x 3), with minor antithetic westerly-dipping faults, is recognised, and inversion tectonics appear to concentrate in the thickest depocentres to the east (X and Y on Figures 8c and 8d), in agreement with experimental models [*Brun and*

Nalpas, 1996]. The combined reactivation of diverging normal faults results in extrusive uplifted wedges which do not completely cancel the previous extensional fault offsets. According to *Morley et al.* [1999c] from geometrical estimates, the maximum amount of uplift on the depth-converted section of figure 8d is about 1 km.

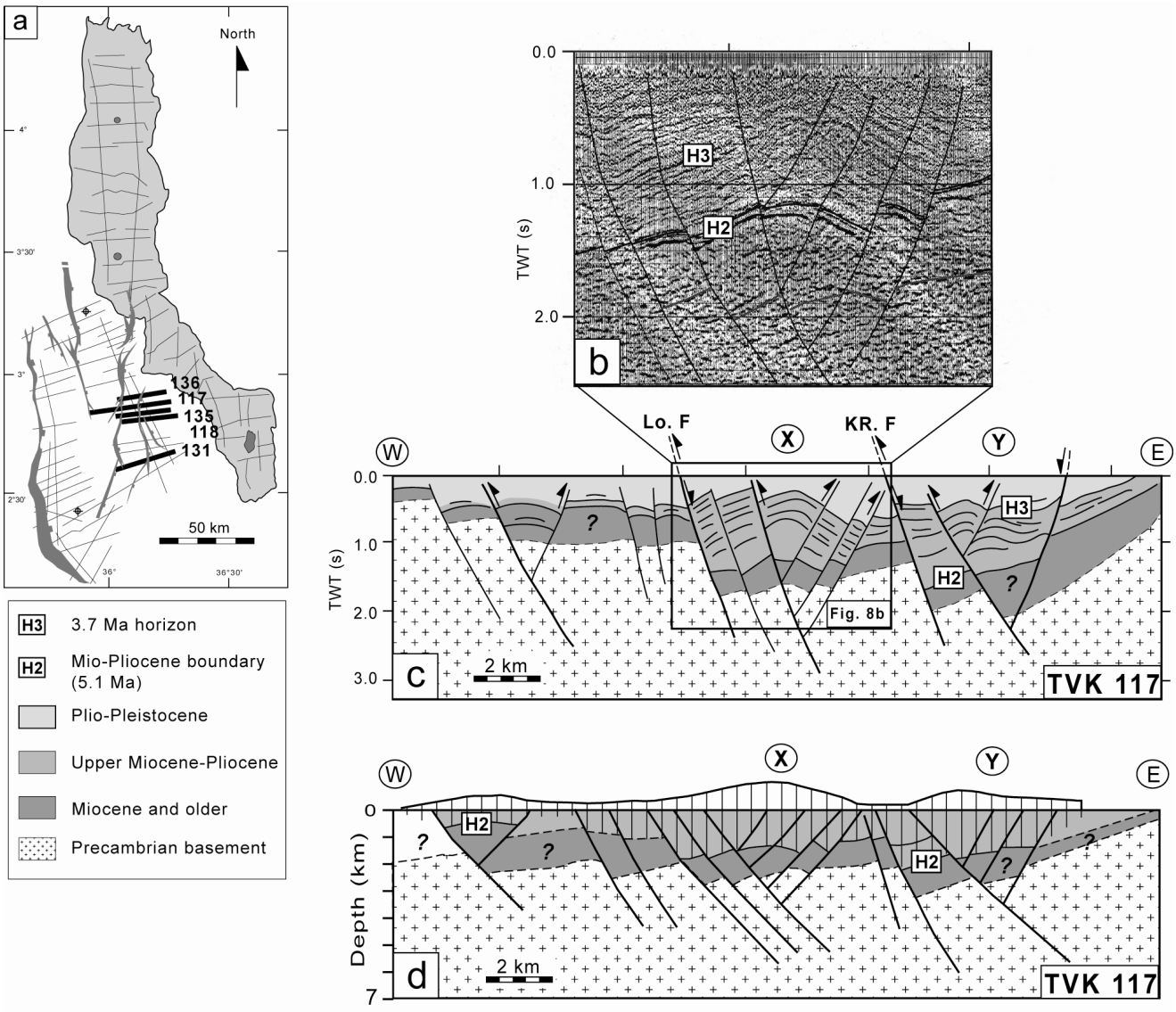

Figure 8. *Upright folding and reverse faults in the North Kerio basin. (a) Similar location map as Figure 2a. (b) Portion of migrated seismic line TVK 117 across the small graben-like basin named 'X' on Figure 8c. A diverging fan of earlier normal faults displaying reversal of motion cuts inversion anticlines. (c) Interpreted seismic line TVK 117 showing the positive inversion of the deepest parts (called X and Y) of the North Kerio basin. The localized distribution of the dense fault network is drawn on the map of figure 9 (see text for discussion). (d) Depth-converted profile TVK 117 showing the amount of eroded section above the inverted zones, after Morley et al. [1999c].*

3.3.3.2. Origin of the Turkana inverted structures

3.3.3.2.1. Spatial distribution

Morley et al. [1999c] tried to explain the restriction of known inversion structures within the Kenya rift to only the Western Turkana region in terms of the interaction of local buoyancy forces with far-field stresses. Two key-aspects of the inversion in Turkana basins which need to be explained by any putative mechanism are the short time-span and the geographically-restricted distribution of related structures. From calibrated seismostratigraphy, the onset of inversion tectonics in the Turkana rift basins is assumed to have occurred during Upper Pliocene times, later than 3.7 Ma (post-H_3). Secondly, on the basis of the existing seismic grid, five discrete inverted zones are distinguished (Figure 9). Three main large areas extend as elliptic cartographic zones (20 x 40 km) with a NS/N160°E-trending axis at the northern extremity of the North Kerio basin and in its offshore prolongation. Two of them form the immediate hangingwall of the Lothagam and Kerio faults, onshore. Two smaller and round-shaped inverted areas also exist to the NW in the onshore Turkana basin. The absence of inverted deformations within the Lokichar half-graben to the west is noticeable. In map-view, the overall inverted area is a ~40 x 100 km elongate zone, trending at N160°E, close to the oblique and central segment of modern Lake Turkana. It roughly coincides (except the Central lake basin to the east) with a high-density zone of normal faulting, reported from seismic reflection data [*Morley et al.,* 1999a] (Figure 9b), and shown as closely-spaced and fan-verging reactivated structures on profile TVK 117 of Figure 8. With regards to the entire Turkana extensional fault network, the high-density fault zone forms a ~40 km-wide transverse corridor at N160°E, in which fault traces swing markedly from a NS regional trend to a N20°E oblique direction (Figure 9b).

The overall linearity of the Turkana NS rift system is thus locally disturbed over a N160°E elongate corridor, resulting firstly in the higher frequency and bifurcation of the previous extensional fault network, and secondly, in its reverse reactivation (Figure 9b). The spatial coincidence between inversion tectonics and anomalous extensional structures suggests a causal link between these two features. That leads us to precise the lateral extent and the origin of the anomalous fault zone from surface geological markers, and then to attempt to find timing and kinematic indicators for addressing its tectonic significance with respect to the long-lived evolution of the Turkana rift.

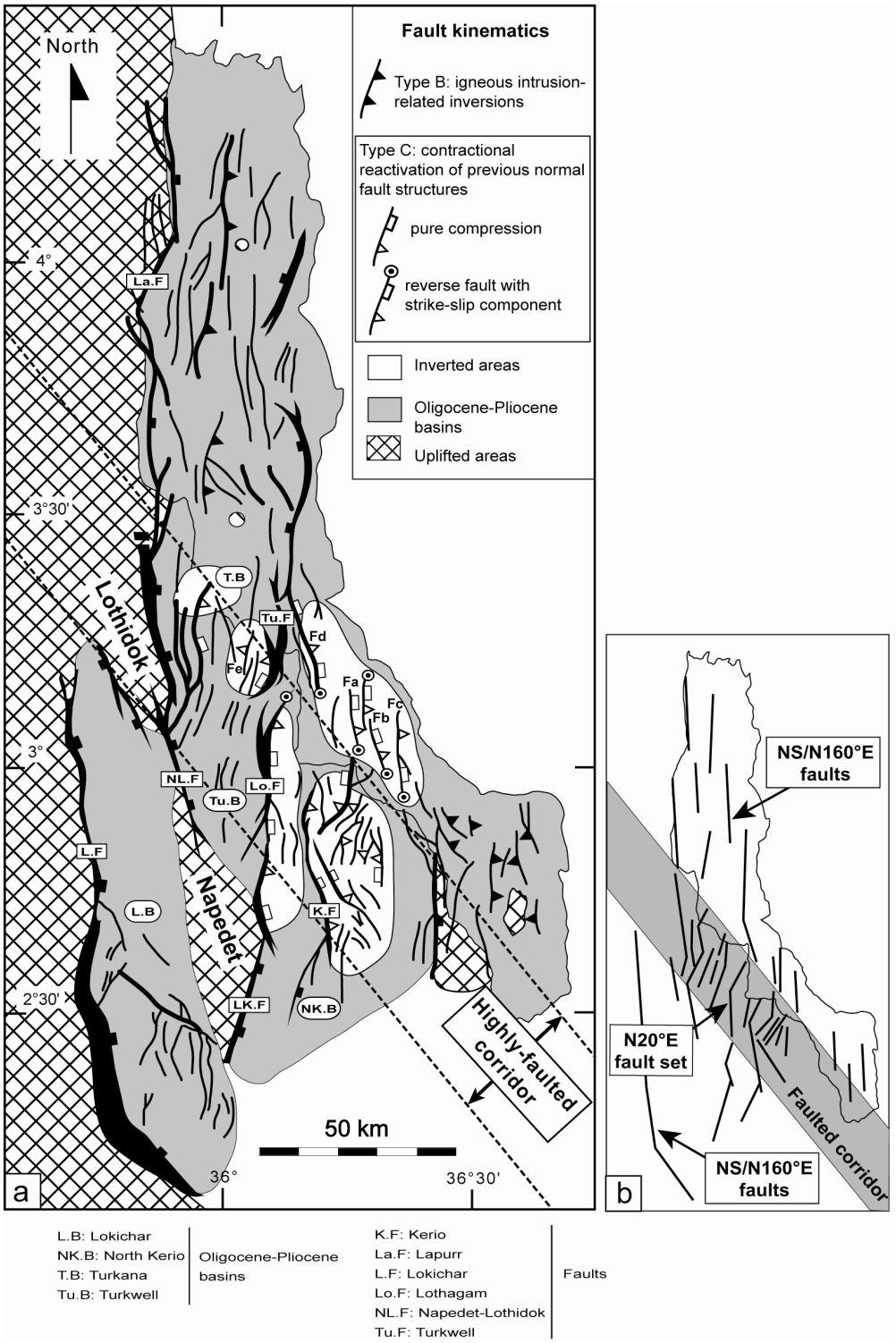

Figure 9. *Map distribution of faults in the main onshore basins (Lokichar, North Kerio, Turkwell and Turkana) of the Turkana rift. (a) Restricted spatial location of inverted structures within discrete elongated areas occurring in a large-scale transverse corridor. This 40 km-wide structural corridor is also marked by a denser network of short and intra-basinal faults that swing at N20°E. Fa, Fb, Fc and Fd refer to fault structures cited in the text. (b) Sketch structural maps illustrating the change of fault direction within the N140°E-trensing highly faulted corridor.*

3.3.3.2.2. Evidence for pre-existing oblique discontinuities

Interpretation of two Landsat TM images (169-058, 23/10/1999 and 170-058, 18/01/2000) allows us to identify a number of structures that differ in nature and age along a regional-scale lineament lying over more than 300 km from the Lothidok plateau to the NW, to the southeastern edge of Lake Turkana, e.g. nearly along part of the above-mentioned anomalous rift zone (Figure 10).

1. In the southern wedge-shaped segment of the Lothidok (Miocene) volcanic plateau, both fracture network and traces of tilted lava flows curve toward parallelism (from NS to N160°E) with the oblique fault-like limit bounding sharply the plateau to the SW (Figure 10a).

2. In the Loriu Hills, on the southwestern side of Lake Turkana, the trace of the Proterozoic foliation plane is dextrally deflected along a 15 km-long linear faulted zone, striking at ~N140°E, parallel to the lake shoreline (Figure 10b). In the same area to the NW, the multistage rejuvenation of N140°E-striking fault/fractures is also inferred from a number of Tertiary dykes following a NW-SE trend, and from the southern faulted termination of Turkana Grits **(**Cretaceous or Miocene in age) exposures.

3. In the Mount Porr area, on the opposite (eastern) side of Lake Turkana (Figure 10d), the E-W arrangement of Quaternary lacustrine sediments is disrupted by a set of N140°E lineamentary fault-like structures that probably root at depth along Cenozoic faults bringing into contact Miocene volcanics and synrift sedimentary series (Turkana Grits).

4. At a greater scale, the Proterozoic basement terrains exposed on the eastern side of the Central Kenya rift pass abruptly eastwards into the Anza-Chalbi Plain along a NW-SE-trending morphological scarp, laterally offset by oblique structures (Figure 10c).

Figure 10. *Evidence for a long-lived transverse (N140°E) fault zone (N'Doto) in the Turkana Cenozoic rift. (a) Structural interpretation of the Landsat TM scene 169-058 in the southern extremity of the Lothidok Miocene volcanic plateau (see figure 10d for location). The faulted origin of this boundary is evidenced by both the sharp southern termination of the volcanics and the cartographic virgation of both faults and lava flows. (b) Sketch map of the Loriu area (SW onshore side of Lake Turkana, see figure 10d for location) from interpretation of the Landsat satellite scene TM 169-058. Note the oblique trend of the lakeshore and the cartographic inflection of basement foliation along a N140°E (dextral?) fault inferred to be part of the NTFZ. (c) Detail view of SRTM (Shuttle Radar Topography Mission) digital elevation model (data from the NASA) showing the transverse faulted boundary of the N'Doto basement relief, SE of Lake Turkana (see figure 10d for location). The NTFZ is expressed by a 20 km-wide zone of highly fractured relief (with a maximum topographic elevation of 2000 m in the cross-section XY drawn on map 10c). Within the N140°E fault zone, fault block uplift occurs along NS-trending structures following basement fabrics. (d) Synthetic structural map of the Turkana rift showing the distribution of inversion tectonics with regards to the first-order extensional and transverse fault networks identified in the present study from seismic and remote sensing dataset. Same abbreviations as figure 9a. The Kataboi and Buluk transverse fault zones (TFZ) are not discussed in the paper.*

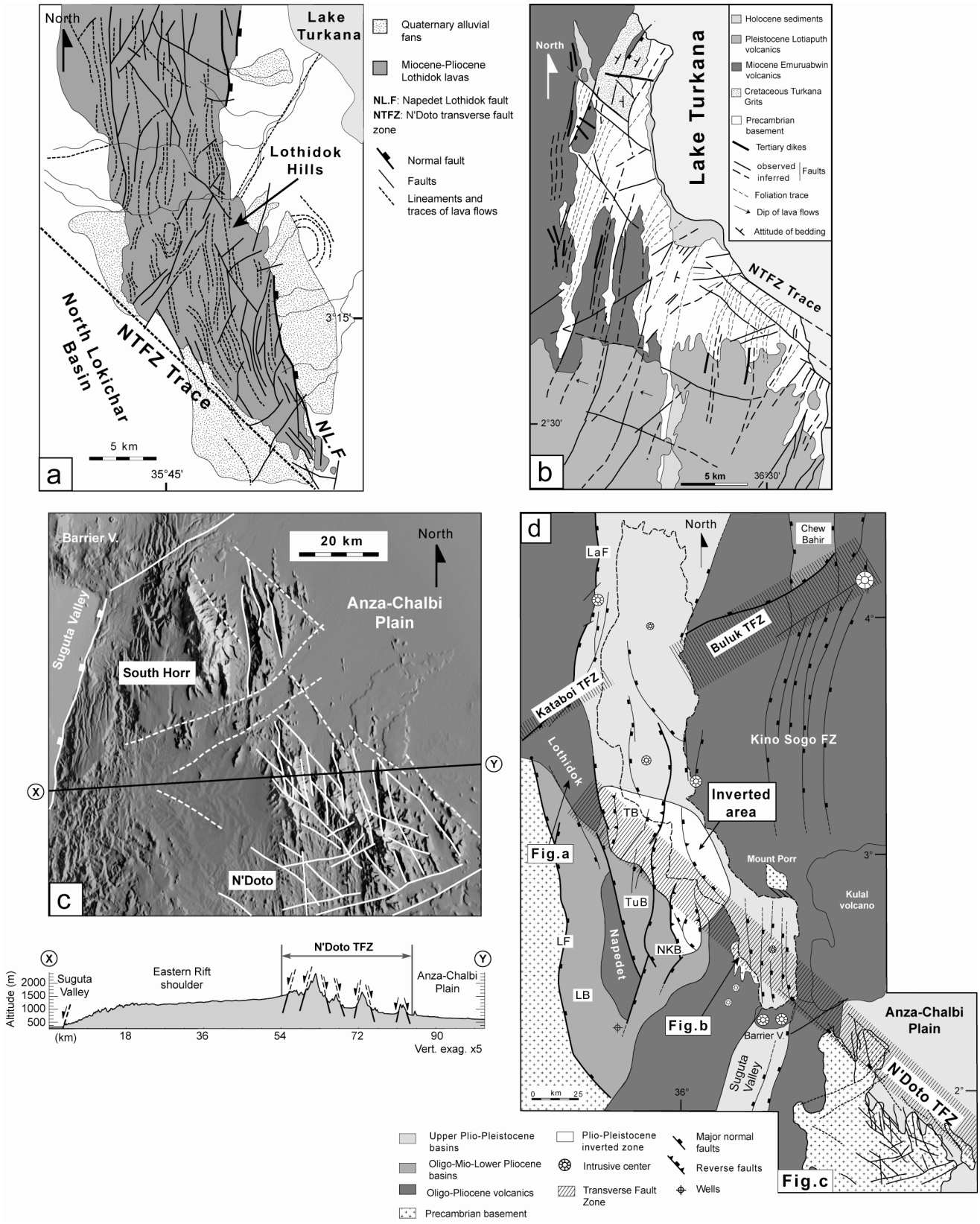
North
Lake Turkana
Lothidok Hills
North Lokichar Basin
NTFZ Trace
NL.F
3°15'
5 km
35°45'
a
Quaternary alluvial fans
Miocene-Pliocene Lothidok lavas
NL.F: Napedet Lothidok fault
NTFZ: N'Doto transverse fault zone
Normal fault
Faults
Lineaments and traces of lava flows
Holocene sediments
Pleistocene Lotiaputh volcanics
Miocene Emuruabwin volcanics
Cretaceous Turkana Grits
Precambrian basement
Tertiary dikes
observed
inferred
Faults
Foliation trace
Dip of lava flows
Attitude of bedding
NTFZ Trace
2°30'
5 km
36°30'
b
Barrier V.
20 km
North
Anza-Chalbi Plain
Suguta Valley
South Horr
N'Doto
c
X
Y
N'Doto TFZ
Suguta Valley
Eastern Rift shoulder
Anza-Chalbi Plain
Altitude (m)
2000
1500
1000
500
(km)
18
36
54
72
90
Vert. exag. x5
d
North
LaF
Chew Bahir
Buluk TFZ
Kataboi TFZ
Lothidok
Kino Sogo FZ
Inverted area
TB
Fig.a
Mount Porr
Kulal volcano
TuB
LF
Napedet
NKB
LB
Fig.b
Barrier V
Anza-Chalbi Plain
Suguta Valley
N'Doto TFZ
4°
3°
2°
36°
0 km 25
Upper Plio-Pleistocene basins
Oligo-Mio-Lower Pliocene basins
Oligo-Pliocene volcanics
Precambrian basement
Plio-Pleistocene inverted zone
Intrusive center
Transverse Fault Zone
Major normal faults
Reverse faults
Wells
Fig.c

This topographical boundary is outlined to the east in the South Horr-N'Doto range by a narrow (~20 km-wide) strip of anomalously elevated relief (as high as 2000 m) that suggests recent vertical movement. The location of this large-scale transverse faulted corridor, about 50 km east of the Suguta axial valley, excludes its origin from rift-flank uplift. It correlates on AMOCO seismic lines with the SW border fault system of the Anza rift and that indicates its nucleation at depth along Cretaceous structures that have been repeatedly rejuvenated in Middle-Miocene, as evidenced by apatite fission-tracks thermo-chronology [*Foster and Gleadow,* 1992].

From the line of structural evidence above, it is proposed that the Turkana Cenozoic rift comprises a large-scale basement-rooted discontinuity, referred to as the N'Doto transverse fault zone (NTFZ hereafter), as long as 300 km and with a maximal width of nearly 40-50 km over the E-W trending segment of modern Lake Turkana (Figure 10d). The NTFZ is part of a complex deep-seated fault network, involving also the so-called Kataboi and Buluk transverse fault zones (Figure 10d), and responsible for the structural segmentation of the Turkana rift, as a whole [*Vétel and Le Gall,* submitted]. The possible contributing role of the NTFZ with respect to the inverted deformation in part of the Turkana rift is discussed in the kinematic model below.

3.3.3.2.3. Kinematic hypotheses

Applying a kinematic model to any deformed areas requires the accurate characterisation of the principal strain axes and/or those of the corresponding applied stress field ($\sigma_1/\sigma_2/\sigma_3$) [see *Ziegler and Cloetingh,,* 2004, for example]. The data and assumptions discussed below about the Turkana rift lead us to establish a three-stage evolutionary model dominated by rapid changes of the stress field conditions during recent periods (<5 Ma.) (Figure 11). In contrast, the long-lived (33-5 Ma.) earlier rifting stage is inferred to have occurred under a constant extensional stress field (Figure 11a) with a ~N90°E-directed horizontal extension (σ_3) only deduced from the ~NS orientation of the master syndepositional rift fault network (Lokichar, Kerio) [*Morley et al.,* 1992]. Reliable data are not available to constrain the palaeo-stress field of the Turkana rifted zone during the onset of basin inversion (<5 Ma.). Field measurements of recent fault planes are too few and the kinematics of seismically-imaged faults is poorly known. Despite these limitations, kinematic hypotheses are attempted, based on the 2D-mapped arrangement of extensional and inverted fault networks (Figures 11b and 11c), as well as on the recent rift kinematics known elsewhere in the EARS, and compared with experimental models.

Comparing the two fault maps of stages 5-3.7 Ma. and 3.7 Ma.-Present shows the preferential development of young anomalous rift structures, involving both extensional and inverted

deformation, above the long-lived NTFZ discontinuity. These characteristics suggest similarity with models of deformed cover sequences on top of a basement fault reactivated in a dominantly strike-slip mode [*Richard et al.,* 1989 and 1995; *Higgins and Harris,* 1997]. According to these experiments, the trace of en-echelon extensional fractures makes an angle of 45° in plan-view to the shear direction [*Tchalenko,* 1970; *Sylvester,* 1984]. Similar angular relationships are observed in the present case study between the (initially normal) N20°E fault network (assimilated to T-type fractures) and the N140/160°E orientation of the NTFZ, hence considered as a possible (40 km-wide) dextral shear zone. In such a dominant strike-slip fault regime, the horizontal axis of shortening (σ_1) should be oriented N20°E, parallel to the tensional fractures, while the corresponding extension direction (σ_3) should be N110°E (Figure 11b). From these assumptions, it is therefore suggested that major kinematic changes occurred in the Early Pliocene, marked by the permutation of the principal stress axes σ_1/σ_2 and the transition from normal fault extension to strike-slip regime. The new stress field favoured lateral fault displacement along suitably oriented structures such as the NTFZ which is likely to have undergone dextral reactivation (Figure 11b). Strike-slip tectonics is dominated by initiation of extensional features (T-type fractures) within the shear zone, hence indicating, at first approximation, compressional and extensional axes oriented respectively N20°E and N110°E. A slight (20°) clockwise rotation of extension, from N90°E to N110°E, is thus believed to have also occurred during stress permutation (Figures 11a and 11b). Inversion tectonics developed later under changing stress field conditions dominated by a N130°E-directed extension, as deduced from the N40°E alignment of recent fissure-style volcanic cones throughout the <1 Ma-old Hurri, Asie and Marsabit shied volcanoes [*Key and Watkins,* 1988], in the Anza-Chalbi desert to the east of the study area (Figure 11c). A similar switch of the extension direction to NW-SE during Upper Pliocene is also proposed by other authors for other parts of the EARS [*Strecker et al.,* 1990; *Bosworth et al.,* 1992; *Delvaux et al.,* 1992; *Bosworth and Strecker,* 1997]. The corresponding shortening direction was thus nearly N40°E, i.e. slightly oblique to the NS and N20°E trends of earlier tensional fault/fracture networks that are likely to have been reactivated as oblique reverse structures.

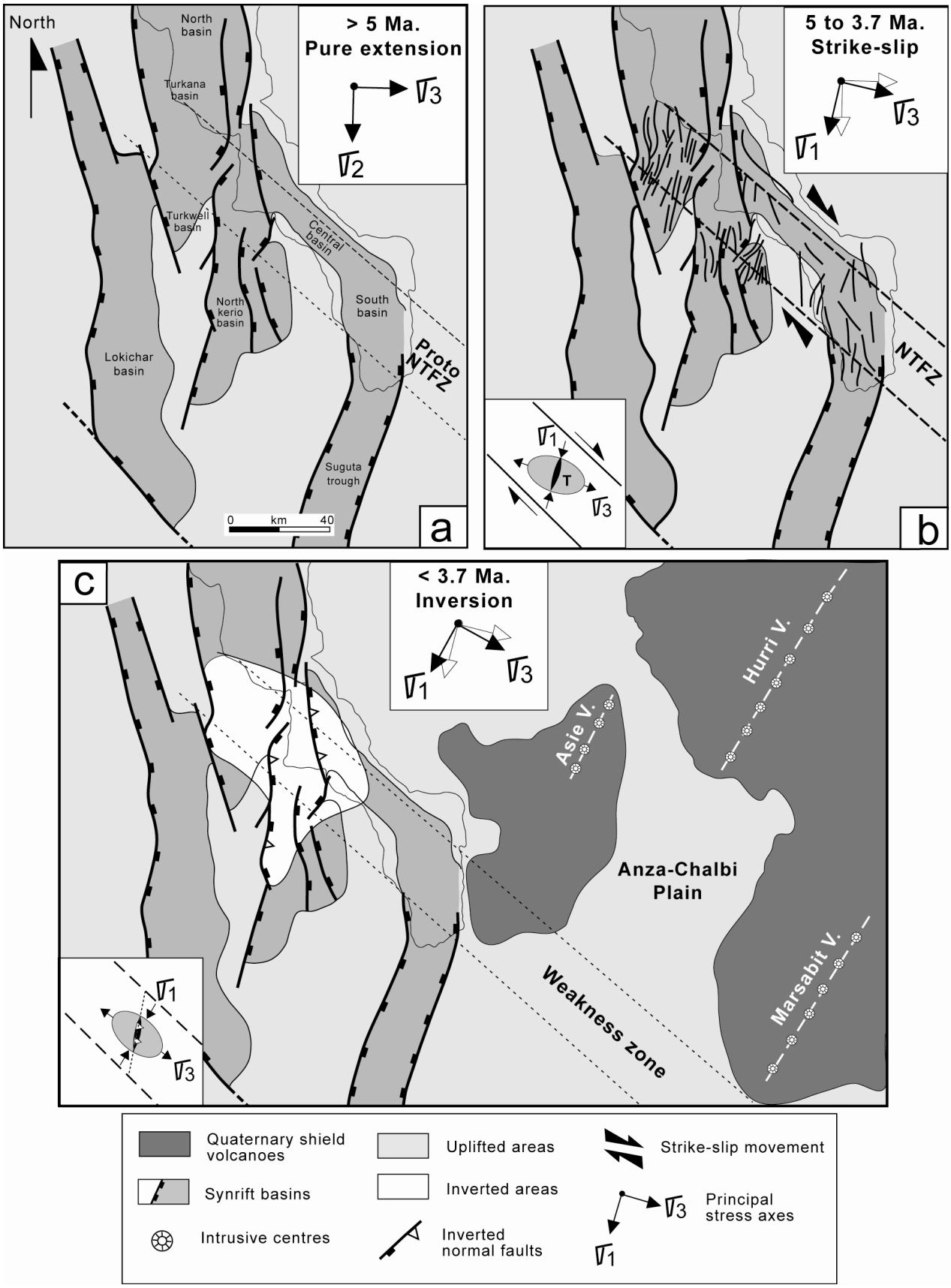
North
North basin
Turkana basin
Turkwell basin
Central basin
North kerio basin
South basin
Lokichar basin
Proto NTFZ
Suguta trough
0 km 40
a
> 5 Ma.
Pure extension
σ3
σ2
5 to 3.7 Ma.
Strike-slip
σ1
σ3
NTFZ
T
b
c
< 3.7 Ma.
Inversion
Hurri V.
Asie V.
Anza-Chalbi Plain
Marsabit V.
Weakness zone
Quaternary shield volcanoes
Synrift basins
Intrusive centres
Uplifted areas
Inverted areas
Inverted normal faults
Strike-slip movement
Principal stress axes

Figure 11. *Three-stage kinematic model for the Turkana rift from Miocene times onwards. For each evolutionary stage, the trace of modern Lake Turkana is drawn as a geographical reference. (a) Major basin development during Miocene times under pure EW extensional regime. (b) First increment of strike-slip (dextral) reactivation of the N'doto transverse basement fault zone (NTFZ) as the result of permutation of stress axes (σ1 and σ 2) and the clockwise rotation (~20°) of horizontal principal stress axes. The dense tensional fault pattern in the North Kerio, Turkwell and Turkana basins might have formed as 'T' Riedel-type structures within a transverse corridor controlled at depth by the reactivated NTFZ. (c) Basin inversion stage illustrating the rejuvenation of earlier extensional faults under an oblique shortening regime. The ~N130°E direction of the corresponding extension (σ3) is deduced from aligned Quaternary intrusive centres. At this stage, the NTFZ is no longer dextrally reactivated.*

One consequence of this recent stress axes rotation (~20° in a still clockwise sense) is that the direction of the inferred regional shortening axis (~N40°E) is at high angle (nearly 80°) to the NTFZ, hence preventing any further strike-slip reactivation of the N140°E fault system (Figure 11c).

As mentioned above about the spatial distribution of inverted deformation, rift-parallel fault structures (NS to N20°E) lying outside the NTFZ with a similar reactivation potential (Lokichar and Lapurr faults, as well as the Kino Sogo and Suguta fault systems drawn on figure 10d) show no evidence of inversion. It thus appears that strain preferentially concentrated within the NTFZ, probably as the result of a decreasing crustal strength caused by steep mechanically weak planes in the basement. The key-role of pre-rift anisotropies on the existence of such crustal weakness zones (analogue to the NTFZ) in rift systems is commonly reported elsewhere [*Ziegler et al.,* 1995; *Ziegler and Cloetingh,* 2004].

We therefore come to the conclusion that basin inversion in the Turkana rift mainly results from the combined effects of stress field changes (permutation and, to a lesser extent, clockwise rotation of principal stress axes $\sigma_1/\sigma_{2)}$, and the mechanical behaviour of a long-lived crustal-scale weakness zone oblique to the rift axis.

3.4. Conclusions

Three kinds of folded structures are present in the Turkana rift, one kind arose during extension, the other two are associated with inversion of extensional structures. Around Lake Turkana, folds are found adjacent to igneous intrusion complexes, and appear to have originated as a result of intrusion emplacement during the Pliocene. The third kind of inverted structures is the main focus of this study. The inversion structures occurred later than 3.7 Ma and have a patchy distribution in five main areas, predominantly in the eastern parts of the onshore rifts, extending into Lake Turkana. The region affected by inversion is confined to an elongate transverse corridor trending

N160°E, with dimensions about 40 km x 100 km, and referred to as the N'Doto transverse fault zone (NTFZ). The NTFZ appears to be related to basement discontinuities oblique to the rift that have been described in a related study [*Vétel and Le Gall,* submitted]. It is proposed in this study that partial inversion of the Turkana rift basins results from two major changes in the stress regime during Pliocene times. The first kinematic stage is dominated by stress axes permutation σ_1/σ_2 that leads to the transition from an extensional regime, where the least principal stress was oriented N90°E, to a transpressional wrench regime where extension was furthermore slightly rotated (~20°) to N110°E. The tensional faults formed within the dextral shear zone (NTFZ) are subsequently inverted, in association with strata folding, as the result of the ongoing clockwise rotation (~20°) of the shortening direction (N40°E) which is thus oblique to the N20°E extensional structures. Similar conclusions about causal links between inversion tectonics and permutation of stress axes have been envisaged elsewhere [*Illies and Greiner,* 1978], and more locally for the recent kinematic evolution of the Malawi rift, in the southern part of the EARS [*Ring et al.,* 1992].

The suggestions made above about the recent kinematic framework of the Turkana rifted zone are tentative and should be further properly evaluated with an integration of additional field data dealing with recent fault motion.

Acknowledgements

Fieldwork was supported by the ECLIPSE (Environnements et Climats du Passé) Program INSU-CNRS (Dir. H. Roche). Authors thank the National Oil Corporation of Kenya for providing the seismic dataset and for field logistics. They are also grateful to the two referees for their helpful comments and more particularly to Damien Delvaux for his thorough review which was very useful for improving the paper. This publication is the contribution n° 935 of the IUEM, European Institute for Marine Studies (Brest, France).

4. Geometry and growth of an inner rift fault pattern: the Kino Sogo Fault Belt, Turkana Rift (North Kenya)

William Vétel[a], Bernard Le Gall[a] & John Walsh[b]

[a] UMR-CNRS 6538 'Domaines Océaniques', Institut Universitaire Européen de la Mer, Place Nicolas Copernic, 29280 Plouzané, France.

[b]Fault Analysis Group, Department of Geology, University College Dublin, Belfield, Dublin 4, Ireland.

Submitted to Journal of Structural Geology (November, 29, 2004).
Manuscript reference SG-D-04-00103

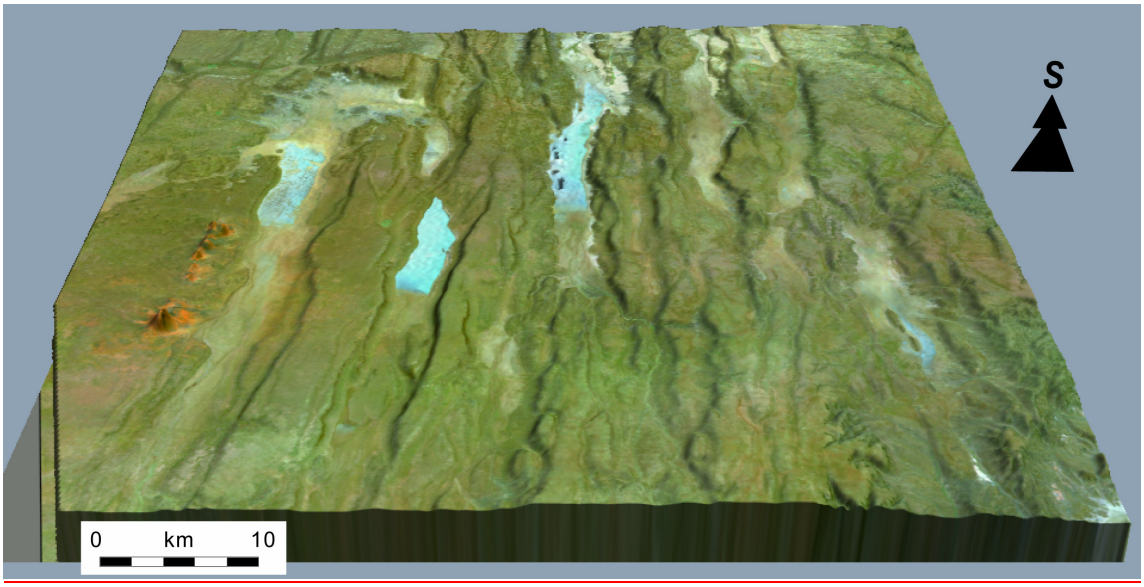

Perspective view of a portion of the Landsat image 169-057 overlain on the digital topography SRTM in the region of the Kino Sogo fault belt (view to the south, light from West, vert. exag. x3).

Abstract

A quantitative analysis is presented on the scaling properties of faults within the exceptionally well-exposed Kino Sogo Fault Belt from the eastern part of the 200 km-wide Turkana rift, Northern Kenya. The Kino Sogo Fault Belt comprises a series of horsts and grabens within an arcuate 40 km-wide zone that dissects Miocene-Pliocene lavas overlying an earlier asymmetric fault block. The fault belt is ~150 km-long and is bounded to the north and south by transverse (N50°E and N140°E) fault zones. An unusual feature of the fault system is that it accommodates very low strains (<1%) and since it is no older than 3 Ma., it could be characterised by extension rates and strain rates which are as low as ~0.1mm/yr and $10^{-16}s^{-1}$ respectively. Despite its immaturity, the fault system comprises segmented fault arrays with lengths of up to 40 km, with individual fault segments ranging up to ~9 km in length. Fault length distributions subscribe to a negative exponential scaling law, as opposed to the power-law scaling typical of other fault systems. The relatively long faults and segments are however characterised by maximum throws of no more than 100 m, providing displacement/length ratios which are significantly below those of other fault systems. The under-displaced nature of the fault system is attributed to early stage rapid fault propagation possibly arising from reactivation of earlier magmatic-related fractures or underlying basement structures/fabrics. Combined with the structural control exercised by pre-existing transverse structures, the Kino Sogo Fault Belt demonstrates the strong influence of older structures on rift fault system growth and the relatively rapid development of under-displaced fault geometries at low strains.

Keywords: Rift extension, recent grid faults, fault growth model, remote sensing, Kino Sogo Fault Belt, Turkana Rift, Kenya.

4.1. Introduction

In many continental rifts active deformation is focussed in a graben-like inner depression where syntectonic fluvio-lacustrine sediments accumulate, in association with extensive lava flows emitted from axial volcanoes. As a consequence, rift-related structures exposed on the floor of the inner trough are often partly or totally concealed beneath recent syn-rift cover, a factor that complicates any attempts to define fault system geometry. In these circumstances, numerous uncertainties arise concerning the geometry and kinematics of faults (nucleation, propagation and fault linkage) and even the calculation of bulk extension. Similar difficulties are often encountered in the axial trough of the East African Rift System (EARS hereafter) and along the eastern magmatic branch in Kenya, in particular (Fig. 1). The inner fault pattern of the Kenya Rift is, however, exceptionally well exposed in three specific areas (Fig. 1b), consisting of the Kino Sogo fault system (KSFB), the Maji-Moto fault system and

the Magadi fault system (Hackman et al., 1990; Le Turdu, 1998; Gloaguen, 2000). A common feature of these well-exposed fault systems is that they are developed within recent (<3 Ma.) lava flows that are devoid of any overlying sedimentary deposits. Previous quantitative studies of the Maji-Moto and Magadi fault systems have provided improved definitions of either their extensional strain rate (Gloaguen, 2000) or their palaeo-stress fields (Le Turdu, 1998).

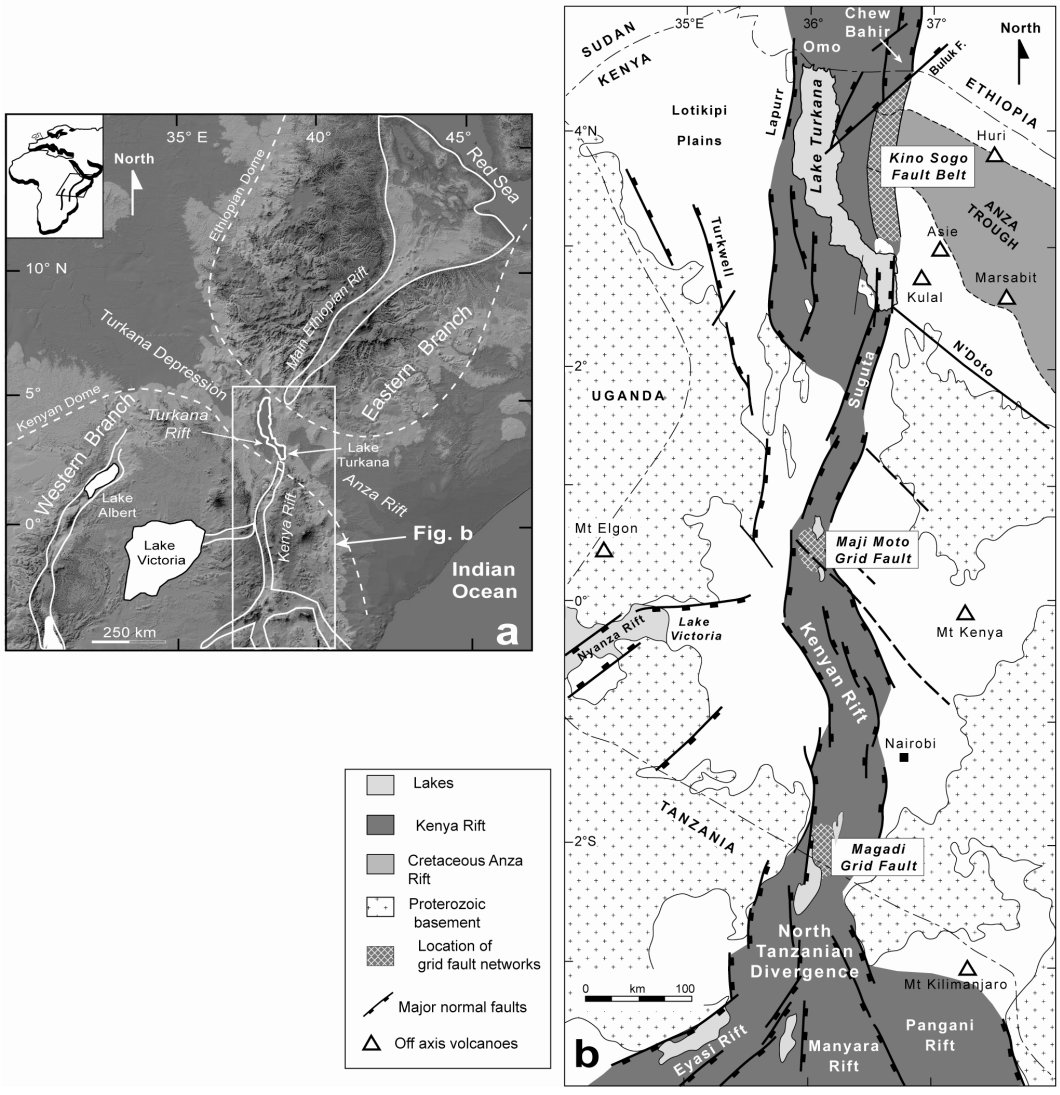

Figure 1. *General setting of the Turkana rift along the eastern branch of the East African Rift System (EARS). a. Digital elevation model of the eastern part of the EARS (from Gtopo 30 data elevation data). The N140°E Turkana depression extends between the Ethiopian and Kenyan domes (dashed lines) following the trace of the Cretaceous Anza rift. b. Structural map of the Kenya rift. Active deformation is concentrated along the linear and narrow Kenya trough excepted at its two extremities where the axial rift splits into 3 branches in the North Tanzanian Divergence to the south and into a more subdued 200 km-wide rift zone along the Turkana area to the north. Inner deformation is concealed by volcanics or sedimentary infill with the exception of three grids fault exposed in the Kino Sogo (under study), the Maji-Moto and the Magadi areas.*

In this paper, we present a description and analysis of the geometry and growth of the KSFB using data constraints derived from outcrop studies, remote sensing data and digital elevation models (Fig. 2). Quantitative analysis of the KSFB is greatly helped by the excellent definition of the fault system on the upper surface of Pliocene lava flows that are not disrupted by either younger volcanic edifices or later sediments. The fault system geometry accommodates only ~1% of fault-related extension during the past 3 Ma. with potentially extremely low extension rates (0.1 mm/yr) and displays scaling properties, including displacement/length scaling and fault populations, that differ from those established from many fault systems characterised by higher strains (Schlische et al., 1996). We attribute these fault geometries and scaling properties either to structural inheritance from rift-parallel Proterozoic crystalline basement fabrics underlying the 200 m-thick Eocene-Pliocene lava pile and/or to the rejuvenation of a younger fracture network generated by bending stress at the top of a volcanic dome. The significance of earlier transverse structures is supported by the presence of cross-cutting, and possibly also contemporaneous faults, which parallel the N50°E and N140°E-oriented discontinuities bounding the KSFB to the north and south. The NW-SE fault trend is known to follow the trace of Anza Cretaceous-Palaeogene rift (Greene et al., 1991; Bosworth, 1992; Smith & Mosley, 1993; Bosworth & Morley. 1994; Dindi, 1994; Ring, 1994; Morley et al., 1999b; Vétel & Le Gall, submitted).

4.2. Geological setting

Within the Turkana depression, the EARS is a polyphased rift system developed since Eocene-Oligocene times (~35 Ma.; Dunkelman et al., 1989; Hendrie et al., 1994; Morley et al., 1999a; Vétel & Le Gall, submitted). The KSFB is part of the youngest rift domain that mainly extends along the easternmost edge of the ~200 km-wide previously rifted zone (Figs. 1b and 2; Gabriel & Aronson, 1987; Ebinger et al., 1993; Ebinger et al., 2000). Because of the subdued and intricate topography of this eastern sector, typical rift morphologies are not easily recognised and a variety of contrasting models have been advanced for the spatio-temporal evolution of the rift. According to Dunkelman et al. (1988 & 1989), the active zone of deformation is concentrated within the offshore basins of Lake Turkana and southwards into the linear, graben-like, trough of the Suguta valley (Bosworth & Maurin, 1993; Dunkley et al., 1993). In contrast, Hackman et al. (1990) proposed a double-armed rift system comprising the Lake Turkana faulted basins to the west and the KSFB into the Chew Bahir trough to the east (Gabriel & Aronson, 1987; Ebinger et al., 2000), with or without both arms linking southwards into the Suguta valley (Fig. 3). This model is favoured by our studies of both recent and earlier Cenozoic extensional fault patterns in the Turkana depression (see also Vétel & Le Gall., submitted).

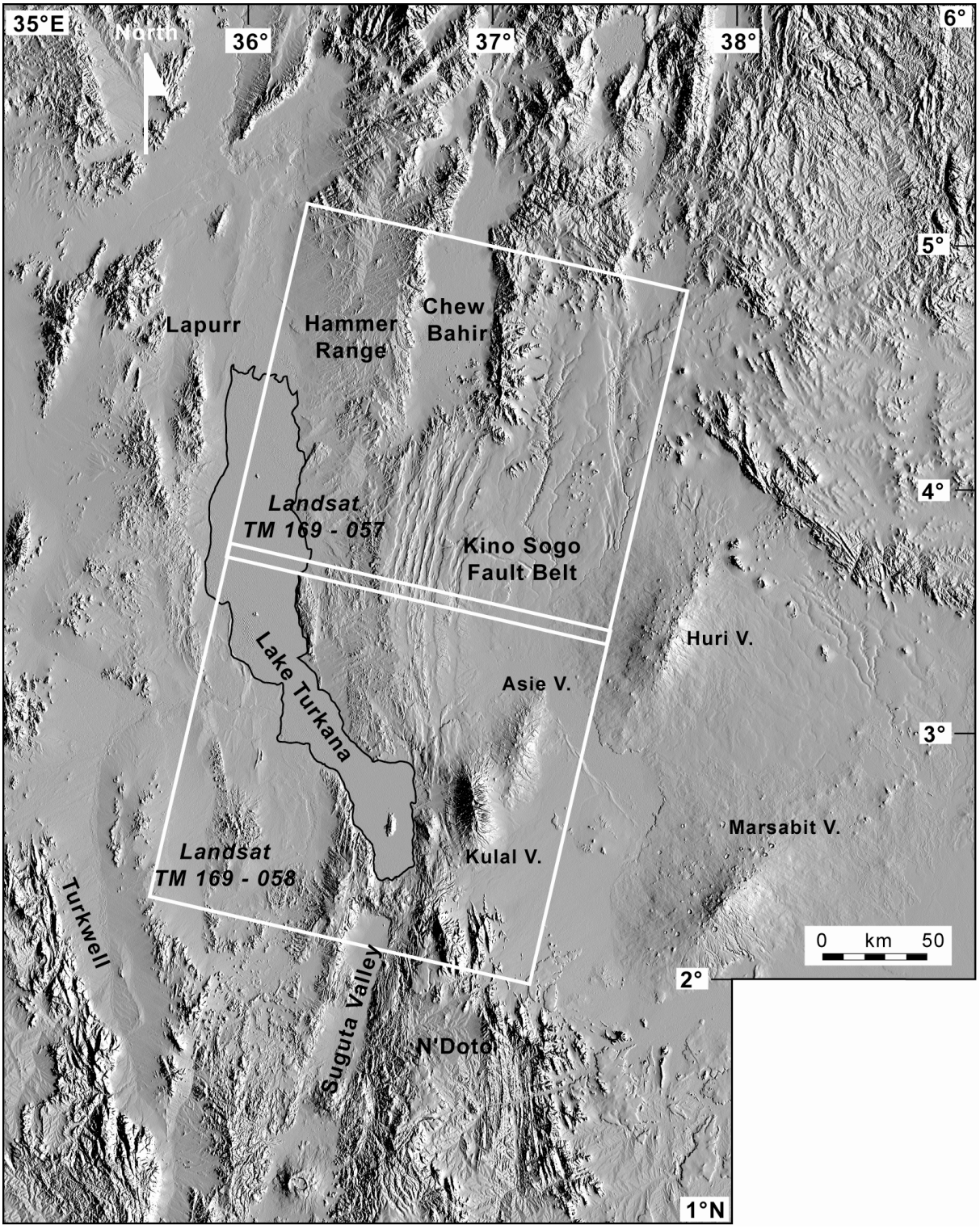

Figure 2. *SRTM (Shuttle Radar Topography Mission) digital elevation model of the broad Turkana rifted zone (resolution 90 m in lateral, 16 m in vertical). White squares indicate the Landsat TM coverage. Note the more subdued topography of the Turkana depression by contrast with Ethiopian and Kenyan relief to the north and south, respectively. The elevated Kino Sogo fault network cuts through volcanics and is well-exposed with regards to the adjoining depressed Chew Bahir graben, Suguta trough, and Lake Turkana basin.*

Using new topographic and remote sensing datasets we also investigate the extent to which the N140°E Cretaceous Anza-type and N50°E structures of the Buluk transverse fault zone (BTFZ) might have influenced the faulting process in the KSFB-Chew Bahir fault zones (Figs. 1 and 3).

Over the past ~35 Ma., the Kino Sogo area *sensu lato* was a dominantly volcanic domain comprising Eocene-Miocene lavas of the Balesa Koromto and Jarigole Fms in the west, overlain to the east by the Pliocene volcanics of the Gombe Fm. (north) and the Hurran Hurra Fm. (south) (Fig. 4; Charsley, 1987; Key & Watkins, 1988; Ochieng et al., 1988; Wilkinson, 1988; Haileab et al., 2004). This dominantly-basaltic complex thins dramatically eastwards over an uplifted footwall block bounded by three major syn-magmatic extensional faults (Figs. 4b and 4d): (i) the N50°E-trending Buluk Fault in the north, belonging to the 30 km-wide BTFZ which displays an array of NE striking faults that partly accommodated the early development of the Chew Bahir basin during Miocene times (Vétel & Le Gall, submitted), (ii) the Allia Bay fault (Fab) in the west which is mainly documented from the rapid westerly sequence growth of the Eocene-Miocene Balesa Koromto/Jarigole Fms (Fig. 4c), and (iii) the Hoi fault in the east which bounds the westernmost exposures of Miocene grits in the Anza basin (Fig. 4b; Morley et al., 1999b). During Eocene-Miocene times, the combined effect of these extensional faults led to the formation of an asymmetric horst block, with a general tilt to the SE (Figs. 4 and 5). This block is believed to have been subjected to significant internal extension along NS-trending fault structures that might have controlled the emplacement of Miocene intrusions such as the Jibisa volcanic complex to the NE (Hackman et al., 1990), adjacent to the transverse structures of the BTFZ (Fig. 4). The uplifted nature of the Kino Sogo fault block prior to the deposition of the Jarigole-Gombe volcanics is supported by the following lines of evidence: (i) the presence of a condensed, 250 m thick, Eocene-Pliocene volcanic sequence directly overlying basement, (ii) the rapid (six-fold) increase in thickness of this volcanic sequence to the west of the Allia Bay Fault (Fig. 4c), (iii) the preservation of scattered inliers of Pliocene lacustrine deposits of the Koobi Fora Fm. (Wilkinson, 1988; Feibel et al., 1989) within the Hurran Hurra low-relief area to the south (Fig. 7b) hence representing the transgression of high-lake levels along a palaeo-embayment to the south of the Kino Sogo area. Continued uplift of the Kino Sogo block following deposition of the Pliocene Gombe volcanics is defined by a gradual 200 m decline in terrain towards the east away from the Allia Bay Fault (cross-section 2 on figure 5). The KSFB post-dates and cuts through this tilted fault block into unexposed Proterozoic metamorphic rocks of the Mozambic belt at depth (Figs. 4 and 7; Smith & Mosley, 1993; Maurin & Guiraud, 1993; Shackelton, 1993; Hetzel & Strecker, 1994). Since the fault system cross-cuts Pliocene Gombe Fm. volcanics, it records deformation that is no older than ~3 Ma. (Hackman et al., 1990; Haileab et al., 2004). A younger age of faulting (<2.25 Ma.) is possible if the aligned intrusive bodies of the Kokurfo Bolol dated complex (Wilkinson, 1988) are controlled and dissected by the easternmost fault of the KSFB (Fe on Fig. 4b).

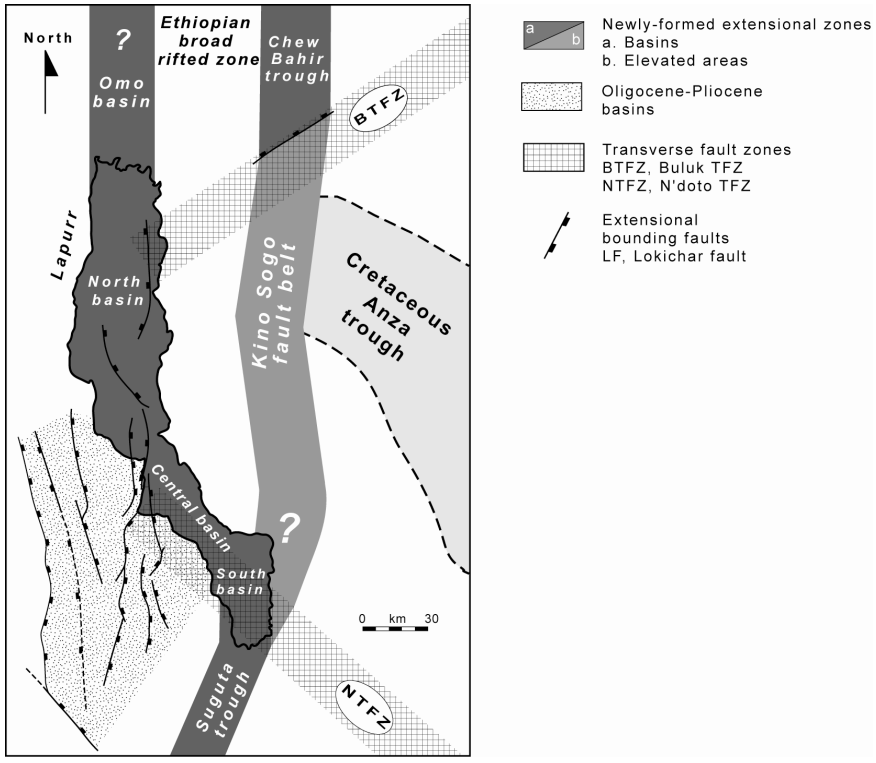

Figure 3. *Structural sketch map showing the location of recent/active deformation (<3 Ma.) within the Turkana rifted zone. Note (1) the existence of Oligo-Pliocene deep half-grabens to the SW, not discussed in this work (see e.g. Morley et al., 1999a for further details), (2) the two parallel zones of recent deformation (Suguta, Lake Turkana basins, Kino Sogo and Chew Bahir) and (3) the similar width of the two rift branches despite their contrasted structural styles.*

4.3. Morphology and geometry of the Kino Sogo Fault Belt

The geometry of the KSFB (Figs. 2 and 4) has been defined from satellite imagery (Landsat Enhanced Thematic Mapper Plus) and recently available topographic data (SRTM; Shuttle radar topography mission; www2.jpl.nasa.gov/srtm). The study area is covered by two Landsat ETM+ images (169-058, 23/10/1999 and 169-057, 27/01/2000). These images have been improved using Geomatica 9.2 and ENVI 4.1 softwares, by merging the panchromatic band that displays the best ground resolution (unit pixel size of 15x15 m) with spectrometric band 2 (green 0,52 to 0,60 μm), band 4 (near infrared 0,76 to 0,90 μm) and band 7 (middle infrared, 2,08 to 2,35 μm) images with lower ground resolution (unit pixel size 30x30 m; Girard and Girard, 1999). These bands provide pixel reflectance and contrast that permit to better constrain the structural interpretation of satellite images. The digital elevation model has a lower lateral resolution (90x90 m) but provides a 3D-visualisation of the fault system and definition of fault throws >16 m. Since numerous smaller faults, with throws <16 m, are resolved by the Landsat scene, the datasets are complementary together providing a more complete overview of the Kino Sogo fault system (Figs. 4 and 7).

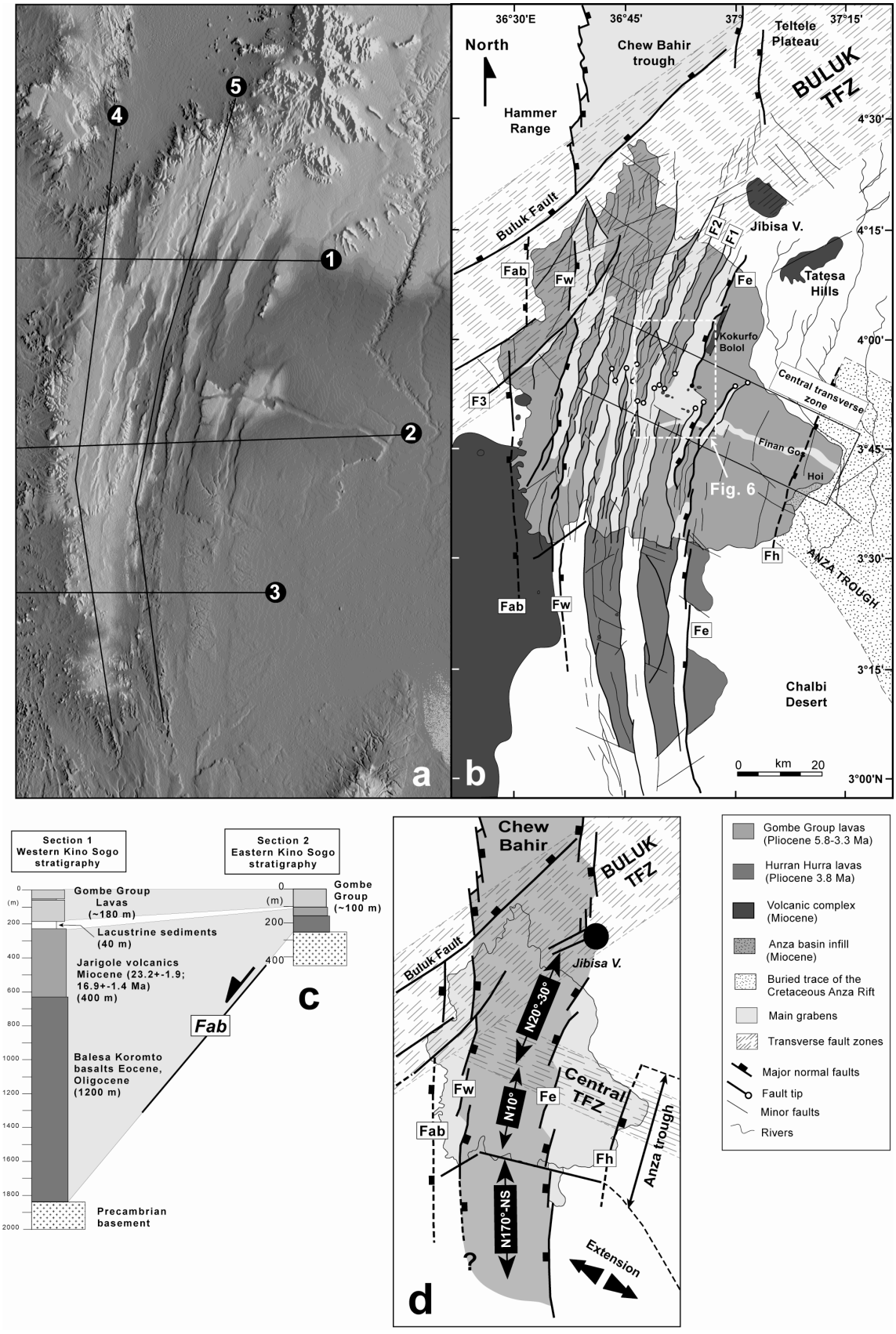
a
b
c
d
North
Chew Bahir trough
Hammer Range
Buluk Fault
BULUK TFZ
Teltele Plateau
Jibisa V.
Tatesa Hills
Kokurfo Bolol
Central transverse zone
Finan Gof
Hoi
Fig. 6
ANZA TROUGH
Chalbi Desert
Fab
Fw
Fe
Fh
F1
F2
F3
36°30'E
36°45'
37°15'
4°30'
4°15'
4°00'
3°45'
3°30'
3°15'
3°00'N
0 km 20
Section 1 Western Kino Sogo stratigraphy
Section 2 Eastern Kino Sogo stratigraphy
Gombe Group Lavas (~180 m)
Lacustrine sediments (40 m)
Jarigole volcanics Miocene (23.2+-1.9; 16.9+-1.4 Ma) (400 m)
Balesa Koromto basalts Eocene, Oligocene (1200 m)
Precambrian basement
Gombe Group (~100 m)
Chew Bahir
Central TFZ
N20°-30°
N10°
N170°-NS
Extension
Anza trough
Gombe Group lavas (Pliocene 5.8-3.3 Ma)
Hurran Hurra lavas (Pliocene 3.8 Ma)
Volcanic complex (Miocene)
Anza basin infill (Miocene)
Buried trace of the Cretaceous Anza Rift
Main grabens
Transverse fault zones
Major normal faults
Fault tip
Minor faults
Rivers

Figure 4. *Geological and morphostructural context of the extensional Kino Sogo Fault Belt (KSFB). a. Shaded SRTM digital elevation model of the Kino Sogo area (light from east and no vertical exaggeration). The location of sections in figure 5 is shown here. b. Structural interpretation from SRTM data of figure a (same scale). The KSFB is subdivided into two distinct faulted areas, the Gombe highly faulted domain to the north and the Hurran Hurra less deformed domain to the south. The Gombe domain is separated from the Chew Bahir trough to the north by the Buluk transverse (N50°E) fault zone. The first-order structures of the KSFB are dominated by a dense system of horst and graben controlled by normal faults that show variations in structural style along-strike. This system is bounded to the west and east by two inward-facing normal faults (Fw and Fe). c. Rapid thickness variations in the volcanic cover from the Kino Sogo (section 2) westwards (section 1) via the Allia Bay extensional fault (Fab). d. Structural sketch map of the KSFB showing the early limits of the easterly Kino Sogo tilted fault block (Fab, Allia Bay fault; Fh, Hoi fault). The three segments of the Pliocene fault system (<3 Ma.) are oriented from N170°E to N30°E northwards between left 'en-echelon' border faults.*

Apart from mapping the fault system, a variety of fault parameters (azimuth, length, spacing, throw) have been extracted from the 2D- and 3D-datasets as a prelude to our quantitative analysis of the fault system.

The KSFB is defined by a 40 km-wide system of extensional faults cross-cutting the pre-existing SE-dipping fault block (Figs. 4 and 5). In map-view, it forms a 150 x 40 km arcuate fault system that is convex to the west and trends between N170°E, in the south, and N30°E, in the north (Figs. 4 and 7). It contains horst and graben structures bounded by two external inward-facing faults (Fw and Fe on figures 4 and 5). The easternmost fault (Fe) extends over the entire length of the fault system. Its southern trace, up to the middle part of the Gombe domain (i.e. the area defined by the Gombe volcanics), is composed of 4 NS-N10°E-oriented left-stepping fault segments, each ~20 km-long (Fig. 4d). Further north, the trace of Fe is laterally offset by ~10 km to the west (and left) and then continues northwards as 2 almost co-linear, but nevertheless left-stepping, segments oriented at N20°-N30°E. 'En echelon' left-stepping fault segments also outline the trace of the western fault (Fw) which is however disrupted by Buluk-type transverse faults in the north. The southern extent of fault Fw is much less visible within the weathered Eocene-Miocene lavas. Indeed the southern part of the KSFB, north of the Kulal volcano and to the immediate W and NW of Asie volcano (Figs. 2 and 7), is poorly defined within the topographically subdued Hurran Hurra domain (i.e. where the Hurran Hurra basalts outcrop), that is partly concealed by recent eolian sands and Eocene-Miocene lavas.

Structural cross-sections across the fault system illustrate the gradual decline of the summit-level altitude towards the east, from 850 m down to 600 m close to Chalbi desert (Fig. 5). Along-strike (i.e. NS) sections show the elevated position (~800 m above sea level, on average) of the Gombe domain with regards to the subdued area (~600 m) of the Hurran Hurra and older basalts to the south.

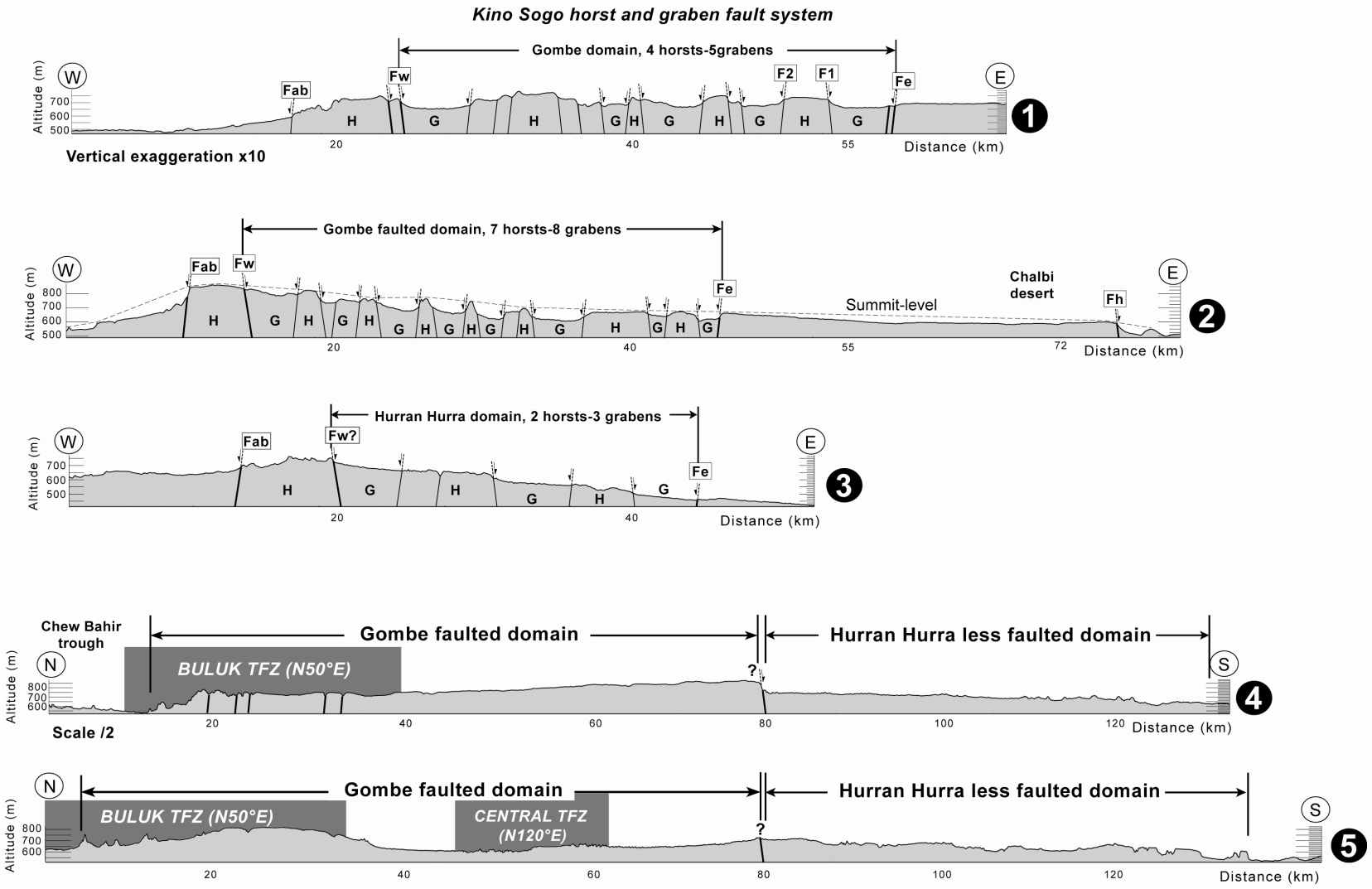
Kino Sogo horst and graben fault system
Gombe domain, 4 horsts-5grabens
W
E
Fab
Fw
F2
F1
Fe
H
G
Altitude (m)
700
600
500
20
40
55
Distance (km)
Vertical exaggeration x10
1
Gombe faulted domain, 7 horsts-8 grabens
Fab
Fw
Fe
800
700
600
500
Summit-level
Chalbi
desert
Fh
72
2
Hurran Hurra domain, 2 horsts-3 grabens
Fw?
3
Chew Bahir
trough
N
S
Gombe faulted domain
Hurran Hurra less faulted domain
BULUK TFZ (N50°E)
?
Scale /2
4
CENTRAL TFZ
(N120°E)
5

Figure 5. *Five structural sections thoughout the Kino Sogo Fault Belt (vertical exaggeration x10). 3 cross-sections (1, 2 and 3) and 2 along-strike sections (4 and 5), (see figure 4a for location). Note the horst and graben system with structural style variations along-strike from the Gombe domain (sections 1 and 2) to the Hurran Hurra domain to the South (section 3). Summit-level line on section 2 shows the asymmetric morphology of the Kino Sogo-easterly tilted block. Along-strike sections 4 and 5 cutting through two transverse faulted corridors (N50°E Buluk TFZ and N120°E Central TFZ) and the faulted limit between the Gombe and Hurran Hurra domains.*

The Gombe domain gives way to lower elevation areas to the north and south across topographic scarps, approximately oriented at N50°E (north) and N120°E (south), and probably related to transverse faulting. This change in elevation is particularly clear on along-strike sections (see sections 4 and 5 on figure 5) crossing the boundary between the well-preserved highly-faulted Gombe basalts to the north and the less well preserved and apparently less deformed terrain of the Hurran Hurra volcanics to the south.

The overall structure of the Gombe domain is dominated by a system of horsts and grabens bounded by first-order faults with maximum lengths of 35-40 km and vertical displacements that do not exceed 100 m (for example, F1 and F2 faults on Fig. 4b). In the North, the fault system comprises 5 pairs of N20°E-striking horst-graben with typical wavelengths of 8 km (see cross-section 1 on Fig. 5). The main bounding faults along the two easternmost horst-graben pairs are relatively continuous and linear, but are cross-cut and apparently offset by transverse (N50°E) faults of the ~30 km-wide BTFZ. The truncation and offset of individual graben across certain faults (e.g. F3 on Fig. 4b) are not however consistent, a feature which suggests that the transverse structures pre-date and are partly contemporaneous with the faults of the KSFB. In the south, the pronounced easterly-tilted topography is cut by an increased number of horst-graben pairs (7 on the cross-section 2 of Fig. 5) that are narrower than, and have strikes that are between 10° and 20° anticlockwise of, those in the north. The change from north to south appears to be defined by a 10 km-wide N120°E-trending depressed zone cutting across the central part of the Gombe domain (Figs. 4b and 6). On the radar DEM, numerous mapped faults appear to tip out within this zone, though closer inspection of the processed 2D-remote sensing data (lateral resolution of 15 m) reveals that some of the large faults splay into dense swarms of more segmented and smaller displacement faults within this zone (see F2 on figure 6). The resulting intricate fault patterns observed in this area evidentally serve to allow southward transfer of fault-related strain onto a system with more, and therefore narrower, horst-graben pairs. This fault complexity is spatially associated with discrete N120°E-oriented discontinuities marked at the surface by a number of aligned circular intrusions (Figs. 4 and 6). These transverse faults may also extend 20 km further to the ESE along the linear course of the Finan Gos palaeoriver trace.

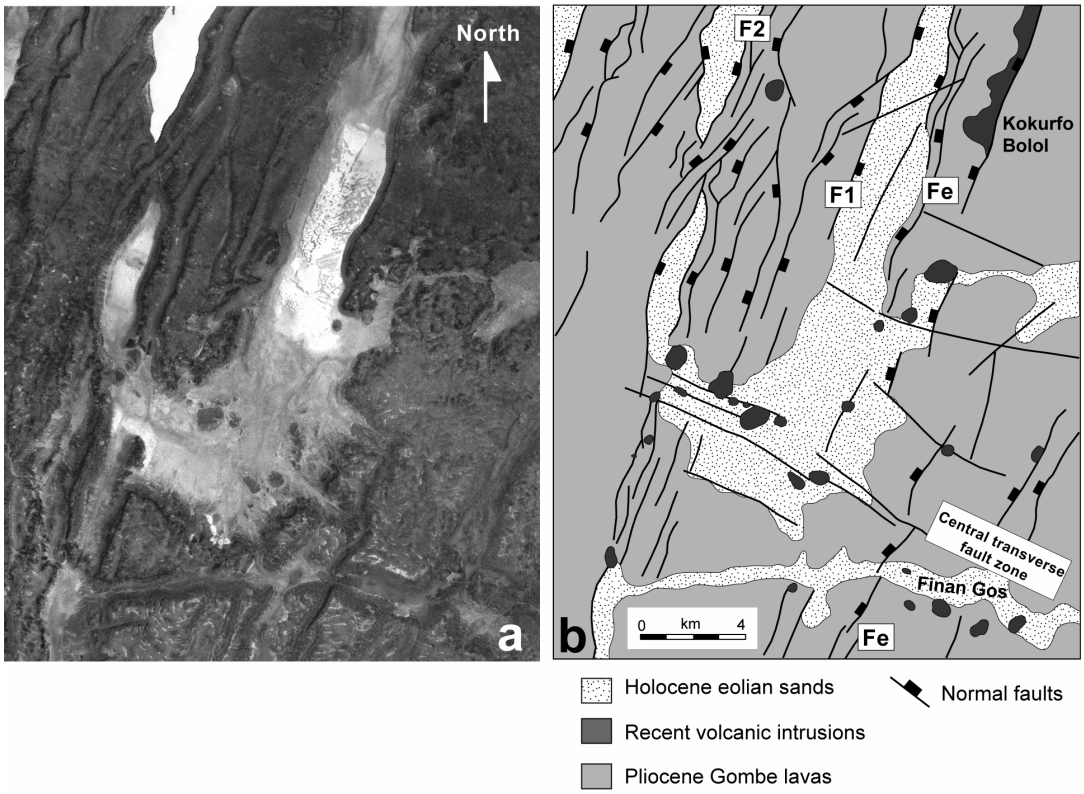

Figure 6. *Structural and magmatic expression of the N120°E-trending Central transverse fault zone. a. Detailed view of the Finan Gos area extracted from Landsat TM satellite image. b. Structural interpretation of figure a showing fault geometry complexities marked by (1) a denser swarm of more segmented and smaller rift-parallel faults over the Central transverse fault zone, (2) an approaching convergent transfer zone between two finger-like graben terminations and (3) N120°E transverse trends outlined by faults and numerous recent volcanic intrusions.*

Though the origin of this transverse zone of displacement transfer and complexity is unclear, its alignment sub-parallel to the earlier Cretaceous-Palaeogene Anza Rift, would be consistent with some influence on the geometry of the Kino Sogo fault system by earlier reactivated cross-cutting structures. Further to the south within the Hurran Hurra basalts, most of the mapped faults are difficult to trace, though 3 of the horst-graben pairs are visible (cross-section 3 on figure 5). Despite the poor preservation of the fault system, the N170°E-striking faults are intensely disrupted by an array of N120°E faults (Anza-type) that occur as far north as the contact between Gombe and Hurran Hurra lavas (Fig. 7). These structures may also represent earlier reactivated faults associated with the southern margin of the Anza Rift.

4.4. Statistics of the Kino Sogo Fault Belt

Quantitative data for the Kino Sogo fault system have been derived for both the fault and fault segment populations defined from SRTM radar data and Landsat images (Figs. 2 and 7).

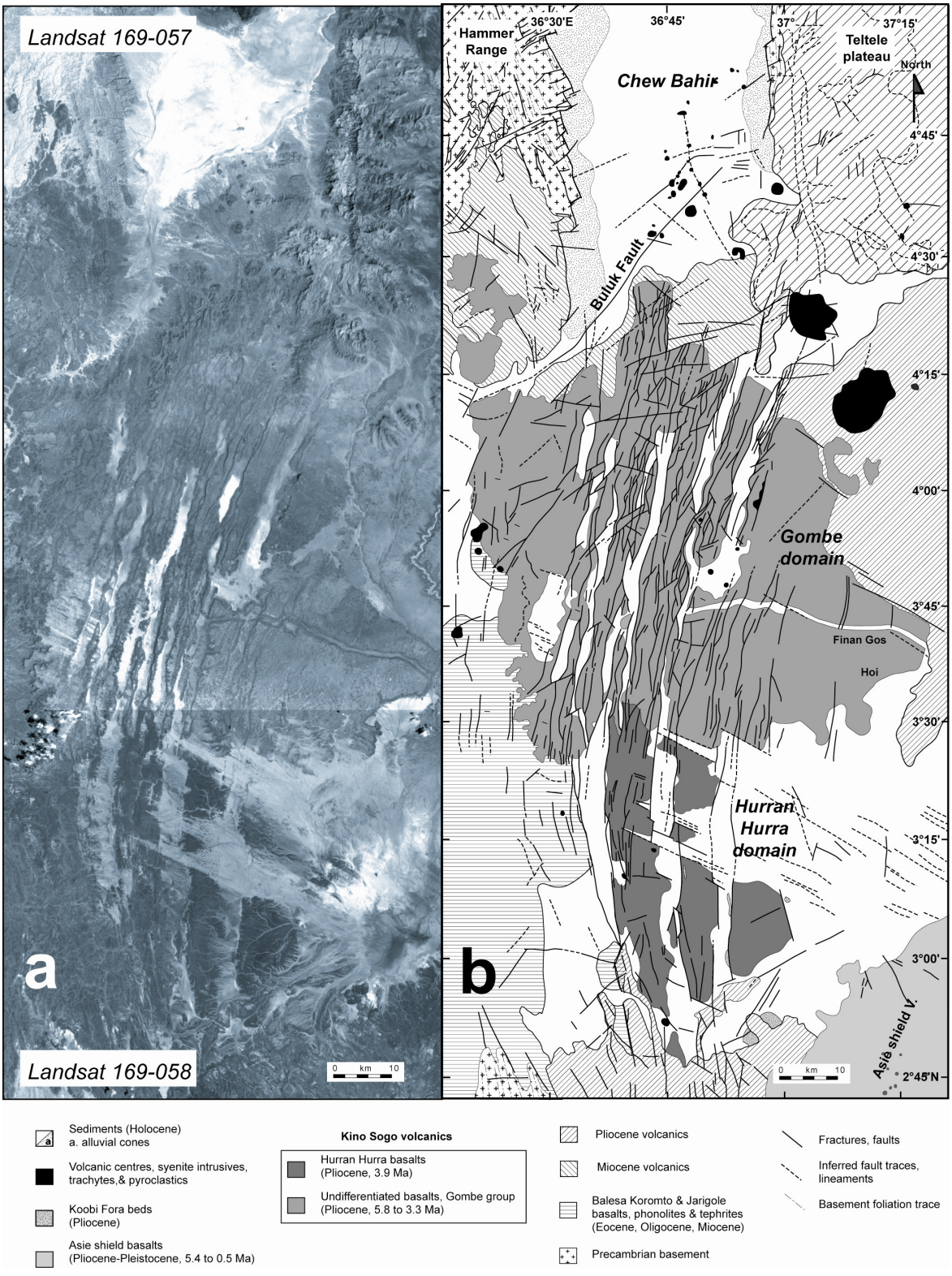

Figure 7. *Structural map of the KSFB. a. Detailed view of the KSFB extracted from Landsat TM processed satellite image. b. Structural interpretation of figure a. Note the structural contrast between the Gombe and the Hurran Hurra faulted domains.*

The purpose of this analysis is to establish the basic scaling properties of the fault system as a means of testing a variety of models related to the geometry and kinematics of the system. Following a brief description of the methodology for defining individual faults and fault segments, orientation analysis is used to emphasize the importance of transverse faults, the presence of which is related to well-established earlier structures. We then use fault length population analysis to highlight the significant difference between this system and other fault systems, a feature which may reflect either the immaturity of the system and/or the role of inheritance from underlying structures. The spatial distributions of faults are presented for completeness, though their significance remains unclear. Displacement analysis, using available radar data, is then used to provide an estimate of the bulk extension, and limiting strain rates, across the system and to permit definition of fault displacement-length scaling which is shown to be quite different from those of previously published fault systems. In our later discussion, we attempt to reconcile the unusual scaling characteristics of the KSFB with existing fault growth models.

4.4.1. Fault and fault segment sampling

Faults and fault segments were mapped from Landsat images with a lateral resolution of 15 m (Fig. 7). Individual fault segments were discriminated on the basis of the presence of fault tips, marked variations of fault azimuth or cross-cutting faults. Whether a fault segment is an element of a longer fault, or segmented fault array (Walsh et al., 2003), was determined on the basis of: (i) the presence of a relay zone with a narrow separation relative to fault segment length, (ii) equivalence of throw and downthrow direction between segments, (iii) similarity of footwall dips on adjacent segments (e.g. Peacock & Sanderson 1991; Cartwright et al., 1995; Cardon, 1999; Gloaguen, 2000; Walsh et al., 2003). A total of 427 individual faults were identified in the Gombe and Hurran Hurra domains, with 1718 fault segments. The high ratio of segments to faults (4/1) reflects the highly segmented nature of the entire fault system, as evidenced by the segmented bounding faults in particular (Fe and Fw on figure 4). The preservation of relay zones is not however surprising given the low displacements on individual segments and the relatively high overlap lengths and separations of many relays. Along the southern portion of the eastern bounding fault, for example, overlap lengths in excess of 2 km are developed between 5 successive segments with 100 m throw, geometries that require relay ramp gradients of less than 1/20 (i.e. 3° ramp dip), values that are well within the range of typical intact relay ramps (Imber et al., 2004). Later we suggest that this highly segmented fault system is partly attributable to the very low displacements, and therefore strains, accommodated by the system.

4.4.2. Fault and segment-trace orientations

The orientation distributions of the faults and fault segments of the Gombe and Hurran Hurra domains are presented in figure 8. These plots highlight the presence of three distinct trends. The dominant faults are N350-30°E-striking structures corresponding to the general trend of the Cenozoic rift. Two other distinct secondary trends correspond to the N50°E and N140°E faults of the BTFZ and Anza rift, respectively. As previously discussed, the latter are best seen in the Hurran Hurra domain to the south, where they generally correspond with the lateral extension of the Anza rift, whilst the former are widely developed in the Gombe domain to the north and arise from the cross-cutting BTFZ. Although these relationships reinforce the notion that earlier structures have influenced, to some extent, the geometry of the fault system, much of the central Gombe domain is relatively unaffected apart from the possible Central transverse structure (Anza-type), already referred to, that appears to be responsible for enhanced fault and horst-graben segmentation.

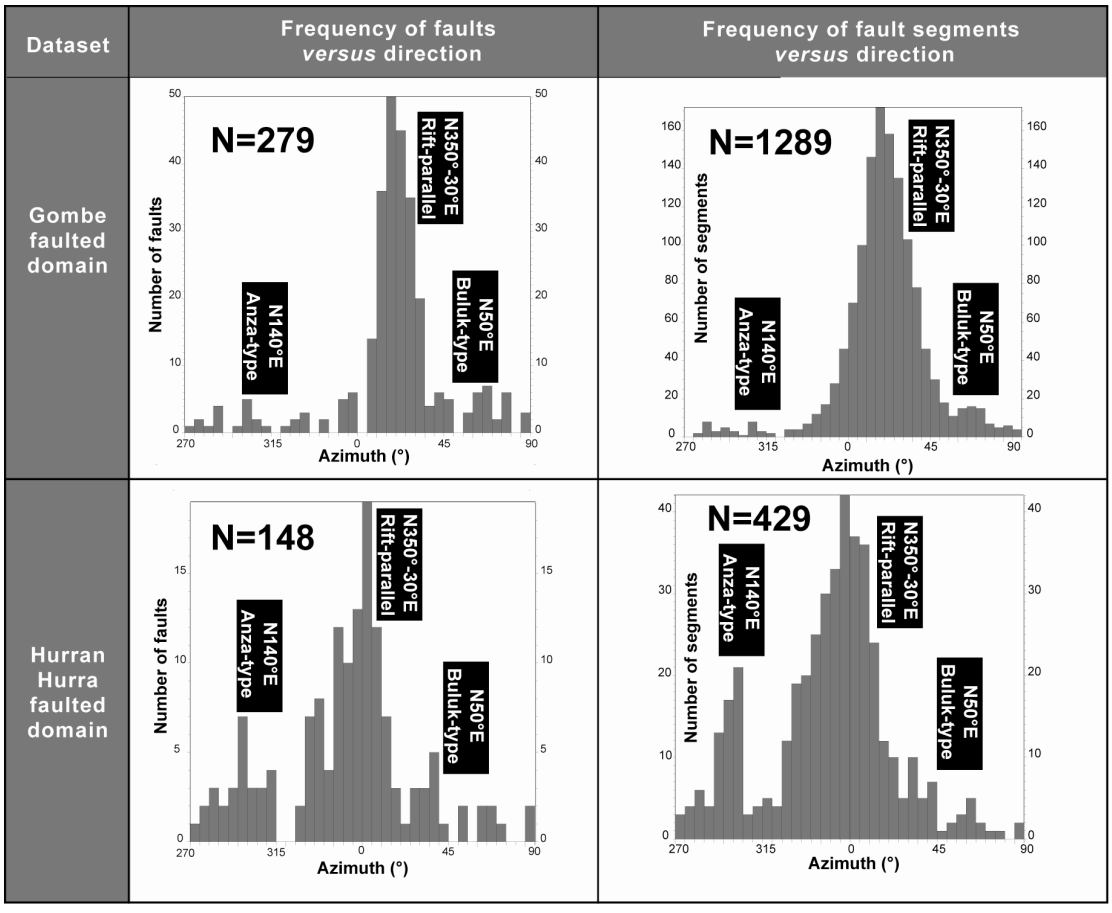

Figure 8. *Histograms illustrating the frequency of faults and fault segments versus direction in the Gombe and Hurran Hurra domains. Three main directions of structures prevail as the dominant N350-N30°E rift-parallel faults and two subsidiary N50°E (Buluk-type) and N140°E (Anza-type) transverse features. Note the swing of fault azimuths from N170°E to N30°E northwards.*

4.4.3. Length of fault and fault segment

In this section, the fault and segment length statistics are presented for the main rift-parallel faults (N350-30°E) of the Kino Sogo fault system. Emphasis is placed on characteristics of the better exposed faults and fault segments of the Gombe domain, for which rift-parallel faults are far more numerous and longer than other trending structures (Table 1), because the Hurran Hurra domain data are likely to be strongly biased by poorer exposure and partial burial by eolian sands. Histograms of fault and segment length show a marked decrease in the frequency of faults and segments with lengths below 5 km and 2 km respectively, values that are much greater than the lateral resolution of the Landsat images (>15 m) (Figs. 9a and 9b). Because our comparison of the Landsat and radar fault maps suggests that the Landsat map contains faults that are significantly below the vertical resolution of available digital elevation models (<< 16 m), it is unlikely that the decrease in fault frequency can be attributed to fault throw resolution. The frequency distributions therefore suggest that there is a real decrease in the frequency of short faults and segments, a feature which is not consistent with the often described fractal nature of other fault systems (Main, 1996; Yielding et al., 1996; Cardon, 1999).

Gombe fault length (L)			
	NS-N30° Rift-parallel	N40°-60° Buluk-type	N120°-140° Anza-type
Number	211	16	10
L. max (km)	37	24	20
Cumulative L.	2046	244	75
Mean L.	9.7	7	6.5

Gombe fault segment length (L)			
	NS-N30° Rift-parallel	N40°-60° Buluk-type	N120°-140° Anza-type
Number	930	74	14
L. max (km)	14	24	10.5
Cumulative L.	1964	240	70
Mean L.	2	3.3	5.4

Hurran Hurra fault length (L)			
	NS-N30° Rift-parallel	N40°-60° Buluk-type	N120°-140° Anza-type
Number	45	5	12
L. max (km)	35	11.4	26
Cumulative L.	347	34	85
Mean L.	7.7	6.8	4

Hurran Hurra fault segment length (L)			
	NS-N30° Rift-parallel	N40°-60° Buluk-type	N120°-140° Anza-type
Number	127	13	35
L. max (km)	8	4.5	25
Cumulative L.	342	42	167
Mean L.	2.7	3.2	4.8

Table 1. *Principal statistic parameters of the Gombe and Hurran Hurra faults and fault segments lengths.*

The scaling properties of length populations are explored further using conventional cumulative frequency *versus* length distributions, which plot the cumulative number of faults or segments (N) with lengths greater than a given value (L). When plotted in log-log and linear-log space, this type of plot permits identification of different types of distribution, in particular power-law and exponential. Exponential-law relationships provide straight line distributions in linear-log plots and are defined by:

$$N(L) = \alpha . e^{-\lambda L} \quad (1)$$

where N is the number of faults, or segments, with length greater than or equal to L, α is the total number of measures and λ is a scale parameter. Power-law relationships provide straight-line distributions on log-log plots and are defined by:

$$N(L) = \alpha . L^{-C} \quad (2)$$

where N is the number of faults, or segments, with length greater than or equal to L, α is a constant and C is the power-law exponent.

Examination of both the fault length and segment length populations for the Gombe domain suggests that the Kino Sogo fault system does not ascribe to the power-law, or fractal, nature of fault populations from many other fault systems (Figs. 9c and 9d; e.g. Childs et al., 1990; Scholz & Cowie, 1990; Walsh et al., 1991; Nicol et al., 1996; Yielding et al., 1996).

Not only do the population distributions on log-log plots provide non-linear curves, which cannot be attributed to sampling issues such as truncation at small lengths or censoring at large lengths (fault lengths are much shorter than the length of the study area), potential straight line portions of the distributions (between 10 and 30 km fault length) have excessively high exponents (i.e. significantly higher than the usual 1-2 range from other fault systems; see Cladouhos & Marrett, 1996). By contrast, the length populations are much more consistent with an exponential distribution (Figs. 9e and 9f), which are relatively rarely described but have previously been variously attributed to either the early fault initiation phase of fault system evolution, when the initiation of new small faults dominates the growth of existing faults (Villemin & Sunwoo, 1987; Cowie et al., 1995), or the final phase of fault system evolution when large faults cut through the brittle layer thickness (Ackermann & Schlische, 1997). Whilst the relatively low strains associated with the Kino Sogo fault system (see below) may be consistent with an early growth stage, the very long fault lengths observed in the area would generally be taken as an indicator of fault system maturity. This apparent conflict is returned to in a later section.

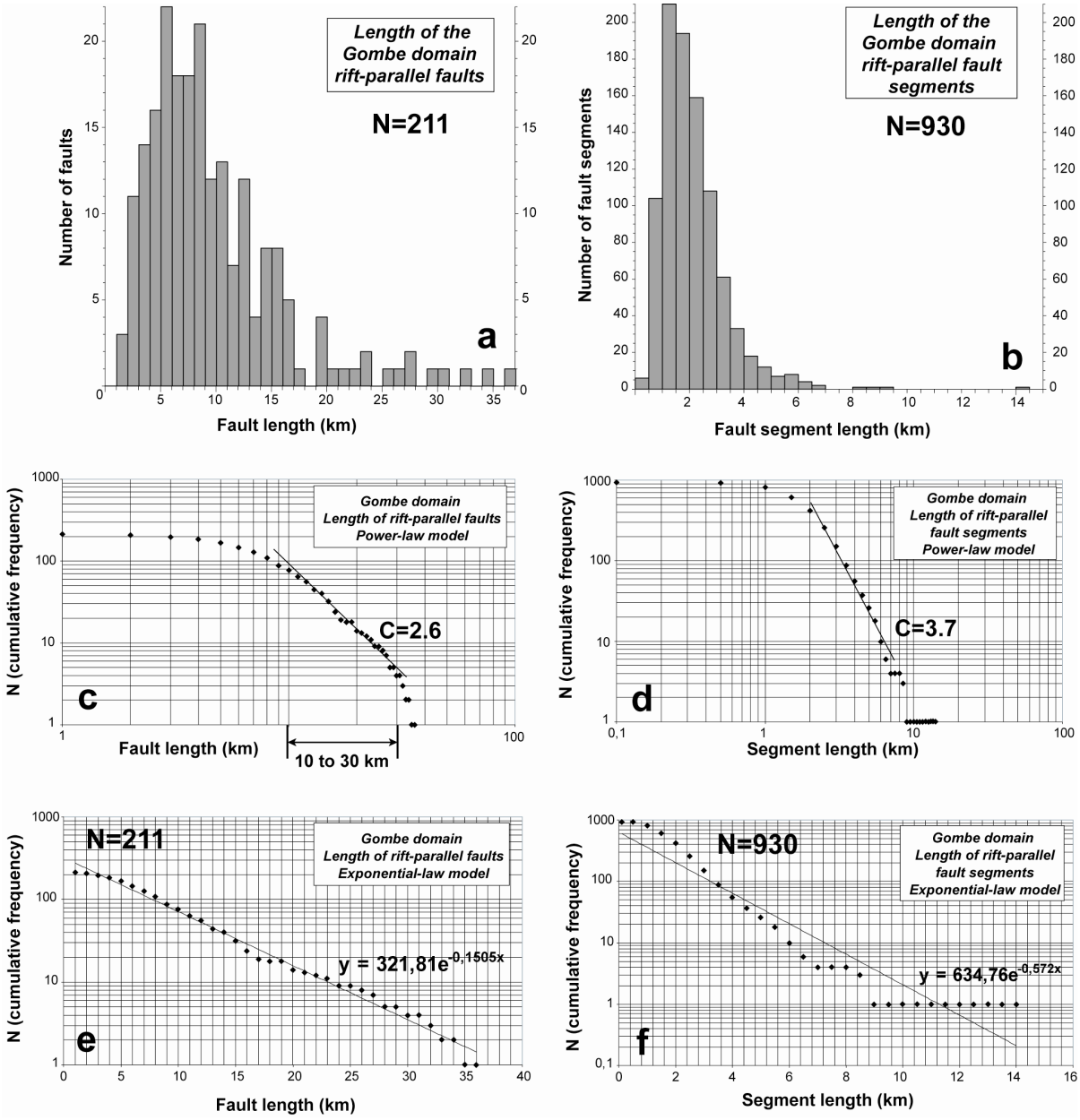

Figure 9. *Distribution of rift-parallel faults and fault segment populations in the Gombe domain. a. and b. Frequency of rift-parallel faults (each km) and fault segments (each 500 m) versus length. The absence of faults <5 km and fault segments <2 km is not due to censoring effects. c-f. Cumulative frequency plot of rift-parallel structures versus length and fit with statistic law models. c. and d. Log-log cumulative frequency plots of faults and fault segments versus length showing a poor fit with power-law. Left and right hand truncation are not due to undersampling effect and area scale effect. The slope of C=2.6 is calculated for the central segment of the length curve between 10 and 30 km. e. and f. Log-linear cumulative frequency plots of faults and fault segments versus length showing a good fit with exponential-law.*

4.4.4. Fault spacing

The best indication of the spatial distributions of the Kino Sogo fault system is the relatively consistent spacing of horst-graben pairs along fault-perpendicular sections (Figs. 4 and 5). Fault maps indicate an increase in the number of horst-graben pairs in the south, with a corresponding decrease in spacing, the origin of which is unclear. For completeness, however, we have calculated 162 fault spacing measurements between adjacent rift-parallel faults on five ~EW cross-sections (15 km apart) in the Gombe domain. Plots of fault spacing *versus* cumulative frequency are characteristic of an exponential-law model rather than a power-law model (Fig. 10). Taken together, the relatively systematic spacing of horst-graben pairs and the exponential spacing distributions, suggest the presence of some dominating km-scale structural control complicated by randomly distributed smaller faults. Although other studies have suggested that regular large-scale fault spacings could be related to the thickness of a faulted layer or crustal thickness (Wu & Pollard, 1995), this explanation is not easily applied to the Kino Sogo system.

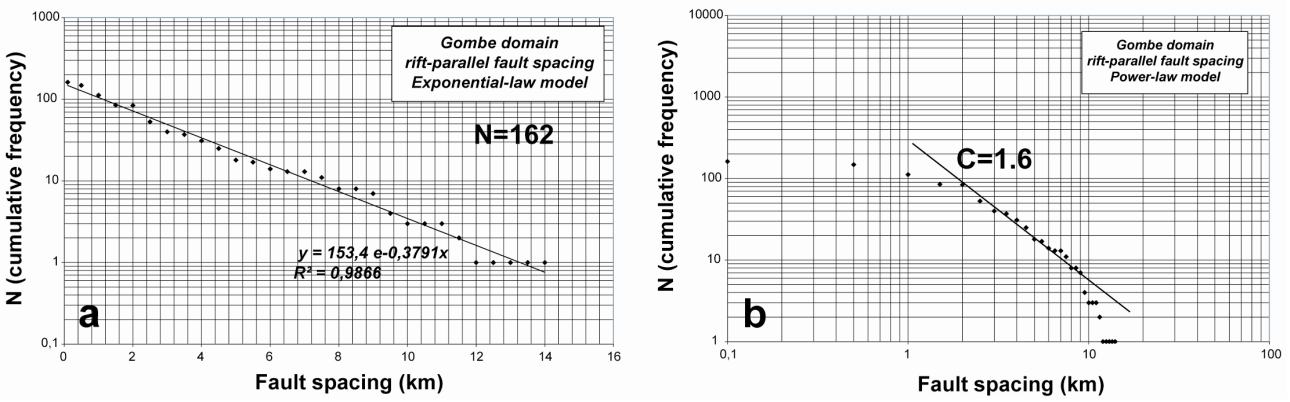

Figure 10. *Log-linear (a) and log-log (b) cumulative frequency plot of rift-parallel fault spacing in the Gombe domain. Spacing data best correlates with exponential law.*

4.4.5. Maximum fault displacements

The maximum throws of 30 of the larger faults within the Gombe domain have been derived from the topographic elevations along fault scarps resolved by the SRTM dataset (16 m vertical resolution). For each of the faults, vertical throws were measured at approximately 5 km intervals along the lengths of their fault scarps. The range of maximum throw is between 30 and 100 m for faults that are between 9 km and 36 km in length (Fig. 11); throws as low as 16 m have been measured but maximum throws are always >30 m. Although the range of fault throws and lengths is relatively narrow, faults from the Kino Sogo system show a weak positive correlation between displacement and length. Similar positive relationships between

fault length and displacement have been established by numerous previous studies and have underpinned the development of different fault growth models in which the maximum displacement (D) of faults scales with fault length (L), following the expression:

$$D=cL^n \quad (3)$$

where c is a constant and n is between 1 and 1.5 (Walsh & Watterson, 1988; Cowie & Scholz, 1992; Gillespie et al., 1992; Dawers et al., 1993; Schlische et al., 1996).

This scaling law (3) is generally taken to be a growth trend and underpins fault growth models involving a sympathetic increase in both the lengths and maximum displacements of faults as a fault system evolves (Walsh & Watterson, 1988; Cowie & Scholz, 1992). The distinctive feature of the Kino Sogo fault system is that although it provides a weak positive correlation between fault displacement and length, it defines a field which falls well below other fault systems, so that faults of a given length are significantly under-displaced compared to similar length faults from other systems (Fig. 11). Before considering the significance of this feature, we first derive estimates for the bulk extension and strain rates associated with the Kino Sogo fault system.

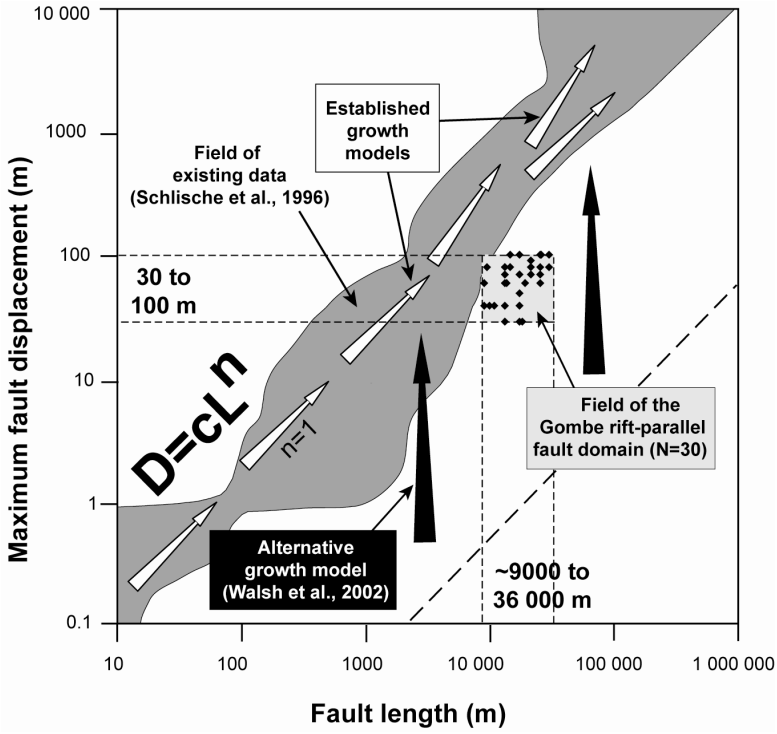

Figure 11. *Log-log plot of maximum fault displacement versus length showing the 'under-displaced' nature of the rift-parallel normal faults in the Gombe domain in contradiction with the growth paths of fault predicted by previous established models (white arrows). Shaded area outlines the field of published data from Schlische et al. (1996). By contrast, Kino Sogo fault data are in agreement with an alternative fault growth model (Walsh et al., 2002) (black arrows) where (1) fault lengths are near-constant from an early stage and (2) growth is achieved by increase in fault displacement.*

4.5. Rift extension and strain rate

The cumulative fault-related extension has been calculated directly from the available SRTM data using the following procedure. Firstly, aggregate throw is calculated from the measured throws at the intersection points of all faults with four regular spaced E-W sections across the fault system. The average cumulative throw for the 40 km-long cross-sections is then used to compute the cumulative heave for a range of plausible fault dips. Fault dips cannot be measured from SRTM data, but previous studies in the Kenya rift suggest average fault dips in the range 60°-70° (Walsh & Watterson 1988; Le Turdu, 1998; Gloaguen, 2000). The cumulative fault throw and fault dips combine to provide cumulative heaves of between 450 m and 285 m for the 40 km-wide rift, values which indicate extensions of between 1.1% and 0.7% and stretching factors (β) of between 1.01 and 1.007. These values are much lower than those described for other parts of the Kenya rift where extension ratio range between 3% and 8% in the Magadi axial trough (Fig. 1b) (Gloaguen, 2000). Even accounting for the possible contribution of faults with throws less than 16 m, the strains associated with the KSFB are nearly an order of magnitude lower than those of typical rifts, a feature that has profound implications for the growth of the fault system (see below).

Estimates of rift extension rates and regional strain rates require definition of the entire period of faulting. The 3 Ma. age of the host lavas defines an upper limit to the possible period of activity and associated minimum estimates of both extension rate (0.15-0.095mm/yr) and strain rate ($1.16 \times 10^{-16} – 7.4 \times 10^{-17}$). It is not possible, however, to estimate a lower limit for the period of fault activity though regional considerations suggest that the fault system was active for recent periods (Holocene?). The extended period of fault activity (3 Ma. to Present) provides estimates of extension rate that are a small fraction of the 1-4 mm/yr extension rate estimates for the adjacent Kenyan or Ethiopian rifts over the period from Pliocene to Present (Morley et al., 1999a; Ebinger et al., 2000; Gloaguen, 2000). Assuming similar rates applied to the multi-rift Turkana zone, then if the KSFB were at any time to have been the sole active component of the zone, it could not have been active for more than ~300,000 years. To reconcile our estimate of the KSFB deformation rates and those of the Turkana rift zone therefore requires that it was either active continuously at very low strain rates or that it had a short-lived history (~ 300,000 years) within that 3 Ma period. Although we cannot yet define the period of fault activity, the most significant issue for the purposes of this article is that the fault system is characterised by very low strains.

4.6. Discussion

The most distinctive feature of the rifting accommodated by the Kino Sogo fault system is the very low recorded extension of ~1% across the 40 km-wide rift. Such very low strains potentially may also provide a rationale for other characteristic features of the fault

system including the under-displaced nature of individual faults, the highly segmented nature of the fault system and the fault size scaling properties. Displacement-length data for the KSFB define a field below that occupied by conventional fault growth trends and indicating relatively low displacement/length ratios (Fig. 11). Their under-displaced nature is however consistent with an alternative fault growth model, described by Walsh et al. (2002), in which fault lengths are established during rapid early stage fault propagation, followed by a more protracted period of displacement accumulation with retarded fault propagation arising from interaction between adjacent faults. The earliest phases of growth are therefore characterised by under-displaced faults, which grow into conventional 'growth' trends rather than along them (Fig. 11). Walsh et al. (2002) showed that a fault system within the Timor Sea characterised by fault-related extension of ~3% now shows displacement/length scaling within the general field for other fault systems, but that early stage fault growth was characterised by lower displacement/length ratios. Their model would therefore predict that fault systems with very low extensions of ~1%, such as the KSFB, should have under-displaced faults. This prediction is consistent with both the under-displaced nature of Kino Sogo faults and the strongly segmented nature of faults within the system. Further displacement accumulation would be expected to result in progressive relay breaching and the map view linkage of fault segments with progressively larger separations and overlap lengths (Imber et al., 2004). The relatively small separations between adjacent fault segments and the displacement conservation along their combined lengths suggest that individual segments link at depth and that later map-view linkage would change the fault map but would otherwise have a limited impact on fault growth (Walsh et al., 2003).

Although rapid fault propagation within the Timor Sea fault system in the past 6 Ma. has been attributed to the reactivation of pre-existing, and underlying, Jurassic normal faults, Walsh et al. (2002) suggest that rapid early stage fault propagation may be typical of fault systems that have developed *ab initio*. The rapid generation of fault lengths, with a broad range of size, contrasts with conventional fault growth models in which the nucleation of smaller faults is followed by the progressive increase in both the length and displacement of some faults. No direct observational constraints favour either the conventional or alternative fault model in previously unfaulted volumes. The potential influence of earlier structures cannot however be ruled out in the case of the KSFB, where there are at least three types of pre-existing structures which could be responsible for the rapid fault propagation and the 'under-displaced' nature of faults (Fig. 12):

(i) Ductile basement foliation planes, showing a N170°E to N30°E sigmoid structural grain, are clearly visible along the N'Doto Proterozoic basement massif exactly in the southern prolongation of the KSFB (Figs. 12a and 12b). The arcuate trace (convex to the west) of the Kino Sogo fault grid displays a quite similar wavelength (~200 km) as those of the basement strain trajectory (convex to the east) in the N'Doto massif. Taking into account the Hammer Range to the north, the basement pattern in the Turkana rift as a whole is seen to

involve a sinusoidal-shaped fabrics dissected by nearly orthogonal (N50°E and N140°E) transverse fault zones at the inflection points (Fig. 12b). It is possible therefore that the rift fault system in the KSFB could have been promoted by the existence of curved underlying Precambrian basement fabrics.

(ii) Proterozoic faults might have existed within the basement rocks underlying the faulted Gombe lavas, but their existence is not easily demonstrated because they would have been subsequently eroded, on the uplifted flanks of the Allia Bay fault (Fab) to provide an apparently unfaulted surface upon which the lavas were deposited. It is possible, nevertheless, that at some time prior to 3 Ma., a fault system may have existed along the KSFB and could therefore have linked the Chew Bahir trough, in the north, to the Suguta trough, in the south.

(iii) Bending stress fractures are likely to have developed at the top of thermal-induced domes inferred to have formed in the Kino Sogo volcanic area during two successive volcanic events at 35-12 Ma. and 6-3 Ma. (Watkins, 1986) (Figs. 12b-d). Under WNW-ESE extension, these extrados-type fractures were oriented at ~NS and they could have subsequently guided the propagation of extension throughout the Kino Sogo domain during the deflation phase following the Pliocene volcanic/doming activity. Supportive evidence for such a fault/fracture propagation model are provided by similar dome/faulting interactions on the western part of the Turkana rift during Miocene times (Vétel & Le Gall, submitted).

To summarise, the existence of earlier fabrics and faults within the basement and/or the presence of magmatic-related bending stress fractures would, on their own, provide a rationale explanation, not only for rapid fault propagation within the Gombe lavas, but also for the longer and, in that respect, apparently more mature geometry of the fault system, as suggested by the exponential frequency fault size distributions (Ackermann & Schlische, 1997).

Concerning the key-role played by transverse fault zones (N50°E and N140°E) on the KSFB development, it is well established that the Chew Bahir graben to the north had a protracted history of rifting prior to the deposition of the Gombe lavas.

Combined with the uplifted nature of the Kino Sogo area and the presence of the westward downthrowing Fab fault, it is clear that at some stages, the Buluk transverse zone must have transferred the strain associated with the Chew Bahir graben westward into the Lake Turkana rift (Vétel & Le Gall, submitted). The co-linearity of the KSFB and the Chew Bahir graben indicates that for some time during the past 3 Ma. a through-going 40 km-wide rift extended directly southwards possibly extending as far south as the Suguta Valley (Fig. 12b), a situation which may also have prevailed at some earlier time. Why such a radical change in rift geometry should occur is unknown, though it presumably reflects some diminution, however temporary, of the influence of the BTFZ. Moreover, the KSFB is transected by a N140°E-trending transverse central zone across which displacement is transferred southwards to an increased number of horst-graben pairs. The orientation of this zone is parallel to that of the pre-existing Cretaceous Anza rift, perhaps reflecting an associated change in crustal

structure, the nature of which is unknown. Other similarly-oriented transverse faults to the south, together with those within the BTFZ, attest to the continued influence of long-lived transverse structures on rift fault geometry.

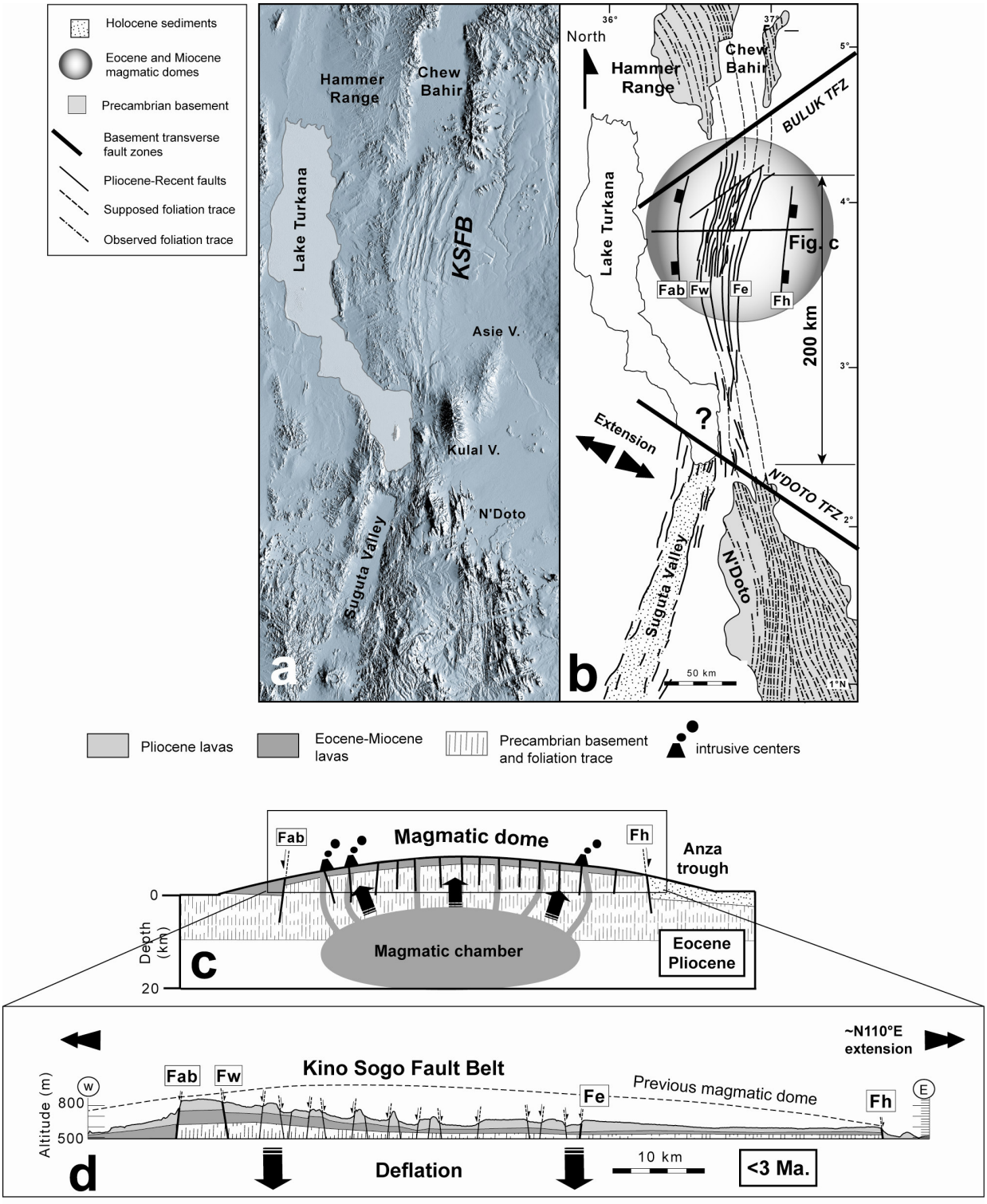

Figure 12. *Pre-existing structures susceptible to have been reactivated during the formation of the KSFB. a. and b. SRTM elevation data show the sigmoid trace of the ductile/brittle structures in the N'Doto and Hammer Range basement massif in the continuity of the KSFB. The sinusoidal-shaped fabrics is dissected by two major transverse fault zones, the so-called N'Doto TFZ (N140°E) and Buluk TFZ (N50°E). Note the location of a previous Eocene-Miocene and Pliocene magmatic dome over the Kino Sogo area. c and d. Eocene to Pliocene volcanic events created a thermal dome susceptible to have formed some bending stress fractures at the top of the magmatic flexure. d. Detailed cross-section of the top of the previous magmatic dome. The deflation of the thermal-induced dome led to the formation of the Kino Sogo Fault Belt by reactivation of pre-existing dome-related fractures (see figure 12b for location).*

4.7. Conclusions

The Kino Sogo Fault Belt is a 40 km wide arcuate zone cutting through a thin (<200m) Pliocene lava sequence on the eastern part of the broad Turkana rift zone (~200 km-wide). Prior to the recent KSFB rifting event (<3.0 Ma.), the early geometry of the Kino Sogo volcanic rifted area was defined by an asymmetrical uplifted fault block, tilted to the E-SE, and bounded by transverse discontinuities to the north (N50°E Buluk fault) and south (N140°E Anza-type structures). The present-day internal organisation of the KSFB is dominated by a regular horst and graben system with no dominant structures and with along-strike variations in structural style (density, direction and linkage of faults) suggesting the existence of three sub-segments separated by two NW-SE transverse fault zones.

The fault system accommodates very low strains (<1%) and since it is no older than 3 Ma. it could be characterised by extension rates and strain rates which are as low as ~0.1mm/yr and $10^{-16}s^{-1}$ respectively. Fault scaling properties, such as fault length distributions, define negative exponential distributions, as opposed to the power-law scaling typical of other fault systems. Other unusual features of the system include the highly-segmented characteristics of the system and the under-displaced nature of the faults, which show displacement/length scaling properties that lie outside of the field generally defined by faults. The scaling properties of the KSFB are most easily reconciled with an alternative model for fault growth (Walsh et al., 2002) in which fault lengths are established rapidly in response to the reactivation of inherited underlying structures. The three potential controls on structural inheritance for the KSFB are the reactivation of either underlying Proterozoic ductile/brittle basement fabrics or bending stress fractures on top of Cenozoic volcanic domes. Combined with the structural controls exercised by earlier transverse structures, the KSFB demonstrates the strong influence of pre-existing structure on fault system growth and the relatively rapid development of under-displaced fault geometries at low strains.

5. Recent tectonics in the Turkana Rift (North Kenya): an integrated approach from drainage network, satellite imagery and reflection seismic analysis

William Vétel[1], Bernard Le Gall[1] & Tom Johnson[2]

[1] UMR 6538 'Domaines Océaniques', Institut Universitaire Européen de la Mer, UBO, CNRS, 4 Place Nicolas Copernic, 29280, Plouzané - FRANCE

[2] Large Lakes Observatory, University of Minnesota, Duluth, MN 55812 - USA

Published in Basin Research 16, 165-181, 2004.
(Received, May, 10, 2003; Revised, December, 2003; Accepted, February, 12, 2004)

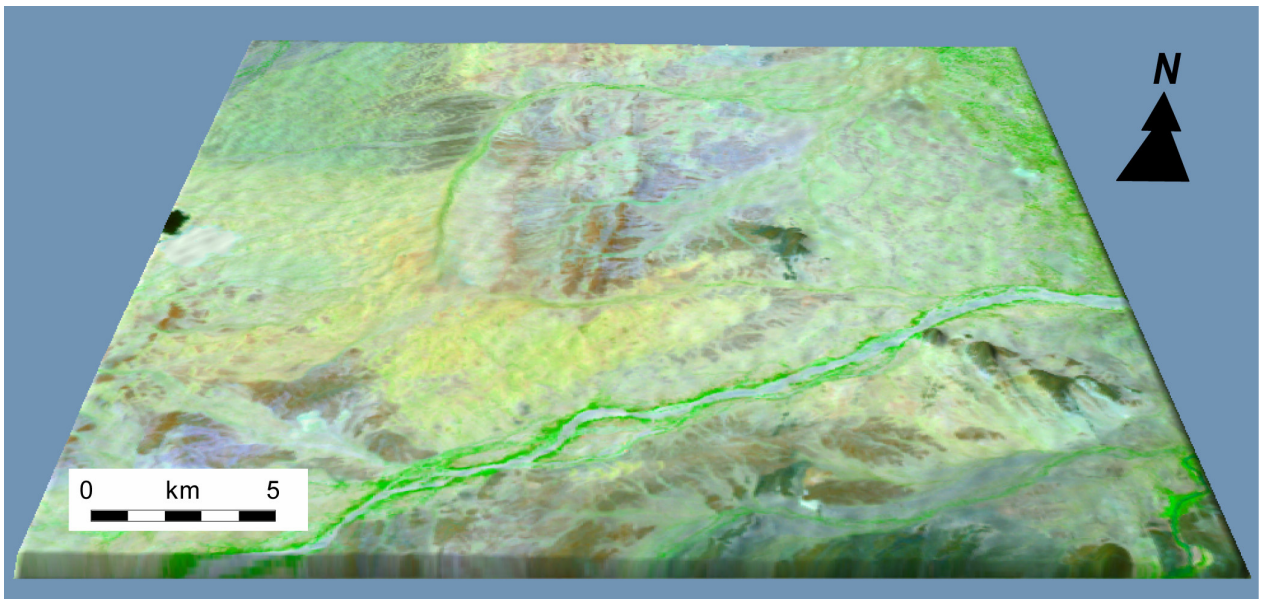

Perspective view of a portion of Landsat image 169-058 on the digital topography SRTM in the region of the circular Kalabata drainage anomaly (view to the North, light from West, vert. exag. x4).

ABSTRACT

The Turkana rifted zone in northern Kenya is a long-lived and polyphased rift system where the lack of well-marked rift morphology makes it difficult to identify the zone of active deformation. A high-density river network is exceptionally well developed over the study area and shows evidence of drainage anomalies that suggest recent fault-induced movements at various scales. Correlation of surface drainage anomalies with Landsat remote sensing and deep seismic reflection data permits to characterize the deep geometry of the inferred fault structures. Seismic stratigraphy further allows distinction between the inherited (Oligo-Pliocene) and the newly-formed (< 3.7 Ma) origin of the recent deformation. Evidence for neotectonics are observed (1) along a large-scale transverse (EW) fault rooted at depth along a steep basement discontinuity (Turkwell), (2) along a rift-parallel (NS) fault zone probably emplaced during the Plio-Pleistocene and currently bounding the Napedet volcanic plateau to the west, and (3) over a round-shaped uplifted zone caused by positive inversion tectonics (Kalabata). The major contribution of this work is the recognition of a broad (80 km-wide) zone of recent/active extensional deformation in the Turkana Rift in contrast with the narrow (20 km-wide) N10°E-trending axial trough forming the Suguta valley to the south, and the Chew Bahir faulted basin to the north. These along-strike variations in structural style are partly controlled by the occurrence of rejuvenated Oligocene-Miocene rift faults and long-lived transverse discontinuities in the Turkana Rift area. More generally, this study has implications for the use of river drainage network about recent/active extensional domains with subdued topography and slow deformation rate.

5.1. INTRODUCTION

The NS-trending Turkana Rift is a 200 km-long portion of the Cenozoic East African Rift System (EARS hereafter), extending between the Ethiopian and Kenyan domes, oblique to the N140°E Turkana depression (Fig. 1). The topography of the inner active zone in the Southern Ethiopian and Central Kenya rifts is linear and well expressed along the narrow Chew Bahir and Suguta troughs, respectively, to the north and south of the Lake Turkana area (Bosworth & Maurin, 1993; Ebinger *et al.,* 1993) (Fig. 2A). When crossing the Turkana depression, the axial rift loses its linear character, showing a poorly defined morphology where it becomes difficult to follow the trace of the active deformation zone.

The lack of well-marked rift morphology over most of the depressed zone has led some authors to propose alternative models for recent rift propagation.

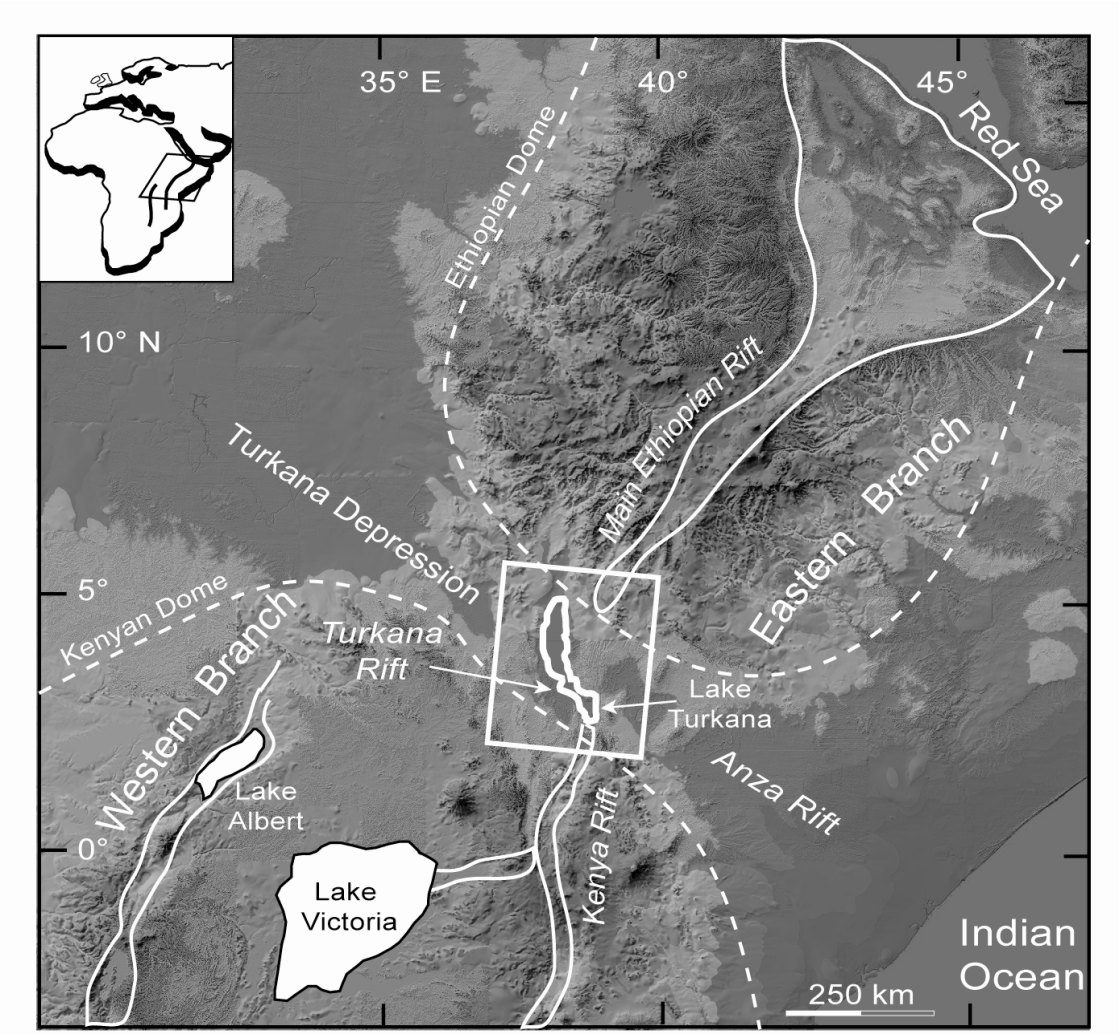

Figure 1. *Digital elevation model of the eastern part of the East African Rift system (GTopo 30 elevation data). The white contour mark the trace of the rift and the white square shows the location of the study area. The N140°E Turkana depression extends between the Kenyan and Ethiopian domes (dashed lines). The trace of the Turkana rift, centred on Lake Turkana, is poorly expressed compared to the highly linear and narrow Kenyan and Ethiopian Rift Valleys.*

According to Dunkelman *et al.* (1989), the recent/active zone of deformation should extend along the offshore basins of Lake Turkana (Fig. 2). Conversely, Hackman *et al.* (1990) and Bosworth & Maurin (1993) considered the horst and graben system of the Kino Sogo plateau farther east as the result of the northerly-propagating deformation within a complex relay zone between the Ethiopian and Kenyan rifts. The tectonic meaning of the Turkana depressed zone has been greatly improved in the 1990's during oil seismic surveys that revealed a system of deep NS-trending Oligocene-Pliocene half-grabens (up to 6-7 km-deep) on the western side of Lake Turkana (Morley *et al.,* 1992).

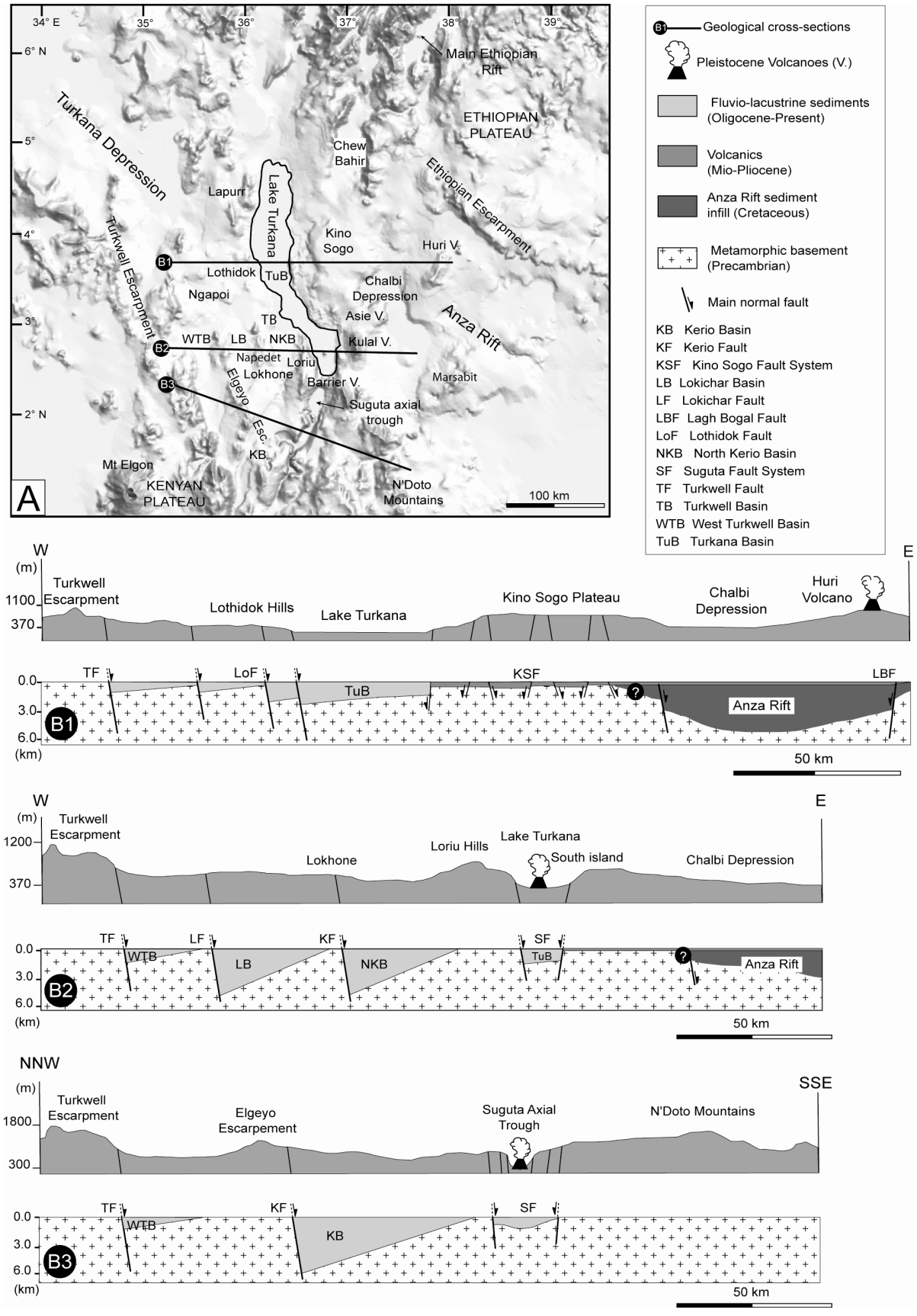
34° E
35°
36°
37°
38°
39°
6° N
5°
4°
3°
2° N
Main Ethiopian Rift
ETHIOPIAN PLATEAU
Turkana Depression
Chew Bahir
Ethiopian Escarpment
Lapurr
Lake Turkana
Kino Sogo
Huri V.
Turkwell Escarpment
B1
Lothidok
TuB
Chalbi Depression
Ngapoi
Asie V.
TB
Anza Rift
WTB
LB
NKB
Kulal V.
B2
Napedet
Loriu
Lokhone
Barrier V.
Marsabit
Elgeyo Esc.
B3
Suguta axial trough
KB
Mt Elgon
KENYAN PLATEAU
N'Doto Mountains
100 km
A
Geological cross-sections
Pleistocene Volcanoes (V.)
Fluvio-lacustrine sediments (Oligocene-Present)
Volcanics (Mio-Pliocene)
Anza Rift sediment infill (Cretaceous)
Metamorphic basement (Precambrian)
Main normal fault
KB Kerio Basin
KF Kerio Fault
KSF Kino Sogo Fault System
LB Lokichar Basin
LF Lokichar Fault
LBF Lagh Bogal Fault
LoF Lothidok Fault
NKB North Kerio Basin
SF Suguta Fault System
TF Turkwell Fault
TB Turkwell Basin
WTB West Turkwell Basin
TuB Turkana Basin
W
E
(m)
1100
370
Turkwell Escarpment
Lothidok Hills
Lake Turkana
Kino Sogo Plateau
Chalbi Depression
Huri Volcano
TF
LoF
KSF
LBF
TuB
Anza Rift
0.0
3.0
6.0
(km)
B1
50 km
W
E
(m)
1200
370
Turkwell Escarpment
Lokhone
Loriu Hills
Lake Turkana
South island
Chalbi Depression
TF
LF
KF
SF
WTB
LB
NKB
TuB
Anza Rift
B2
50 km
NNW
SSE
(m)
1800
300
Turkwell Escarpment
Elgeyo Escarpement
Suguta Axial Trough
N'Doto Mountains
TF
KF
SF
WTB
KB
B3
50 km

Figure 2. A. *Digital elevation model of the Turkana Rift (Digital Chart of the World elevation data). The relief of the Turkana depression, situated between the Ethiopian and Kenyan plateaus, is relatively low. The trace of the rift is well expressed along the Suguta valley to the south of Lake Turkana, and in the Chew Bahir trough to the NE, but it is diffuse in the vicinity of the lake.* ***B.*** *Three cross-sections of the Turkana rift illustrating the topographic expression of the rift at the surface (vertical exaggeration x10) and the Oligocene-Pliocene sedimentary basins at depth.*

These synrift basins are arranged within a ca. 60 km-wide zone of extension that primarily formed during a major rifting event during Oligo-Miocene. Because of the poor resolution of seismic data in the upper part of the profiles, the occurrence of recent/active tectonics west of the deformed zones (Lake Turkana basins and Kino Sogo plateau) as advocated by previous models (Dunkelman *et al.,* 1989; Hackman *et al.*, 1990; Bosworth & Maurin, 1993) is not detectable. Thus the partial or total reactivation of this wide zone of ancient deformation during recent rifting is not documented, although being an important issue for determining the distribution of neotectonics in the Turkana rifted zone as a whole.

We present in this work a complementary approach that attempts to correlate the deep basinal structures imaged on the seismic profiles with the morphotectonic features and river drainage data supplied by satellite imagery.

This study demonstrates the interest of such an approach, combining surface and deep dataset, in order to reveal neotectonics in extensional faulted domains with subdued topography. Drainage network analyses have been applied successfully in numerous neotectonic studies (e.g. Leeder & Jackson, 1993; Pubellier *et al.,* 1994; Collier & Gawthorpe, 1995; Deroin & Deffontaines, 1995; Goldsworthy & Jackson, 2000). Drainage network analysis is applied here to the Turkana extensional area, which displays a dense river network, exceptionally developed over part of the Oligo-Pliocene basins mentioned above. Drainage anomalies are identified and interpreted according to classical criteria (Deffontaines, 1990). Three of the drainage systems provide new insights on the recent evolution of the western part of the Turkana Rift area, with respect to transverse basement-rooted faults (Turkwell River anomaly), newly formed extensional faults (Lokichar River anomaly), and inversion tectonics (Kalabata River anomaly). Therefore, emphasis is put in the present study on the ability of river drainage analysis in supplying additional surface evidences for neotectonics in extensional faulted terrains with low associated relief.

5.2. DATASET AND METHODS

5.2.1. Dataset

This study is principally based on two Landsat thematic mapper images (169-058, October 1999 and 170-058, January 2000). Each satellite scene is 180 x 180 km with a spatial resolution of about 30 x 30 m relative to the unit pixel size (Girard & Girard, 1999). The deep geometry of the recent deformation observed at the surface on Landsat images is illustrated on seven onshore seismic lines (Amoco TVK sections) that image the structure of the sedimentary synrift infill (5 sec. TWT.) in the Lokichar, North Kerio and Turkana basins (Figs. 2 & 3).

Topography is derived from the world data Gtopo 30 and DCW (digital chart of the world) with low resolution (100 m vertical), but large coverage (Figs. 1 & 2A). At a smaller scale, the major limitation of the present work is the almost complete lack of 1/50 000 topographic maps over the study area. Only two maps (with 20 m vertical resolution) are available on the southernmost part of the Lokichar drainage pattern where one digital elevation model has been processed (Fig. 3).

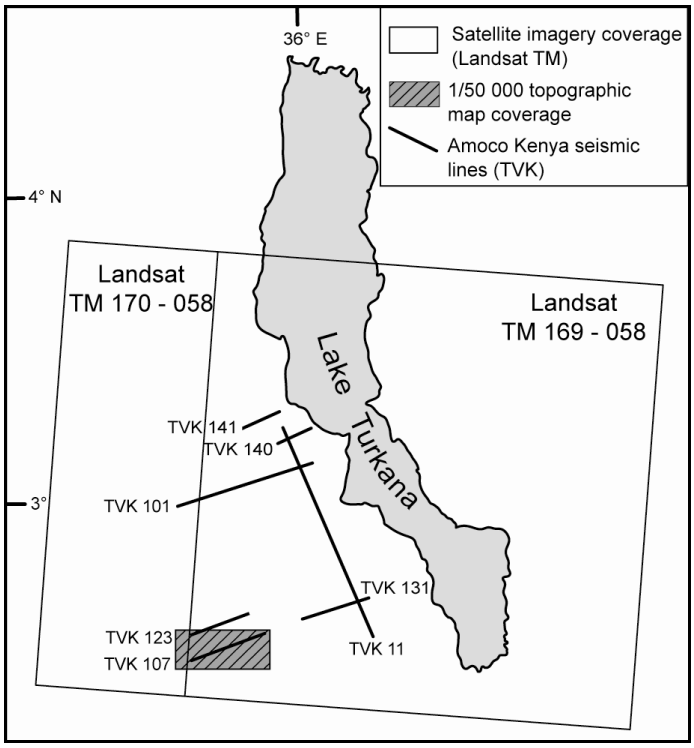

Figure 3. *Location map of the three different types of dataset used in this study: two Landsat Thematic Mapper satellite images (TM 170-057, 18/01/2000; TM 169-058, 21/10/1999), two topographic sheets (1/50 000) and seven Amoco seismic reflection profiles on the western side of Lake Turkana.*

5.2.2. Methods

Our drainage network analysis consisted first of extracting the traces of intermittent rivers by using the channel 7 of the Landsat imagery (middle infrared wavelength of about 1400 to 2000 nm) that reveals humid zones (Girard & Girard, 1999). The preferred distribution of the drainage pattern over Quaternary sediments in depressed zones is clearly expressed, in contrast with adjoining volcanic plateaus where rivers are less visible as a function of reflectance criterion (Kadirov, 1998) (Fig. 5). The stream frequency is dependent on various parameters such as the permeability of the substratum, the thickness of the alteration zone and the climatic setting (Phillips & Schumm, 1987). It is also linked to the amplitude of vertical neotectonic displacements (Goldsworthy & Jackson, 2000), as well as to the lithology and structural arrangement of the exposed rocks (Phillips & Schumm, 1987; Stark, 1991).

The second stage of the drainage network study consists of identifying drainage anomalies that are usually expressed as diversions of river courses along lithological, tectonic or morphological discontinuities (Deffontaines, 1990). Such diversions are known to be sensitive to minor slope variations of a few degrees that could in turn indicate modest recent/active deformation. The anomalies can occur at both regional and local scales and in various tectonic environments including extensional (Jackson & Leeder, 1994), strike-slip (Gaudemer *et al.*, 1989), or compressional settings (Marple & Talwani, 1993). The ability of stream courses to accommodate rapidly changing topography constitutes a first-order approach for neotectonic studies (Gaudemer *et al.,* 1989; Jackson *et al.,* 1996). By contrast, river networks that recorded relatively ancient increments of deformation are no longer expressed in the present morphology because of either active erosion or subsequent sedimentary burial (Dumont, 1993).

5.3. MORPHOLOGICAL AND STRUCTURAL SETTINGS

The Turkana transverse depression separates the Ethiopian and Kenyan domes that both rise to about 3500-4200 meters (Baker *et al.,* 1972; Morley *et al.,* 1999a) (Fig. 1). The northern and southern terminations of the two domes are dissected by the Chew Bahir and Suguta axial troughs where active deformation is focused and results in a dense network of normal faults (Gabriel & Aronson, 1987; Bosworth & Maurin, 1993; Dunkley *et al.,* 1993; Ebinger *et al.,* 2000) (Fig. 2). This typical graben-like morphology is no longer observed in the 300 km-wide Turkana depression, which instead displays a much more diffuse morphological organization where elevations range between 300 and 2000 meters (Fig. 2B). Relief is mainly constituted by: (1) discrete volcanic edifices, Pliocene-Pleistocene in age, such as the Barrier, Kulal, Asie and Huri

volcanoes (Ochieng' *et al.,* 1988; Wilkinson, 1988; Hackman *et al.,* 1990; Bosworth & Maurin, 1993), (2) tabular volcanic plateaus (Lothidok, Napedet and Kino Sogo) involving principally Miocene-Pliocene lavas (Boschetto *et al.,* 1992, Morley *et al.,* 1999a), and (3) basement uplifted blocks and their overlying Miocene-Recent volcanic cover, as observed in the footwall of the Chew Bahir, Loriu and Lapurr fault systems (Walsh & Dodson, 1969; Key & Watkins, 1988; Ebinger *et al.,* 2000) (Figs. 2 & 5). The lowest part of the Turkana depression is occupied by the sigmoid-shaped Lake Turkana that lies at an altitude of 375 m and is locally bordered to the west by NS-trending linear fault scarps in the Loriu and Lapurr areas. Its southern extremity extends into the Suguta valley, and best expresses active deformation in the Turkana depression (Bosworth & Maurin, 1993; Dunkley *et al.,* 1993).

The large-scale structure of the Turkana depression results from two major episodes of rifting that occurred during the Cretaceous-Palaeogene in the N140°E Anza rift to the SW (Greene *et al.,* 1991; Bosworth, 1992; Dindi, 1994; Morley *et al.,* 1999b) and in the Oligocene-Recent in the NS Turkana Rift zone *sensu stricto* (Morley *et al.,* 1992) (Fig. 2). Since the continuation of Cretaceous structures to the NW beneath the Turkana area is not yet proved, their eventual influence on Cenozoic rifting is not considered in the present work.

The dominant NS-trending structures in the Turkana Rift principally correspond to Oligo-Pliocene half-grabens referred to as the Lokichar, North Kerio and Turkana basins from seismic reflection profiling on the west side of Lake Turkana (Figs. 2B & 5A) (Morley *et al.,* 1999a, c). Their dimensions are about 50 to 100 km-long, 20 km-wide and up to 7 km-deep, filled with fluvio-lacustrine sediments and volcanic deposits (Dunkelman *et al.,* 1989; Morley *et al.,* 1992).

Supportive evidences for Plio-Pleistocene rifting are known to occur in the eastern part of the Turkana Rift from both morphological and seismic data. The present morphology in the Suguta and Kino Sogo areas exhibits dense fault networks striking at N10°E and cutting through volcanic rocks dated at 4.2-2.6 Ma (Suguta) and at 5.8-3.3 Ma (Kino Sogo) (Bosworth & Maurin, 1990; Dunkley *et al.,* 1993; Wilkinson, 1988; Hackman *et al.,* 1990). This inferred <2.6 Ma-old major faulting episode might be responsible also for the tilted attitude of 120 ka-old lacustrine levels in the Suguta trough (Casanova, 1986). Coeval extension probably occurred farther north in the Lake Turkana offshore basins (Dunkelman *et al.,* 1989), but there, youngest tectonic activity is also documented from the deformation of the lake floor and Holocene sediments (Johnson *et al.,* 1987). In order to get a general overview of the structural development of the Turkana Rift, it is essential to identify the westerly extent of recent extensional faulting throughout the Oligo-Miocene rift domain by using drainage network anomalies.

5.4. DRAINAGE NETWORK CHARACTERISTICS AND ANOMALIES

5.4.1. First-order drainage network

The Turkana drainage pattern (TDP hereafter) is dominated by Lake Turkana, which is the largest closed water body in the Eastern Branch of the EARS (surface of 7500 km²; length of 250 km; width of 15 to 30 km; maximum water depth of 114 m) (Fig. 4) (Yuretich, 1979; Butzer, 1980). The climate of the Turkana area is semi-arid, with two rainy seasons in April-May and September-November, providing a total of 200 to 500 mm of water depending on altitude (Butzer, 1980; Vincens, 1984). As in most closed lakes, Lake Turkana's level has been drastically subjected to climatically induced fluctuations during Pliocene-Pleistocene and Holocene times (Butzer, 1980; Owen *et al.,* 1982; Johnson *et al.,* 1987, 1990; Feibel *et al.,* 1989). Palaeolake long-lived highstand levels dated at around 5 ka and located at 60-70 m above present lake level (375 m), are visible on satellite images along the sedimentary plains fringing the actual shoreline.

Three major rivers feed Lake Turkana: the Omo River from the north and the Turkwell and Kerio rivers, flowing from the west and south (Fig. 4). The Omo River is the only perennial river among them. It is the major axial drainage to the lake and provides nearly 90 % of the lake's fresh water annually (Butzer, 1980). This river drains the humid tropical Ethiopian highlands to the north, and flows for 1000 km into the lake's axis. In contrast, the Turkwell and Kerio rivers both run with a NS rift-parallel trend along most of their courses (Figs. 4 & 5B). They are intermittent features that provide lateral drainage to the lake. The headwaters of these two rivers are located in the Kerio half-graben (Kerio River), and in the Turkwell escarpment (Turkwell River) (Fig. 4).

The Turkwell River traces an elliptical course resulting in the rapid swing of its trend from NS along its southern part to EW farther north, at about 3° N in the Lodwar area (Figs. 5B & 6A). There, the Kagwalas River joins the Turkwell River after flowing along the southern edge of the Ngapoi volcanic plateau. The abrupt change in the trend of the Turkwell River, from a rift-parallel axial drainage to a perpendicular EW trend, defines a main drainage anomaly in the region (anomaly 1 on Figure 5B). At the eastern extremity of the Turkwell anomalous drainage segment, the river empties into the lake via a large delta extending close to a marked embayment of the Lake Turkana where the Kerio and Lokichar rivers are also seen to reach the lake.

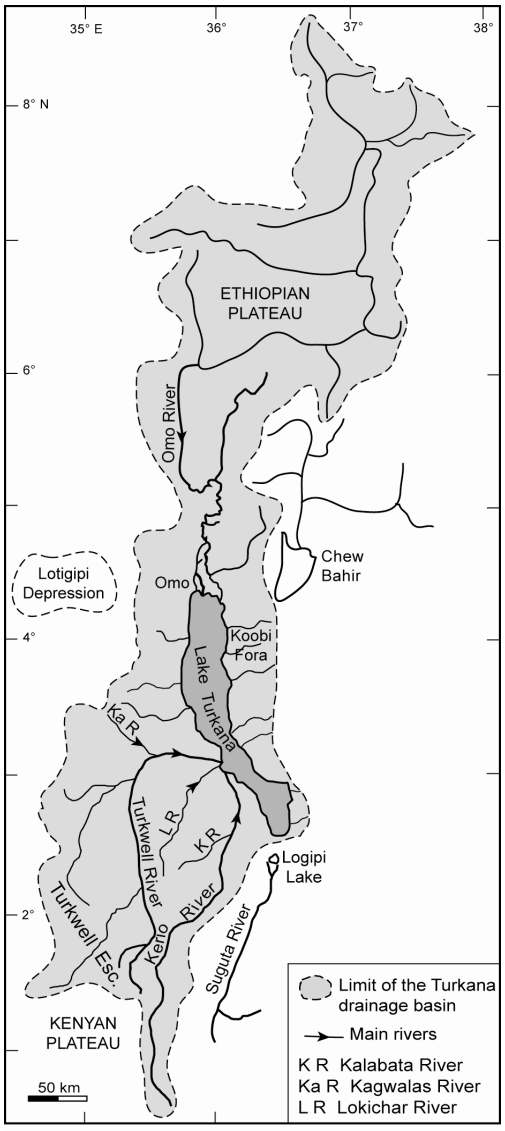

Figure 4. *Map of the Lake Turkana drainage basin and its first-order drainage network. The Omo permanent river supplies 90% of water to the lake from the Ethiopian plateaus to the north. The Tukwell and Kerio intermittent rivers drain the Kenyan plateau and the Kerio half-graben to the south.*

5.4.2. Second-order network

The TDP is extremely dense on the southwestern side of Lake Turkana, covering a surface of about 150 x 100 km (Fig. 5B), and hence forming one of the most important river complexes of the EARS as a whole. Given the relatively low annual rainfall rate measured in the Turkana region, this unexpectedly dense drainage network might have been initiated during older wet periods. Today it carries water only during the rainy seasons (Vincens, 1984).

The second-order river network is inhomogeneously distributed within two roughly NS-trending domains that have different drainage frequencies (Fig. 5). Special attention is paid to the high-frequency drainage zone to the west (the so-called Turkwell-Ngapoi zone), whereas the poorly

developed drainage to the east, in the so-called Lothidok-Kerio zone, also encompasses interesting features, which are briefly described.

5.4.2.1. The Turkwell-Ngapoi zone

The Turkwell-Ngapoi high-frequency drainage area is bounded by two nearly rift-parallel structures, the Turkwell escarpment to the west and the Napedet volcanic plateau to the east. It is subdivided into three subhomogeneous stream zones (Fig. 5B), according to classical drainage pattern criteria used elsewhere (Deffontaines, 1990):
(1) To the north, a dense stream system is symmetrically distributed with regards to the Kagwalas River, but with marked changes in its typology and organization on both sides of the river. The southern side is dominated by a sub-parallel and northeasterly flowing pattern, whilst to the NE, a radial dense network develops around discrete basement relief.

(2) South of the N70°E-trending Nakaton River, the main drainage area is subdivided into the Turkwell (W) and the Lokichar (E) subhomogeneous zones along a NS watershed line following discontinuous basement outcrops.
To the west, the Turkwell River drainage is assumed to develop entirely on a basement substratum that is only exposed along the watershed line (E) and in the Turkwell escarpment (W). The presence of significant Oligo-Miocene half-grabens at depth (similar to the Lokichar basin) is not documented by geophysics in the Turkwell area.
The symmetrical distribution of the dendritic-parallel type stream network on both sides of the Turkwell River disappears northwards, close to the easterly deflection of the river, where the eastern drainage network progressively follows the rotation of the Turkwell River to the east, whilst the western one does not show such a changing direction of flow.

(3) To the east, the Lokichar subhomogeneous zone forms a NS elongated zone (25 x 100 km) bounded to the east by a sharp cartographic limit lying close to the western edge of the Napedet volcanic plateau. The arrangement and typology of its dense river network are strongly controlled by the lithology of the substratum exposed on both sides of the Lokichar eroded master fault (Morley, 1999c) (Fig. 5A). The river drainage evolves from a radial type, flowing around smooth hills of basement lithology in the footwall block to the west, to a dense, parallel-type network flowing to the east over Quaternary alluvium capping the hangingwall basinal domain.
The drainage system is locked to the east against a prominent NS-trending lineament, 60 km-long with no marked topographic expression and followed by the intermittent Lokichar River (Joubert, 1966).

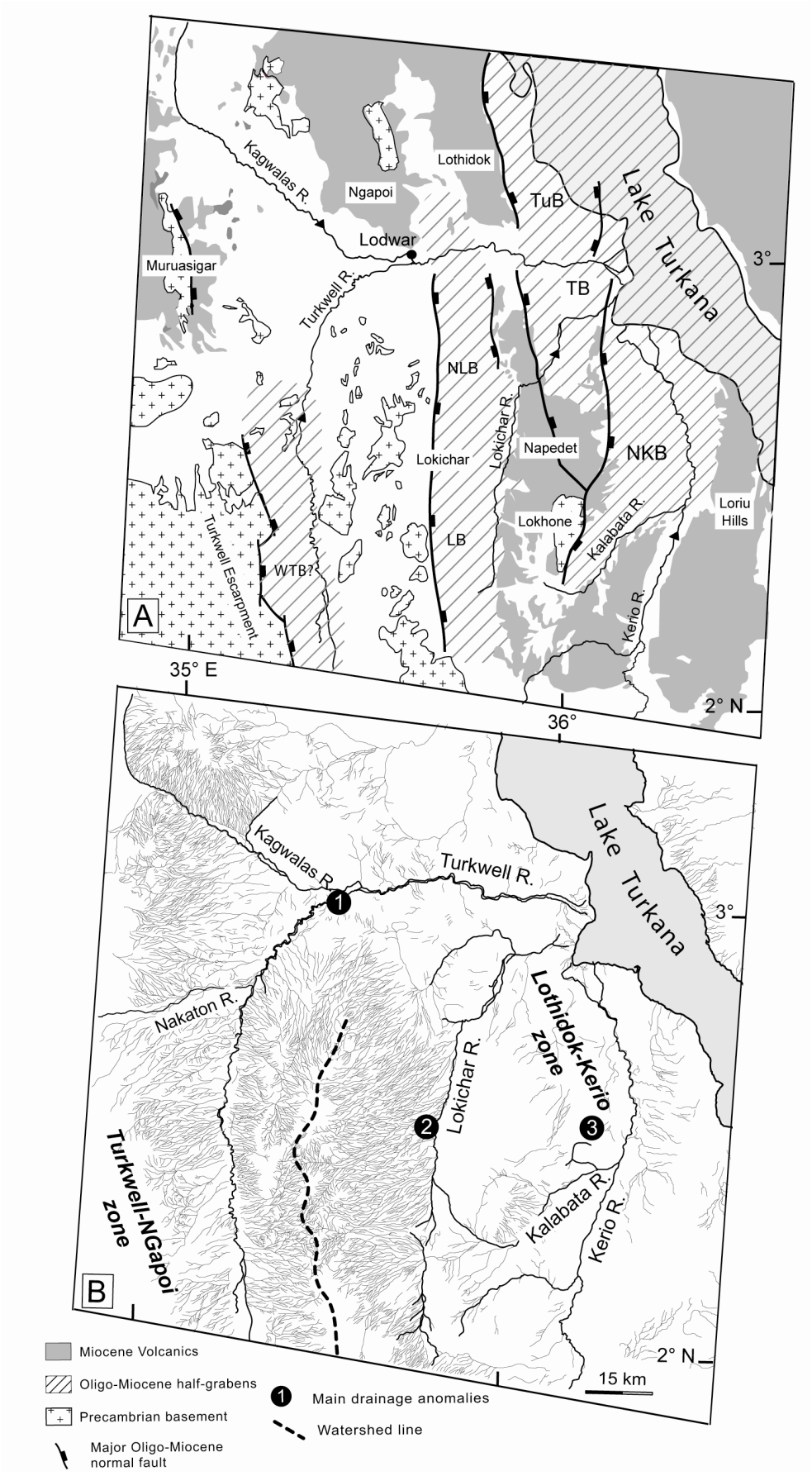
Kagwalas R.
Lothidok
Ngapoi
TuB
Lake Turkana
Lodwar
3°
Muruasigar
Turkwell R.
TB
NLB
Lokichar R.
Napedet
NKB
Lokichar
Loriu Hills
Lokhone
Kalabata R.
LB
Turkwell Escarpment
WTB?
Kerio R.
A
35° E
36°
2° N
Kagwalas R.
Turkwell R.
Lake Turkana
3°
Nakaton R.
Lothidok-Kerio zone
Lokichar R.
Turkwell-NGapoi zone
Kalabata R.
Kerio R.
B
2° N
15 km
Miocene Volcanics
Oligo-Miocene half-grabens
Precambrian basement
Major Oligo-Miocene normal fault
Main drainage anomalies
Watershed line

Figure 5. *Influence of lithology and structure (A) on the distribution and frequency of river drainage network (B) on the western side of Lake Turkana. For ease of comparisons, the two maps are drawn at the same scale.* ***A.*** *Simplified geological map of the study area and Oligocene-Pliocene basins organization from Morley et al. (1999a).* ***B.*** *First-order and tributary drainage network of the west Turkana area extracted from two Landsat TM satellite images. Note the lack of secondary drainage on the Napedet, Loriu, Lothidok and Ngapoi volcanic plateaus. In contrast, it is extremely developed on the Quaternary sedimentary cover in the Lokichar, Turkwell and Ngapoi areas, on the western part of the Turkana area. The watershed limit separates the Napedet-Lokichar and Turkwell domains. Three main drainage network anomalies are fully discussed in the text.*

This first-order feature outlines the mapped boundary between synrift lavas and sediments forming the flexural margin of the Lokichar Miocene half-graben. Such a cartographic arrangement, in addition to the progressive swing of the general flow direction from E to NE northwards, constitutes the so-called Lokichar drainage anomaly (anomaly 2 on figure 5B).

5.4.2.2. The Lothidok-Kerio zone

In the Lothidok-Kerio area, the low-frequency tributary system is totally absent in the Napedet (S) and Lothidok (N) volcanic plateaus. It preferentially develops on the eastern side of the Kerio River, probably fed by water coming from the relief of the 1800 m high Loriu uplifted block. In the Lokhone sector to the south, a denser drainage occurs in a restricted subcircular area where the N10° limit of a palaeo-basement horst (Miocene in age) is clearly outlined by the sharp disappearance of a centrifugal-parallel river network to the west over crystalline eroded basement rocks. Farther to the NE, an anomalous isolated circular stream, about 3 km in diameter, (anomaly 3 on Figure 5B) is observed on the northwestern side of the Kalabata River, over Pliocene sediment-lava alternations of the North Kerio half-graben.

5.5. DRAINAGE PATTERN ANOMALIES

According to the TDP organization in relation to the geological and morphological context, three drainage anomalies, the Turkwell, the Lokichar and the Kalabata have been selected to provide insights at various scales about river drainage evolution and neotectonic movements.

5.5.1. The Turkwell River anomaly

Since accurate topographic data are not yet available in the Turkana area, the large-scale deflection of the Turkwell River to the east is not easily linked to recent rift-induced morphology.

However its structural control is documented by a line of evidence dealing with the general arrangement of the Oligocene-Pliocene half-graben system seismically imaged in the Lothidok-Lothagam hill area (Fig. 6B, C).

Once superposed on the tectonic sketch map of the Oligo-Pliocene rift basins (Morley *et al.,* 1999a) (Fig. 6C), the trace of the Turkwell River appears to cut the Lokichar fault at a high angle to the west, whilst farther east, it lies over a roughly EW-trending corridor, 15 km-wide, where some of the major NS extensional structures show complex lateral fault linkages. From W to E, the river first intercepts an oblique relay zone (structure (a) in Fig. 6C) between the Napedet and Lothidok fault segments that bound, respectively, the Turkana and the Turkwell basins to the west. The river's eastern trace lies over an approaching divergent transfer zone (structure (b) in Fig. 6C) (according to the nomenclature of Morley, 1999b) that separates adjacent faulted basins with opposite polarities. Indeed, the dominantly westward-dipping extensional structures forming the Turkwell fault system on the dip-seismic lines TVK 140-141 across the southern termination of the Turkana basin pass laterally southwards into an array of easterly-facing normal faults within the Turkwell and North Kerio basins (Profile TVK 101 on Figure 6B2).

Borehole stratigraphy (Eliye Springs-well, Morley, 1999a) (see location in Fig. 6B1, C), reveals that the two opposite fault systems involve Late Pliocene (< 3.7 Ma) to Recent (Pleistocene?) sequences (Fig. 6B). This indicates the recent age of extension within the EW-trending corridor, called here the Turkwell Transfer Fault Zone (TTFZ in the text).

Lateral correlation with EW-trending fault structures observed in the Mount Porr area on the eastern shore of Lake Turkana (Fig. 6C) suggests that the TTFZ is a long-lived transverse rift structure controlled at depth by a pre-existing basement discontinuity (Vétel & Le Gall, submitted).

With regards to the recent evolution of the Turkana Rift, two kinematic models can account for the structural control of the Turkwell River anomaly by a transverse fault zone.

Figure 6. *Evidence for anomalous EW-trending structures in the Turkana rift from river drainage and the rift fault network.* ***A.*** *Satellite image of the Turkwell River drainage pattern. The Turkwell River course is deflected from a general NS trend to an anomalous EW direction, 20 km before reaching the lake.* ***B.*** *Seismic sections through Oligocene-Pliocene basins in the Turkwell area. LF: Lokichar Fault; LotF: Lothagam Fault; NLF: Napedet-Lothidok Fault; TF: Turkwell Fault; WNF: West Napedet Fault.* ***B1-B2.*** *Dip-section showing opposite facing extensional faults in terrains extending on both sides of the EW trace of the Turkwell River. Note the westerly and easterly dips of the Turkwell and Lothagam faults, respectively* ***C.*** *Structural map of the Turkwell area from surface (river drainage) and deep (seismic) data sets. The image faults controlling the Oligocene-Pliocene basins are drawn from Morley et al. (1999a). The EW-trending segment of the Turkwell River flows above a zone of increasing complexity in the Miocene rift fault network (relay and overlapping zones).*

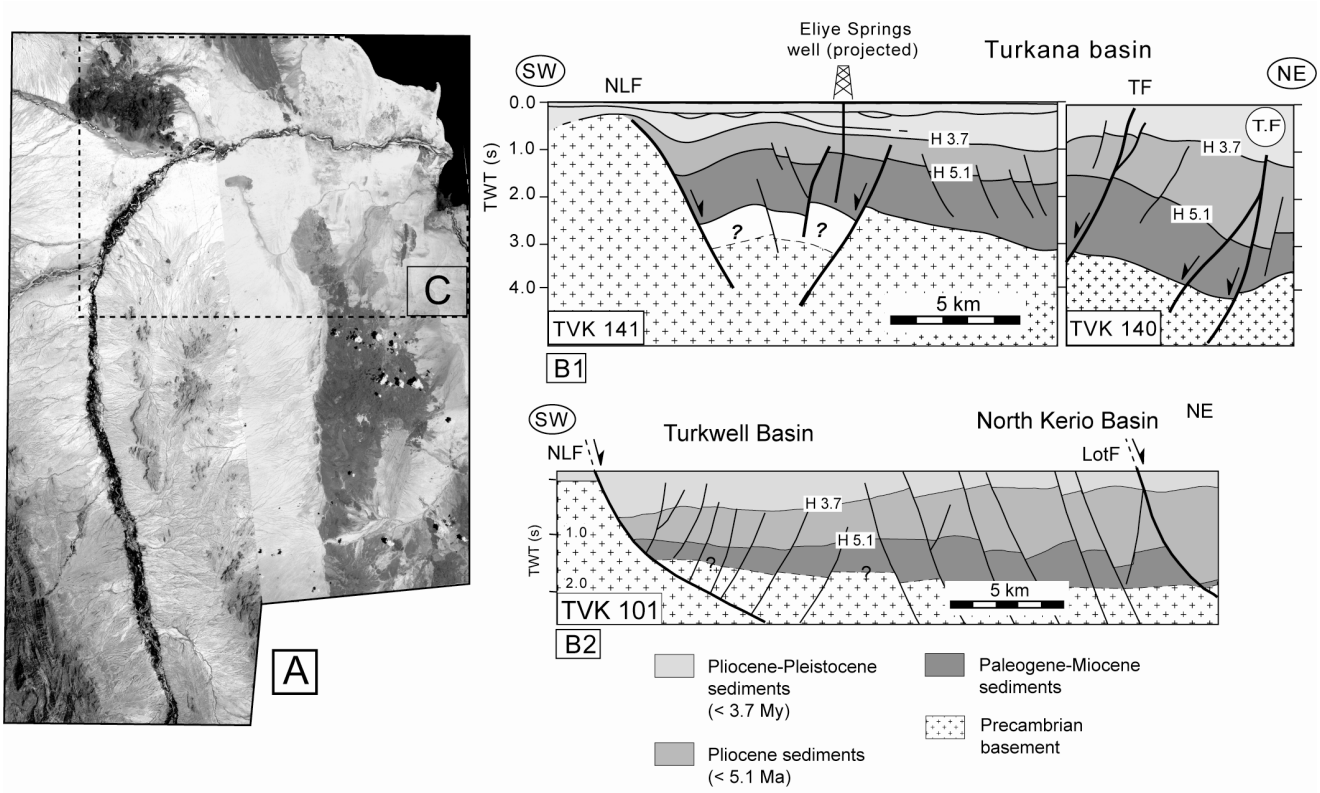
A
C
Eliye Springs
well (projected)
Turkana basin
SW
NE
NLF
TF
T.F
TWT (s)
0.0
1.0
2.0
3.0
4.0
H 3.7
H 5.1
?
5 km
TVK 141
TVK 140
B1
Turkwell Basin
North Kerio Basin
LotF
TVK 101
B2
Pliocene-Pleistocene sediments (< 3.7 My)
Pliocene sediments (< 5.1 Ma)
Paleogene-Miocene sediments
Precambrian basement

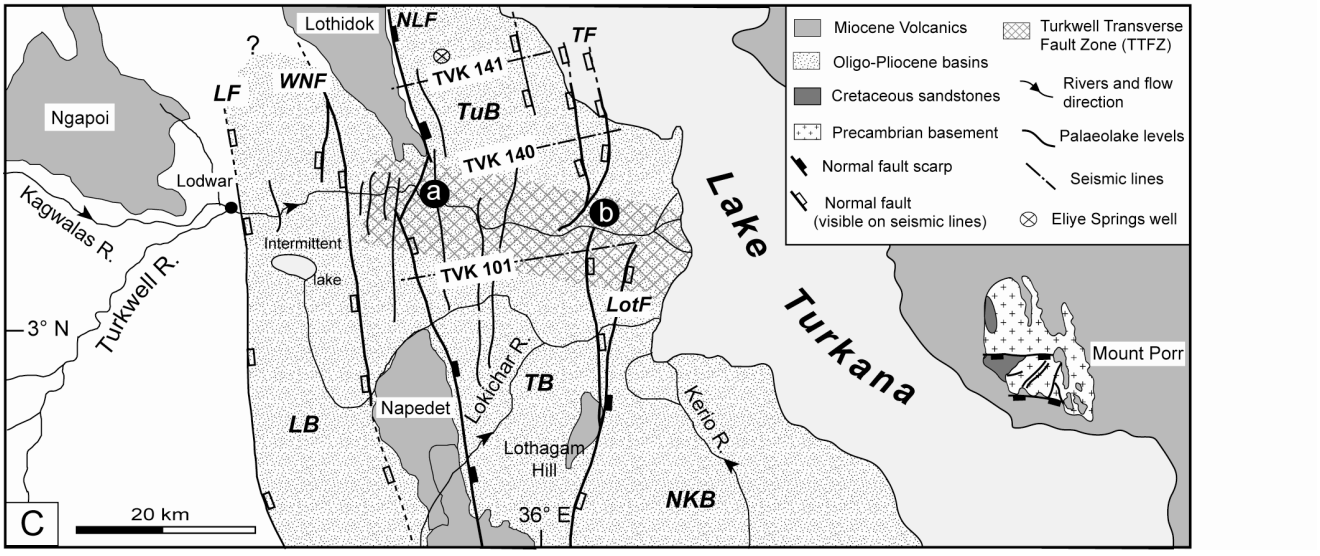
Lothidok
NLF
TF
WNF
LF
TVK 141
TuB
TVK 140
Ngapoi
Lodwar
Kagwalas R.
Turkwell R.
Intermittent
lake
TVK 101
LotF
3° N
Napedet
Lokichar R.
TB
LB
Lothagam
Hill
Kerio R.
NKB
36° E
20 km
C
Lake Turkana
Mount Porr
Miocene Volcanics
Oligo-Pliocene basins
Cretaceous sandstones
Precambrian basement
Normal fault scarp
Normal fault (visible on seismic lines)
Turkwell Transverse Fault Zone (TTFZ)
Rivers and flow direction
Palaeolake levels
Seismic lines
Eliye Springs well

A first model implies that the Lothidok faulted block to the north has been significantly uplifted along the TTFZ, hence inducing the lock of the Turkwell River course along the foot of the elevated zone in a similar way as depicted by Jackson *et al.* (1996) in the Otago active fault zone (New Zealand). However, the lack of EW-trending morphological fault scarps on the northern side of the Turkwell River does not support this first hypothesis. An alternative model is favored here from several lines of evidence dealing mainly with the spatial distribution of palaeolake levels (probably Holocene in age) as they are expressed on Landsat images by dense arrays of short and parallel features high reflectance lineaments. They occur principally over a narrow NS-trending strip of Quaternary sediments bounded to the west by the Lothidok and Napedet volcanic scarps (Fig. 6C).

Other palaeolake levels extend farther west over a narrow EW-trending corridor strictly superposed on the TTFZ. The most peripheral lake levels extend 15 km west of the Lothidok-Napedet scarp, in the vicinity of a small intermittent swamp or lake (Fig. 6C). The westerly transgression of Lake Turkana along the inferred Turkwell transverse palaeoembayment probably occurred during an upper Holocene highstand lake level, which is documented in the Koobi Fora and Omo areas (Fig. 4) (Butzer, 1980; Owen *et al.,* 1982).

It is also likely that the Turkwell embayment has exploited a more erodable and weathered transverse zone developed on top of the disrupted zone of complex Miocene-Pliocene fault linkage structures forming the TTFZ. Such fault patterns are known to be the locus of preferential erosion (Jackson & Leeder, 1994) (Fig. 7), and they might result, at a larger scale, in the capture of first-order rivers as applied here to the Turkwell River.

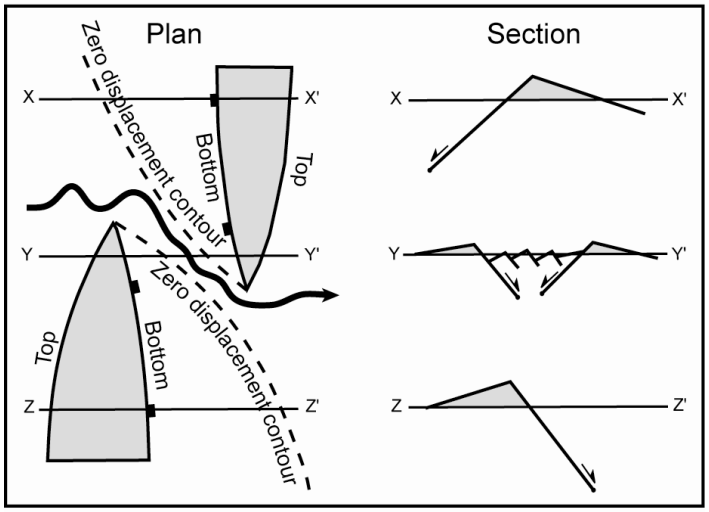

Figure 7. *Morphological and river drainage frameworks related to overlapping and extensional fault networks. Map-view and cross-sections showing the trace of a river between the tip zones of two synthetic overlapping faults and the subdued topography related to secondary fault structures (modified from Jackson & Leeder, 1994).*

5.5.2. The Lokichar River anomaly

The Lokichar drainage anomaly occurs along the contact between Miocene basalts of the Napedet plateau to the east and sedimentary cover of the Lokichar half-graben to the west (Fig. 8). Joubert (1966) have noted an atypical arrangement of the river network in this area but did not formulate an evolution model for this zone. Such drainage organization generally typifies fault-induced topography in zones of active deformation (Peakall *et al.,* 2000; Schumm *et al.,* 2000). However field investigations along the Lokichar anomaly indicate subdued topography, with no evidence for a fault scarp (Fig. 8C). Instead, Miocene basalts dipping gently to the west (3-4°) are seen to disappear beneath the recent alluvial sediments of the Lokichar plain (Joubert, 1966) and form the modest relief on the Napedet plateau to the east (Figs. 8D2 & D3). The general tilt of the Napedet volcanics on the eastern flexural margin of the Lokichar half-graben conforms to the westerly polarity of the basin (Morley *et al.,* 1999a).

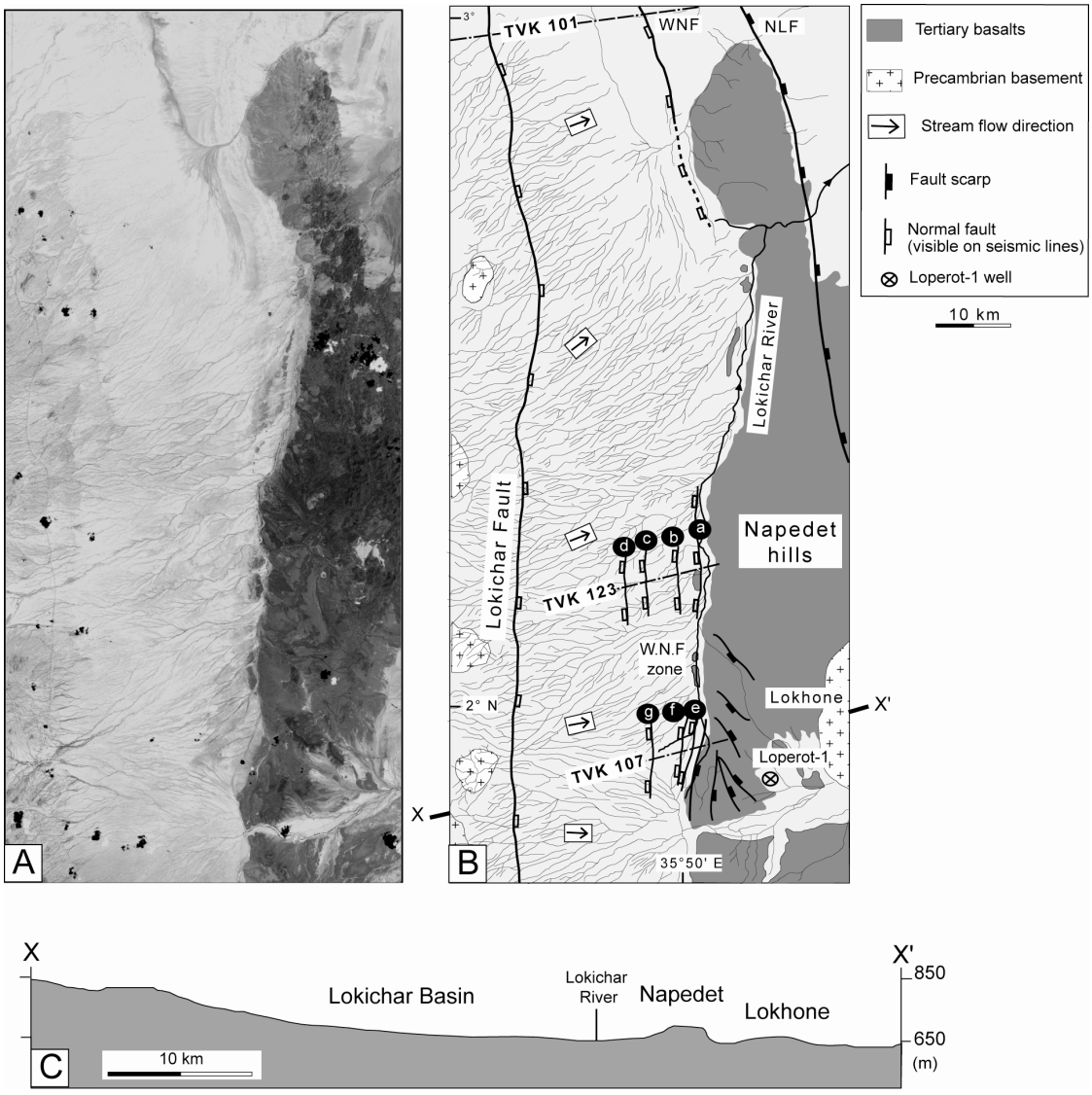

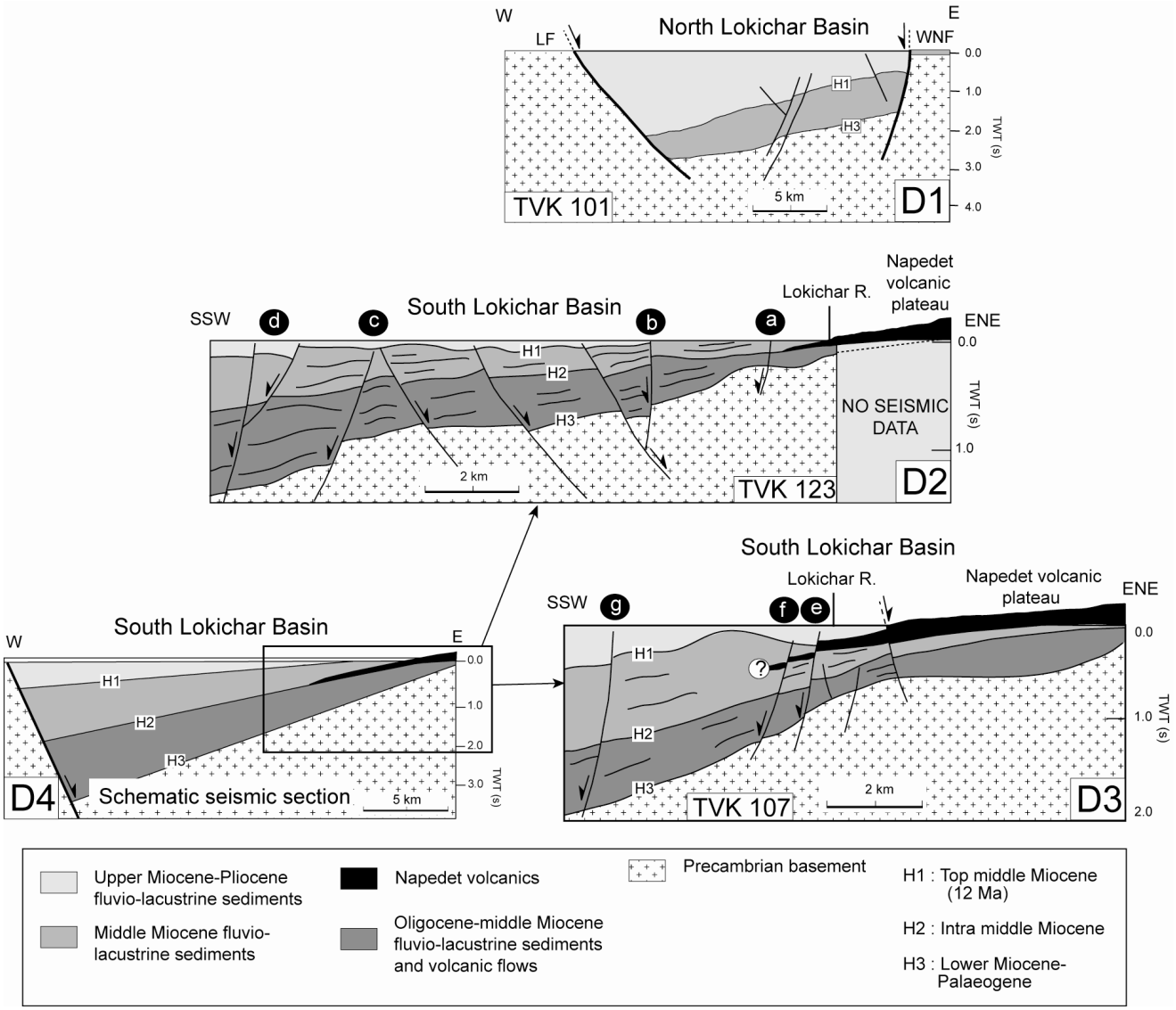

Figure 8. *The structural significance of the Lokichar-Napedet river drainage anomaly.* ***A.*** *General view of the Napedet-Lokichar area extracted from a Landsat TM satellite image.* ***B.*** *Morphostructural interpretation of figure A showing the abrupt termination of the EW/SW-NE Lokichar secondary stream network along the NS western edge of the Napedet volcanic hills.* ***C.*** *Topographic profile (XX') (vertical exaggeration x25) illustrating the east-dipping gentle slope (1%) of the Lokichar basin and the low relief of the western limit of the Napedet plateau to the east.* ***D.*** *Amoco seismic reflection lines crossing the eastern flexural margin of the Lokichar half-graben, and showing the deep structure of the boundary between the Napedet volcanic plateau to the east and the Quaternary cover to the west.* ***D1.*** *Dip-section TVK 101 across the northern termination of the graben-like Lokichar basin. Note that significant post-H1 displacement occurred along the WNF.* ***D2-D3.*** *Dip-sections (TVK 123 and 107) through the flexure of the Lokichar half-graben (D4). The Lokichar River occurs in the vicinity of a faulted zone involving minor westerly-dipping normal structures and to which we assign the control of the Lokichar River course by downthrown blocks no longer visible in the present-day topography.*

Three dip-seismic profiles across the flexural part of the Lokichar basin cut the Lokichar anomaly at high angles (Fig. 8B, D). The seismic reflectors, interpreted according to the Loperot-1 well (Morley, 1999c) (Fig. 8B), involve a thick Oligo-Pliocene sedimentary wedge subdivided into a number of fluvio-lacustrine sequences (Morley, 1999c). Because of the limited seismic resolution at shallow depth, the relation between the top Middle Miocene series (post-H1) and the recent (Quaternary?) cover is poorly defined. However, a series of minor extensional faults, dipping mostly to the west, are clearly imaged close to the surface. On the seismic line TVK 101, the West Napedet Fault (WNF) forms a steep border fault bounding the Lokichar asymmetrical graben to the east (Fig. 8D1). Given its important throw during recent time (post-H1), the WNF is likely to have extended much farther south than deduced from the Middle Miocene isopach map (Morley *et al.,* 1999a) (Fig. 8B). The postulated topographic scarp that might have formed at the northern termination of the Napedet volcanic edge is no longer preserved in the present morphology, but it is likely to have locked the eastern course of the palaeo-Lokichar River.

About 30 km farther south, the graben-like geometry of the Lokichar basin gives way to a flexural margin imaged on profiles TVK 123 and 107 (Figs. 8D2 & D3). Shallowly-dipping sequences are cut by a series of antithetic extensional faults dipping to the west. Two of them (labeled (a) and (b) on Fig. 8D2) occur with a steeper attitude and modest displacement in the easternmost part of the basin, in the vicinity of the Lokichar River area. Fault (a) lies close to the western limit of the Napedet volcanics at the surface, hence suggesting that it has been reactivated during recent times. The resulting (probably minor) westerly-downthrow is thought to have been sufficient to create a topographic scarp along which the palaeo-Lokichar river drainage was deviated. The morphologic expression of the inferred scarp is no longer visible in the present-day topography.

A similar fault geometry is observed farther south on the eastern portion of seismic line TVK 107 where three west-dipping normal faults, labeled (e), (f) and (g), involve the entire synrift sedimentary package up to sequence H1 (Fig. 8D3). The easternmost fault (e) strictly extends in the southern continuation of fault (a) and lies close to the western outcrop edge of the Napedet volcanics. This spatial coincidence suggests similar kinematics for fault (e) as applied to fault (a).

Correlating seismically-imaged rift fault structures with river drainage anomaly at the surface permits a determination of the structural evolution of the flexural margin of the Lokichar basin from Palaeogene-Miocene up to present. A four-staged evolutionary model (Fig. 9) illustrates the sequential development of faulting within the entire basin:

(1) Initiation of the Lokichar half-graben occurs in Upper Oligocene-Lower Miocene along the Lokichar border fault (Fig. 9A1). Deposition of sequence H3 takes place in the Loperot/Lokhone lakes (Morley *et al.,* 1999a).

(2) The maturity stage in the Miocene (Fig. 9A2) results in the deposition of thick lacustrine and fluvio-deltaic sequences (H3-H2-H1) during the main development of the Lokichar fault which accommodates most of the extension. The NS basement relief formed in the uplifted footwall block of the Lokichar fault is probably drained by a stream network flowing eastwards into the lake hangingwall area (Morley *et al.,* 1999a). At this stage, the general topography of the Lokichar basin is slightly tilted to the west, in agreement with the easterly polarity of the border fault. This general slope direction leads to the development of a dense parallel-type stream network flowing westward into the basin, as classically observed in most extensional basins (Leeder & Jackson, 1993; Schumm *et al.,* 2000). The volcanic relief emplaced in the Napedet marginal area to the east might have also emphasized the formation of this lateral river drainage.

(3) During the Upper Miocene (Fig. 9A3), the deformation migrates eastwards from the western faulted border, where the Lokichar master fault is abandoned while its footwall is progressively eroded, to the flexural margin of the basin to the east which is dissected by the West Napedet fault system. The easterly shift of the deformation results in two modifications in the shallow structure of the basin: (1) the reversal of polarity (from W to E) of the drainage network in relation with tilted-block rotation along the WNF system, and (2) the locking and NS channeling of the secondary stream along the corresponding topographic fault scarp. Although displacement and rotation along the WNF system are minor (see above), the resulting gentle slope topography is believed to have been sufficient to initiate parallel-type river drainage. That assessment is supported by analogue modeling that shows similar drainage with a minimum slope of 3 % (Phillips & Schumm, 1987).

(4) The erosional processes that dominate the Pliocene-Pleistocene evolution of the entire Lokichar basin may account for the subdued topography of the WNF area to the east. Given the differential erosion of the lithologically-contrasted material in the WNF system (sediments in the hangingwall and basalts in the footwall), the Lokichar drainage anomaly is still preserved today without any topographic fault scarp (Fig. 9A4).

At a regional scale, the Lokichar subsidiary river system shows abrupt changes in flow direction from EW in the southern part of the basin, to N70°E in the central part, up to N45°E farther north, in the WNF area (Fig. 9B). This diverging river pattern probably results from a change of slope direction from EW in the south (perpendicular to the normal fault network) to NE farther north in response to greater downthrow and subsidence along the WNF (Fig. 9B).

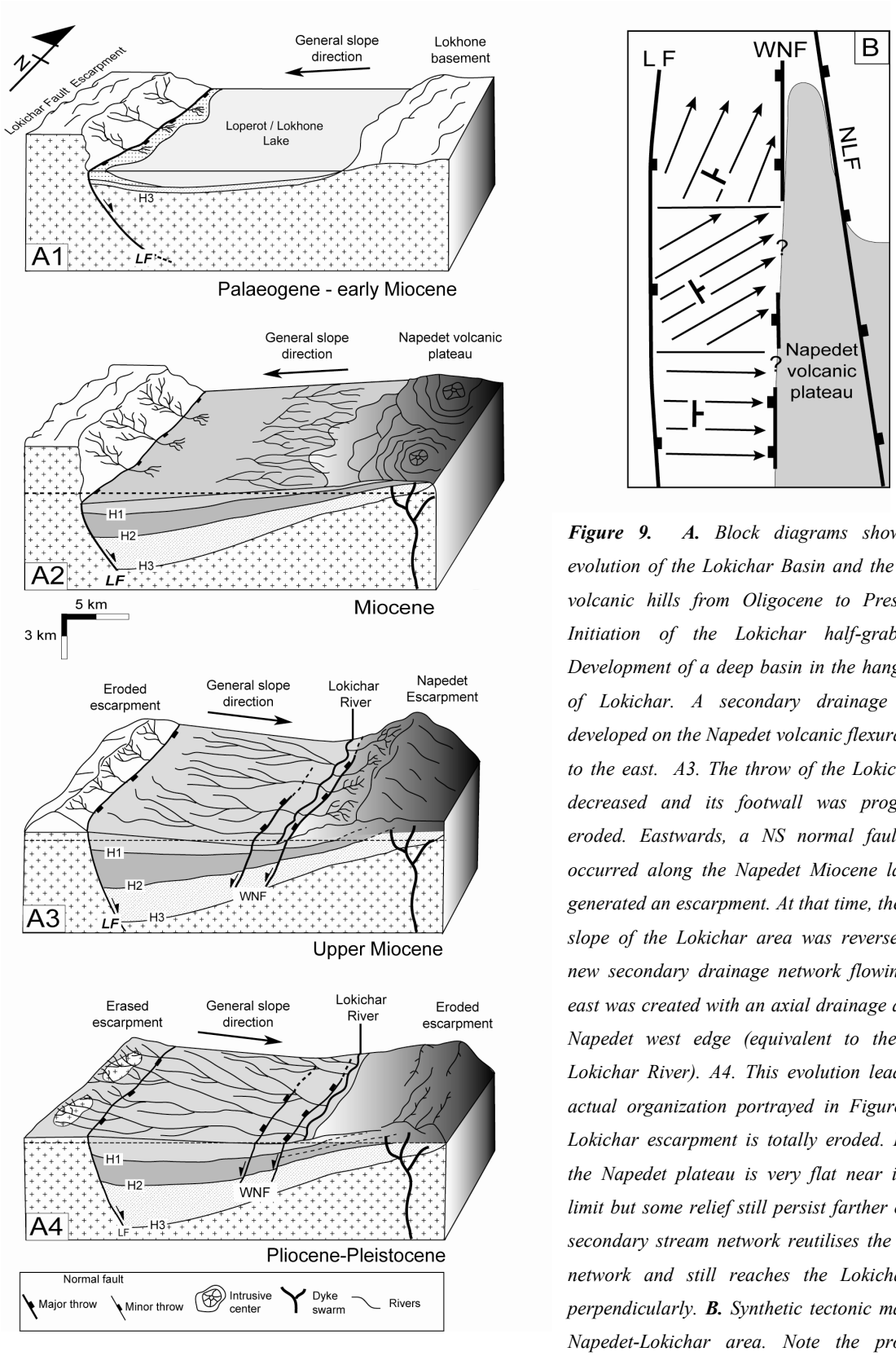

Figure 9. ***A.*** *Block diagrams showing the evolution of the Lokichar Basin and the Napedet volcanic hills from Oligocene to Present. A1. Initiation of the Lokichar half-graben. A2. Development of a deep basin in the hanging wall of Lokichar. A secondary drainage network developed on the Napedet volcanic flexural border to the east. A3. The throw of the Lokichar fault decreased and its footwall was progressively eroded. Eastwards, a NS normal fault system occurred along the Napedet Miocene lavas and generated an escarpment. At that time, the general slope of the Lokichar area was reversed and a new secondary drainage network flowing to the east was created with an axial drainage along the Napedet west edge (equivalent to the present Lokichar River). A4. This evolution leads to the actual organization portrayed in Figure 8. The Lokichar escarpment is totally eroded. Likewise, the Napedet plateau is very flat near its linear limit but some relief still persist farther east. The secondary stream network reutilises the Miocene network and still reaches the Lokichar River perpendicularly.* ***B.*** *Synthetic tectonic map of the Napedet-Lokichar area. Note the progressive change direction of rivers from south to north, according to the tectonic setting.*

5.5.3. The Kalabata River circular anomaly

The tributary network of the Kalabata River is poorly developed at the southern extremity of the Lothidok-Napedet drainage subdomain (Fig. 5B). One of its western affluent draws a sub-circular anomalous course (diameter of ca. 3 km) on Pleistocene-Recent sediments overlying the southern part of the North Kerio basin (Figs. 5 & 10). Inside the anomaly, prominent NS-trending lineaments are clearly distinguished from pale sediments on the Landsat image. They can be correlated with Miocene basalts that form discrete outcrops on the SE part of the anomaly (Ochieng *et al.,* 1988). The Kalabata circular anomaly typically resembles morphological features induced by domal uplift or volcanic intrusions (Marple & Talwani, 1993; Merrits & Hesterberg, 1994; Schumm *et al.,* 2000). Its structural interpretation is constrained at depth by seismic data from line TVK 131 (Fig. 10C).

The Kalabata anomaly is located over a small Miocene depocenter in the hangingwall of the Kerio fault (Morley *et al.,* 1999a). These strata are deformed into a system of open upright folds dissected by diverging reverse faults. This leads to a succession of small-scale triangular and pop-up zones that typify inversion tectonics. This inverted tectonic phase is assumed to be < 3.7 Ma in age with regards to similar compressional structures restricted to the North Kerio basin as a whole (Morley *et al.,* 1999c, Le Gall *et al.,* in press). The NS-trending basaltic lineaments identified by remote sensing in the hangingwall of the Kerio fault are a trace of folded Miocene lava flows imaged by the seismic profiles. The subcircular drainage anomaly in the Kalabata area is therefore attributed to local domal uplift caused by the positive inversion of a minor depocenter during post-Pliocene times.

Whatever the origin of the driving forces responsible for recent compression in the North Kerio half-graben (Morley *et al.,* 1999c; Le Gall *et al.,* in press), our structural interpretation of the Kalabata River anomaly is consistent with previous studies of similar round-shaped anomalies elsewhere (Marple & Talwani, 1993; Merrits & Hesterberg, 1994).

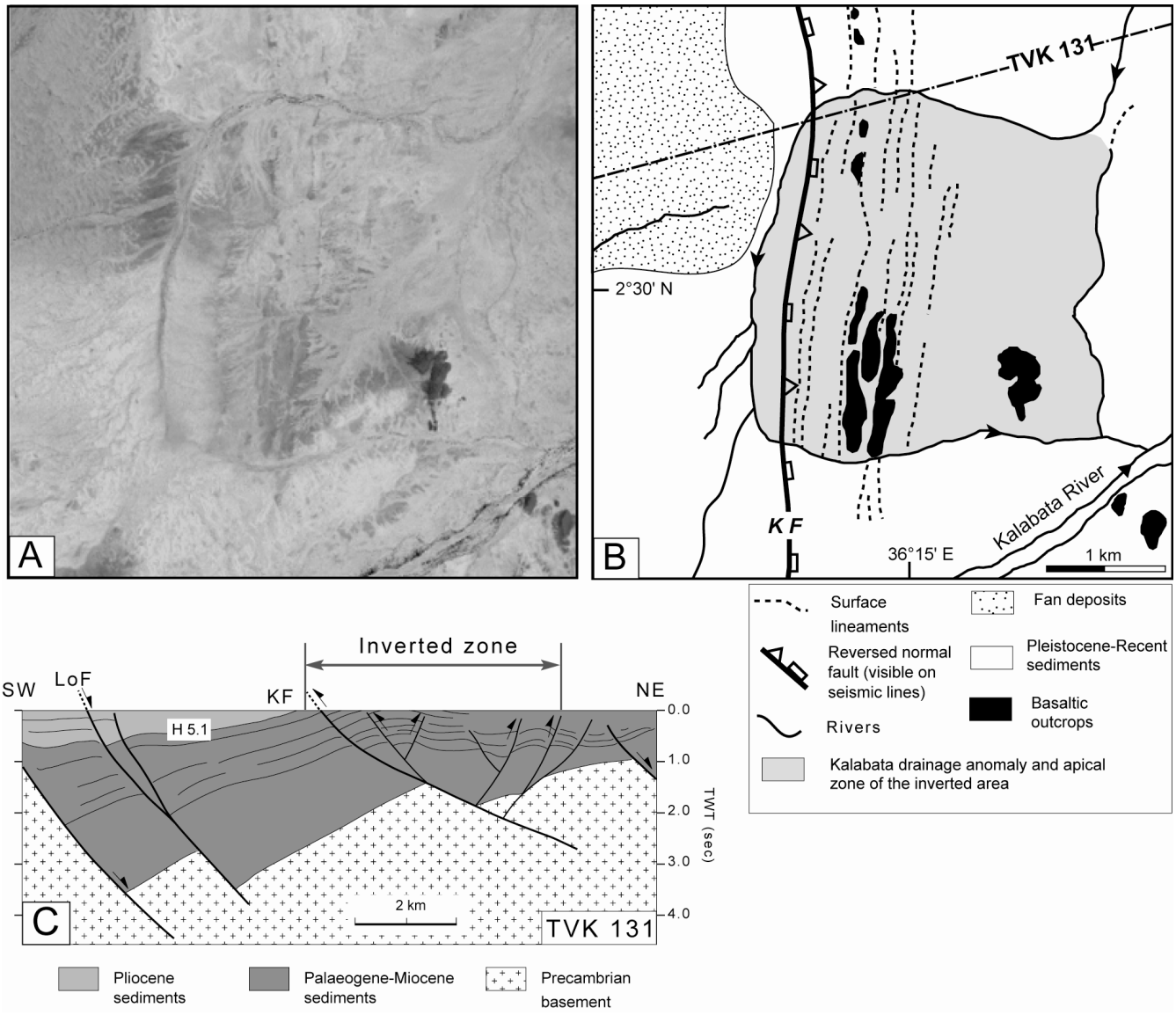

Figure 10. *Kalabata river drainage anomaly related to inversion tectonics in the southern part of the North Kerio Basin.* ***A.*** *Detailed view of the Kalabata anomaly extracted from a Landsat TM satellite image. The subcircular trace of the river is clearly observed as are also a group of NS dark lineaments.* ***B.*** *Morphostructural interpretation.* ***C.*** *EW-trending seismic line (TVK 131) crossing the northern end of the area surrounded by the Kalabata River anomaly. This up-domed area correlates with recent (< 5.1 Ma) inverted fault/fold structures at depth.*

5.6. DISCUSSION AND CONCLUSIONS

The main episode of extension in the Turkana Rift zone occurred during Upper Oligo-Pliocene times, resulting in large 6-7 km-deep half-grabens on the western part of modern Lake Turkana. Most of the associated flank uplift morphology has been removed by erosion in the footwalls of

the Lokichar, West Napedet, Napedet-Lothidok, Lothagam and Turkwell master faults (LF, WNF, NLF, LoF, TF, respectively) (see Fig. 6C).

Younger (< 5.1 Ma) fault displacements, of either extensional or (more locally) compressional types, are documented by seismics along the easternmost structures (WNF, NLF, LoF, TF).

These recent deformations no longer have clear topographic expression. However, their trace at the surface can be deduced from the analysis of the regional drainage network. This approach, when combined with deep seismic data highlights recent structural features of the Turkana Rift (Fig. 11), and emphasizes the use of river drainage analysis for better constraining recent faulting in extensional zones with subdued morphology.

First-order river deflection, perpendicular or oblique to a given extensional system, may be used as a key-marker for identifying large-scale transverse fault zones that do not benefit from deep structural constraints. This assessment is supported by the recent evolution of the TTFZ which involves < 3.7 Ma series at depth and coincides with a 15 km-wide topographically-depressed corridor, occupied by the EW course of the Turkwell River (Anomaly 1). This transverse zone of disrupted rift fault linkage was as a zone of preferred weathering, expressed at the surface by a palaeoembayment that guided the westerly transgression of Lake Turkana during an upper Holocene highstand lake level, and also the capture of first-order river.

Palaeo-river drainage anomalies may outline the trace of recent structures that are badly (or not) documented because of subdued topography, and poor quality seismic data at shallow depth. The Lokichar and Kalabata anomalies (2 and 3 on Fig. 11) supply evidence for such neotectonic deformation in relation to both extensional and compressional contexts. The excellent conservation of the corresponding fault-controlled subsidiary river drainages, still flowing at present, suggests the relatively young age (Quaternary?) of the associated fault patterns, whilst the lack of fault scarps implies that these latter are no longer active.

River drainage analysis presented in this work leads us to identify recent minor extensional deformation on the western shore of Lake Turkana, as far west as the eastern margin of the Lokichar basin (Fig. 12). It is therefore suggested that post-Miocene rifting in the Turkana sector takes place in a nearly 80 km-wide zone of diffuse deformation involving 1) to the east, the active basins of south and central Lake Turkana where a focussing of stress is observed, and 2) to the SW, a weakly deformed zone where earlier (Miocene) faults are slightly reactivated. If considering the time interval 5 Ma-Present, the < 3.7 Ma-old deformation in the Kino Sogo faulted ‘belt’ should be also included in the Turkana neotectonic zone.

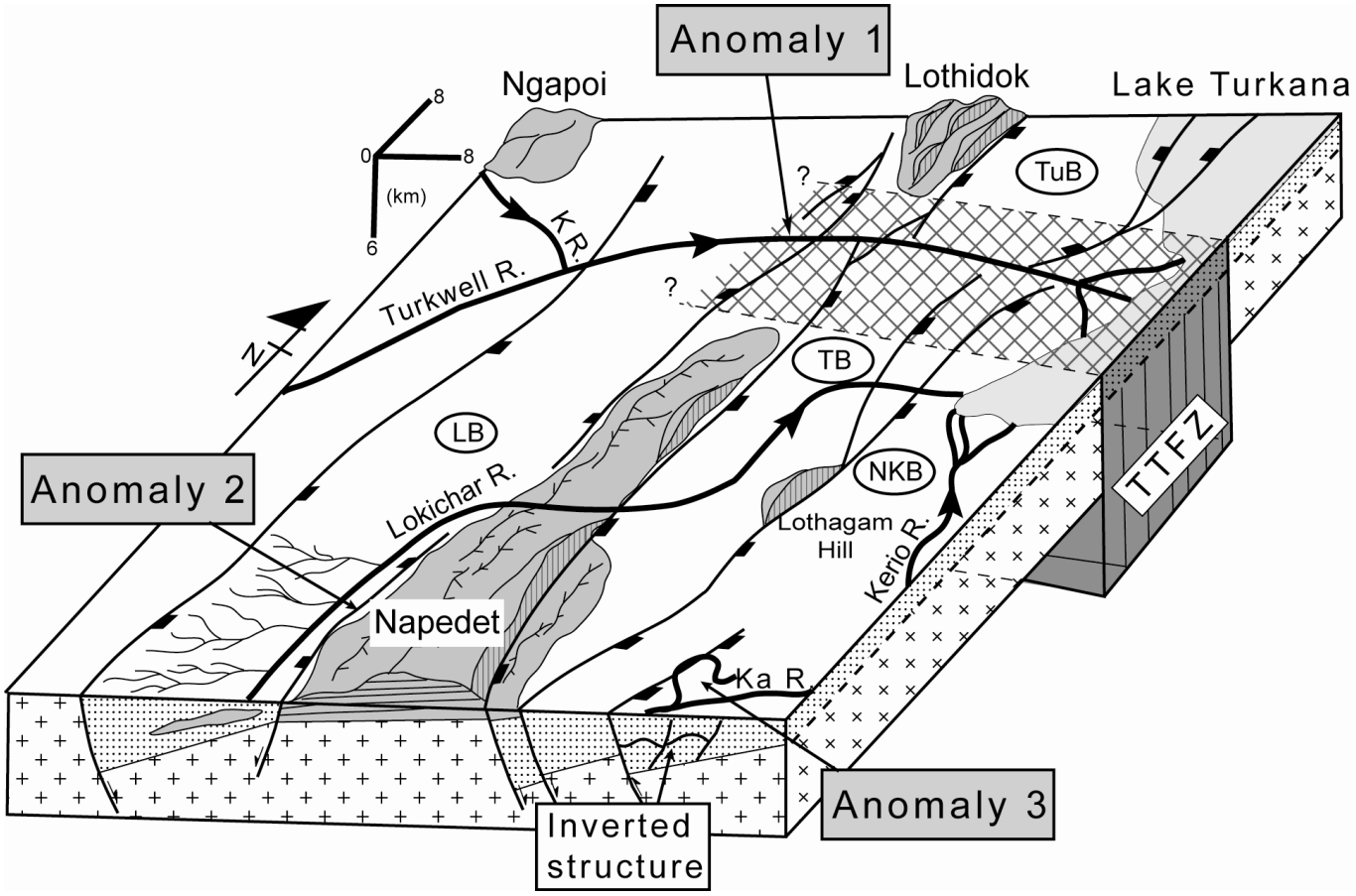

Figure 11. *3D block-diagram synthesizing the three types of river drainage anomalies identified in the Turkana area rift zone. Anomalies (1) (Turkwell) and (2) (Lokichar) are large-scale structures induced by an EW transverse discontinuity, and NS reactivated normal faults, respectively. Anomaly (3) (Kalabata) is related to the positive inversion of a local depocenter in the immediate hangingwall of the North Kerio border fault at Pliocene times.*

However, further morphotectonic studies of the Kino Sogo grid fault are highly needed to accurately estimate the amount of extension across this eastern-rifted area, in order to get a more comprehensive overview of the neotectonic domain in the Turkana Rift and propose a kinematic model for recent/active deformation in this atypical sector. More generally, our work highlights the interest of combining drainage network anomalies deduced from remote sensing with subsurface data (seismic reflection) for documenting recent structural features with low topographic expression.

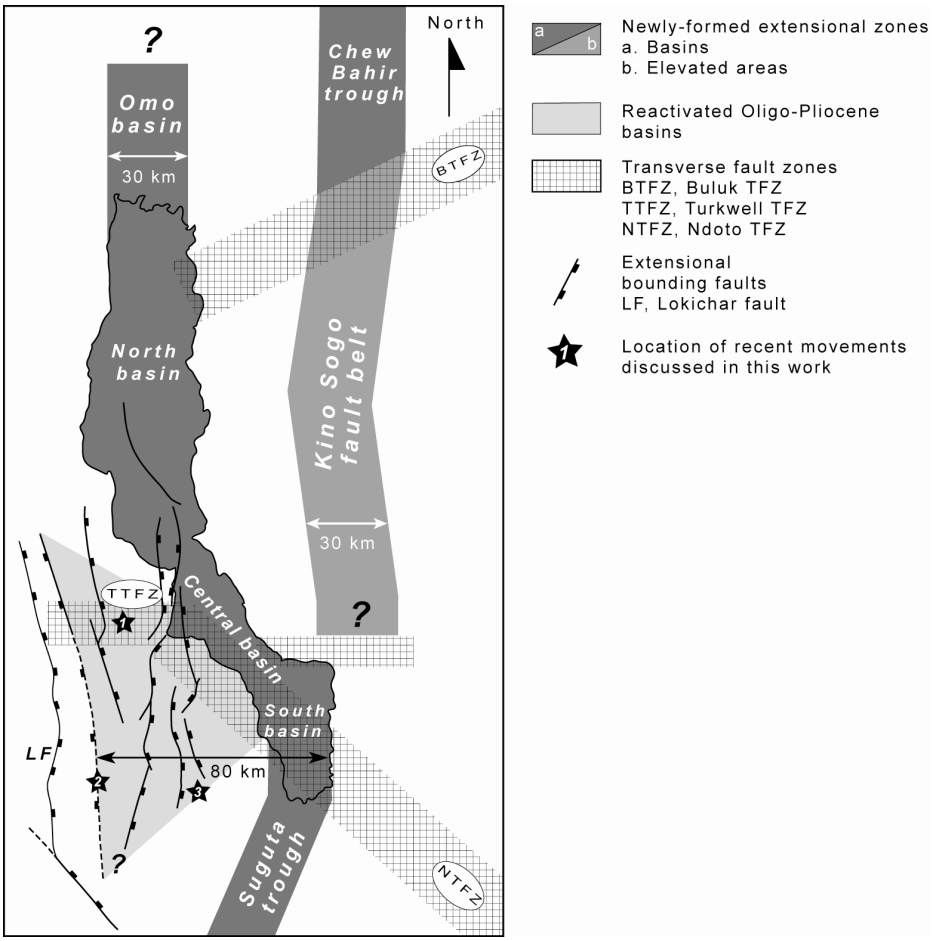

Figure 12. *Structural sketch map showing the location of recent deformation (< 5 Ma) within the Turkana rifted zone. Note 1) the two parallel narrow deformation zones of newly formed axes (Suguta, Lake Turkana basins, Kino Sogo, Chew Bahir) and 2) the 80 km-wide diffuse deformation zone to the SW, including reactivated Oligocene-Pliocene basins.*

ACKNOWLEDGEMENTS

This work is part of a co-operative program conducted between the National Oil Corporation of Kenya (NOCK) and the UMR 6538 “Domaines Océaniques”, Institut Universitaire Européen de la Mer, Plouzané, France. Financial support was provided by the 3D-3G Project supported by Elf Petroleum Norge AS (grant N° 2231-01 ELF), the ECLIPSE (Environnements et Climats du passé) Program of INSU-CNRS, as well as by grants from SUCRI-2E and UMR CNRS 6538 “Domaines Océaniques”. Research authorization was provided by the Ministry of Education, Science and Technology of the Republic of Kenya. The authors express their thanks to NOCK Managing Director for permission to publish this work, and to Dr. A. Maende, NOCK Exploration and Production Manager, for scientific, administrative and logistic support. We also thank J-J. Tiercelin

for providing the remote sensing data, as well as B. Collet for his contribution in elaborating digital elevation models. Special thanks are due to H. Roche and the French-Kenyan archaeological team for their hospitality in the field. This publication is IUEM contribution No. 907. This is publication No. 153 of the International Decade of East African Lakes (IDEAL) programme. The authors would like to thank the reviewers M. Leeder, P. A. Cowie and M. Strecker for their helpful and constructive comments.

6. SYNTHESE GENERALE ET CONCLUSIONS

Ce travail de recherche aborde les problèmes de mise en place d'un segment du Rift Est Africain (REA), en étroite relation avec l'héritage structural, d'une part (couloirs de socle faillés, système rifté oblique antérieur crétacé,…), et la présence de domaines magmatiques, d'autre part. L'exemple choisi est celui de la portion de rift Turkana (Nord Kenya) dont les premiers épanchements de laves ainsi que les bassins syn-rifts les plus anciens débutent à l'Eocène (~45 Ma.), pour se poursuivre jusqu'à l'Actuel.
Les principaux acquis de ce travail, basés pour l'essentiel sur l'interprétation d'images satellites Landsat ETM+, de modèles numériques de terrain (SRTM) et de profils de sismiques réflexion, précisent les modes de nucléation et de propagation de l'extension et apportent de nouvelles contraintes pour les modèles de formation et d'évolution des bassins syn-rifts en contexte magmatique.

6.1. Méthodologie

Différentes approches méthodologiques ont été appliquées avec succès au rift Turkana au cours de ce travail et permettent d'étudier en détail les 45 Ma. d'histoire du rifting et plus particulièrement les déformations récentes/actives (<5 Ma.).

- La combinaison de l'interprétation de l'imagerie satellitale avec les modèles numériques de terrain, nous a permis d'identifier les différents ensembles lithologiques en présence (socle précambrien, grès crétacés, laves éocènes-quaternaires et sédiments récents) et de cartographier le champ de fracturation, en considérant l'âge relatif des déformations.

- Des conditions d'affleurement exceptionnelles du réseau de failles en lanières du Kino Sogo, sur le flanc est du lac Turkana, ont autorisé une étude géométrique et statistique de la fracturation ainsi qu'une quantification de l'extension.

- L'analyse détaillée du réseau de drainage, extrait des images satellites a servi de révélateur pour des mouvements verticaux d'amplitude modeste le long de structures faillées de dimensions inférieures à la résolution des méthodes mises en œuvre.

L'approche méthodologique proposée dans ce travail peut être facilement transposée à l'étude d'autres secteurs similaires où la topographie est peu marquée en réponse à un taux d'extension faible, distribué au travers d'une zone déformée de grande dimension.

6.2. Modalités de l'extension associées au rifting cénozoïque Turkana

6.2.1. Nucléation et propagation de la déformation

Concernant la dynamique du rift Turkana *sensu stricto* depuis l'Eocène, nous retiendrons les principaux résultats suivants :

- L'identification de deux couloirs transverses faillés intra-socle, d'échelle régionale, de direction N140°E (N'Doto-Karisia; NKFZ) et N50°E (Kataboi, Buluk; KBFZ). La NKFZ (100x600 km), de dimensions comparables à celles du linéament d'Assoua (Coussement, 1995), n'avait jamais été identifiée par les études antérieures. Une troisième zone transverse discontinue, orientée EW (Turkwell-Mount Porr ; TMFZ) et d'échelle plus réduite (20x100 km), est également mise en évidence. Le rôle fondamental tenu par les deux zones transverses de premier ordre (NKFZ, BKFZ) sur la nucléation et la propagation des bassins du rift Turkana ainsi que sur la localisation des zones magmatiques est clairement démontré par la reconstitution de l'évolution du segment de rift Turkana à cinq stades du processus de rifting (45-23 Ma. ; 23-15 Ma. ; 15-6 Ma. ; 6-2.6 Ma. et 2.6 Ma.-Actuel). Les cartes tectono-magmatiques 'restaurées' correspondantes montrent que :

1) les bassins syn-rifts s'initient et se propagent à l'intérieur du couloir transverse NKFZ N140°E, à la faveur des relations angulaires optimales à l'ouverture entre les structures N140°E et les failles NS (angle obtus). Ces observations sont en accord avec le modèle de propagation proposé par Lezzar et al. (2002) pour les bassins du lac Tanganyika (branche ouest du REA).

2) à l'inverse, la propagation des failles NS est soit, bloquée lors de leur interaction avec les structures N50°E (angle aigu), soit transférée en latérale, ce qui a contribué à élargir considérablement la zone riftée du Turkana et à distribuer la déformation dans une zone d'environ 200x200 km comportant 3 'branches' de rift diachrones (Lac Turkana, Kino Sogo, Ririba).

2) l'allure losangique des bassins (N140°-NS) et leur dimension finale (~30x100 km) sont directement imposées par la géométrie de la fracturation interne à la zone transverse NKFZ et notamment par les relations angulaires entre les différentes familles de failles qui s'intersectent mutuellement.

3) la segmentation du rift Turkana en cellules d'allure triangulaire directement fonction de la structure des couloirs NKFZ et KBFF.

- La mise en place de domaines volcaniques et leur migration latérale (vers l'E et le S) à des stades successifs du rifting permet de discuter la nature des relations entre magmatisme et déformation. Après la disparition des dômes thermiques (70-200 km de diamètre) liés à l'activité volcanique, le rôle déterminant des structures syn-magmatiques (fentes d'extrados au toit des dômes, failles) sur la propagation des bassins à travers les paléo-dômes est

démontré à deux reprises : 1) dans la zone centrale du Turkana (domaine Lothidok-Kino Sogo) pour la période miocène et 2) plus à l'E au niveau du Kino Sogo au Pliocène.

- A grande échelle, ce travail suggère l'absence de bassins crétacés sous le rift Turkana au-delà de la faille de Hoi, qui limite à l'est le domaine du Kino Sogo, sur le flanc oriental du lac Turkana. Les arguments en faveur de cette hypothèse sont : 1) l'initiation et la propagation du rift cénozoïque dans une zone épargnée par le rifting crétacé et localisée entre les extrémités déconnectées des bassins d'Anza et du Soudan, 2) le mode de croissance et la géométrie du réseau de failles du Kino Sogo qui implique une faible épaisseur de laves éocènes-pliocènes surmontant directement le socle précambrien et incompatible avec la présence d'un bassin profond crétacé sous-jacent et 3) l'absence de structures N140°E dans le prolongement direct d'Anza au NW où des structures N50°E (type KBFZ), fortement obliques à la direction du bassin crétacé sont par contre prédominantes.

- L'origine de la dépression transverse du Turkana, ainsi que son caractère déprimé tout au long du processus de rifting, sont également expliqués par l'interaction des processus lithosphériques associés à la migration de la plaque Afrique (1000 km vers le NE en 50 Ma.) au dessus de deux panaches mantelliques cénozoïques. L'absence de soulèvement topographique associé lors du passage de la zone du Turkana à la verticale d'un panache vers 35 Ma. suggère deux hypothèses : 1) la migration latérale du matériel mantellique sous la lithosphère pré-étirée au crétacé (Anza-Soudan) annule les effets du soulèvement thermique, selon le modèle de 'thin-spot' de Thompson & Gibson (1991) ou 2) le 'durcissement' mécanique de la lithosphère, lié au refroidissement du matériel mantellique sous-plaqué au Crétacé qui empêche le bombement à grande longueur d'onde de cette dernière sous l'effet du panache.

6.2.2. Evolution néotectonique (<5 Ma.)

Après avoir déterminé le mode de mise en place du rift Turkana depuis l'Eocène, nous nous sommes attachés à caractériser l'origine et la cinématique des déformations récentes/actives (<5 Ma.) visibles en surface et dans les bassins syn-rifts imagés par sismique. A propos des processus tectoniques récents, nous retiendrons :

- Le rôle déterminant joué par la zone transverse NKFZ sur la cinématique récente du rifting et plus particulièrement lors de la formation d'inversions tectoniques positives, localisées à la verticale de la NKFZ. Un modèle cinématique en trois temps est proposé, impliquant des variations importantes du champ de contrainte: 1) avant 5 Ma., le régime est purement extensif ($\sigma 3$ horizontal orienté N90° et $\sigma 1$ vertical), 2) entre 5 et 3.7 Ma., une rotation horaire de $\sigma 3$ (~20°) induit la réactivation en dextre de la NKFZ et la formation d'un réseau de failles intra-bassins orientées N20°E à la verticale de la NKFZ et 3) après 3.7 Ma.,

une rotation horaire de σ3 (~20°), associée à une permutation σ1/σ2, qui entraînent la réactivation inverse des failles N20°E dans des zones compressives le long de la NKFZ. La formation d'antiformes en surface, en réponse à cette phase d'inversion récente, est confirmée par l'anomalie de drainage circulaire de Kalabata qui souligne l'inversion d'un dépocentre au pied de la faille de Kerio.

- La réactivation au Plio-Pléistocène de la faille bordière Ouest Napedet, d'âge oligo-miocène, entraîne le blocage d'un réseau dense de rivières secondaires le long de cette discontinuité et démontre ainsi l'existence de mouvements récents/actifs (<5 Ma.) dans les bassins syn-rifts du secteur ouest du rift Turkana.

- Sur le flanc est du lac Turkana, le réseau de failles du Kino Sogo (150x40 km), d'âge <3 Ma., recoupe une faible épaisseur de laves mio-pliocènes déposées au toit d'un bloc asymétrique de socle précambrien, bordé par des structures N140°E (type NKFZ), N50°E (KBFZ) et NS. L'étude géométrique et statistique de ce système de horsts et grabens nous permet : 1) de quantifier l'extension (<1%) ainsi que le taux de déformation qui est de l'ordre de ~0.1 mm/an soit 10^{-16} s^{-1}, 2) d'établir la corrélation à une loi mathématique, de type exponentielle, à propos de la longueur des failles et des segments de faille, en opposition avec les modèles classiques qui privilégient des lois de puissance (e.g. Nicol et al., 1996) et 3) de démontrer le caractère sous-déplacé de l'ensemble du réseau de faille avec un rapport rejet/longueur (≤ 100 m /9-40 km) inférieur à ceux décrits sur des réseaux de failles similaires (e.g. Schlische et al., 1996 ; Gloaguen, 2000). Ce caractère mature mais sous-déplacé des failles nous amène à proposer un modèle de croissance de failles dominé par la réactivation de structures pré-existantes intra-socles (foliation/failles) où initiées à un stade magmatique antérieur (fentes d'extrados, failles) au toit d'un paléo-dôme volcanique.

L'étude du rift Turkana apporte d'une façon plus générale, des éléments de réponse sur la mise en place de la branche orientale du REA (Fig. 1), qui semble s'ouvrir, non pas du nord vers le sud comme cela est souvent suggéré (Baker et al., 1972 ; Dunkley et al., 1993), mais à partir de cellules extensives isolées (oligo-miocènes), localisées dans un premier temps au niveau de zones transverses majeures (NKFZ pour le rift Turkana ; Assoua pour le rift Kenyan sud) et qui s'inter-connectent à un stade plus jeune du processus (plio-pléistocène) pour former une vallée axiale (Suguta). Les conclusions des modèles cinématiques ont également des implications importantes sur les variations du champ de contraintes durant les 5 derniers Ma. au niveau du Turkana et pourraient expliquer certaines structures encore mal comprises dans d'autres secteurs du REA.

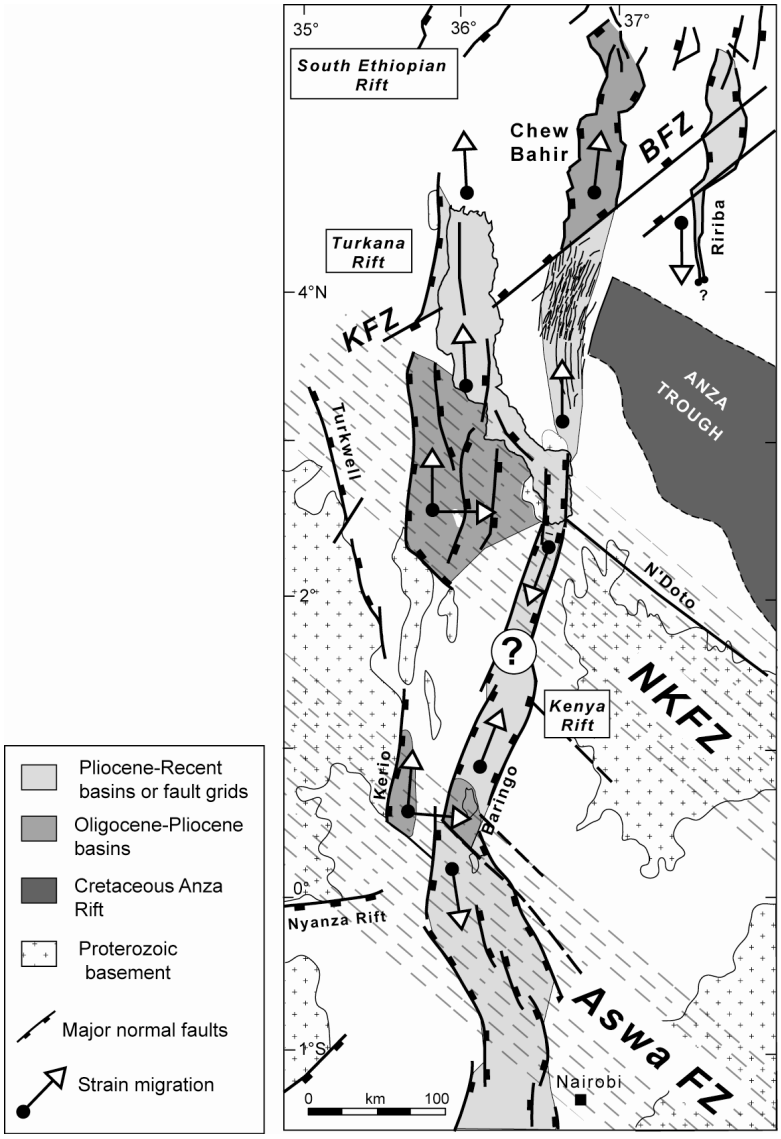

Figure 1. *General structural map of the Turkana rift and the adjoining Ethiopian and Kenyan rifts. Turkana rift basins initiated within the NKFZ during Oligo-Pliocene times while contemporaneous Kerio and Baringo basins occur further South along the Aswa fault zone. Note the quite similar dimensions and orientations of NKFZ and Aswa zones (~100 km-wide). Kenyan rift is deviated from N10°E to N160°E-trending along the Aswa zones and forms a triple junction with the poorly-known Nyanza rift whereas only the central Lake Turkana basin is trending at N140°E with regards to the NS Turkana rift basins.*

6.3. Implications pétrolières

La NOCK (National Oil Corporation of Kenya), ainsi que les compagnies pétrolières Amoco et Shell se sont largement impliquées dans deux projets de recherche d'hydrocarbure dans le secteur rifté du Turkana, en relation avec 1) la présence éventuelle de réservoirs pétroliers dans les dépôts gréseux du bassin crétacé d'Anza, comparables aux réserves déjà découvertes dans les bassins crétacés du Soudan au NW (Bosworth, 1992) et 2) l'existence de réservoirs

dans les différents bassins syn-rifts oligo-pliocènes du rift Turkana, dans lesquels des indices d'huile ont été identifiés par forage dans des roches mères d'origine lacustre et riches en matière organique (black-shales; TOC ~8%) (Morley et al., 1992). Concernant ces deux axes de recherche industriels, les résultats de notre étude démontrent que :

- L'absence de prolongation du bassin crétacé d'Anza vers le NW au-delà du domaine du Kino Sogo restreint largement les potentiels de réservoirs d'huile d'origine crétacée sous la zone du Turkana. De plus, l'absence de connexion entre les bassins d'Anza et du Soudan implique des histoires sédimentaires et une maturation des roches mères et/ou des roches réservoirs (diagénèse) propres à chaque bassin qui ne permettent pas de transposer les paramètres du Soudan à la zone d'Anza.

- La présence d'inversions tectoniques positives au sein des bassins syn-rifts oligo-miocènes est susceptible d'avoir agit sur les réservoirs d'huile potentiels selon deux modes : 1) la formation d'anticlinaux en réponse à la phase compressive récentes (<3.7 Ma.) peut avoir générer des remaniements des réservoirs (migration dans les niveaux hauts le long des failles) et créer des pièges sous les antiformes favorables au piégeage d'hydrocarbures et/ou 2) la formation d'un réseau dense de failles et leur jeu inverse peut avoir entraîner des ruptures de réservoir et la diffusion des ressources.

D'une façon plus générale, notre travail procure une vision cinématique et géométrique complète d'un système de bassins syn-rifts fluvio-lacustres à potentiel pétrolier (Anza et Turkana). La géométrie initiale des dépocentres ainsi que leur mode de développement par rapport à l'héritage structural et au magmatisme sont relativement bien contraints et peuvent être aisément transposés à l'étude de bassins pétroliers analogues.

6.4. Implications sur la dynamique de l'extension continentale

Les résultats de ce travail de thèse apportent à diverses échelles de nouvelles contraintes sur la dynamique générale de l'extension continentale en contexte magmatique, à savoir :

- Les relations entre un panache et une lithosphère pré-étirée induisent l'absence de soulèvement thermique et la persistance d'une dépression topographique en surface calquée sur la trace de la zone étirée.

- Les relations entre deux structures riftées obliques d'âge différent (Anza N140°E Crétacé et Turkana NS Cénozoïque) sont abordées et démontrent qu'un rift néoformé s'initie et se développe au-delà des limites de l'ancien domaine rifté, en accord avec le modèle thermo-mécanique de Negredo et al. (1995).

L'étude du rift Turkana aboutit également à la mise en évidence de plusieurs modèles concernant principalement :

1) le rôle déterminant tenu par les couloirs transverses faillés pré-existants sur le contrôle de la nucléation et la géométrie finale des bassins syn-rifts, ainsi que les complications tectoniques entraînées par les variations récentes (<5 Ma.) du champ de contrainte, permettent de mieux comprendre les relations entre l'héritage, l'extension et les bassins syn-rifts.

2) les relations entre magmatisme et déformation démontrent que la propagation en latérale des bassins est favorisée par la réactivation des structures internes de dômes magmatiques après cessation de l'activité volcanique. Ce mécanisme va à l'encontre du modèle proposé par Callot et. (2001, 2002) qui stipule que la déformation se concentre d'abord dans les domaines magmatiques avant de migrer en latéral.

3) le modèle atypique de croissance des failles proposé pour le domaine magmatique du Kino Sogo entre en contradiction avec les modèles classiques de propagation de failles (e.g. Schlische et al., 1996). Notre modèle alternatif, en accord avec celui proposé par Walsh et al. (2002), apporte de nouvelles contraintes sur la nucléation, le mode de croissance des failles, les taux d'extension et de déformation présentés par de tels systèmes de failles en contexte extensif.

7. PERSPECTIVES DE RECHERCHE

Dans la continuité directe de ce travail de thèse, deux thématiques de recherche nous paraissent intéressantes à développer. Elles concernent :

- La notion d'héritage structural, qui sera discutée, par le biais de modélisations analogiques, à propos de l'influence de discontinuités transverses sur la nucléation de la déformation et le développement des bassins syn-rifts.
- La quantification des processus d'érosion intervenant au niveau des escarpements et des blocs soulevés associés aux principales failles du rift.

La première thématique, partiellement traitée au chapitre 2, se focalisera sur les conditions mécaniques et cinématiques des expérimentations envisagées. Par contre, l'accent sera mis sur le second axe de recherche qui traite d'un problème peu ou pas évoqué dans le présent manuscrit.

7.1. Modélisation analogique

Cette approche sera abordée au laboratoire de modélisation analogique de l'université de Rennes en collaboration avec Olivier Dauteuil. Bien que les structures extensives étudiées dans ce travail se développent en contexte magmatique, c'est à dire aux dépens d'une croûte thermiquement modifiée, l'influence du paramètre thermique sur la nucléation de la déformation ne sera pas prise en compte.

7.1.1. Originalité de l'approche

La plupart des modèles analogiques appliqués jusqu'à présent aux dispositifs extensifs, afin de caractériser l'influence de discontinuités transverses pré-existantes, ne considèrent que des structures, soit de dimensions 1D et alors localisées à la limite des deux plaques mobiles (e.g. Withjack et Jamison, 1986 ; Tron & Brun, 1991 ; McClay & White, 1995 ; Morley, 199d ; Mart et Dauteuil, 2000 ; Dubois et al., 2002), soit de dimension 2D et matérialisées dans ce cas par une bande de latex en position horizontale entre les deux plaques (Clifton et Schlische, 2001).
Les perturbations structurales identifiées dans le rift Turkana correspondent à des structures à 3 dimensions et à comportement mécanique contrasté, qu'il s'agisse du couloir de failles transverses recoupant sur une largeur d'environ 100 km la zone d'étude ou de la croûte amincie associée au rift crétacé d'Anza. La modélisation de ces structures héritées nécessite d'introduire dans le modèle des discontinuités rhéologiques 3D selon la procédure décrite dans le paragraphe suivant.

7.1.2. Dimensionnement, contraintes géométriques et cinématiques

Compte tenu de la géométrie initiale du dispositif anté-rift (Fig. 1a), deux types de discontinuités transverses seront prises en compte dans les modèles expérimentaux, à savoir :

- Le couloir faillé N140°E de la NKFZ, oblique par rapport à l'extension cénozoïque ($\sigma 3$ horizontale et comprise entre N90°E à N130°E). Cette discontinuité de premier ordre, considérée comme verticale, présente en surface une largeur d'environ 100 km, c.a.d. environ la longueur totale d'un bassin syn-rift de type Lokichar. Cette zone comprend elle-même 3 discontinuités majeures, régulièrement espacées (~30 km), orientées parallèlement à la direction générale de la NKFZ. A une échelle inférieure, la NKFZ présente également un réseau de fractures secondaire N140°E avec un espacement d'environ 2 à 5 km. D'un point de vue dimensionnement du modèle, le couloir de failles sera matérialisé par un parallélépipède de silicone (plus déformable), de 50 cm de large, et recoupant en oblique l'ensemble du modèle de 1x1 m (Fig. 1g1). Les failles de second-ordre à l'intérieur de la zone de faiblesse correspondront aux limites verticales entre deux ou trois bandes de silicones à rhéologies différentes (selon des critères de faisabilité qui restent à déterminer).
- Le système rifté d'Anza et du Soudan, considéré comme un domaine pré-étiré et peu déformable, sera assimilé à deux blocs rigides orientés parallèlement aux discontinuités précédentes (Figs. 1a et 1h).

La première expérience ne concerne que le couloir de failles N140°E, soumis à trois extensions successives, de directions variables et en contexte de rift oblique. L'interaction de ce couloir avec les blocs rigides type Anza est modélisée dans la seconde expérience, toujours selon une extension oblique.

Limitations des modèles

En plus du paramètre thermique évoqué précédemment, d'autres facteurs ne peuvent pas être actuellement intégrés dans les dispositifs expérimentaux pour des raisons techniques. Il s'agit de :

- La fabrique pénétrative intra-socle, constituée par la foliation régionale en position subverticale et orientée NS (Fig. 1a).
- La zone de fractures KBFZ qui recoupe la partie nord de la zone d'étude à l'azimut N50°E (Fig. 1a).

7.1.2.1. Expérience 1

Cette première expérience comportera une zone fragile, de direction N140°E, placée dans un milieu isotrope soumis à des variations progressives du champ de contraintes (Figs. 1g1 et g2). Cette configuration tentera de reproduire le comportement de la discontinuité transverse majeure NKFZ (~100 km de large) à l'échelle du Turkana (200x200 km) (Fig. 1a).

- Cet ensemble sera dans un premier temps soumis à une contrainte σ3, oblique de 50° par rapport à la discontinuité. Cette contrainte s'exercera jusqu'à atteindre le taux de déformation enregistré par les bassins oligo-pliocènes du Turkana (Fig. 1g1). Il s'agira de tester si 1) les structures initiales du rift se localisent préférentiellement dans la zone transverse (domaine fragilisé) (Fig. 1b), 2) la déformation migre au sein du couloir fragile et 3) si le comportement des structures néoformées évolue à l'approche des limites extérieures de la zone N140°E, en accord avec les modélisations proposées par Clifton & Schlische (2001) (Figs. 1b et 1c).
- Une rotation horaire de la contrainte extensive (~20°) sera ensuite appliquée au modèle (σ3 horizontal et σ1 vertical) afin de tester l'apparition d'une composante décrochante (dextre ?) le long des structures transverses, en réponse à la réduction de l'angle entre celles-ci et la direction d'extension (Fig. 1g2). Ceci a pour objectif de refléter le comportement de la NKFZ lors de la rotation récente (<5 Ma.) de l'extension (Fig. 1e).
- Au cours du dernier stade, le modèle sera soumis à une légère compression selon un axe subperpendiculaire (~20°) à la discontinuité, la direction d'extension correspondante ayant subit une rotation horaire de 20° (Fig. 1g2). Ce dernier dispositif expérimental devrait permettre d'estimer les conditions angulaires nécessaires à la réactivation inverse des failles normales (Fig. 1f).

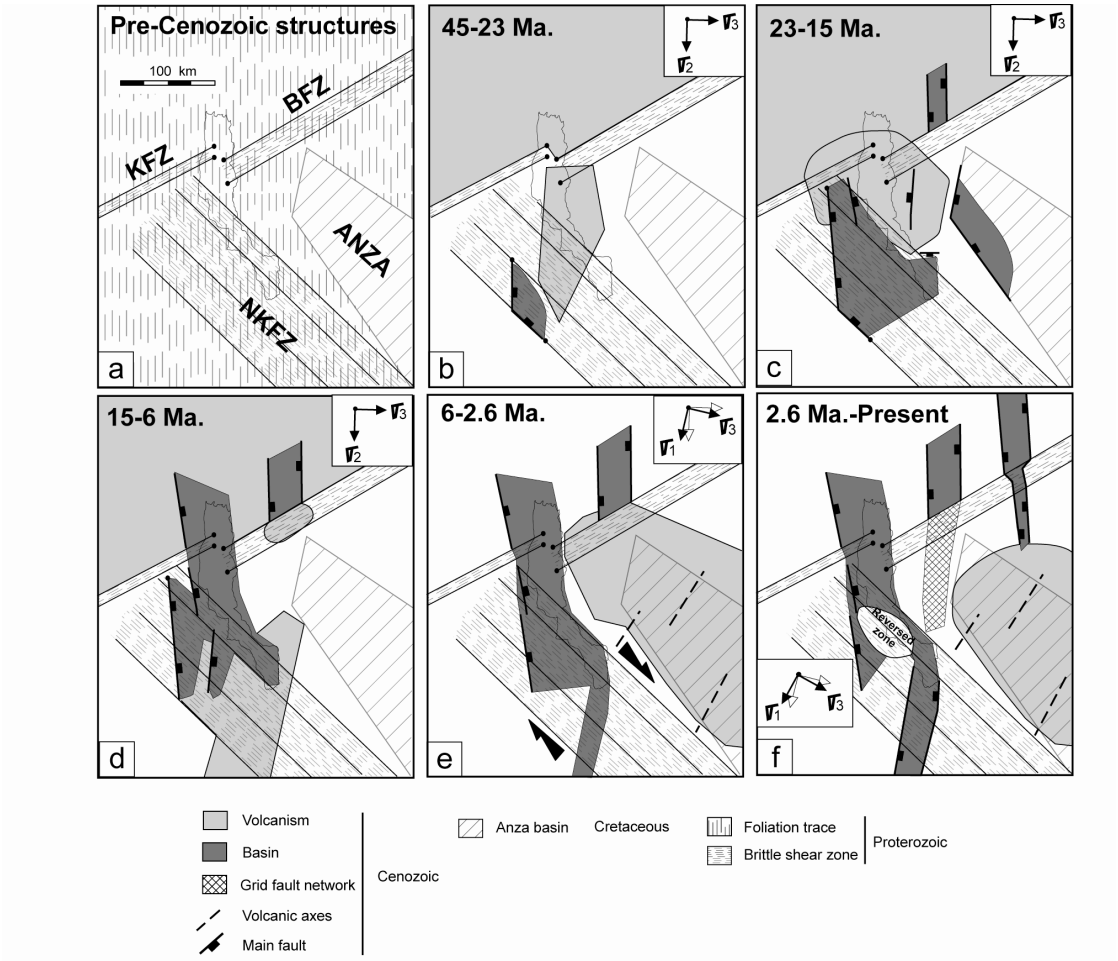

Analogue modelling experiences

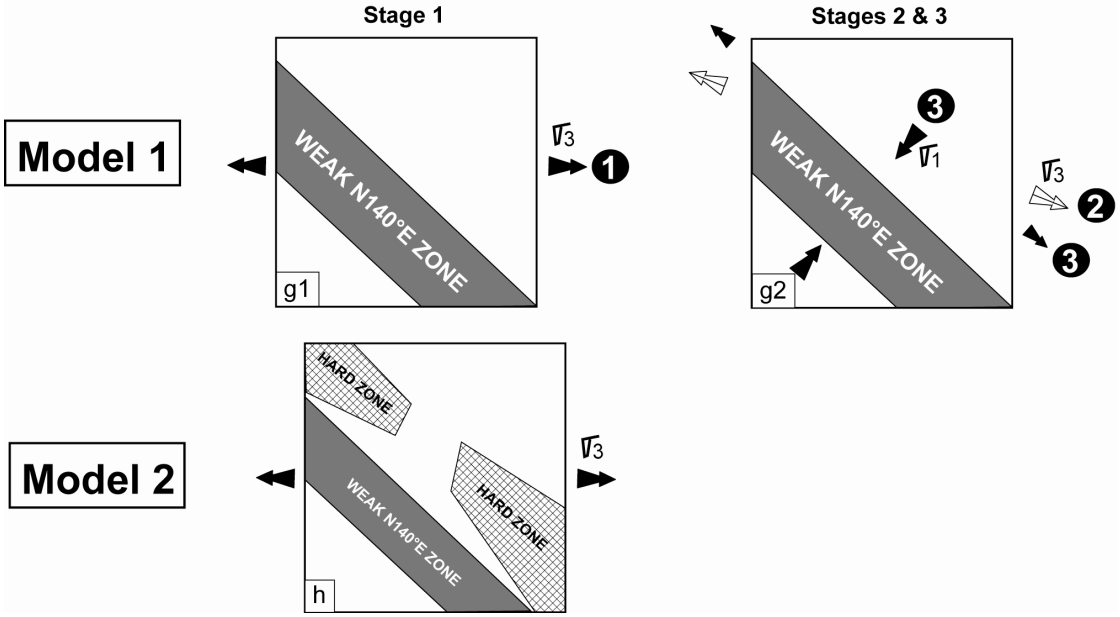

***Figure 1**. a-f) Schémas structuraux simplifiés de l'évolution du rift Turkana depuis 45 Ma. (g-h) Modèles analogiques envisagés pour tester 1) le comportement d'une zone pré-fracturée N140°E (g1-g2) soumise à des variations du champ de contraintes et 2) la localisation de la déformation dans un système comportant une zone transverse fragile et deux blocs rigides (lithosphère pré-étirée crétacée) (h).*

7.1.2.2. Expérience 2

Cette seconde expérience se propose de modéliser les mécanismes de la déformation à une échelle plus grande (facteur ~1.5) (Fig. 1h). Il s'agit de tenter de reproduire le comportement de la déformation entre les terminaisons des bassins crétacés Anza-Soudan et la zone N140°E NKFZ. Les zones pré-étirées crétacées sont considérées comme peu ou pas déformables lors du rifting cénozoïque (Fig. 1a-f). Le modèle comportera deux blocs rigides N140°E déconnectés, directement bordés au sud par la zone N140°E, et soumis à une extension oblique (50°) selon un taux de déformation identique à celui de la phase 1 de la première expérience (Fig. 1g1).
L'objectif est de confirmer les conclusions du chapitre 2 qui stipulent que la zone de nucléation de la déformation se situe dans l'axe de la zone 'inter-blocs'.

7.2. Evolution morphostructurale des escarpements de failles

L'étude morphostructurale des escarpements de failles, abordée en collaboration avec François Guillocheau et Stéphane Bonnet du laboratoire Géosciences Rennes, comportera deux approches complémentaires :

- La première approche sera consacrée à la quantification des phénomènes d'érosion responsables, au niveau de la zone d'étude, de l'abrasion totale d'escarpements, et des blocs soulevés associés, d'âge >5 Ma. (Lokichar, Kerio sur la figure 2)
- La seconde approche concernera l'évolution structurale d'un système extensif complet comprenant : le bloc soulevé, la faille normale et le bloc effondré, en relation avec des structures transverses. Les phénomènes de nucléation, propagation et segmentation des structures seront discutés par analogie avec ceux observés le long du système de failles Lapurr-Lothidok (d'âge 11 Ma.-Actuel).

7.2.1. Thématique 1 : bilan d'érosion et de transfert de matière

Les données sismiques disponibles sur la zone d'étude fournissent une image 3D des remplissages sédimentaires syn-rifts, qui sont par ailleurs calibrés par forages. Ceci permet de contraindre la chronologie et l'amplitude maximale des déplacements verticaux le long des failles bordières (Fig. 2).

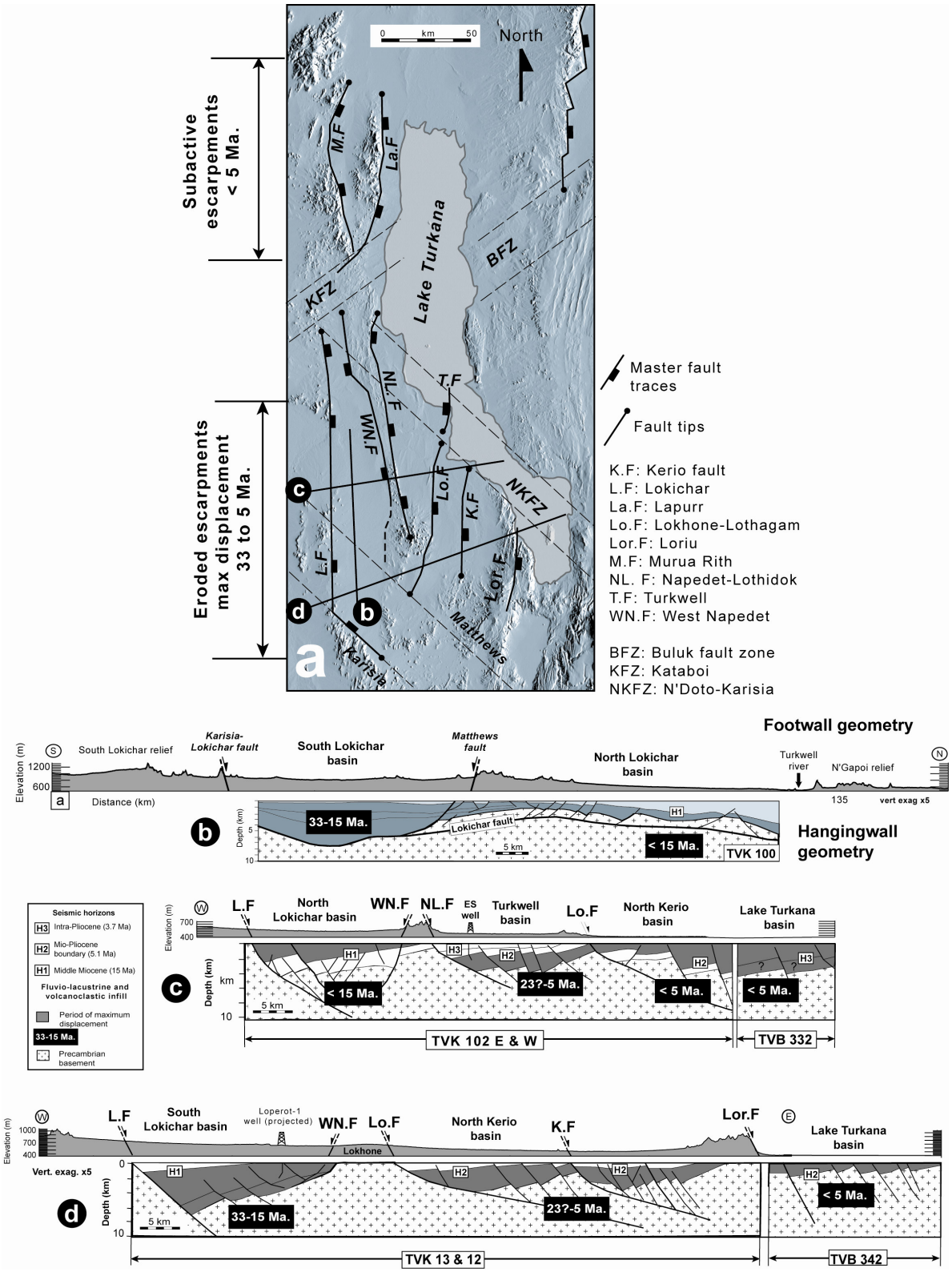

Figure 2. *Topographie des escarpements associés aux failles oligo-pliocènes. a) MNT général d'après les données SRTM. b-d) Coupes structurales EW et NS établies à travers les bassins syn-rifts à partir des données de sismique réflexion et SRTM.*

Dans le cas où le bloc soulevé associé est totalement ou partiellement érodé, son élévation initiale peut être estimée à partir de chartes existantes en fonction de l'espacement des blocs, de la géométrie des failles et de la quantité d'extension (Jackson & McKenzie, 1983 ; Barr, 1987 ; Bott, 1997) (Fig. 3). Sur la base de ces contraintes géométriques et chronologiques, nous proposons d'établir le bilan des matières érodées en tenant compte également des facteurs climatiques et lithologiques.

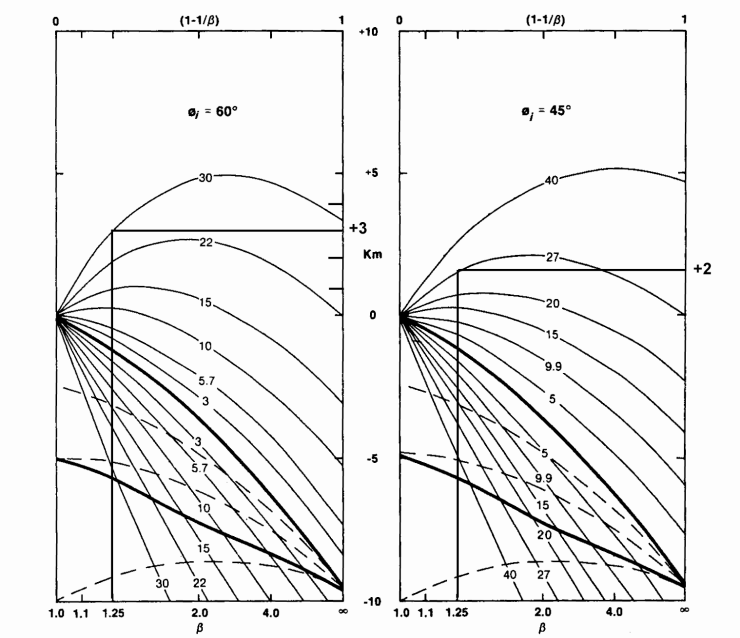

Figure 3. *Courbes illustrant le soulèvement et la subsidence d'un système de bloc basculés en 'domino' contrôlé par des failles normales de pendage 60° ou 45° (modifié d'après Barr, 1987). Les chiffres sur les courbes indiquent l'espacement entre deux failles. Les données de notre étude (~30 km d'espacement entre les failles et un β~1.25) implique un soulèvement compris entre 2000 et 3000 m.*

7.2.2. Thématique 2 : Evolution structurale d'un système couplé bloc soulevé-bloc effondré

Le système extensif de Lapurr-Lothidok bénéficie d'un jeu quasi-complet de données à la fois dans le bloc soulevé (imagerie satellite, topographie, datations K/Ar, observations de terrain) et dans le bloc effondré (données de surface et coupes sismiques) (Figs. 4, 5 et 6). Parmi les principales observations que nous pouvons faire à partie de ces données, nous retiendrons :

- La segmentation longitudinale du bloc effondré en trois sous-bassins de taille variable (<11 Ma), séparés par des zones hautes (Lapurr, Kataboi, Turkana).
- La variété de style structural de chacun des bassins marquée par l'approfondissement (>2000 m) des deux bassins latéraux.
- La migration (vers le sud) du dépocentre récent au sein du bassin nord (Lapurr).
- Le blocage des bassins le long d'accidents transverses (N50°E).

- La compartimentation du bloc soulevé en une succession de blocs séparés par des structures transverses (N140°E ou N50°E). La trace de ces discontinuités obliques se prolonge dans les séries plio-quaternaires au pied de l'escarpement et témoignent donc de leur activité récente.
- La décroissance rapide des reliefs entre 1) un bloc nord (Lapurr), élevé (~1200 m) et contenant les laves les plus anciennes (oligo-miocènes) et 2) un bloc sud (Lothidok-Kataboi), peu élevé (~600 m) et impliquant des laves plus récentes (mio-pliocènes).
- La rupture topographique intervient brutalement à l'approche de la zone transverse de Kataboi.

L'objectif de cette approche est de contraindre l'évolution de ces deux dispositifs segmentés (blocs inférieur et supérieur) et préciser si les mouvements interviennent de façon synchrone ou diachrone entre les différents blocs :

- les reliefs les plus hauts sont-ils associés aux bassins les plus profonds ?
- les blocs les plus segmentés sont-ils les plus érodés ?

La thématique 1 peut également être appliquée à propos du couplage soulèvement/érosion en parallèle avec le taux de subsidence du bloc effondré.

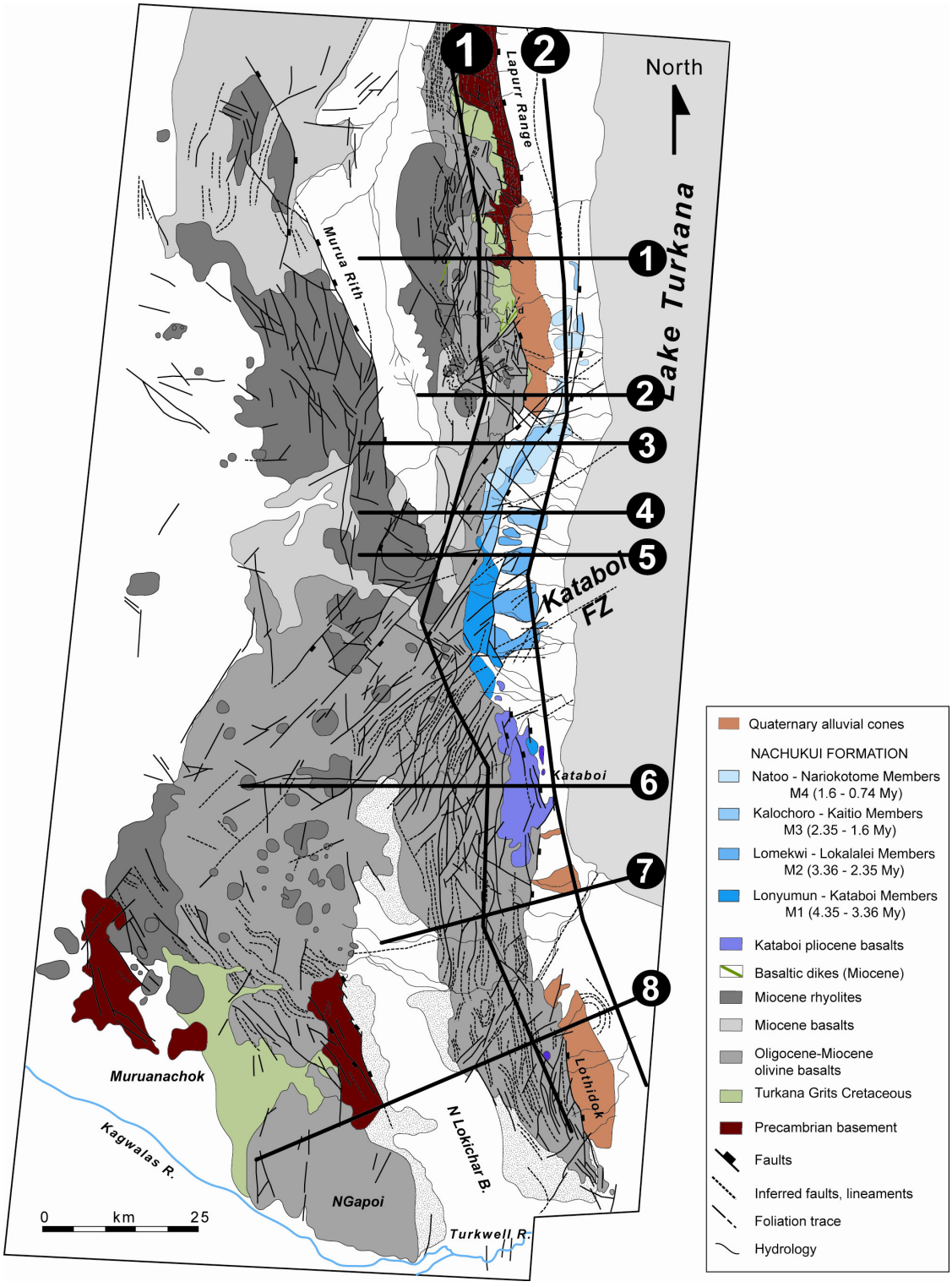

Figure 4. *Interprétation structurale de la zone de Lapurr-Lothidok d'après l'imagerie satellitale. Localisation des coupes structurales des figures 5 et 6.*

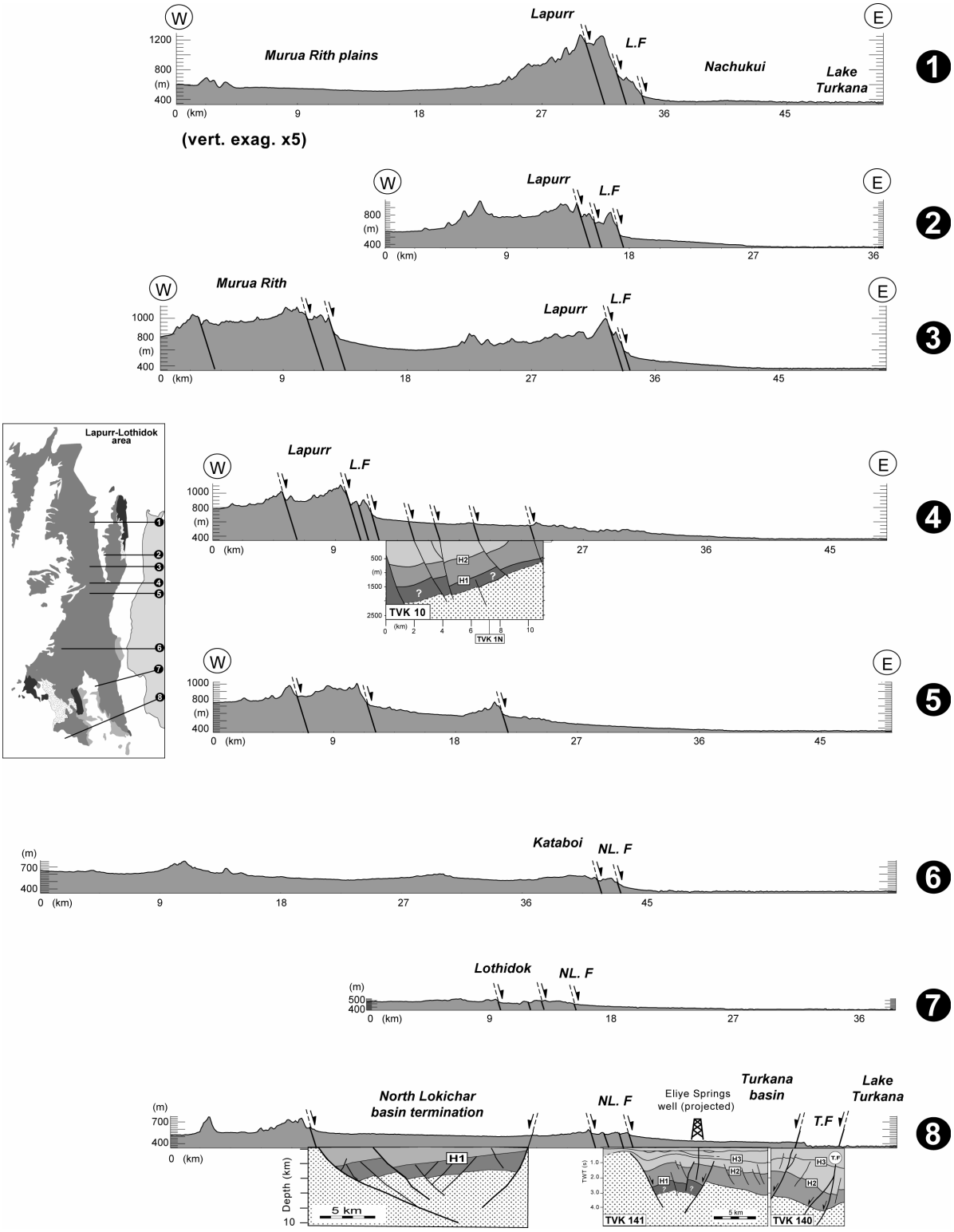

Figure 5. *Coupes structurales EW à travers l'escarpement de Lapurr-Lothidok. La géométrie profonde est illustrée par les lignes sismiques TVK 10, 3, 141.*

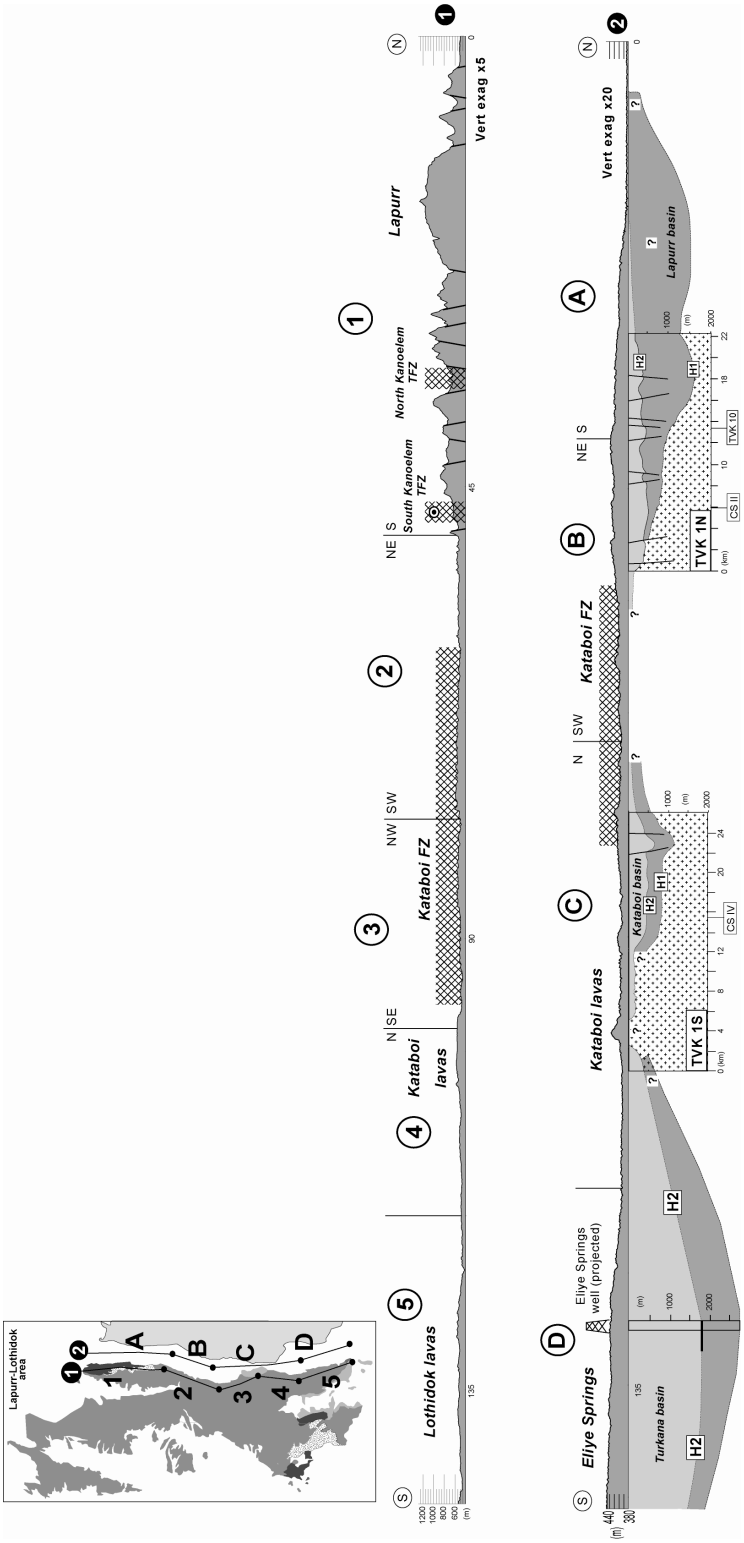

Figure 6. *Coupes structurales NS dans le bloc soulevé de Lapurr-Lothidok et dans le bloc effondré. La géométrie profonde est illustrée par la ligne sismique TVK 1.*

LISTE DES FIGURES

Introduction

1. Données et méthodes

2. Dynamic of continental extension in magmatic rifts. The study case of the Turkana Rift since the last 45 Ma. (Northern Kenya)

3. Inversion tectonics during continental rifting : The Turkana Cenozoic rifted zone, Northern Kenya

4. Geometry and growth of an inner rift fault pattern: the Kino Sogo Fault Belt, Turkana Rift (North Kenya)

5. Recent tectonics in the Turkana Rift (North Kenya) : an integrated approach from drainage network, satellite imagery and reflection seismic analysis.

6. Synthèse générale et conclusions

Figure 1. p 152. Carte structurale du Rift Kenyan montrant le mode de mise place du rift depuis l'Eocène.

7. Perspectives de recherche

Figure 1. 158. Schémas structuraux de l'évolution du rift Turkana depuis 45 Ma. et modèles analogiques envisagés pour modéliser le comportement d'une zone pré-faillée N140°E (g1-g2) soumise à des variations du champ de contrainte et (h) la localisation de la déformation dans un système pré-existant marqué par une zone transverse fragile et deux blocs rigides réprésentant la lithosphère pré-étirée crétacée.

Figure 2. p 160. Expression topographique actuelle des escarpements associés au jeu des failles syn-rift oligo-pliocènes. a) MNT général d'après les données SRTM. b-d) Coupes structurales EW et NS à travers les bassins syn-rift à partir des données de sismique réflexion et les données SRTM.

Figure 3. p 161. Courbes illustrant le soulèvement et la subsidence des blocs soulevés et effondrés dans un système en faille normale avec un pendage initial de 60° ou 45° (modifié d'après Barr, 1987).

Figure 4. p 163. Interprétation structurale de la zone de Lapurr-Lothidok d'après l'imagerie satellitale.

Figure 5. p 164. Coupes structurales EW à travers l'escarpement de Lapurr-Lothidok. La géométrie profonde est illustrée par les lignes sismiques TVK 10, 3, 141.

Figure 6. p 165. Coupes structurales NS dans le bloc soulevé de Lapurr-Lothidok et dans le bloc effondré. La géométrie profonde est illustrée par la ligne sismique TVK 1.

Annexes

Annexe 1. Tableaux récapitulatifs des mesures de stratification et de failles observées dans la zone ouest du lac Turkana (mission 2002)

Annexe 2. Echantillons et datations des laves oligo-pliocènes de la zone ouest Turkana (Mission 2002)

Tableau 1. Récapitulatif des échantillons de laves oligo-pliocènes récoltés au cours de la mission de 2002. Certains d'entre eux ont été datés par méthode K/Ar au laboratoire de Brest (resp : H. Bellon) (voir figure 1 pour localisation).

Figure 1. Carte de localisation des échantillons datés sur la zone de Lapurr-Lothidok.

Figure 2. Carte de localisation et tableau récapitulatif des échantillons datés le long de la gorge de Lapurr.

Figure 3. Log stratigraphique de la série volcanique de Lapurr.

Annexe 3. Echantillons et datations des paléoniveaux holocènes de la zone ouest du lac Turkana (Mission 2002)

Tableau 3. Récapitulatif des échantillons de paléoniveaux lacustres holocènes de la zone ouest du lac Turkana récoltés au cours de la mission de 2002. Certains d'entre eux ont été datés par méthode C^{14} au laboratoire de Gif sur Yvette, Paris (resp : J.F. Saliège)(voir figure 4 pour localisation).

Figure 4. a) Courbe de variations du niveau Holocene du lac Turkana (modifié d'après Butzer, 1980). b) Carte de localisation des échantillons de paléoniveaux lacustres datés (C14).

Tableau 4. Synthèse des datations et altitudes des sédiments lacustres et des formations littorales du lac Turkana pour la période Holocene (10 000 ans.–Actuel).

REFERENCES BIBLIOGRAPHIQUES

- A -

ACKERMAN, R. V. & SCHLISCHE, R. W. 1997. Anticlustering of small normal faults around larger faults. *Geology*, 25 (12), 1127-1130.

ARAMBOURG, C. 1943. Les Formations Pretertiaires de la bordure occidentale du Lac Rudolphe (Afrique Orientale). *Comptes Rendus de l'Académie des Sciences de Paris,* 197, 1663-1665.

ARTHAUD, F., CHOUKROUNE, P. & ROBINEAU, B. 1980.Tectonique, microtectonique et évolution structurale du golfe de Tadjoura et du Sud de la dépression Afar (Rép. De Djibouti). *Bull. Soc. Géol. France*, *XXII, 6,* 901-908.

- B -

BAKER, B. H., MOHR, P. A. & WILLIAMS, L. A. 1972. Geology of the Eastern Rift System of Africa. *The Geological Society of America*, Special paper 136.

BARR, D. 1987. Structural/stratigraphic models for extensional basins of half-graben type. *Journal of Structural Geology,* 9, 491-500.

BELLIENI, G. E., VICENTIN, J., ZANETTIN, B. & PICIRILLO, E. M. 1981. Oligocene transitional tholeiitic magmatism in northern Turkana (Kenya): comparison with coeval Ethiopian volcanism. *Bulletin Volcanologique,* 44, 411-427.

BONAVIA, F., CHOROWICZ, J. & COLLET, B. 1995. Have wet and dry Precambrian crust largely governed Cenozoic intraplate magmatism from Arabia to east Africa? *Geophysical Research Letters*, 22, 2337-2340.

BOSCHETTO, H. B., BROWN, F. H. & McDOUGALL, I. 1992. Stratigraphy of the Lothidok Range, northern Kenya, and K/Ar ages of its Miocene primates. *Journal of Human Evolution*, 22, 47-71.

BOSWORTH, W. 1992. Mesozoic and early Tertiary rift tectonics in East Africa. *Tectonophysics*, 209, 115-137.

BOSWORTH, W., STECKER, M. R. & BLISNIUK, P. M. 1992. Integration of East African paleostress and present-day stress data: implications for continental stress field dynamics. *Journal of Geophysical Research,* 97, B8, 11851-11865.

BOSWORTH, W. & MAURIN, A. 1993. Structure, geochronology and tectonic significance of the northern Suguta Valley (Gregory Rift), Kenya. *Journal of the Geological Society of London,* 150, 751-762.

BOSWORTH, W. & MORLEY, C.K. 1994. Structural and stratigraphic evolution of the Anza rift, Kenya, *Tectonophysics, 236,* 93-115.

BOSWORTH, W. & STRECKER, M.R. 1997. Stress field changes in the Afro-Arabian rift system during the Miocene to Recent period, *Tectonophysics, 278,* 47-62.

BOTT, M. H. P. & KUSZNIR, N. J. 1979. Stress distribution associated with compensated plateau uplift structures with applications to the continental splitting mechanism. *Geophys. J. R. Astron. Soc,* 56, 451-459.

BOTT, M. H. P. 1997. Modelling the deformation of half-graben using realistic upper crustal rheology, *Journal of Geophysical Research*, 102, G11, 24605-24617.

BOULET, S. 2003. Stratigraphie sismique et séquentielle de dépots fluvio-lacustres en contexte de rift. Application au bassin oligo-miocène de Lokichar, région du lac Turkana, Rift Est-Africain, *DEA Rapport, Univ. Brest,* 47 p.

BREKKE, H. & RIIS, F. 1987.Tectonics and basin evolution of the Norwegian shelf between 62°N and 72°N, *Norsk Geologisk Tisskrift, 67,* 295-322.

BRUN, J. P. & NALPAS, T. 1996. Graben inversion in nature and experiments, *Tectonics, 15,* 23, 677-687.

BUCK, W.R. 1991. Modes of continental lithospheric extension. *Journal of Geophysical Research*. 96, 20161-20178.

BUTZER, K. W. ISAAC, G. L., RICHARDSON, J. L. & WASHBOURN-KAMAU, C. 1972. Radiocarbon dating of east African lake levels. *Science,* 175, 1069-1076.

BUTZER, K. W. 1980. The Holocene lake plain of North Rudolph, East Africa. *Physical Geography*, 1, 42-58.

- C -

CALLOT, J. P. GRIGNE, C., GEOFFROY, L. & BRUN, J. P. 2001. Development of volcanic margins: two-dimensional laboratory models. *Tectonics*, 20, 148-159.

CALLOT, J. P., GEOFFROY, L. & BRUN, J. P. 2002. Development of volcanic margins: three-dimensional laboratory models. *Tectonics*, 21 (6), 1052 (doi: 10.1029/2001TC901019).

CARDON, H. 1999. Mécanisme de propagation des réseaux de failles : l'exemple du Rift Gregory (Kenya). *Unpublished PhD thesis, Univ. Claude Bernard Lyon,* 200 p.

CARTWRIGHT, J.A., MANSFIELD, C. & TRUGGILL, B. 1995. The growth of faults by segment linkage : evidence from the Canyonlands grabens of S. E. Utah. *Journal of Structural Geology* 17, 1319-1326.

CASANOVA, J. 1986. Les stromatolites continentaux: Paleoecologie, paleohydrologie, paleoclimatologie. Application au rift Gregory. *Thesis, University Aix-Marseille,* 200 p.

CASTAING, C., BOURGINE, B., CHILES, J. P., GENTER, A., OUILLON, G. & SORNETTE, D. 1995. Multiscale organization of joints and faults revealed by geostatistical, multifractal and wavelet techniques, *In :* Terra Abstract, EUG8, p. 186, Strasbourg (France).

CHAPMAN, G. R., LIPPARD, S. & MARTIN, J. E. 1978. The stratigraphy and structure of the Kamasia range, Kenya rift valley. *Journal of the Geological Society of London*, 135, 265-281.

CHARSLEY, T. J. 1987. Geology of North Horr area. Ministry of environment and natural resources, Mines and geology department, Republic of Kenya, 40 p.

CHILDS, C., WALSH, J. J. & WATTERSON, J. 1990. A method for estimation of the density of fault displacements below the limit of seismic resolution in reservoir formations. In *: North Sea Oil and Gas Reservoir II* (edited by Buller, A. T. *et al.*). The Norwegian Institute of Technology, Graham and Trotman, London, 309-318.

CHOROWICZ, J. & MUKONKI, M. B. 1980. Linéaments anciens, zones transformantes récentes et géotectoniques des fossés dans l'Est Africain, d'après la télédétection et la microtectonique : Museum Royal Africa Central, Tervuren, Belgium. Department of Geology and Mineralogy Annual Report, 143-146.

CLADOUHOS, T. T. & MARRETT, R. 1996. Are fault growth and linkage consistent with power-law distributions of fault lengths? *Journal of Structural Geoloy* 18, 281-293.

CLIFTON, A. & SCHLISCHE, R. W. 2001. Nucleation, growth, and linkage of faults in oblique rift zones: Result from experimental clay models and implications for maximum fault size. *Geology,* 29, 5, 455-458.

COLLET, B., PARROT, J. F. & TAUD, H. 2000. Orientation of absolute African plate motion revealed by tomomorphometric analysis of the Ethiopian dome. *Geology*, 28, 12, 1147-1149.

COLLIER, R. E. L. & GAWTHORPE, R. L. 1995. Neotectonics, drainage and sedimentation in Central Greece: insights into coastal reservoir geometries in syn-rift sequences. From Lambiase, J. J. (eds.), *Hydrocarbon Habitat in Rift Basins, Geol. Soc. Spec. Publication*, 80, 165-181.

CORDELL, L. 1978. Regional geophysical setting of the Rio Grande Rift. *Geological Society of America Bulletin,* 89, 1073-1090.

CORTI, G., BONINI, M., CONTICELLI, S., INNOCENTI, F., MANETTI, P. & SOKOUTIS, D. 2003. Analogue modelling of continentale extension: a review focused on the relations between the patterns of deformation and the presence of magma. *Earth-Science Reviews*, 63, 169-247.

COUSSEMENT, C. 1995. Structures transverses et extension intracontinentale. Le rôle des zones de failles d'Assoua et Tanganyika-Rukwa-Malawi dans la cinématique néogène du système de Rift Est-Africain. *PhD Thesis, Université de Bretagne Occidentale, Brest*, 222 p.

COWARD, M.P. 1996. Balancing sections through inverted basins, from Buchanan, P.G. and Nieuwland, D.A. (eds), Modern development in structural interpretation, validation and modelling, *Geological Society special publication, 99,* 51-77.

COWIE, P. A. & SCHOLZ, C. H. 1992. Displacement-length scaling relationship for faults: data synthesis and discussion. *Journal of Structural Geology,* 14 (10), 1149-1156.

COWIE, P. A., SORNETTE, D. & VANNESTE, C. 1995. Multifractal scaling properties of a growing fault population. *Geophysical Journal International,* 122, 457-469.

CUREWITZ, D. & KARSON, J.A. 1998.Geological consequences of dike intrusion at mid-ocean ridge spreading centers, in Faulting and magmatism at mid-ocean ridges, edited by Buck, W.R., P.T. Dealney, and J.A. Karson, *American Geophysical Union, 106,* 117-136.

- D -

DALY, M. C., CHOROWICZ, J. & FAIRHEAD, J. D. 1989. Rift basin evolution in Africa: the influence of reactived steep basement shear zones. From Cooper, M. A. & Williams, G. D. (eds.), Inversions tectonics, *Geological Society Special Publications,* n°44, 309-334.

DAVY, P. 1993. On the frequency-length distribution of the San Andreas fault system. *Journal of Geophysical Research,* 98, B7, 12141-12151.

DAWERS, N. H., ANDERS, M. H. & SCHOLZ, C. H. 1993. Fault length and displacement: scaling laws. *Geology,* 21, 1107-1110.

DE CHABALIER, J. B. & AVOUAC, J. P. 1994. Kinematics of the Asal Rift (Djibouti) determined from the deformation of Fieale volcano. *Science,* 265, 1677-1681.

DEFFONTAINES, B. 1990. Développement d'une méthode géomorphologique et morphostructurale; Analyse des surfaces enveloppes, du réseau hydrographique et des modèles numériques de terrain; Applications au Nord-Est de la France. *PhD Thesis, University Paris VI,* 230 p.

DELVAUX, D., LEVI, K. KAJARA, R. & SAROTA, J. 1992. Cenozoic paleostress and kinematic evolution of the Rukwa-North Malawi rift valley (East African Rift System), *Bull. Centres Rech. Explo. ELF Aquitaine, 16,* 2, 383-40.

DEROIN, J. P. & DEFFONTAINES, B. 1995. Morphostructurale analysis for linking streamflow, lithology, and structure: comparison with remote sensing data on the Cévennes (French Massif Central). *Z. Geomorph.*, 1, 97-116.

DINDI, E. W. 1994. Crustal structure of the Anza graben from gravity and magnetic investigations. *Tectonophysics*, 236, 359-371.

DORE, A.G. & LUNDIN, E.R. 1996. Cenozoic compressional structures on the NE Atlantic margin: nature, origin and potential significance for hydrocarbon exploration*, Petroleum Geoscience, 2,* 299-311.

DORE, A.G., LUNDIN, E.R., FICHLER, C. & OLESEN, O. 1999. Patterns of basement structure and reactivation along the NE Atlantic margin, *Journal of the Geological Society of London, 154,* 85-92.

DUBOIS, A., ODONNE, F., MASSONAT, G., LEBOURG, T. & FABRE, R. 2002. Analogue modelling of fault reactivation : tectonic inversion and oblique remobilisation of grabens. *Journal of Structural Geology*, 24, 1741-1752.

DUMONT, J. F. 1993. Lake patterns as related to neotectonics in subsiding basins: the example of the Ucamara depression, Peru. *Tectonophysics*, 222, 69-78.

DUNBAR, J.A. & SAWYER, D. S. 1988. Continental rifting at pre-existing lithosphere weakness. *Nature,* 333, 450.

DUNKELMAN, T. J., KARSON, J. A. & ROSENDAHL, B. R. 1988. Structural style of the Turkana Rift, Kenya. *Geology,* 16, 258-261.

DUNKELMAN, T. J., ROSENDAHL, B. R. & KARSON, J. A. 1989. Structure and stratigraphy of the Turkana rift from seismic reflection data. *Journal of African Earth Sciences,* 8, 489-510.

DUNKLEY, P. N., SMITH, M., ALLEN, D. J. & DARLING. W. G. 1993. The geothermal activity and geology of the northern sector of the Kenya Rift Valley. From *Research report SC/93/1*, British Geological Survey for Kenyan Ministry of Energy. 183 p.

- E -

EBINGER, C. J., YEMANE, T., WOLDEGABRIEL, G., ARONSON, J. L. & WALTER, R. C. 1993. Late-Eocene-Recent volcanism and faulting in the southern main Ethiopian rift. *Journal of the Geological Society of London*, 150, 99-108.

EBINGER, C. J. & IBRAHIM, A. 1994. Multiple episodes of rifting in Central and East Africa: A re-evaluation of gravity data, *Geol. Rundsch. 83,* 689-702.

EBINGER, C. J. & SLEEP, N. 1998. Cenozoic magmatism throughout East Africa resulting from impact of a single plume. *Nature,* 395, 788.

EBINGER, C. J., YEMANE, T., HARDING, D. J., TESFAYE, S., Kelley, S. & Rex, D. C. 2000. Rift deflection, migration and propagation: Linkage of the Ethiopian and Eastern rifts, Africa. *Geological Society of America Bulletin*, 112, 163-176.

ENGLAND, P.C. 1983. Constraints on extension of continental lithosphere. *Journal of Geophysical Research*, 88, 1145-1152.

- F -

FEIBEL, C. S., BROWN, F. H. & McDOUGALL, I. 1989. Stratigraphic context of fossil hominids from the Omo group deposits: Northern Turkana basin, Kenya and Ethiopia. *American Journal of Physical Anthropology*, 78, 595-622.

FERGUSON, A.J. & HARBOTT, B.J. 1982. Geographical, physical and chemical aspects of Lake Turkana, in Lake Turkana: A report on the findings of the Lake Turkana Project 1972-1975, edited by Hopson, A.J., London Overseas Development Administration, 1-107.

FOSSEN, H. & RORNES, A. 1996. Properties of fault populations in the Gullfaks field, northern North Sea. *Journal of Structural Geology,* 18, 179-190.

FOSTER, D.A. & GLEADOW, A.J. 1992. The morphotectonic evolution of rift-margin mountains in central Kenya: constraints from apatite fission-track thermochronology, *Earth and Planetary Science Letters, 113,* 157-171.

FOSTER, D. A. & GLEADOW. A. J. W. 1996. Structural framework and denudation history of the flanks of the Kenya and Anza Rifts, East Africa. *Tectonics,* 15, n° 2, 258-271.

- G -

GABRIEL, G. W. & ARONSON, J. L.**,** 1987. Chow Bahir rift: A "failed" rift in southern Ethiopia. *Geology*, 15, 430-433.

GAUDEMER, Y., TAPPONNIER, P. & TURCOTTE, D. L. 1989. River offsets across active strike-slip faults. *Annales Tectonicae*, III, 2, 55-76.

GAULIER, J. M. & HUCHON, P. 1991. Tectonic evolution of the Afar triple junction. *Buletin de la Société Géologique de France,* 162 (3), 451-464.

GEORGE, R., ROGERS, N. & KELLEY, S. 1998. Earliest magmatism in Ethiopia: Evidence for two mantle plumes in one flood basalt province. *Geology,* 26, 10, 923-926.

GEORGE, R. M. & ROGERS, N. W. 2002. Plume dynamics beneath the African plate inferred from the geochemistry of the Tertiary basalts of southern Ethiopia. *Contrib. Mineral. Petrol,* 144, 286-304.

GIBBS, A.D. 1984. Structural evolution of extensional bsin margins, *Journal of the Geological Society of London, 141,* 609-620.

GILLCRIST, R., COWARD, M.P. & MUGNIER, J. L. 1987. Structural inversion, examples from the Alpine foreland and the French Alps, *Geodinamica Acta, 1,* 5-34.

GILLESPIE, P. A., WALSH, J. J. & WATTERSON, J. 1992. Limitations of dimension and displacement data from single faults and the consequences for data analysis and interpretation. *Journal of Structural Geology,* 14, 1157-1172.

GIRARD, C.M. & GIRARD, M. C., 1999. Traitement des données de Télédétection. *Dunod*. 528 p.

GLOAGUEN, R. 2000. Analyse quantitative de l'extension continentale par imagerie satellitale optique et radar. Application au rift sud-kenyan. *Unpublished PhD Thesis, University of Brest*, 200 p.

GOLDSWORTHY, M. & JACKSON, J., 2000. Active normal fault evolution in Greece revealed by geomorphology and drainage patterns. *Journal of the Geological Society of London,* 157, 967-981.

GREENE, L. C., RICHARDS, D. R. & JOHNSON, R. A., 1991. Crustal structure and tectonic evolution of the Anza rift, northern Kenya. *Tectonophysics*, 197, 203-211.

GREENE, W. V., ACHAUER, U. & MEYER, R. P. 1991. A three-dimensional seismic image of the crust and upper mantle beneath the Kenya rift. *Nature,* 354, 199-203.

GUIRAUD, R. & MAURIN J. C. 1992. Early Cretaceous rifts of Western and Central Africa: an overview. *Tectonophysics,* 213, 153-168.

- H -

HACKMAN, B. D., CHARSLEY, T. J., KEY, R. M. & WILKINSON, A. F. 1990. The development of the East African Rift system in noth-central Kenya. *Tectonophysics*, 184, 189-211.

HAILEAB, B., BROWN, F.H., McDOUGALL, I. & GATHOGO, P. N. 2004. Gombe Group basalts and initiation of Pliocene deposition in the Turkana depression, northern Kenya and southern Ethiopia. *Geological Magazine, 141* (1), 41-53.

HARDING, T.P. 1983. Seismic characteristics and identification of negative flower structures, positive flower structures and positive structural inversion, *American Association for Petroleum Geologist Bulletin, 69,* 582-600.

HARRIS, J. M., BROWN, F. H. & LEAKEY, M. G. 1988. Stratigraphy and paleontology of Pliocene and Pleistocene localities west of Lake Turkana, Kenya. *Contrib. Sci.* 399, 1-128.

HAUTOT, S., TARITS, P., WHALER, K., LE GALL, B., TIERCELIN, J. J. & LE TURDU, C. 2000. Deep structure of the Baringo rift basin (Central Kenya) from three-dimensional magneto-telluric imaging. Implications for rift evolution. *Journal of Geophysical Research*, 105, B10, 23,499-23,518.

HENDRIE, D.B., KUSZNIR, N.J. MORLEY, C.K. & EBINGER, C. J. 1994. Cenozoic extension in northern Kenya: a quantitative model of rift basin development in the Turkana region, in Crustal and Upper Mantle Structure of the Kenya Rift, edited by Prodehl C., G.R., Keller, and M.A. Khan, *Tectonophysics 236,* 409-438.

HETZEL, R. & STRECKER, M. R. 1994. Late mozambique belt structures in western Kenya and their influence on the evolution of the Cenozoic Kenya Rift. *Journal of Structural Geology,* 16, 2, 189-201.

HIGGINS, R.I. & HARRIS, L.B. 1997. The effect of cover composition on extensional faulting above reactivated basement faults: result from analogue modelling, *Journal of Structural Geology*, 19*,* 1, 89-98.

HILL, K.C. & COOPER, G.T. 1996. A strategy for palinspatic restoration of inverted basins: thermal and structural analyses in SE Australia, from Buchanan, P.G. and Nieuwland, D.A. (eds), Modern development in structural interpretation, validation and modelling, *Geol. Soc. special publication, 99,* 99-115.

- I -

ILLIES, J.H. & GREINER, G. 1978. Rhinegraben and the Alpine system, *Geological Society of America Bulletin, 89,* 770-782.

ILLIES, J. H. 1981. Mechanism of graben formation. *Tectonophysics,* 73, 249-266.

IMBER, J., TUCKWELL, G. W., CHILDS, C., WALSH, J. J., MANZOCCHI, T., HEATH, A. E., BONSON, C. G. & STRAND, J. 2004. Three-dimensional distinct element modelling of relay growth and breaching along normal faults. *Journal of Structural Geology,* 26, 1897-1911.

- J -

JACKSON, J. & McKENZIE, D. P. 1983. The geometrical evolution of normal fault systems. *Journal of Structural Geology*, 5, 471-482.

JACKSON, J. & LEEDER, M.**,** 1994. Drainage systems and the development of normal faults: an example from Pleasant Valley, Nevada. *Journal of Structural Geology*, 16, 8, 1041-1059.

JACKSON, J., NORRIS, R. & YOUNGSON, J.**,** 1996. The structural evolution of active fault and fold systems in central Otago, New Zealand: evidence revealed by drainage patterns. *Journal of Structural Geology*, 18, 217-234.

JOHNSON, T. C., HALFMAN, J. D., ROSENDAHL, B. R. & LISTER, G. S.**,** 1987. Climatic and tectonic effects on sedimentation in a rift-valley lake: Evidence from high-resolution seismic profiles, Lake Turkana, Kenya. *Geological Society of American Bulletin*, 98, 439-447.

JOHNSON, T. C., HALFMAN, J. D. & SHOWERS, W. J. 1990. Paleoclimate of the past 4000 years at Lake Turkana, Kenya, based on the isotopic composition of authigenic calcite. *Palaeogeography, Palaeoclimatology, Palaeoecology,* 85, 189-198.

JOUBERT, P., 1966. Geology of the Loperot area. Report 74, Geological Survey of Kenya, 52 p.

- K -

KADIROV, U., 1998. Traitement d'image, approche par analyse fréquentielle et spatiale et approche par morphologie mathématique, étude de l'urbanisme de la ville de Tachkent et de l'environnement de la Touranie. *Thesis, University Paris VI*, 245 p.

KEY, R. M. & WATKINS, R. T.**,** 1988. Geology of the Sabarei area. Report 111, Ministry of environment and natural resources, Mines and geology department, Ministry of Kenya, 57 p.

KRISP Working Group. 1991. The Kenyan Rift: pure shear extension above a mantle plume. *Nature,* 345, 223-227.

KUSZNIR, N.J., MARSDEN, G. & EGAN, S.S. 1991. A flexural cantilever simple-shear/pure shear model of continetal lithosphere extension: application to the Jeanne d'Arc Basin, Grand Banks and Viking Graben, North Sea. In: The Geometry of Normal Faults (edited by Roberts, A.M., Yielding, G. & Freeman, B.). *Spec. Publ. Geol. Soc. London,* 56, 41-60.

- L -

LAHITTE, P., GILLOT, P. Y. & COURTILLOT, V. 2003. Silicic central volcanoes as precursors to rift propagation: the Afar case. *Earth and Planetary Science Letters,* 207, 103-116.

LEEDER, M. R. & JACKSON, J. A., 1993. The interaction between normal faulting and drainage in active extensional basins, with examples from the western United States and central Greece. *Basin Research,* 5, 79-102.

LE GALL, B., VETEL, W. & MORLEY, C, K. Inversion tectonics during continental rifting: The Turkana rifted zone, Northern Kenya. *Tectonics*, in press.

LE TURDU, C. 1998. Modèles tectono-sédimentaires 3D des bassins en extension. Exemples du Rift du Kenya (Baringo-Bogoria et Magadi), du Rift Ethiopien (Ziway-Shala) et du Fossé Nord-Tanganyika. *Thèse de doctorat de l'UBO,* 416 p.

LEZZAR, K. E., TIERCELIN, J. J., LE TURDU, C., COHEN, A. S., REYNOLDS, D. J., LE GALL, B. & SCHOLZ, C. A. 2002. Control of normal fault interaction on the distribution of major Neogene sedimentary depocenters, Lake Tanganyika, East African rift. *American Association of Petroleum Geologists Bulletin,* 86, 6, 1027-1059.

- M -

MAIN, A. 1996. Statistical physics, seismogenesis and seismic hazard. *Reviews of Geophysics*, 34, 433-462.

MARPLE, R. T. & TALWANI, P., 1993. Evidence of possible tectonic upwarping along the South Carolina coastal plain from an examination of river morphology and elevation data. *Geology*, 21, 651-654.

MARR, D. & HILDRETH, E. 1980. Theory of edge detection. *Proc. R. Soc. Lond.,* B207, 187-217.

MARRETT, R. 1996. Aggregate properties of fracture populations. *Journal of Structural Geology*, 18, 169-178.

MART, Y. & DAUTEUIL, O. 2000. Analogue experiments of propagation of oblique rifts. *Tectonophysics,* 316, 121-132.

MAURIN, J. C. & GUIRAUD, R. 1993. Basement control in the development of the Early Cretaceous West and Central African Rift System. *Tectonophysics*, 228, 81-95.

McCLAY, K. R. & WHITE, M. 1995. Analogue models of orthogonal and oblique rifting. *Marine and Petroleum Geology,* 12, 137-151.

McCONNELL, R. B. 1972. Geological development of the rift system of eastern Africa. *Geological Society of America Bulletin,* 83, 2549-2572.

McDONALD, R. 1994. Petrological evidence regarding the evolution of the Kenya Rift Valley. *Tectonophysics,* 236, 373-390.

McDOUGALL, I. & WATKINS, R. T. 1988. Potassium-Argon ages of volcanic rocks from northeast of Lake Turkana, northern Kenya. *Geological Magazine,* 125, 15-23.

McDOUGALL, I. & FEIBEL, C. S. 1999. Numerical age control for the Miocene-Pliocene succession at Lothagam, a hominoid-bearing sequence in the northern Kenya Rift. *Journal of Geological Society, London,* 156, 731-745.

McKENZIE, D.P. 1978. Some remarks on the development of sedimentary basins. *Earth and Planetary Science Letters,* 40, 25-32.

McKENZIE, D. P. & BICKLE, M. J. 1988. The volume and composition of melts generated by extension of the lithosphere. *Journal of Petrology*, 29, 625-679.

MECHIE, J., KELLER, G.R., PRODEHL, C., GACIRI, S., BRAILE, L.W., MOONEY, W.D., GAJEWSKI, D. & SANDMEIER, K.J. 1994. Crustal structure beneath the Kenya Rift from axial profile data. In: C. Prodehl, G.R. Keller and M.A. Khan (Editors). Crustal and Upper Mantle Structure of the Kenya Rift. *Tectonophysics,* 236, 179-199.

MERRITS, D. J. & HESTERBERG, T., 1994. Stream Networks and long-term surface uplift in the New Madrid seismic zone. *Science*, 265, 1081-1084.

MOHR, P.A. & WOOD, C.A. 1976. Volcano spacing and lithospheric attenuation in the Eastern Rift of Africa, *Earth and Planetary Science Letters,* 33*,* 126-140.

MORLEY, C.K. 1994. Interaction of deep and shallow processes in the evolution of the Kenya rift. *Tectonophysics,* 236, 81-91.

MORLEY, C.K., 1999a. Influence of Preexisting Fabrics on Rift Structure, in C. K. Morley ed., Geoscience of Rift Systems-Evolution of East Africa: *AAPG Studies in Geology*, 44, 151-160.

MORLEY, C. K. 1999b. Aspect of Transfer Zone Geometry and Evolution in East African Rifts, in C. K. Morley ed., Geoscience of Rift Systems-Evolution of East Africa: *AAPG Studies in Geology*, 44, 161-171.

MORLEY, C. K. 1999c. Marked along-strike variations in dip of the normal faults-the Lokichar fault, N. Kenya rift: a possible cause for metamorphic core complexes. *Journal of Structural Geology*, 21, 479-492.

MORLEY, C. K. 1999d. How successful are analogue models in addressing the influence of pre-existing fabrics on rift structure? *Journal of Structural Geology,* 21, 1267-1274.

MORLEY, C. K., WESCOTT, W. A., STONE, D. M., HARPER, R. M., WIGGER, S. T. & KARANJA, F. M., 1992. Tectonic evolution of the northern Kenyan Rift. *Geological Society of London*, 149, 333-348.

MORLEY, C. K, WESCOTT, W. A., HARPER, R. M., WIGGER, S. T., DAY, R. A. & KARANJA, F.M. 1999a. Geology and Geophysics of the Western Turkana Basins, Kenya, in C. K. Morley ed., Geoscience of Rift Systems-Evolution of East Africa: *AAPG Studies in Geology*, 44, 19-54.

MORLEY, C. K., DAY, R. A., LAUCK, R., BOSHER, R., STONE, D. M., WIGGER, S. T., WESCOTT, W. A., HAUN, D., BASSETT, N., & BOSWORTH, W. 1999b. Geology and Geophysics of the Anza Graben, in C. K. Morley ed., Geoscience of Rift Systems-Evolution of East Africa: *AAPG Studies in Geology,* 44, 67-90.

MORLEY, C. K, HARPER, R. M. & WIGGER, S. T. 1999c. Tectonic Inversion in East Africa, in C. K. Morley ed., Geoscience of Rift Systems-Evolution of East Africa: *AAPG Studies in Geology*, 44, 193-210.

MOUCHOT, M. C. 2000. Introduction au traitement d'images. Ecole Nationale Supérieure des Télécommunications de Bretagne, 114 p.

- N -

NEEDHAM, D. T., YIELDING, G. & FOX, R. J. 1996. Fault population description and prediction using examples from the offshore UK. *Journal of Structural Geology*, 18, 155-167.

NEGREDO, A, FERNADEZ, M. & ZEYEN, H. 1995. The lateral syn- and post-rift evolution of lithospheric yield strength. Constraints on modes of rifting. *Earth and Planetary Science Letters,* 134, 87-98.

NICOL, A., WALSH, J. J., WATTERSON, J. & GILLESPIE, P. A. 1996. Fault size distributions-are they really power-law? *Journal of Structural Geology,* 18, 2/3, 191-197.

- O -

OCHIENG J. O., WILKINSON, A. F., KAGASI, J. & KIMONO, S., 1988. Geology of the Loiyangalani area. *Ministry of Environment and Natural Resources*, Mines and Geological Department, Republic of Kenya, 53 p.

OPHEIM, J.O. & GUDMUNSON, A. 1989. Formation and geometry of fractures, and related volcanism, of the Krafla fissure swarm, northeast Iceland, *Geol. Soc. Am. Bull., 101,* 1608-1622.

OWEN, R.B., BARTHELME, J. W., RENAUT, R. W. & VINCENS, A., 1982. Palaeolimnology and archaeology of Holocene deposits north-east of lake Turkana, Kenya. *Nature*, 5874, 523-529.

- P -

PEACOCK, D. C. P. & SANDERSON, D. J. 1991. Displacements, segment linkage and relay ramps in normal fault zones. *Journal of Structural Geology,* 13, 721-733.

PEAKALL, J., LEEDER, M., BEST, J. & ASHWORTH, P., 2000. River response to lateral ground tilting: a synthesis and some implications for the modelling of alluvial architecture in extensional basins. *Basin Research*, 12, 413-424.

PHILLIPS, L. F. & SCHUMM, S. A., 1987. Effect of regional slope on drainage networks. *Geology*, 15, 813-816.

PRICE, S., BRODIE, J., WITHAM, A. & KENT, R. 1997. Mid-Tertiary rifting and magmatism in the Traill O region, east Greenland, *J. Geol. Soc., London, 154,* 419-434.

PRODEHL, C., JACOB, B., THYBO, H., DINDI, E. & STANGL, R. 1994. Crustal structure on the northeastern flank of the Kenya Rift. In: C. Prodehl, G.R. Keller and M.A. Khan (Editors). Crustal and Upper Mantle Structure of the Kenya Rift. *Tectonophysics,* 236, 271-290.

PUBELLIER, M., DEFFONTAINES, B., QUEBRAL, R. & RANGIN, C., 1994. Drainage network analysis and tectonic of Mindanao, southern Philippines. *Geomorphology,* 9, 325-342.

- R -

REEVES, C. V., KARANJA, F. M. & McLEOD, I. N. 1987. Geophysical evidence for a failed Jurassic rift and triple junction in Kenya, *Earth and Planetary Science Letters, 81,* 299-311.

RICHARD, P. D., BALLARD, J.F., COLLETTA, B. & COBBOLD, P. R. 1989. Fault initiation and development above a basement strike-slip fault: analogue modelling and tomography, *Comptes Rendu Académie des Sciences, 309,* 11, 2111-2118,

RICHARD, P.D., NAYLOR, M.A. & KOOPMAN, A. 1995. Experimental models of strike-slip tectonics, *Petroleum Geoscience,* 1, 71-80,

RING, U. 1994. The influence of pre-existing structure on the evolution of the Cenozoic Malawi rift (East African rift system), *Tectonics,* 13, 313-326.

RING, U., BETZLER, C. & DELVAUX, D. 1992. Normal versus strike-slip faulting during rift development in East Africa: The Malawi Rift, *Geology, 20,* 1015-1018.

ROCHE, H., DELAGNES, A., BRUGAL, J. P., FEIBEL, C., KIBUNJIAS, M., MOURREL, V. & TEXIER, P. J. 1999. Early hominid stone tool production and technical skill 2.34 Myr ago in West Turkana, Kenya. *Nature,* 399, 57-60.

ROGERS, N., McDONALD, R., FITTON, J. G., GEORGE, R., SMITH. M. & BARREIRO, B. 2000. Two mantle plumes beneath the East African rift system: Sr, Nd and Pb isotope evidence from Kenya Rift basalts. *Earth and Planetary Science Letters,* 176, 387-400.

ROSENDAHL, B.R., 1987. Architecture of the continental rifts with special reference to East Africa, Ann. Rev. *Earth and Planetary Science Letters,* 15*,* 445-503.

ROSENDAHL, B. R., KILEMBE, E. & KACZMARICK, K. 1992. Comparison of the Tanganyika, Malawi, and Turkana Rift zones from analyses of seismic reflection data. *Tectonophysics,* 213, 235-256.

RUBIN, A.M. & POLLARD, D. D. 1988. Dike-induced faulting in rift zones of Iceland and Afar, *Geology, 16,* 413-417.

- S -

SCHLISCHE, R. W., YOUNG, S. S., ACKERMANN, R. V. & GUPTA, A. 1996. Geometry and scaling relations of a population of very small rift-related normal faults. *Geology,* 24, 683-686.

SCHOLZ, C.H. & COWIE, P. A. 1990. Determination of total strain from faulting using slip-measurements. *Nature,* 346, 837-839.

SCHULL, T.J. 1988. Rift basins of interior Sudan: Petroleum exploration and discovery, *American Association of Petroleum Geologist Bulletin,* 72, 1128-1162.

SCHUMM, S. A., DUMONT, J. F. & HOLBROOK, J. 2000. Active Tectonics and Alluvial Rivers. *Cambridge University Press*, 274 p.

SENGÖR, A. M. C. & BURKE, K. 1978. Relative timing of rifting and volcanism on Earth and its tectonic implications. *Geophysical Research Letter*, 5, 419-421.

SHACKELTON, R. M. 1993. Tectonics of the Mozambique Belt in East Afri~ In: Magmatic processes and Plate Tectonics (edited by Richard, H. M., Alabaster, T., Harris, N. B. W. & Neary, C. R.) 76, *Spec. Publ. Geol. Soc. London,* 345-362.

SHELL Report, Well Resume Eliye Springs-1, 1992. National Oil Corporation of Kenya, Nairobi, 40p.

SMITH, M. & MOSLEY, P. 1993. Crustal heterogeneity and basement influence on the development of the Kenya Rift, East Africa. *Tectonics*, 12, 591-606.

SPETCH, T.D. & ROSENDAHL, B.R. 1989. Architecture of the Lake Malawi rift, East Africa, *Journal of African Earth Science*, 8, 393-413.

SPOHN, T. & SCHUBERT, G. 1982. Convective thinning of the lithosphere: a mechanism for the initiation of continental rifting. *Journal of Geophysical Research,* 87, 4669-4681.

STARK, C. P. 1991. An invasion percolation model of drainage network evolution. *Nature*, 352, 423-425.

STEWART, K & ROGERS, N. 1996. Mantle plumes and lithosphere contributions to basalts from southern Ethiopia. *Earth and Planetary Science Letters,* 139, 195-211.

STRECKER, M.R., BLISNIUK, P.M. & EISBACHER, G.H. 1990. Rotation of extension direction in the central Kenya Rift, *Geology,* 18, 299-302.

SYLVESTER, A.G. 1984. Wrench fault tectonics, *American Association of Petroleum Geologists Reprint Series,* 28, 374 p.

- T -

TCHALENKO, J.S. 1970. Similarities between shear zones of different magnitudes, *Geological Society of America Bulletin,* 81, 1625-1640.

THEUNISSEN, K., KLERX, J., MELNIKOV, A. & MRUMA, A. 1996. Mechanisms of inheritance of rift faulting in the western branch of the East African Rift, Tanzanie. *Tectonics,* 15, 776-790.

THOMPSON, R. N. & GIBSON, S. A. 1991. Subcontinental mantles plumes, hotspots and pre-existing thinspots. *Journal of the Geological Society, London*, 148, 973-977.

THOUE, F. 1993. Quantification par imagerie tridimensionnelle de l'extension continentale et des déplacements associés. Exemples au Kenya et au Yemen. *PhD Thesis Univ. Grenoble*, 200 p.

TONGUE, J. A., MAGUIRE, P. K. H. & YOUNG, P. A. V. 1992. Seismicity distribution from temporary earthquake recording networks in Kenya. *Tectonophysics,* 204, 71-79.

TRON, V. & BRUN, J. P. 1991. Experiments on oblique rifting in brittle-ductile systems. *Tectonophysics,* 188, 71-84.

- V -

VAN WYK DE VRIES, B. & MERLE, O. 1996. The effect of volcanic constructs on rift fault patterns. *Geology,* 24, 7, 643-646.

VELDE, B., DUBOIS, J., TOUCHARD, G. & BADRI, A. 1990. Fractal analysis of fractures in rocks: The Cantor's Dust Method. *Tectonophysics,* 179, 345-352.

VELDE, B. & DUBOIS, J. 1991. Fractal analysis of fractures in rocks: The Cantor's Dust Method-Reply. *Tectonophysics,* 198, 112-115.

VERSFELT, J. & ROSENDAHL, B. R. 1989. Relationship between pre-existing structure and rift architecture in Lakes Tanganyika and Malawi, East Africa. *Nature,* 337, 354-356.

VETEL, W., LE GALL, B. & JOHNSON, T.C. 2004. Active tectonics in the Turkana Rift (North Kenya). An integrated approach from drainage network, satellite imagery and reflection seismic analyses. *Basin Research,* 16 (2), 165-181.

VETEL, W., LE GALL, B. & WALSH, J.J. Geometry and growth of an inner rift fault pattern: the Kino Sogo Fault Belt, Turkana Rift (North Kenya). Submitted to *Journal of Structural Geology.*

VETEL, W. & LE GALL, B. Dynamic of continental extension in magmatic rifts. The study case of the Turkana Rift since the last 45 Ma. (Northern Kenya). Submitted to *Tectonophysics*.

VILLEMIN, T. & SUNWOO, C. 1987. Distribution logarithmique self-similaire des rejets et longueurs de failles: exemple du Bassin Houiller Lorrain. *Compte Rendu de l'Académie Sciences, Paris.* Série II, 305, 1309-1312.

VILLEMIN, T., BERGERAT, F. ANGELIER, J. & LACASSE, C. 1994. Brittle deformation and fracture patterns on oceanic rift shoulders: the Esja peninsula, SW Iceland, *Journal of Structural Geology,* 16, 12, 16541-1654.

VINCENS, A., 1984. Environnement végétal et sédimentation pollinique lacustre dans le bassin du lac Turkana (Kenya). *Journal of palaeobiology,* Vol. special, ISSN 0253-6730, 235-242.

- W -

WALSH, J. & DODSON, R. G.**,** 1969. Geology of the Northern Turkana. Report 82. Geological Survey of Kenya, 48 p.

WALSH, J. J. & WATTERSON, J. 1988. Analysis of the relationship between the displacements and dimensions of faults. *Journal of Structural Geology,* 10, 239-247.

WALSH, J. J., WATTERSON, J. & YIELDING, G. 1991. The importance of small-scale faulting in regional extension. *Nature,* 351, 391-393.

WALSH, J. J., NICOL, A. & CHILDS, C. 2002. An alternative model for the growth of faults. *Journal of Structural Geology*, 24, 1669-1675.

WALSH, J. J., BAILEY, W. R., CHILDS, C., NICOL, A. & BONSON, C. G. 2003. Formation of segmented normal faults: a 3-D perspective. *Journal of Structural Geology,* 25, 1251-1262.

WATKINS, R. T. 1986. Volcano-tectonic control on sedimentation in the Koobi For a sedimentary basin, Lake Turkana. From Frostick, L. E. et al. (eds), Sedimentation in the African Rifts, Geological Special Publication, n°25, 85-95.

WESCOTT, W. A., WIGGER, S. T., STONE, D. M. & MORLEY, C. K. 1999. Geology and geophysics of the Lotikipi plain, *in* C. K. Morley ed., Geoscience of Rift Systems-Evolution of East Africa: AAPG Studies in Geology N°44, 55-65.

WILKINSON, A. F. 1988. Geology of the Allia Bay area. Report 109, *Ministry of Environment and Natural Resources*, Mines and Geological Department, Republic of Kenya, 54 p.

WILLIAMSON, P. G. & SAVAGE, R. J. G. 1986. Early rift sedimentation in the Turkana basin, northern Kenya, *From* Frostick, L. E., *et al*. (eds), *Sedimentation in the African rifts: Geological Society of London Special Publication*, 25, 267-283.

WINN, R.D., STEINMETZ, J.C. & KEREKGYARTO, W.L. 1993. Stratigraphy and rifting history of the Mesozoic-Cenozoic Anza Rift, Kenya, *Am. Assoc. Petrol. Geol. Bull., 77,* 11, 1989-2005.

WITHJACK, M. O. & JAMISON, W. R. 1986. Deformation produced by oblique rifting. *Tectonophysics,* 126, 99-124.

WOLFENDEN, E., EBINGER, C., YIRGU, G., DEINO, A. & AYALEW, D. 2004. Evolution of the northern Main Ethiopian rift: birth of a triple junction. *Earth and Planetary Science Letters,* 224, 213-228.

WU, H. & POLLARD, D. D. 1995. An experimental study of the relationship between joint spacing and layer thickness. *Journal of Structural Geology,* 17, 887-905.

- Y -

YIELDING, G., NEEDHAM, T. & JONES, H. 1996. Sampling of fault populations using sub-surface data: a review. *Journal of Structural Geology,* 18, 2/3, 135-146.

YURETICH, R. F.**,** 1979. Modern sediments and sedimentary processes in Lake Rudolf (Lake Turkana), eastern rift valley, Kenya. *Sedimentology*, 26, 313-331.

- Z -

ZANETTIN, B., VISENTIN, J., BELLIENI, G., PICCIRILLO, E. M. & RITA, F. 1983. Le volcanisme du bassin Nord-Turkana (Kenya) : âge, succession et évolution structurale. Bull. *Cent. Rech. Explor. Prod. Elf-Aquitaine,* 7, 249-255.

ZHANG, Y. S. & TANIMOTO, T. 1992. Ridges, hotspots and their interactions as observed in seismic velocity maps. *Nature,* 355, 45-49.

ZIEGLER, P.A. 1987. Compressional intra-plate tectonics in the Alpine foreland, *Tectonophysics, 137,* 389-420.

ZIEGLER, P.A. 1988. Evolution of the Arctic-North Atlantic and the Western Tethys, *American Association of Petroleum Geologist, Memoir, 43,* 198 p.

ZIEGLER, P.A. 1989. Geodynamic model for Alpine intra-plate compressional deformation in Western and Central Europe, in Inversion tectonics, edited by Cooper, M.A., and G.D. Williams, *Geol. Soc. London, Sp. Pub., 44,* 63-85.

ZIEGLER, P.A., CLOETINGH, S. & VAN WEES, J.D. 1995. Dynamics of intraplate compressional deformation: the Alpine foreland and other examples, *Tectonophysics, 252,* 7-59.

ZIEGLER, P.A. & CLOETINGH, S. 2004. Dynamic processes controlling evolution of rifted basins, *Earth-Science Reviews, 64,* 1-50.

ANNEXE 1. Mesures des plans de stratification et des plans de failles de la zone ouest du lac Turkana (mission de terrain 2002)

Mesures de stratification (So) des Formations de la région Ouest Turkana				
Localisation	**Type de roche Description**	**Age**	**Direction**	**Pendage**
SEDIMENTS RECENTS (Plio-Pléistocène)				
KATABOI	Argile, argilite dans laga	9515+-80 ans	160 0	8 NE 4 E
ELIYE SPRINGS	Argile, argilite lacustres	6630+-45 6285+-50 ans	20 130 150 75 30	2 SE 20 NE 10 NE 6 NW 4 NE
LOTHAGAM	Banc à gastéropodes	9795+-100 ans	40	28 NW
NARIOKOTOME	Sédiments du Membre Natoo-Nariokotome	1.6 – 0.74 Ma	10 150 20	2 W 4 SW 6 NW
KAITIO	Tuff, sédiments du Membre Natoo-Nariokotome	1.6 – 0.74 Ma	30 16 70 30 30 130	4 NW 6 NW 8 NW 4 NW 6 NW 12 NE
KALOCHORO	Tuff, sédiments du Membre Natoo-Nariokotome	1.6 – 0.74 Ma	50 10 110 145	12 NW 8 W 14 SW 5 SW
NAYIENA ENGOL	Sédiments du membre Kalochoro-Kaitio	2.35 – 1.6 Ma	0 120	6W 20 SW
LOKALALEI	Sédiments du Membre Lomekwu-Lokalalei	3.36 – 2.35 Ma	20	4 NW
FORMATIONS ANCIENNES (Crétacé - Miocène)				
LOKITAUNG-LAPURR	Contact grès-laves Idem Grès Brèche volcanique Laves Laves	Crétacé-Oligocène	170 0 120 0 150 20 140 130	20 SW 10 W 10 SW 16 E 12 SW 18 NW 20 SW 20 SW
KANOELEM	Grès	Crétacé	130 130 70 50 60 40 10 40 120 170 30 20 80	0 4 SW 4 NW 12 NW 20 NW 12 NW 10 NW 12 NW 6 NE 20 SW 6 NW 52 NW 2 NW

Mesures de stratification (So) des Formations de la région Ouest Turkana				
Localisation	**Type de roche Description**	**Age**	**Direction**	**Pendage**
FORMATIONS ANCIENNES (Crétacé - Miocène)				
MURUANACHOK	Grès	Crétacé	130 160 0 60 55 85	20 NE 5 NE 8 E 20 SE 20 SE 12 SW
LOTHIDOK	Grès (bordure SE)	Miocène	160 170 50	14 SW 20 NW 10 SE
NARIOKOTOME	Laves	Miocène	95 150	10 SW 18 SW
TOPERNAWI	Volcano-sédimentaire	Miocène	100 90 65 70 60 20	8 NE 14 N 80 NW 8 NW 10 NW 10 SE
LOTHAGAM	Grès Volcanisme Idem	????	 20 40 170 40 140 170 0 170 40 130	 10 SE 28 NW 14 SW 12 SE 10 SW 25 SW 20 W 20 SW 10 NW 15 SW
NAPEDET	Grès (N du plateau volcanique Laves Napedet Laves	Miocène	110 160 0 80	12 NE 8 SW 10 W 16 NW

FAILLES (TURKANA)							
			FAILLES		STRIES		
Localisation	**Type de roche affectées**	**Rejet**	**Direction**	**Pendage**	**Plongement**	**Direction**	**Type de mouvement**
LOTHIDOK	Sédiments récents		130 140	20 NE 30 NE	20 20	50 40	normal
LOTHAGAM	Sédiments gastéropodes récents (9800 ans)	50 cm	20	70 NW			normal
NARIOKOTOME	Sédiments du Membre Natoo-Nariokotome	4 m	135	90	70	135	Normalo-senestre
KAITIO	Tuff, sédiments du Membre Natoo-Nariokotome	Faible qqls dm	50 55 60 90 55 40 25 110 75 70 60 10 70 155 70 20 70 60 45 15 60 85 90 20 20 130 95 100 35 50 90 30 90	40 NW 25 NW 34 SE 35 S 30 SE 45 NW 45 SE 30 NE 50 SE 30 SE 45 NW 40 NW 30 SE 55 NE 30 NW 55 SE 20 NW 30 NW 35 SE 20 SE 60 NW 50 SE 65 N 40 SE 70 SE 30 NE 60 NE 45 NE 60 SE 55 NW 65 N 60 SE 60 N	25 25 34 35 30 35 45 30 50 30 45 32 30 55 30 55 20 30 35 20 60 50 65 25 70 20 60 45 35 55 65 60 60	325 325 150 180 145 285 115 20 165 160 330 335 160 65 340 110 340 330 135 105 240 175 0 110 110 40 15 10 125 320 0 120 0	Déformation hydroplastique
KALOCHORO	Tuff, sédiments du Membre Natoo-Nariokotome	Qqls cm	0 60 30	70 E 65 NW 70 SE			normal

			FAILLES		STRIES		
Localisation	**Type de roche affectées**	**Rejet**	**Direction**	**Pendage**	**Plongement**	**Direction**	**Type de mouvement**
LAPURR	Sédiments récents	1 m	0 80 120 100 135	70 E 78 NW 50 SW 50 SW 58 NE	50 58	300 70	normal
LAPURR SOCLE	SOCLE Eponte dyke Laves		160 110 110 140 150 50 60 140 10 50 20 105 20 10	30 NE 80 NE 75 NE 80 SW 50 SW 44 SE 86 SE 66 SW 90 30 SE 35 SE 70 SW 35 SE 80	44 40 40 20 12 80	SE 60 110 270 220 100	normal
KANOELEM	Grès		30 160 55 30 35 140 80 30 70 30 15 0 20 40 10 140 10 10 10 25 30 0 30	70 NW 90 35 NW 65 NW 80 NW 65 NE 90 90 90 80 NW 65 SE 80 W 65 NW 65 NW 55 NW 60 NE 90 40 NW 40 SE 60 SE 55 SE 60 E 75 SE	70 22 30 64 65 70 65 40 65 44 80 26 22 60 55 42	210 340 295 300 20 260 105 330 310 120 10 160 120 115 120 80	

FAILLES (TURKANA)							
			FAILLES		STRIES		
Localisation	Type de roche affectées	Rejet	Direction	Pendage	Plongement	Direction	Type de mouvement
MURUANACHOK	Grès		70	64 SE	40	230	
			130	50 SW	50	220	
			150	80 NE	65	110	
			130	70 NE	70	320	
			145	52 SW	52	235	
			120	70 SW	60	280	
			130	40 NE	40	40	
			100	60 SW	45	250	
			140	30 NE	30	50	
			40	60 SE	0	40	
			110	54 SW	50	250	
			130	40 NE	20	0	
NAPEDET	Sédiments récents ?	5 m	10	60 NW			
			60	90			
			80	70 SE			
			20	65 NW			
			0	90	0	180	
			90	80 N	20	70	
			150	35 NE			
			110	80 NE			
NARIOKOTOME		85	80 NW	80	355		
TOPERNAWI	Volcano-sédimentaire	3 m	60	68 NW	68	330	
		2 m	80	70 SE	70	170	
		5 cm	80	80 NW	80	350	
			70	75 SE			
			45	65 SE	30	30	
			50	60 SE	60	150	
LOTHAGAM	Grès	Qqls dm	170	40 SW			
			110	75 SW			
			0	60 W			
			0	60 W			
			130	28 NE	28	40	
			0	60			
			10	40 NW	40	280	
			165	35 SW			
			0	40 W	40	270	
			40	80 NW			
			0	80 W			
			0	40 W	40	270	
			165	35 SW			
	Volcanisme	30 m	150	65 NE	50	115	
			130	70 NE	40	110	
			0	80 W	80	270	
			160	80 SW	80	250	
			160	80 SW			

ANNEXE 2. Echantillons et datations des laves oligo-pliocènes de la zone ouest Turkana (Mission 2002)

Tableau 1. *Récapitulatif des échantillons de laves oligocènes-pliocènes récoltés au cours de la mission de 2002. Certains d'entre eux ont été datés par méthode K/Ar au laboratoire de Brest (resp : H. Bellon)(voir figure 1 pour localisation).*

ECHANTILLONS	*LOCALISATION*	*TYPE*	*DESCRIPTION, FACIES*	*AGE (MA)*
LAPURR				
LAP 02/01	Gorge de Lapurr N 4° 16' 07,7" E 35° 48' 50,5"	Dyke N56 4 m vertical intrude les grès	Basalte aphyrique sombre, Débit en gros prisme perpendiculaire aux épontes	
LAP 02/02	Gorge de Lapurr N 4° 16' 05,4" E 35° 49' 02,5"	Dyke N70 1,45 m subvertical intrude les grès	Basalte aphyrique sombre	
LAP 02/03	Gorge de Lapurr N 4° 16' 17,4" E 35° 49' 05,7"	Dyke N60 3,50 m subvertical intrude les grès	Basalte aphyrique sombre, inclusions de calcite	
LAP 02/04	Gorge de Lapurr N 4° 16' 17,4" E 35° 49' 05,7"	Dyke NS 4,50 m subvertical intrude les grès et recoupe le LAP 02/03	Basalte aphyrique sombre	
LAP 02/04A et B	Gorge de Lapurr N 4° 16' 02,2" E 35° 49' 12,4"	Dyke N60, 2 types de faciès	Débit en boules et faciès à grain fin	
LAP 02/04C	Gorge de Lapurr	Dyke N40 de 8 m	Débit en boules, faciès à grain fin	
LAP 02/04D	Gorge de Lapurr N 4° 17' 06" E 35° 48' 56,6"	Dyke N50 de 2 m	Débit en boules, faciès à grain fin	
LAP 02/05	Gorge de Lapurr	Dyke N50 25 cm vertical, intrude les grès en deux branches parallèles	Basalte fin	
LAP 02/06	Gorge de Lapurr	Volcanisme, coulée de 8 m, base de la série volcanique	Basalte grenu à débit en boules	
LAP 02/07	Gorge de Lapurr	Volcanisme, coulée de plusieurs m proche du contact avec les grès	Coulée successives de basaltes à grain fin	
LAP 02/09	Gorge de Lapurr N4° 16' 07,3" E35° 47' 06,4"	Volcanisme, coulée de 20 m en petits prismes parfois radiaires	Basalte fin	
LAP 02/09A	Gorge de Lapurr N 4° 16' 13,2" E 35° 47' 18,8"	Volcanisme, coulée de 20 m	Basalte massif en gros prismes	***34.5***
LAP 02/09B	Gorge de Lapurr N 4° 16' 0,6" E 35° 47' 19"	Volcanisme, coulée prismée de 20 m	Basalte	***34 +- 0.9***
LAP 02/09D	Gorge de Lapurr Idem	Dyke N40°, 80 cm, oblique (N40, 38E) passant latéralement en	Basalte à grain fin	

		sill		
LAP 02/09E	Gorge de Lapurr Idem	Dyke N40°, 30 cm, oblique (N40, 80W)	Basalte à grain fin	
LAP 02/09F	Gorge de Lapurr Idem	Sill de 3 m, parallèle à la So (N170, 20SW)	Faciès grenu	
LAP 02/10	Gorge de Lapurr Idem	Volcanisme, coulée prismée de 6,50 m	Basalte fin	***34.7***
LAP 02/11	Gorge de Lapurr N 4° 15' 33,5" E 35° 46' 55"	Volcanisme, coulée de 2 m	Basalte	
LAP 02/12	Gorge de Lapurr N 4° 15' 43" E 35° 46' 33,4"	Volcanisme, coulée prismée de 10 m	Basalte massif	
LAP 02/13	Gorge de Lapurr, près de Lokitaung N 4° 15' 51,6" E 35° 45' 32,9"	Volcanisme, coulée prismée de 10 m	Basalte massif	***38.4***
LAP 02/13A	Gorge de Lapurr N 4° 15' 43,4" E 35° 45' 29"	Volcanisme, coulée de 5 m	Basalte massif	***29.7 +- 0.7***
LAP 02/13B	Gorge de Lapurr Idem	Volcanisme, coulée de 8 m	Basalte massif	
LAP 02/13C	Gorge de Lapurr Idem	Volcanisme, coulée de 2 à 6 m	Basalte	***37.1***
LAP 02/13D	Gorge de Lapurr N 4° 15' 42,6'' E 35° 45' 23,3''	Volcanisme, coulée massive de 15 m	Basalte	***27.9+-0.7***
LAP 02/13E	En arrière de Lokitaung vers Murua Rith N 4° 19' 34,9'' E 35° 39' 46,4''	Volcanisme, coulée prismée de 10 m	Basalte très bien prismé	
LAP 02/13F	Idem proche de Kalin	Volcanisme	Basalte à gros feldspath	
LAP 02/14	Gorge de Lapurr, près de Lokitaung N 4° 15' 54,8" E 35° 45' 39,1"	Volcanisme, coulée prismée de 10 m	Basalte	***37.1***
LAP 02/15	Gorge de Lapurr N 4° 15' 59,5'' E 35° 45' 50''	Volcanisme, coulée de 10 m à gros prisme	Basalte massif	***19.45+-0.55***
LAP 02/16	Gorge de Lapurr N 4° 16' 02,6" E 35° 45' 58,8"	Volcanisme, coulée de 15 m	Basalte massif à grosses géodes (calcite, calcédoine) et lentilles à ooides de malachite	
LAP 02/17	Gorge de Lapurr N 4° 16' 06,4" E 35° 46' 02,5"	Volcanisme, coulée de 15 m	Coulée à grosses vacuoles, géodes, basalte prismé à calcite et opale	
LAP 02/18	Gorge de Lapurr	Volcanisme, coulée de 5 m	Basalte grossièrement prismé, enduit de malachite à la base	
LAP 02/19	Gorge de Lapurr	Volcanisme, coulée bréchique de 10 m	Basalte à géodes	***37.25+-0.9***
LAP 02/20	Gorge de Lapurr	Volcanisme, coulée en prismes grossiers de 3-4 m	Basalte	

LAP 02/21	Gorge de Lapurr	Volcanisme, coulée en prismes grossiers de 6 m	Basalte sombre	
LAP 02/22	Gorge de Lapurr	Volcanisme, coulée en prismes grossiers de 15 m	Basalte (partie médiane de la coulée)	
LAP 02/23	Gorge de Lapurr	Dyke de 10 m recoupant une coulée en gros prismes LAP 02/24	Basalte	
LAP 02/24	Gorge de Lapurr	Volcanisme, coulée prismée de 5 m	Basalte	***38.6***
LAP 02/25	Gorge de Lapurr N 4° 15' 43,3" E 35° 46' 37"	Dyke N10 1,50 m subvertical	Basalte	
LAP 02/26	Gorge de Lapurr N 4° 15' 46" E 35° 46' 43,1"	Volcanisme, coulée prismée 12 m	Basalte massif	***33***
LAP 02/27	Gorge de Lapurr Idem	Volcanisme, coulée de 10 m	Basalte à grain fin	
LAP 02/27A	Gorge de Lapurr N 4° 15' 40,5" E 35° 46' 51,5"	Volcanisme, coulée de 10 m	Base de la coulée LAP 02/27	
NA 02/32	Laga Nariokotome N 4° 07' 02,4" E 35° 47' 16,1"	Volcanisme, coulée prismée	Basalte aphyrique à grain fin dans le lit du laga	***20.6 +- 0.9***
NA 02/33	Idem	Volcanisme, coulée	Faciès à grain fin en base de coulée	***17***
NA 02/34	Idem	Volcanisme	Lave à débit en boules	
NA 02/36	Idem	Volcanisme, coulée	Basalte massif	
NA 02/37	Idem	Volcanisme, coulée de 3,50 m	Coulée régulière à patine blanche	
NA 02/38	Idem	Volcanisme, coulée de 2 m massive à base érosive	Basalte massif	
NAIYENA ENGOL				
NAI 02/01	Naiyena Engol	Sédimentaire, banc décimétrique dans un banc de 4-5 m	Grès induré en milieu de banc	
NAI 02/02	Idem	Sédimentaire	Banc à Melania	
NAI 02/03	Idem	Sédimentaire, banc décimétrique	Lumachelle à gastéropodes fortement cimentée	
Coupe de Naiyena Engol				
NAIA 02/08	Idem	Volcano-sédimentaire	Tuf pulvérulant blanc	
NAIA 02/09	Idem	Volcano-sédimentaire	Grès passant latéralement à un tuf	
NAIA 02/10	Idem	Volcano-sédimentaire, banc de 5 cm	Tuf blanc	
NAY 02/01	Laga Naiyena Engol N 4° 04' 34,5"	Contact sédiments-volcanisme	Volcanisme hydrothermalisé, veine de calcite,	

	E 35° 46' 56,7"		basalte à vacuoles de calcite étirées	
NAY 02/02	Idem	Volcanisme	Lave à vacuole dans les premières collines volcaniques	
NAY 02/03	N 4° 04' 55,2" E 35° 46' 03,7"	Volcanisme	Basalte sombre à grain fin	***29.3 +- 1.4***
KANEOLEM				
KEN 02/03	Kanoelem	Volcanisme	Première coulée en avant de l'escarpement de Lapurr, débit en boules	
KEN 02/05	Kanoelem N 4° 11' 07,4" E 35° 49' 41,5"	Système de dykes et sill au contact grès-volcanisme	Basalte à grain fin	
KEN 02/09	Kanoelem N 4° 11' 50,7" E 35° 49' 46,9"	Dyke NS, 2 m	Basalte	
KEN 02/12	Idem, escarpement	Volcanisme	Lave 'intrusive' entre le grand escarpement et la falaise de grès	***27.2***
KEN 02/14	Idem, au pied de l 'escarpement dans le système de dyke-sill de Kanoelem	Volcanisme	Lave en filon, baguettes d'amphiboles, corps intrusif à altération en boules	***Feldspath 36.1 +- 0.9***
NATOO				
NAT 02/01	Laga Natoo N 4° 12' 42,1" E 35° 49' 36,4"	Sill au contact entre grès et laves	Lave à grain fin	
NAT 02/02	Idem	Idem	Filon à grosses amphiboles	***25.4***
NAT 02/02a	Idem	Idem	Feldspath	***26.5 +- 1.0***
ELIYE SPRINGS				
EL 02/03	Idem	Volcano-sédimentaire, banc de 12 cm	Tuf gris clair un peu verdâtre	
EL 02/06	Idem	Volcano-sédimentaire, banc de 50 cm	Sable fin tufacé	
KATABOI				
KAT 02/03	Kataboi N 3° 44' 30,4'' E 35° 46' 29, 3''	Volcanisme, coulée prismée	Basalte sombre à grain fin (Miocène-Pliocène ?)	
KAT 02/04	Kataboi N 3° 44' 51,2'' E 35° 46' 45,5''	Idem	Idem	***4.41 +- 0.19***
KAT 02/05	Kataboi N 3° 45' 05,5'' E 35° 46' 55,2''	Idem	Idem	***5.05***
LOTHAGAM				
LOT 02/02	Lothagam N 2° 55' 24,4'' E 36° 03' 41,9''	Volcanisme, coulée prismée	Basaltes à grain fin et pyroxènes (Miocène ?)	

NAPEDET				
NAP 02/01 à 05	Napedet E N 2° 47’ 20,3’’ E 35° 55’ 15,5’’	Volcanisme	Boules de basaltes à grain fin et clinopyroxènes inclus dans une brèche de type lahar	
LOTHIDOK				
LOTI 02/03	Lothidok N 3° 11’ 57,1’’ E 35° 51’ 22,1’’	Volcanisme	Basalte sombre à pyroxènes et plagioclases	
KANAMUKUN				
KAN 02/01 et 02	Kanamukun N 4° 20’ 47,5’’ E 35° 52’ 26,3’’	Contact grès-socle	? ? ? ?	
TOPERNAWI				
TOP 02/01	Laga Topernawi	Volcanisme, coulée en pseudo-prismes	Basalte à grain fin	***28 +- 0.7***
TOP 02/03a et b	Idem	Volcano-sédimentaire, banc de 1,50 m d’épaisseur maximum	Tufs ‘soudés’ verdâtres en petits bancs d’épaisseur de 5 à 30 cm, faciès noduleux riche en débris végétaux carbonisés et fragments non carbonisés 02/03a : faciès nodulaire 02/03b : faciès lité au dessus	
TOP 02/04	Idem	Volcano-sédimentaire, banc de 50 cm	Tuf jaune roux	
TOP 02/05	Idem	Volcano-sédimentaire, banc de 2 m	Tuf jaune vert	
TOP 02/06	Idem	Volcano-sédimentaire, banc de 75 cm	Tuf verdâtre à granules et petits graviers	

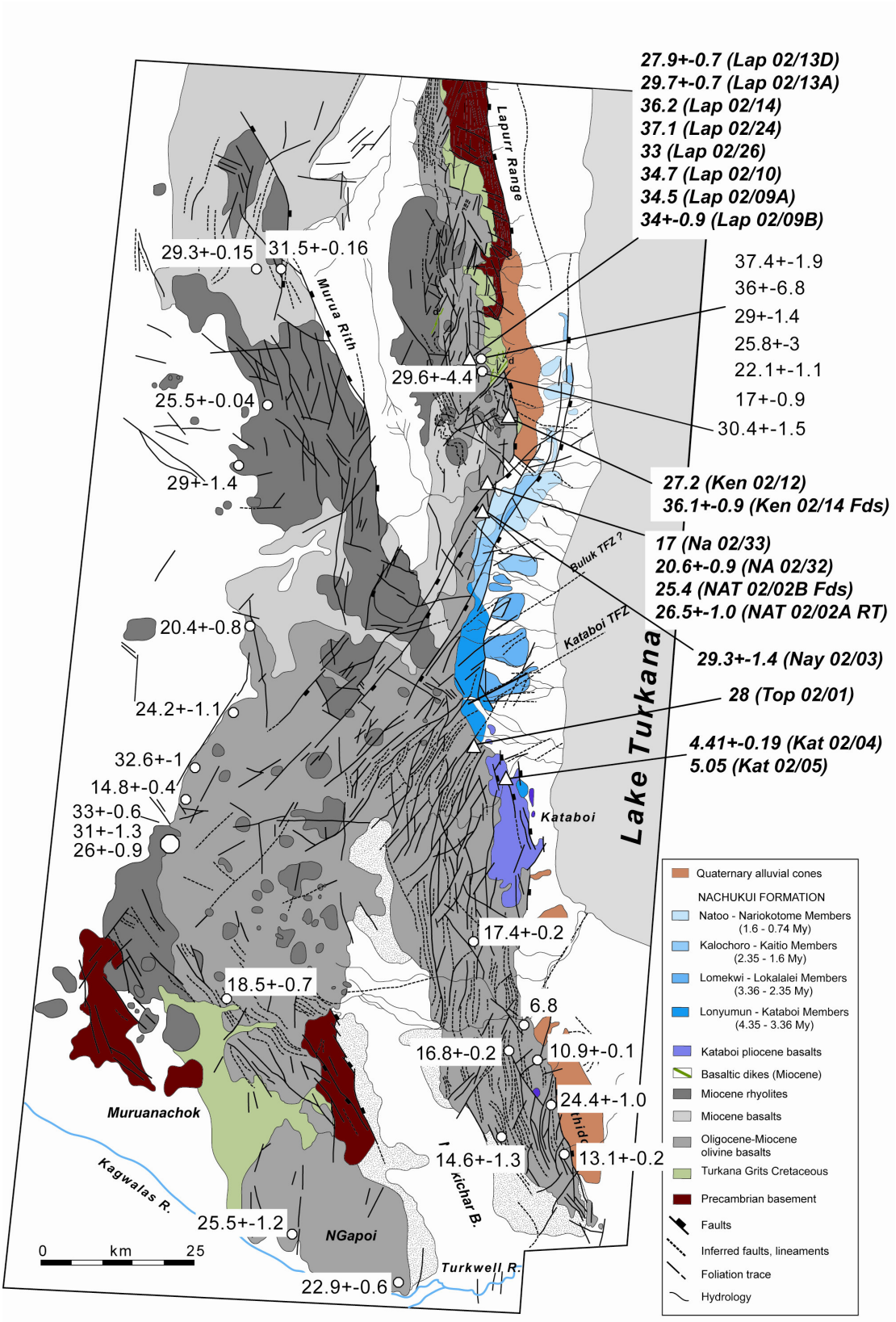

Figure 1. *Carte de localisation des échantillons datés sur la zone de Lapurr-Lothidok (triangles). Datations provenant de la littérature (rond).*

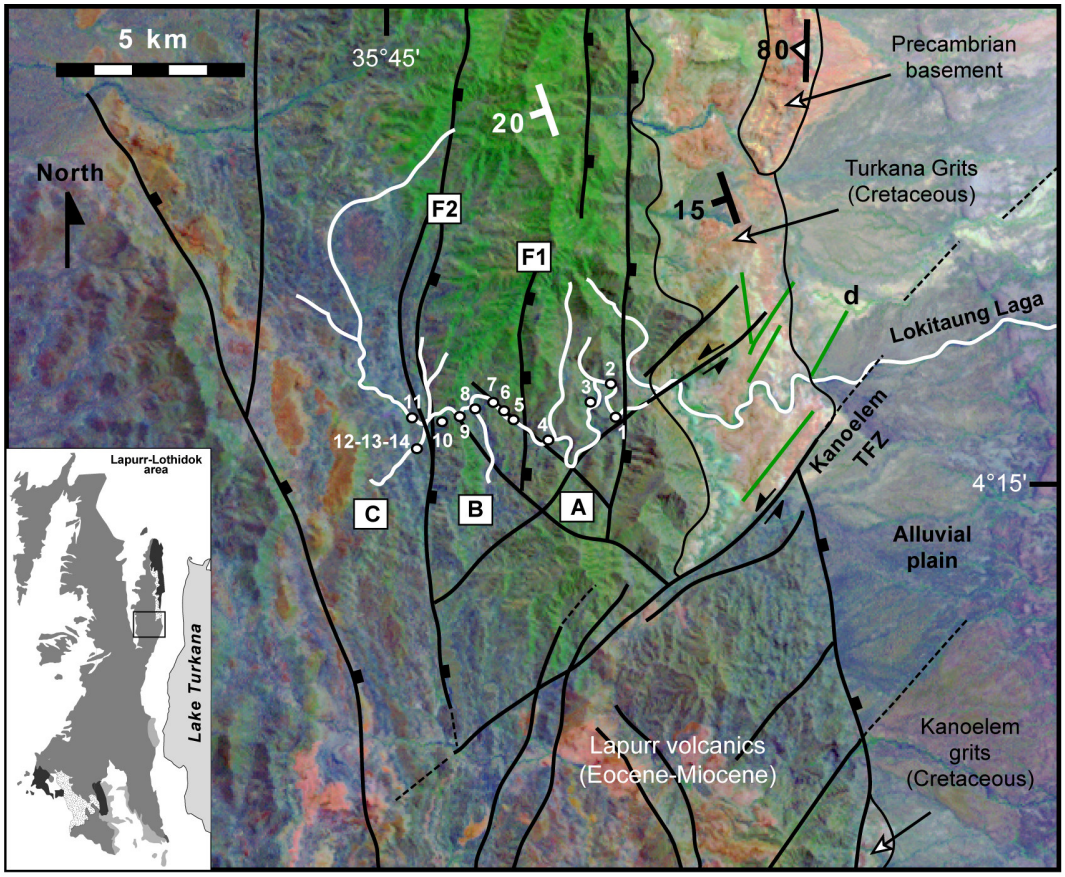

	Sample number	Sample name	Age (Ma)	Location GPS point
Block C	12	LAP 02/13D	28.2	N 4° 15' 43,4" E 35° 45' 29"
	11	LAP 02/13C	37.1	N 4° 15' 43,4" E 35° 45' 29"
Sill ?	10	LAP 02/13A	29.7+-0.7	N 4° 15' 43,4" E 35° 45' 29"
Normal fault	9	LAP 02/13	38.4	N 4° 15' 51,6" E 35° 45' 32,9"
	8	LAP 02/14	37.1	N 4° 15' 54,8" E 35° 45' 39,1"
Sill ?	7	LAP 02/15	19.45+-0.55	N 4° 15' 59,5'' E 35° 45' 50''
Block B	6	LAP 02/19	37.25+-0.9	N 4° 16' 06,4" E 35° 46' 02,5"
	5	LAP 02/24	38.6	N 4° 15' 43,3" E 35° 46' 37"
Normal fault	4	LAP 02/26	33	N 4° 15' 46" E 35° 46' 43,1"
Block A	3	LAP 02/10	34.7	N 4° 16' 0,6" E 35° 47' 19"
	2	LAP 02/09A	34.5	N 4° 16' 13,2" E 35° 47' 18,8"
	1	LAP 02/09B	34+-0.9	N 4° 16' 0,6" E 35° 47' 19"

Top escarpement

Bottom escarpement

***Figure 2**. Carte de localisation et tableau récapitulatif des échantillons datés le long de la gorge de Lapurr. Les redoublement d'âge des séries suggèrent la présence de trois blocs basculés (A, B, C) séparés par deux failles normales (F1, F2). Certains âges récents dans les séries plus anciennes pourraient indiquer des intrusions de type sill.*

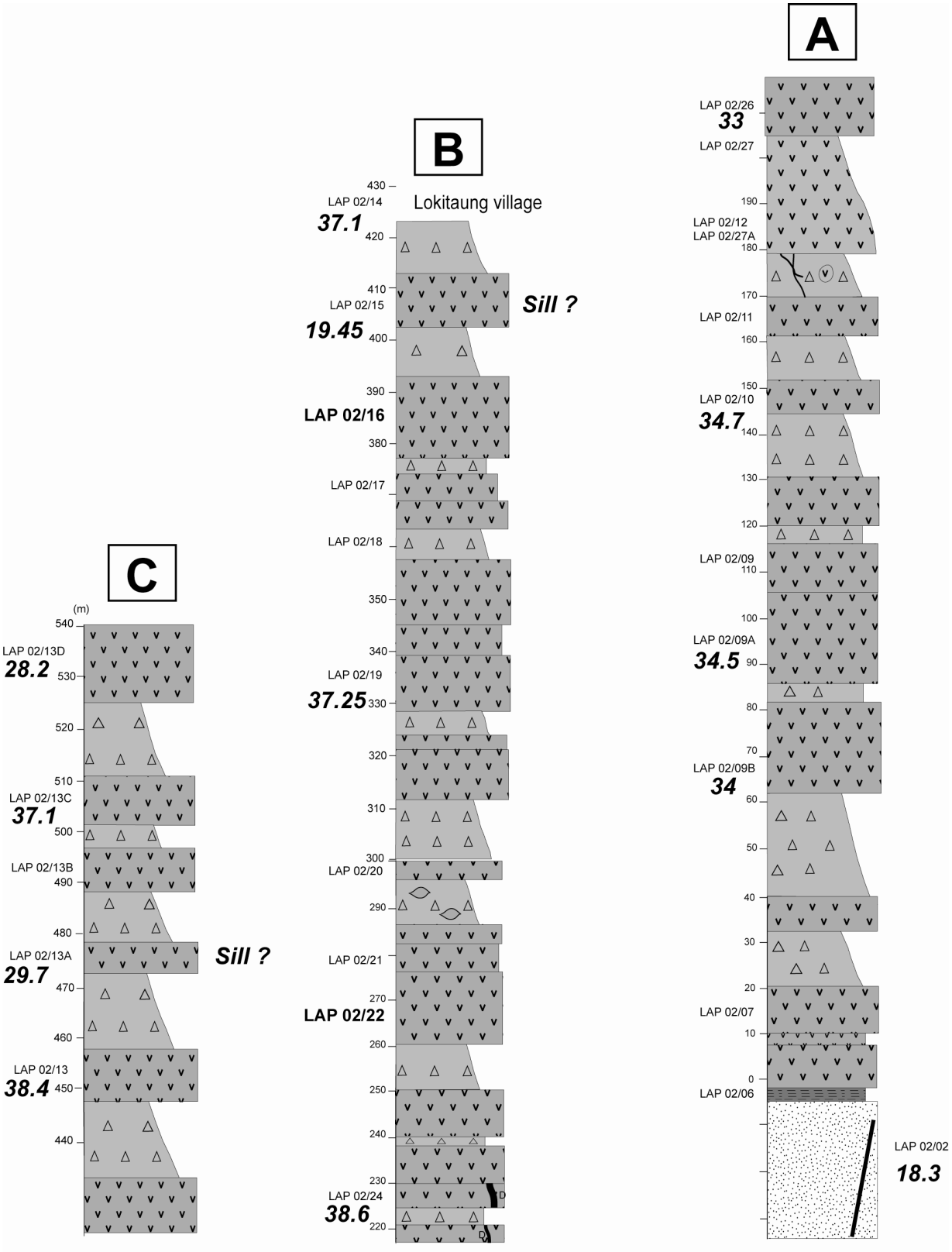

Figure 3. *Log stratigraphique de la Formation volcanique de Lapurr (Eocène-Miocène). Les datations K/Ar font apparaître trois blocs basculés (A, B et C) localement intrudés par des sills.*

ANNEXE 3. Echantillons paléoniveaux lacustres mission Turkana 2002

ECHANTILLONS	*DESCRITION*	*Position géographique*	*Age C14 (BP)*
APALOKWO			
APA 02/01	Encroûtement stromatolitique (croûte et galet encroûté)	4° 10' 51'' 35° 51' 12.7''	
APA 02/02	Niveau à huîtres et encroûtement carbonaté	4° 10' 51'' 35° 51' 12.7''	
ELIYE SPRINGS			
EL 02/01	Coquilles de lamellibranches au sommet d'une formation lacustre	3° 11' 52.4'' 36° 00' 10.5''	
EL 02/14A	Sable coquillé fin micacé sans structure à coquilles de bivalves	3° 13' 6.7'' 36° 00' 11.4''	Datation sur unio **6285 +- 50 yr**
EL 14C	Niveau à gastéropodes	3° 13' 6.7'' 36° 00' 11.4''	
EL 02/15	Argilite brun vert, grasse, micacée à débris de poissons et coquilles de bivalves	3° 13' 6.7'' 36° 00' 11.4''	
EL 02/16	Sable fin micacé riche en coquilles de bivalves et débris de poissons	3° 13' 6.7'' 36° 00' 11.4''	
EL 02/17	Niveau à coquilles	3° 13' 6.7'' 36° 00' 11.4''	Datation sur gastéropodes **6630 +- 45 yr**
KATABOI			
KAT 02/06	Niveau coquillé à gastéropodes et gros bivalves	3° 44' 51.7'' 35° 47' 5.1''	Datation sur unio **9515 +- 80 yr**
LAPURR			
LAPS 02/12	Niveau de diatomites (faillé)	4° 16' 44.7'' 35° 52' 14.2''	
LAPS 02/14	Niveau à huîtres et encroûtement carbonaté (+63 m au dessus du lac actuel)	4° 17' 1.5'' 35° 51' 46.5''	Datation sur huître **5225 +- 80 yr**
LOKALALEI			
LO 02/01	Encroûtement stromatolitique d'épaisseur centimétrique directement sur galet	3° 57' 21.4'' 35° 47' 1.5''	
LO 02/02	Encroûtement stromatolitique d'épaisseur 1-3 cm directement sur huître	3° 57' 21.4'' 35° 47' 1.5''	
LO 02/03	Encroûtement stromatolitique d'épaisseur centimétrique sur huître	3° 57' 21.4'' 35° 47' 1.5''	
LO 02/04	Ensemble de	3° 57' 21.4''	

	galet/huître/encroûtement stromatolitique	35° 47’ 1.5’’	
LO 02/05	Ensemble galet/grosses huîtres/encroûtement stromatolitique	3° 57’ 21.4’’ 35° 47’ 1.5’’	
LO 02/06	Encroûtement stromatolitique épais sur huître	3° 57’ 21.4’’ 35° 47’ 1.5’’	
LOTHAGAM			
LOT 02/01	Banc sableux à gastéropodes (40-50 cm) (faillé)	2° 55’ 53.9’’ 36° 03’ 45.7’’	Datation sur melanias **9795 +- 15 yr**
LOT 02/03	Argilite beige à coquilles de gastéropodes	2° 55’ 14.4’’ 36° 03’ 36.5’’	
NACHUKUI			
NACH 02/01	Niveau à huîtres, +65 m au dessus du niveau du lac actuel	4° 05’ 11.1’’ 35° 49’ 36.4’’	Datation sur huîtres **5260 +- 40 yr**
NACH 02/02	Niveau à huîtres et encroûtement carbonaté, niveau à +75 m au dessus du lac actuel	4° 05’ 11.1’’ 35° 49’ 36.4’’	
NAKOLAK			
A	Niveau à gastéropodes		
B	Niveau à huîtres		
NAK 02/01	Petits oncolites et petits galets encroûtés	4° 09’ 01’’ 35° 51’ 1.8’’	
NAK 02/02	Gros stromatolites autour d’un galet (2 encroûtement différent)	4° 09’ 01’’ 35° 51’ 1.8’’	
NAK 02/03	Huîtres dans cordon de galets de 10 m de largeur	4° 09’ 01’’ 35° 51’ 1.8’’	Datation sur huîtres **5320 +- 35 yr**
NAK 02/04	Niveau à huîtres, 100 m en aval de NAK 02/03	4° 09’ 01’’ 35° 51’ 1.8’’	
NAK 02/05	Encroûtement stromatolitique sur galets dans cordon de galets	4° 09’ 4.8’’ 35° 51’ 7.6’’	
NAK 02/06	Niveau à gastéropodes et bivalves associés à un cordon de galets à huîtres	4° 09’ 4.8’’ 35° 51’ 7.6’’	Datation sur melanias **4965 +- 40 yr**
NARIOKOTOME			
NA 02/24	Niveau à huîtres	4° 07’ 5.7’’ 35° 51’ 2.7’’	
NA 02/26	Gros stromatolites	4° 07’ 5.7’’ 35° 51’ 2.7’’	
NA 02/27	Petits oncolites	4° 07’ 5.7’’ 35° 51’ 2.7’’	
NA 02/32	Niveau à huîtres	4° 07’ 5.7’’ 35° 51’ 2.7’’	Datation sur huîtres **4810 +- 40 yr**
TOPERNAWI			
TOP 02/11	Niveau à huîtres	3° 50’ 41.9’’ 35° 46’ 19.2’’	Datation sur huîtres **5810 +- 70 yr**

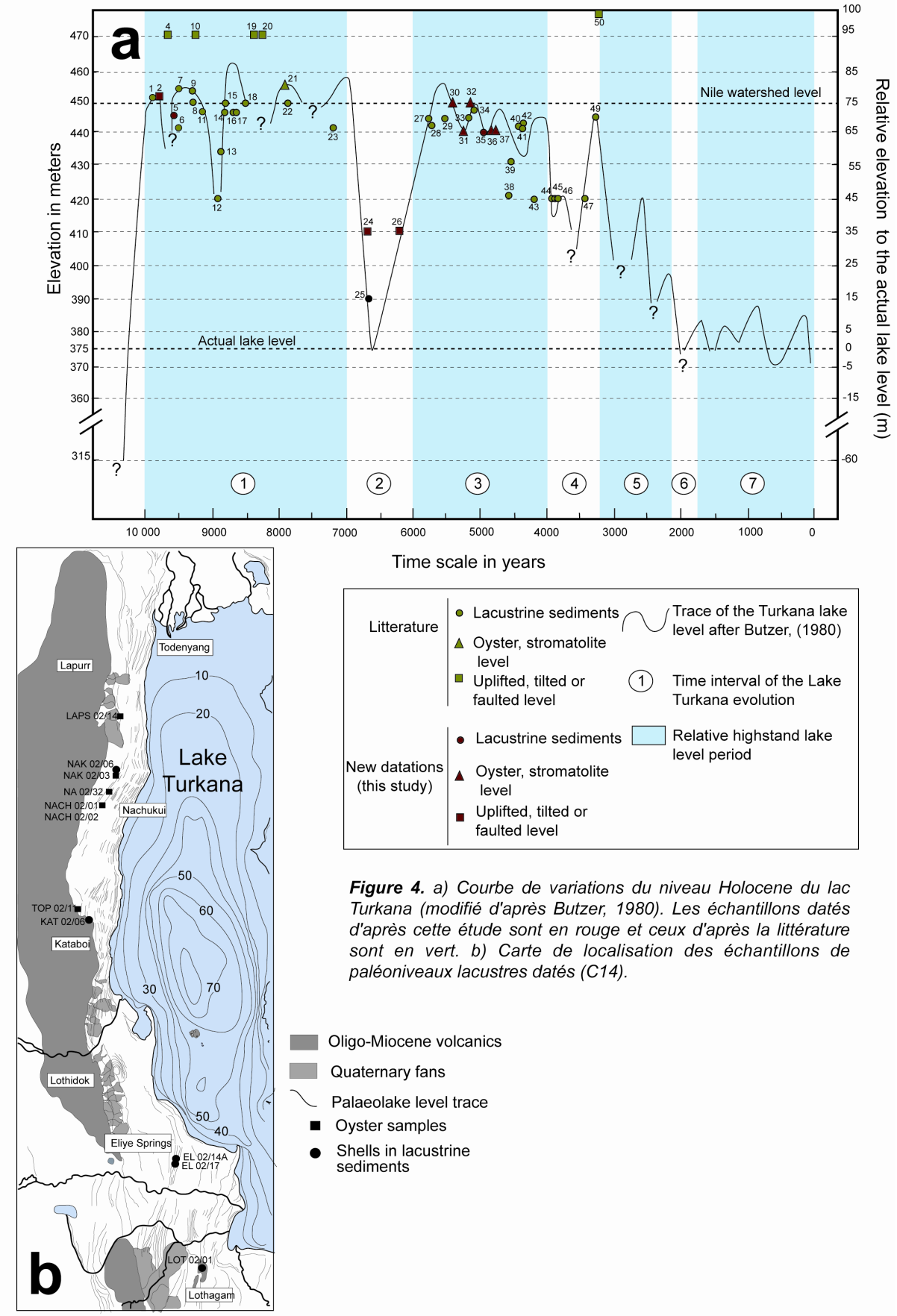

Figure 4. *a) Courbe de variations du niveau Holocene du lac Turkana (modifié d'après Butzer, 1980). Les échantillons datés d'après cette étude sont en rouge et ceux d'après la littérature sont en vert. b) Carte de localisation des échantillons de paléoniveaux lacustres datés (C14).*

Tableau 4. *Synthèse des datations et altitudes des sédiments lacustres et des formations littorales du lac Turkana pour la période Holocene (10 000 ans. – Actuel). En rouge : nouvelles datations, en jaune : cordons d'huîtres, en orange : dépôts déformés ou soulevés.*

Période de temps	***Numéro de site***	***Références***	***Matériel daté***	***Position géographique***	***Altitude (m)***	***Age (années BP)***	***Méthode***
Phase 1 10 000 - 7000 ans	1	Owen et al., 1982	Silt à diatomite	Koobi Fora	+ 75 ? + 80 ?	**9880 +- 670**	^{14}C
	2	LOT 02/01	Coquilles de gastéropodes *(Melania)*	2° 55' 53.9'' 36° 03' 45.7'' Lothagam	?	**9795 +- 15**	^{14}C
	3	Truckle, 1976	Coquilles de gastéropodes	Suguta Namarunu	+ 200	**9660 +- 210**	^{14}C
	4	Owen et al., 1982	Coquilles mollusques	Kokoi horst	+ 95 (soulevé)	**9540 +- 260**	^{14}C
	5	KAT 02/06	Coquilles *(Unionidae)*	3° 44' 51.7'' 35° 47' 5.1'' Kataboi	+ 70	**9515 +- 80**	^{14}C
	6	Butzer et al., 1972	Coquilles *(Corbicula)*	5° 24' 35° 56' Kibish	+ 67	**9500 +- 150**	^{14}C
	7	Butzer et al., 1972	Coquilles *(Unionidae)*	5° 24' 36° 12' Kibish	+ 80	**9500 +- 150**	^{14}C
	8	Owen et al., 1982	Coquilles	Ileret	+ 70 ? + 75 ?	**9360 +- 135**	^{14}C
	9	Butzer et al., 1972	Coquilles *(Unionidae)*	5° 05' 36° 02' Kibish	+ 78	**9300 +- 400**	^{14}C
	10	Owen et al., 1982	Coquilles mollusques	Kokoi horst	+ 95 (soulevé)	**9260 +- 235**	^{14}C
	11	Butzer et al., 1972	Coquilles	5° 24' 35° 57' Kibish	+ 72	**9100 +- 300**	^{14}C
	12	Owen et al., 1982	Coquilles	Koobi Fora	+43 +46	**8915 +- 140**	^{14}C
	13	Butzer et al., 1972	Coquilles	5° 23' 35° 57' Kibish	+ 59	**8900 +- 300**	^{14}C
	14	Butzer et al., 1972	Coquilles *(Corbicula)*	5° 24' 35° 56' Kibish	+ 72	**8800 +- 200**	^{14}C
	15	Owen et al., 1982	Coquilles *(Etheria)*	Koobi Fora	+ 73 + 75	**8710 +- 130**	^{14}C
	16	Butzer et al., 1972	Coquilles *(Corbicula)*	5° 24' 35° 56' Kibish	+ 72	**8700 +- 200**	^{14}C
	17	Butzer et al., 1972	Coquilles *(Corbicula)*	5° 24' 35° 56' Kibish	+ 72	**8650 +- 150**	^{14}C
	18	Owen et al., 1982	Coquilles	Koobi Fora	+ 73 + 75	**8520 +- 130**	^{14}C
	19	Owen et al., 1982	Os de mammifères dans dépôts littoraux	Koobi Fora	+ 95 (soulevé)	**8395 +- 270**	^{14}C

	20	Owen et al., 1982	Os de mammifères et poissons dans dépôts littoraux	Koobi Fora	+ 95 (soulevé)	**8355 +- 235**	^{14}C
	21	Butzer et al., 1972	Coquilles *(Etheria)* dans cordon d'huîtres	5° 05' 35° 55' Kibish	+ 80	**7900 +- 150**	^{14}C
	22	Owen et al., 1982	Os de poissons	Koobi Fora	+ 73 + 75	**7855 +- 160**	^{14}C
	23	Butzer et al., 1972	Coquilles *(Unionidae)*	2° 55' 36° 05' Lotahgam	+ 66 ?	**7160 +- 80**	^{14}C
	24	EL 02/17	Coquille de gastéropodes	3° 13' 6.7'' 36° 00' 11.4'' Elyie Springs	?	**6630 +- 45**	^{14}C
Phase 2 7000 – 6000	25	Butzer et al., 1972	Coquilles	4° 28' 35° 57' Todenyang	+ 15	**6600 +- 150**	^{14}C
	26	EL 02/14A	Coquille de bivalve *(Unionidae)*	3° 13' 6.7'' 36° 00' 11.4'' Elyie Springs	?	**6285 +- 50**	^{14}C
	27	TOP 02/11	Niveau à huîtres	3° 50' 41.9'' 35° 46' 19.2'' Topernawi	+ 65	**5810 +- 70**	^{14}C
	27	Butzer et al., 1972	Coquilles *(Unionidae)*	5° 22' 36° 05' Kibish	+ 69	**5750 +- 100**	^{14}C
	28	Butzer et al., 1972	Coquilles	5° 18' 35° 57' Kibish	+ 67	**5700 +- 100**	^{14}C
	29	Butzer et al., 1972	Coquilles	5° 19' 35° 59' Kibish	+ 69	**5450 +- 100**	^{14}C
	30	NAK 02/03	Coquilles d'huître	4° 09' 01'' 35° 51' 1.8'' Nakolak	+ 74	**5320 +- 35**	^{14}C
	31	NACH 02/01	Coquilles d'huître	4° 05' 11.1'' 35° 49' 36.4'' Nachukui	+ 64	**5260 +- 40**	^{14}C
Phase 3 6000 – 4000	32	LAPS 02/14	Niveau à huîtres et encroûtement carbonaté	4° 17' 1.5'' 35° 51' 46.5'' Lapurr	+ 63	**5225 +- 80**	^{14}C
	32	NACH 02/02	Coquilles d'huître	4° 05' 11.1'' 35° 49' 36.4'' Nachukui	+ 74	**5255 +- 30**	^{14}C
	33	Butzer et al., 1972	Coquilles	5° 10' 35° 35' Kibish	+ 70	**5150 +- 350**	^{14}C
	34	Owen et al., 1982	Dépôts littoraux	Koobi Fora	+ 70 ? + 73 ?	**5060 +- 245**	^{14}C
	35	NAK 02/06	Coquille de gastéropodes *(Melanoides)*	4° 09' 4.8'' 35° 51' 7.6'' Nakolak	?	**4965 +- 40**	^{14}C
	36	NA 02/32	Coquilles d'huître	4° 07' 5.7'' 35° 51' 2.7'' Nariokotome	+ 65	**4810 +- 40**	^{14}C

	37	NA 02/32	Concrétion carbonatée	4° 07’ 5.7’’ 35° 51’ 2.7’’ Nariokotome	+ 65	**4790 +- 30**	^{14}C
	38	Owen et al., 1982	Os de poisson	Koobi Fora	+ 45 + 47	**4580 +- 170**	^{14}C
	39	Owen et al., 1982	Os de mammifères dans niveaux littoraux	Koobi Fora	+ 55 +56	**4560 +- 185**	^{14}C
	40	Owen et al., 1982	Coquilles	Koobi Fora	+ 67	**4540 +- 230**	^{14}C
	41	Butzer et al., 1972	Coquilles *(Etheria)*	3° 08’ 35° 59’ Kerio	+ 66 ?	**4400 +- 100**	^{14}C
	42	Owen et al., 1982	Charbon de bois	Koobi Fora	+ 65 ? + 68 ?	**4390 +- 235**	^{14}C
	43	Owen et al., 1982	Charbon de bois	Koobi Fora	+ 43 + 46	**4160 +- 110**	^{14}C
	44	Owen et al., 1982	Charbon de bois	Koobi Fora	+ 43 + 46	**3970 +- 60**	^{14}C
	45	Owen et al., 1982	Charbon de bois	Koobi Fora	+ 45 + 47	**3960 +- 60**	^{14}C
	46	Owen et al., 1982	Charbon de bois	Koobi Fora	+ 45 + 47	**3945 +- 135**	^{14}C
Phase 4 4000 – 3200	47	Owen et al., 1982	Os de mammifères dans niveaux littoraux	Koobi Fora	+ 45 + 47	**3405 +- 130**	^{14}C
	48	Butzer et al., 1972	Coquilles	5° 19’ 35° 57’ Vallée de l’Omo	+ 70	**3250 +- 150**	^{14}C
	49	Owen et al., 1982	Os de mammifères dans niveaux littoraux	Koobi Fora	+ 100 (soulevé)	**3215 +- 155**	^{14}C
Phase 5 3200 – 2100							
Phase 6 2100 – 1800							
Phase 7 1800 - Actuel							